<u>**Final Report**</u>

Nondestructive Testing for Advanced Monitoring and Evaluation of Damage in Concrete Materials

Prepared for:

Florida Department of Transportation
Project Contract No. BC354 - 57

Prepared By:

Dr. Andrew J. Boyd
Dr. Bjorn Birgisson
Mr. Christopher Ferraro
Mr. Scott Cumming

University of Florida
Department of Civil & Coastal Engineering
P.O. Box 116580, 345 Weil Hall
Gainesville, FL 32611-6580

August 2005

DISCLAIMER

The opinions, findings, and conclusions expressed in this publication are those of the authors and not necessarily those of the State of Florida Department of Transportation.

APPROXIMATE CONVERSIONS TO SI UNITS

SYMBOL	WHEN YOU KNOW	MULTIPLY BY	TO FIND	SYMBOL
LENGTH				
in	inches	25.4	millimeters	mm
ft	feet	0.305	meters	m
yd	yards	0.914	meters	m
mi	miles	1.61	kilometers	km

SYMBOL	WHEN YOU KNOW	MULTIPLY BY	TO FIND	SYMBOL
AREA				
in^2	squareinches	645.2	square millimeters	mm^2
ft^2	squarefeet	0.093	square meters	m^2
yd^2	square yard	0.836	square meters	m^2
ac	acres	0.405	hectares	ha
mi^2	square miles	2.59	square kilometers	km^2

SYMBOL	WHEN YOU KNOW	MULTIPLY BY	TO FIND	SYMBOL
VOLUME				
fl oz	fluid ounces	29.57	milliliters	mL
gal	gallons	3.785	liters	L
ft^3	cubic feet	0.028	cubic meters	m^3
yd^3	cubic yards	0.765	cubic meters	m^3
NOTE: volumes greater than 1000 L shall be shown in m^3				

SYMBOL	WHEN YOU KNOW	MULTIPLY BY	TO FIND	SYMBOL
MASS				
oz	ounces	28.35	grams	g
lb	pounds	0.454	kilograms	kg
T	short tons (2000 lb)	0.907	megagrams (or "metric ton")	Mg (or "t")

SYMBOL	WHEN YOU KNOW	MULTIPLY BY	TO FIND	SYMBOL
TEMPERATURE (exact degrees)				
^oF	Fahrenheit	5 (F-32)/9 or (F-32)/1.8	Celsius	^oC

SYMBOL	WHEN YOU KNOW	MULTIPLY BY	TO FIND	SYMBOL
ILLUMINATION				
fc	foot-candles	10.76	lux	lx
fl	foot-Lamberts	3.426	candela/m^2	cd/m^2

SYMBOL	WHEN YOU KNOW	MULTIPLY BY	TO FIND	SYMBOL
FORCE and PRESSURE or STRESS				
lbf	poundforce	4.45	newtons	N
lbf/in^2	poundforce per square inch	6.89	kilopascals	kPa

http://www.fhwa.dot.gov/aaa/metricp.htm

APPROXIMATE CONVERSIONS FROM SI UNITS

SYMBOL	WHEN YOU KNOW	MULTIPLY BY	TO FIND	SYMBOL
LENGTH				
mm	millimeters	0.039	inches	in
m	meters	3.28	feet	ft
m	meters	1.09	yards	yd
km	kilometers	0.621	miles	mi

SYMBOL	WHEN YOU KNOW	MULTIPLY BY	TO FIND	SYMBOL
AREA				
mm^2	square millimeters	0.0016	square inches	in^2
m^2	square meters	10.764	square feet	ft^2
m^2	square meters	1.195	square yards	yd^2
ha	hectares	2.47	acres	ac
km^2	square kilometers	0.386	square miles	mi^2

SYMBOL	WHEN YOU KNOW	MULTIPLY BY	TO FIND	SYMBOL
VOLUME				
mL	milliliters	0.034	fluid ounces	fl oz
L	liters	0.264	gallons	gal
m^3	cubic meters	35.314	cubic feet	ft^3
m^3	cubic meters	1.307	cubic yards	yd^3

SYMBOL	WHEN YOU KNOW	MULTIPLY BY	TO FIND	SYMBOL
MASS				
g	grams	0.035	ounces	oz
kg	kilograms	2.202	pounds	lb
Mg (or "t")	megagrams (or "metric ton")	1.103	short tons (2000 lb)	T

SYMBOL	WHEN YOU KNOW	MULTIPLY BY	TO FIND	SYMBOL
TEMPERATURE (exact degrees)				
^oC	Celsius	1.8C+32	Fahrenheit	^oF

SYMBOL	WHEN YOU KNOW	MULTIPLY BY	TO FIND	SYMBOL
ILLUMINATION				
lx	lux	0.0929	foot-candles	fc
cd/m^2	candela/m^2	0.2919	foot-Lamberts	fl

SYMBOL	WHEN YOU KNOW	MULTIPLY BY	TO FIND	SYMBOL
FORCE and PRESSURE or STRESS				
N	newtons	0.225	poundforce	lbf
kPa	kilopascals	0.145	poundforce per square inch	lbf/in^2

*SI is the symbol for the International System of Units. Appropriate rounding should be made to comply with Section 4 of ASTM E380. (Revised March 2003)

http://www.fhwa.dot.gov/aaa/metricp.htm

Technical Report Documentation Page

1. Report No.	2. Government Accession No.	3. Recipient's Catalog No.
4. Title and Subtitle Nondestructive Testing for Advanced Monitoring and Evaluation of Damage in Concrete Materials		5. Report Date August 2005 6. Performing Organization Code
7. Author(s) Andrew J. Boyd, Bjorn Birgisson, Christopher Ferraro, Scott Cumming		8. Performing Organization Report No. Project 00026793
9. Performing Organization Name and Address University of Florida Department of Civil & Coastal Engineering 365 Weil Hall, Box 116580 Gainesville, FL 32611		10. Work Unit No. (TRAIS) 11. Contract or Grant No. BC354-57
12. Sponsoring Agency Name and Address Florida Department of Transportation 605 Suwannee ST. MS 30 Tallahassee, FL 32399 Tel: 850-414-4615		13. Type of Report and Period Covered Final Report December 2001 – August 2005 14. Sponsoring Agency Code
15. Supplementary Notes		

16. Abstract

This research program was designed to provide the groundwork for future research aimed at using nondestructive testing to monitor new structures for compliance with FDOT performance specifications, and lead to the understanding necessary to successfully devise nondestructive testing regimes which can be used to monitor new structures to ensure adequate performance and detect defects or damage present in existing structures.

The project included a survey aimed at identifying the deterioration mechanisms and defects most relevant to bridge structures in Florida and review of previously published literature to assist in identifying specific nondestructive techniques, or combinations of techniques, which would be most effective for evaluating the damage mechanisms expected in Florida bridges.

The identified deterioration mechanisms were then reproduced in the laboratory and evaluated using the recommended nondestructive techniques. Recommendations were made concerning the use of nondestructive testing technologies in the evaluation of concrete bridge structures in the State of Florida.

17. Key Word		18. Distribution Statement	
NDT, nondestructive testing, concrete, damage evaluation, sulfate attack		No Restrictions	
19. Security Class. (of this report) Unclassified	20. Security Class. (of this page) Unclassified	21. No. of Pages 238	22. Price

FORM DOT F 1700.7 (8-72) Reproduction of completed page authorized

ACKNOWLEDGEMENTS

This work was supported by the Florida Department of Transportation. The principal investigator appreciates the technical assistance provided by Mr. Charles Ishee (FDOT Project Manager) and Mr. M. Bergin, and the support of the FDOT Structural Materials laboratory and the Corrosion laboratory.

EXECUTIVE SUMMARY

Nondestructive testing (NDT) has the potential to be a powerful investigative tool due in part to its ability to detect problems without inducing further damage, but also because it does so with minimal expenditures of time and manpower. Considering the potential gains associated with nondestructive testing, there is a significant lack of expertise available in the State of Florida as well as a lack of knowledge of the fundamental relevance of NDT results.

This research program detailed herein was designed to provide the groundwork for future research aimed at using nondestructive testing to monitor new structures for compliance with FDOT performance specifications, and lead to the understanding necessary to successfully devise nondestructive testing regimes which can be used to monitor new structures to ensure adequate performance and detect defects or damage present in existing structures.

Identifying the deterioration mechanisms and defects most relevant to bridge structures in Florida was the first step. This goal was accomplished through a survey of relevant structures in Florida by reviewing inspection records, searching the Pontis Bridge Management System database, interviewing FDOT personnel, and examining a limited number of structures in the field.

The most prevalent form of damage was found to be cracking, both macro-scale (induced by structural loading, reinforcement corrosion, shrinkage, creep, etc.) and micro-scale (induced by sulfate attack or wet-dry cycling among others). Other forms of deterioration included surface damage due to seawater exposure and delamination of improperly repaired sections.

Simultaneous with the structural survey, a review of previously published literature was conducted to assist in identifying specific nondestructive techniques, or combinations of techniques, which would be most effective for evaluating the damage mechanisms expected in Florida bridges. When considering factors such as effectiveness, applicability, ease of use, and cost, the most effective nondestructive testing techniques for the evaluation and monitoring of new concrete are those implementing pulse wave velocity measurements, specifically ultrasonic pulse velocity and impact echo. Though not able to actually identify the type or source of damage per se, they are definitely capable of detecting damage and measuring severity on a relative scale over time. They are thus well suited for periodic monitoring of new structures, or even older structures once a baseline condition is assessed. Using these techniques in a tomographic imaging strategy to create a three-dimensional “image” of a concrete member is particularly effective, not only at defining damage but also in locating and delineating the extent of that damage.

In order to evaluate the effectiveness of the chosen NDT techniques, the most prevalent deterioration mechanisms identified in the survey were reproduced in the laboratory. In this case, microstructural cracking was induced through exposure of concrete specimens to a sulfate solution. It was found that the wave velocity techniques were indeed sensitive to small changes in physical properties, which were determined from destructive testing. Field testing showed that these techniques were not only effective in detecting large scale cracking, but could also physically locate such damage precisely when a tomography approach was used.

Finally, recommendations were made concerning the use of nondestructive testing technologies identified in this research in the evaluation of concrete bridge structures in the State of Florida. Though implementation of the tests themselves can be done immediately, more work is necessary in order to formulate a procedure such that bridge inspections can be done in an effective and expeditious manner.

TABLE OF CONTENTS

Chapter 1 – Introduction ... 1
Chapter 2 – Literature Review ... 3
Visual Inspection ... 3
Liquid Penetrant Methods ... 7
Acoustic Sounding ... 9
Surface Hardness Methods ... 12
Penetration Resistance Methods ... 13
Pullout Test ... 14
Break-Off test ... 15
Ultrasonic Testing ... 17
Pulse-Echo Testing ... 27
Impact Echo ... 36
Acoustic Emission ... 56
Impulse Response ... 66
Magnetic Methods ... 71
Ground Penetrating Radar ... 75
Resonant Frequency ... 77
Infrared Thermography ... 80
Radioactive Methods ... 85
Conclusions ... 89
Chapter 3 – Laboratory Testing Program ... 90
Definition of Sufficiency Rating ... 90
Methodology ... 91
Results ... 93
Conclusions ... 94
Personnel Survey ... 95
Chapter 4 – Laboratory Testing Program ... 97
Specimen Evaluation ... 101
Results – Nondestructive Evaluation ... 104
Results – Destructive Testing ... 108
Summary ... 122
Chapter 5 – Analysis of Results ... 124
Correlation of Destructive & Nondestructive Results ... 124
SEM Analysis of Microstructure ... 140
Chapter 6 – Conclusions ... 145
Chapter 7 – Recommendations ... 148

References ... 150

Appendices
A – NDT Monitoring Results ... 158
B – Rebound Hammer Test Results ... 168
C – Core Test Results ... 192
D – Scanning Electron Microscopy Images ... 217

CHAPTER 1
INTRODUCTION

Nondestructive testing of civil engineering structures is a potentially valuable tool for monitoring the performance of new structures or detecting and evaluating deterioration in older structures. The inherent cost savings compared to existing destructive evaluation techniques are considerable. Currently, there are a large number of nondestructive testing techniques available for this monitoring and evaluation, though proper implementation procedures for these techniques must be developed. There is also a need to evaluate the various nondestructive testing techniques available to determine which are best suited for specific types of damage or even the absence of damage.

With a shift from the prescription-based specifications of the past to a new performance-based approach, it will be essential to be able to evaluate and monitor new structures to ensure compliance with these specifications. Currently, a great deal of the quality assurance and forensic work performed on civil engineering structures revolves around the use of destructive testing techniques, which by their very nature require the investigator to damage the structure being investigated. A preferable approach is to use nondestructive techniques that allow determination of the structure's condition without inducing further distress.

Nondestructive testing (NDT) has the potential to be a powerful investigative tool due in part to its ability to detect problems without inducing further damage, but also because it does so with minimal expenditures of time and manpower. Considering the potential gains associated with nondestructive testing, there is a significant lack of expertise available in the State of Florida as well as a lack of knowledge of the fundamental relevance of NDT results.

In the past, NDT has usually been approached in an entirely empirical manner. Typically, this was done by performing large numbers of tests with a particular piece of equipment and then analyzing the results in an attempt to find some pattern that represents the expected damage. Our goal is to initially revisit the fundamentals of NDT from the opposite, but more relevant, direction; by examining the actual damage mechanisms themselves and determining the NDT results produced by these mechanisms.

There are a number of advantages associated with this approach. It will allow proper correlation of NDT results with the type and severity of damage present in the material. It will also help define which tests are the most sensitive to, and thus best suited for, detecting various types of damage. Such information is essential in establishing acceptable performance of new structures by confirming the initial absence of damage and later to monitor the initiation and progress of deterioration.

By combining a laboratory testing program that simulates damage mechanisms in concrete with nondestructive testing technologies this research will identify the parameters most sensitive to a given type of damage. Knowledge of these key material parameters will allow for the selection of appropriate NDT technologies for monitoring changes in these parameters over time. This effort will thus provide the groundwork for future research aimed at using nondestructive testing to monitor new structures for compliance with FDOT performance specifications, and will lead to the understanding necessary to successfully devise nondestructive testing regimes which can be used to monitor new structures to ensure adequate performance and detect defects or damage present in existing structures.

Knowledge of the condition of newly constructed structures will provide FDOT with the quality assurance data necessary to ensure compliance with the performance-based specifications approach currently being adopted. Similarly, the ability to detect, identify and quantify existing damage at an earlier age than conventional techniques will minimize the costs associated with rehabilitation. Finally, a comprehensive NDT based evaluation program will set the stage for a rational framework for actual service life modeling of structures, with an emphasis on providing information for the development of optimum maintenance regimes and rehabilitation techniques.

CHAPTER 2
LITERATURE REVIEW

Introduction to Nondestructive Testing

The purpose of establishing standard procedures for nondestructive testing (NDT) of concrete structures is to qualify and quantify the material properties of in-situ concrete without intrusively examining the material properties. There are many techniques that are currently being research for the NDT of materials today. This chapter focuses on the NDT methods relevant for the inspection and monitoring of concrete materials.

Visual Inspection

Visual inspection refers to evaluation by means of eyesight, either directly or assisted in some way. The visual inspection of a structure is the "first line of defense" and typically involves the search for large-scale deficiencies and deformities. Perhaps the most important aspect related to the preparation for visual inspection is the review of available literature related to the structure or structural element. This should include original drawings, notes and reports from previous inspections, and interviews with personnel familiar with the structure or structural element to be inspected. Although interviews are usually not in themselves considered a type of visual inspection, the interview process can often precipitate a visit to the structure or structural element that can then focus on visible defects noted by site personnel, who usually have the most familiarity with the structure.

Direct visual inspection

The basic principle of direct visual inspection is a meticulous attention to detail. The most common tools used by inspectors include calipers, gauges, templates, micrometers, rulers, levels, chalk, illumination devices, cameras, note taking devices, and other miscellaneous equipment.

Direct visual inspection can be applied to most methods of preventative maintenance and rehabilitation work. Care must be taken to avoid focusing on the search for small-scale deficiencies within a structure to the extent that large-scale deficiencies are overlooked. It is important for the inspector to periodically take a step back and look for larger scale deficiencies. This "can't see the forest for the trees" syndrome can occur especially when less experienced inspection personnel are involved.

Remote visual inspection

Often, field conditions are not conducive to the direct inspection of a structure or its component elements. Sight limitations could be a result of inaccessibility due to obstructions, hazardous conditions or deficiencies of a scale not visible to the naked eye. When such unfavorable field conditions arise, aids may be required to permit effective visual inspection. Usually, remote visual inspection involves the effective use of optical instruments. These instruments include mirrors, borescopes, charged coupled devices (CCD), and remote miniature cameras.

Borescopes

A borescope is an optical instrument composed of a tube designed for the remote inspection of objects. A person at one end of the tube can view an image obtained at the other end. The image is transmitted through the tube via fiber optic bundles, running though the tube, camera, video projection system, or lenses. A borescope that utilizes fiber bundles for its image projection is commonly referred to as a fiber optic borescope or fiberscope. Another method of image transfer is through the use of a small camera at one end of the tube and a monitor at the other end. Lenses can also be used to convey the image to the observer through an eyepiece.

Due to the variety of needs created by industry, there are several types of borescopes. The basic categories are rigid or flexible, as dictated by the configuration of the tube. Figures 2.1 through 2.3 illustrate flexible and rigid borescopes. The borescopes most commonly used today are: fiber optic borescopes, camera borescopes, lens borescopes and microborescopes. The fiber optic and camera variety are usually of the flexible type, while the lens borescope is typically rigid. Microborescopes can be either rigid or flexible.

Borescopes are commonly used for the inspection of objects that have areas of inaccessibility. They are prevalent in the mechanical engineering field more than any other area and are instrumental in the inspection and condition assessment of engines and engine parts. However, borescopes are valuable to civil/structural inspectors and are commonly employed in the inspection of inaccessible structural elements, such as the interior of masonry block or multi-wythe brick walls. Borescopes were instrumental in the Statue of Liberty restoration project, which began in 1984 and was completed in 1990. Olympus Corporation donated flexible fiberscopes, rigid borescopes, halogen light sources and photo recording accessories to the project. The equipment was used by the National Parks Service engineers to examine the Lady's iron skeleton. In depth observations revealed a hazardous array of warps, sags, leaks, and failed joints (Hellier 2001). Without the use of borescopes, the inspectors' efforts would have resulted in an incomplete assessment of the structure. Figures 2.1-2.3 are photographs of the most commonly used borescopes.

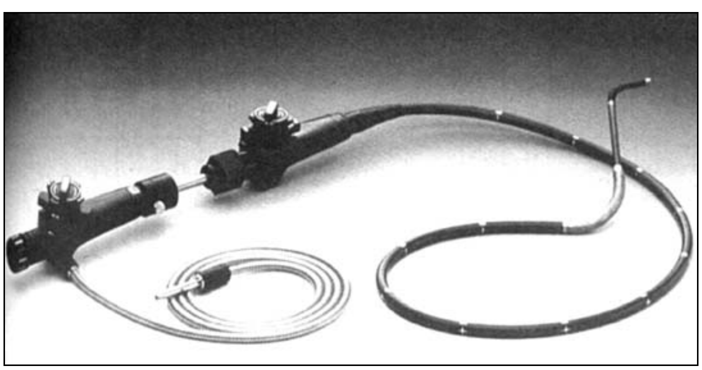

Figure 2.1: Flexible borescope (Hellier 2001)

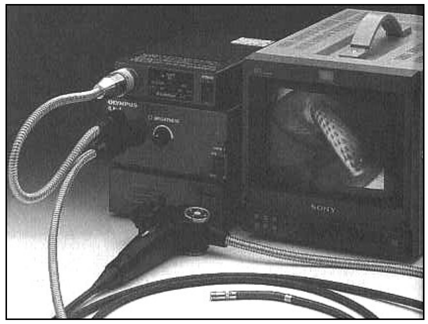

Figure 2.2: Flexible borescope and monitor (Hellier 2001)

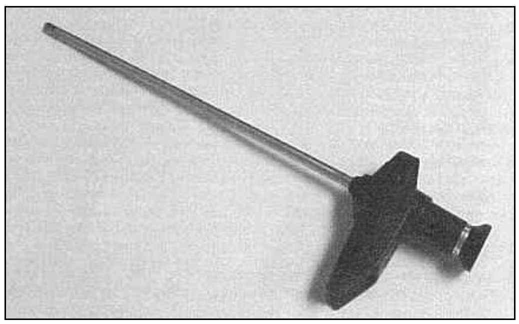

Figure 2.3: Rigid borescope (Hellier 2001)

Charged coupled device

Willard Boyle and George Smith of Bell Laboratories invented the Charged Coupled Device (CCD) in 1970. Since then, CCDs have been used in many of the computer-based optical equipment in use today. CCDs can be found in photocopiers, facsimile machines, cameras, scanners and other optical computer based products.

A CCD is composed of thousands of light sensitive cells, usually referred to as pixels that produce an electrical charge proportional to the amount of light they receive. These pixels can be arranged in either a linear or two-dimensional array, which in turn can be used to produce a digital image. The typical facsimile machine and computer scanner used today have a linear arrangement of CCDs, which progressively traverses the original object in order to progressively build a digital copy. Digital cameras use a two dimensional CCD, also called an area CCD, to instantly create a digital image.

CCDs are of value to the inspection industry as they allow inspectors to capture images of specimens as the traditional camera has done for decades. The advantage of using CCD based technology over film-based cameras is primarily the speed in which the images are developed. Digital photos are usually viewable through the camera instantaneously, which allows personnel on site to observe the image without delay. The person taking the digital photo can then make an on-site decision concerning the quality of the image and whether it needs to be recaptured.

Robotic cameras

Miniature cameras are sometimes considered a variation of fiber optic cameras. In the recent past, both miniature cameras and fiber optic cameras both required a wire or some physical connection to the monitor or viewing device. However, as technology progresses, limitations diminish. Miniature robotic cameras were instrumental in the initial stages of the inspection of the World Trade Center (WTC) disaster site in September 2001. The robots deployed at the WTC site were completely free of cables and were able to gain access to areas where human access was impossible or hazardous. The equipment used in this case employed artificial intelligence, robotics, and CCD technology. Dr. Robin Murphy, an Associate Professor at the University of South Florida, is also the Director of Research for the Center for Robot-Assisted Search and Rescue (CRASAR) in Tampa, Florida. Her research primarily encompasses artificial intelligence in robotics and robot tasking (Murphy 2000).

The robots employed at the WTC disaster site, depicted in 2.4 and 2.5, were used to explore and inspect the inner areas of the wreckage. Remote exploration of the site allowed inspectors to locate victims and visually inspect the structural integrity of the wreckage. The robots were used in several areas of the site, including the collapsed Towers One and Two. This was the first known robot-assisted search and rescue response, and represented the culmination of six years of research and training. The robots were successfully used to find at least five victims, helped rescue teams select voids for further searching, and assisted in the building clearing efforts. Videos of the robots, their interfaces, and views from their sensors were used to illustrate key findings on mobility, sensing, control, and human-robot interaction.

Figure 2.4: Robot used for visual survey at the WTC disaster site (Casper 2002)

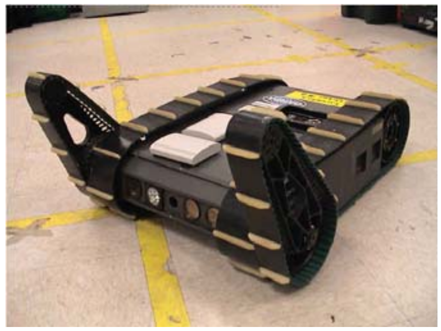

Figure 2.5: Robot used for visual survey at the WTC disaster site (Casper 2002)

Although disaster inspection is a highly specialized and limited field of research, the technology developed and implemented for this work will become more prevalent in the visual inspection industry.

Applications of Visual Inspection

Visual inspection is a fast, convenient and relatively inexpensive technique used to evaluate the overall condition of structures. This technique allows inspectors to make real-time evaluations and recommendations of a given structure, which is particularly valuable in emergency or safety inspections.

Some limitation of the visual inspection technique is sight obstructions, which can be due to lighting, access or obstruction. Another disadvantage of visual inspection is the "human factor" that is often encountered. The susceptibility to human misinterpretation and the requirement for establishing a baseline for defects in general, especially under poor conditions, can lead to inconsistent identification of anomalies, which can give rise to contradicting evaluations (Qasrawi 2000).

Liquid Penetrant Methods

The liquid penetrant examination method can be used to nondestructively evaluate certain nonporous materials. The American Society for Testing and Materials (ASTM) has developed material specific test standards for the penetrant examination of solids (ASTM E165 – 95). Liquid penetrant methods are nondestructive testing methods for detecting discontinuities open to the surface, such as cracks, seams, laps, cold shuts, laminations, through leaks, or lack of fusion. These methods are applicable to in-process, final, and maintenance examinations. They can be effectively used in the examination of nonporous, metallic materials, both ferrous and nonferrous, and of nonmetallic materials such as glazed or fully densified ceramics, certain nonporous plastics, and glass.

Hardened Portland cement concrete is a permeable material due to the properties of the cement matrix. As concrete is batched and mixed, capillary pores are formed in the hydrated cement matrix; penetrant methods of investigation, as described in the relevant ASTM standard, do not apply to concrete because they were developed for testing of nonporous materials. At present, there is no standardized test method available for liquid penetrant examination of porous materials.

However, it is possible to use water as an aid to detect surface flaws in concrete. Inspectors can apply water to a concrete surface and observe the rate of drying. As the water evaporates from the surface, areas containing cracks will hold moisture. As illustrated in Figure 2.6, these moist areas will result in local discoloration of the concrete, which facilitates the visual detection of cracks.

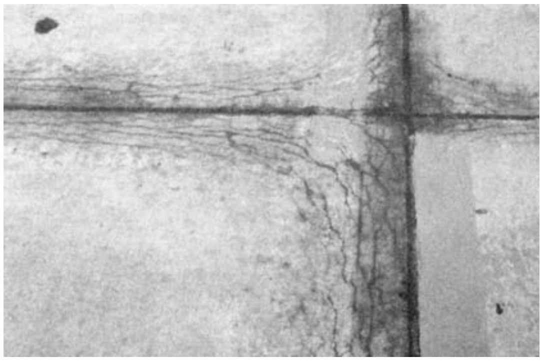

Figure 2.6: Cracks in concrete pavement with moisture present (ACI 201.1 R92)

The principle upon which the liquid penetration method is based is that of capillary suction, a physical phenomenon in which the surface tension of liquids causes them to be drawn into small openings such as cracks, seams, laps, cold joints, laminations and other similar material deficiencies.

The most important property affecting the ability of a penetrant to enter an opening is "wetability". Wetability refers to a liquid's behavior when in contact with a surface (Hellier 2001). The angle created between the free surface of a liquid and a solid surface is referred to as the contact angle. It is an important characteristic related to the penetrability of the liquid. Liquids that have small contact angles have better penetrability than those liquids exhibiting large contact angles. Figure 2.7 depicts contact angles for various liquids.

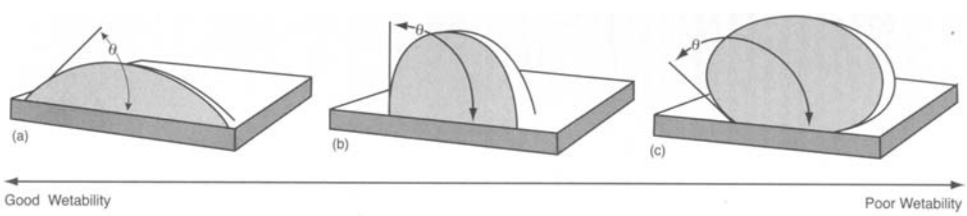

Figure 2.7: Contact angles for various liquids (Hellier, 2001)

Viscosity is another significant property of liquid penetrants. Viscosity is defined as the resistance to flow in a fluid, or semifluid. Liquids with lower viscosities are more desirable for use in liquid penetrant examination since they have superior flow properties.

The visibility of the liquid penetrant is a valuable quality in the penetrant examination procedure. Usually, the visibility or contrast of a liquid penetrant is measured by the dye concentration, which makes the liquid penetrant more visible. Contrast ratio is used to measure the visibility of a penetrant. The contrast ratio scale ranges from 50:1 to 1:1, where a contrast ratio of 1:1 would represent a color in reference to itself, for example, red dye on a red solid surface. Contrast ratios of 40:1 can be achieved through the use of fluorescent dye penetrants under ultraviolet illumination. As a result, ASTM has recognized fluorescent penetrant examination, and standard test methods have been developed. ASTM D4799-03 is the standard test that describes the conditions and procedures for fluorescent penetrant testing for bituminous materials.

Although liquid penetrant methods have been beneficial in the location of surface defects in solids, they have several limitations. Existing liquid penetrant examination techniques are applicable to the inspection of nonporous solids and are thus not applicable to the survey and inspection of concrete structures and buildings. The majority of these are composed of concrete and masonry; both of which are porous materials.

Acoustic Sounding

Acoustic sounding is used for surveying concrete structures to ascertain the presence of delaminations. Delaminations can be a result of poor concrete quality, debonding of overlays or applied composites, corrosion of reinforcement, or global softening. The test procedures used for delineating delaminations through sounding include: coin tap, chain drag, hammer drag, and an electro-mechanical sounding device. The purpose of each test is to sonically detect deficiencies in the concrete. ASTM has created a standard, *ASTM D 4580 – 86*, which covers the evaluation of delaminations. The standard describes procedures for both automated and manual surveys of concrete.

A major advantage to sonic testing is that it produces immediate results on near surface anomalies. The effectiveness of sonic testing relies heavily on the user's expertise in signal interpretation and consistency.

Coin tap test

The coin tap test is one of the oldest and most widely researched methods of sonic testing. The test procedure requires the inspector to tap on the concrete sample with a small hammer, coin, or some other rigid object while listening to the sound resulting from the impact. Areas of nondelaminated concrete will create a clear ringing sound upon impact while regions of delaminated, disbonded, or softened concrete will create a dull or hollow sound. This change in sonic characteristics is a direct result of a change in effective stiffness of the material. As a result, the force-time function of an impact and its resulting frequencies of an impact differ between areas of good and poor quality concrete (Cawley & Adams, 1988). *ASTM D 4580-86* describes the procedure for manually surveying concrete structures for delaminations using the coin tap procedure.

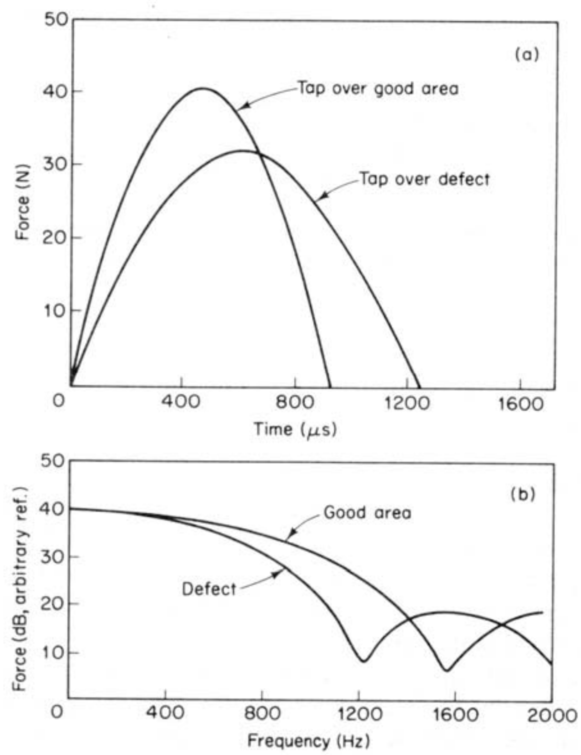

Figure 2.8: Coin tap test results
(a) Force-time histories of solid and disbonded areas of a carbon fiber reinforced skinned honeycomb structure,
(b) Spectra of time histories (Cawley & Adams, 1988)

Figure 2.8 illustrates the shorter force-time history and larger resulting frequency produced by impacts on solid material as opposed to disbonded/delaminated material. Understanding the force-time function aids an inspector's abilities to sonically evaluate a material, as it takes less time for two elastic solids to separate subsequent to a collision. A similar analogy could be made by comparing the effect of walking on a sidewalk to walking in the mud. The sinking phenomenon that one experiences in the mud is similar to the extended time length of impact produced by a delaminated material. The "sinking" of the hammer or coin into the delaminated material results in a plastic deformation of the material, resulting in a more dull or hollow sound.

The electronics industry has provided inspectors with equipment that is capable of detecting and recording the sonic wave signals that are produced by an impact. As a result, there are currently several commercially available products available for such signal acquisition. The most common devices for sonic data acquisition are the instrumented hammer and the smart hammer.

The instrumented hammer was developed for the airline industry to be used in the detection of anomalies in airplane materials. It measures and records the force-time history and amplitude frequency of an impact via the use of an accelerometer embedded in the head of the hammer.

The smart hammer was developed for the shipbuilding industry. This instrument measures and records the sonic response of an impact through a microphone. The microphone uses the sonic data, instead of the force data, to create an acoustic signal.

Both impact-force data generators and impact-sound data generators have been proven to generate useful signals for nondestructive sonic testing. The information gained from both sources has demonstrated their capability of producing consistent and valid experimental results. At the present time, research is being conducted into both impact-force and impact-sound devices to develop improved testing methods. Both devices have created the opportunity for improved standardization of acoustic sounding tests. The objective nature of testing with mechanical devices that are capable of producing consistent and repeatable results can help to improve testing standards for structural and material inspectors. Although the instrumented hammer and smart hammer are considered to be automated delamination inspection equipment, the testing data and procedures produced by these devices are still in the initial stages and an ASTM standard test method for these devices has not yet been created.

Chain drag survey

The chain drag survey provides a low-cost method to inspect delaminated areas in concrete surfaces. The survey allows inspectors to traverse a large area with reasonable accuracy in a short period of time. Since the test is quick and inexpensive it may be used for an initial evaluation to determine the need for further investigation. Like the coin tap and hammer sounding methods, the chain drag test is subjective, and therefore requires an experienced inspector to perform the survey. Due to the nature of the test, localized areas of delaminations are more difficult to detect. Concrete decks or slabs that have comparatively large percentages of deficiencies may require the use one of the more localized tests, like the coin tap or hammer sounding methods, to provide a more accurate picture of the tested structure.

The chain drag survey consists of dragging a chain over the concrete surface. This approach suffers from limitations similar to the electro-mechanical sounding device. The chain drag survey cannot be performed on vertical members of a structure and thus is limited to the topside of concrete slabs and decks. Similar to the coin tap test, areas of nondelaminated concrete will create a clear ringing sound upon contact, and areas of delaminated, disbonded or softened concrete will create a dull or hollow sound. The typical chain used for inspection is composed of four or five segments of 1 inch link chain of ¼” diameter steel approximately 18 inches long attached to an aluminum or copper tube two to three feet in length. The test is performed by dragging the chain across the entire surface of the concrete slab and marking the areas that produce a dull sound. The deficient areas can be recorded and further investigated using other techniques.

Electro-mechanical sounding device

The Electro-Mechanical sounding device is a small, wheeled device equipped with tapping wheels and sonic receivers. Two rigid steel tapping wheels provide the impacts for the delamination survey. The sonic receivers are composed of oil filled tires coupled with piezoelectric transducers. The data acquisition equipment is composed of a data recorder that stores the signals from the sonic receivers (ASTM D4580-86). The electro-mechanical sounding device has become somewhat antiquated as the development of other, more reliable and more efficient, delamination survey techniques have been developed. ASTM D 4580-86 (procedure A) defines the standard practice for performing a delamination survey using this device. It is primarily limited by the nature of the equipment employed, as it cannot perform tests on vertical concrete surfaces, and is thus restricted to the top surface of concrete decks and slabs.

Applications of acoustic sounding

Acoustic sounding has proven to be a reliable supplement to visual and other forms of evaluation due to its capability to conduct near-surface investigations at a relatively rapid rate. These techniques are also valuable in that they are usually relatively low in cost and can be conducted in conjunction with most visual inspections. However, the method is limited in several respects. It remains largely subjective to human interpretation and can be a confusing technique when background noise is prevalent. The method lacks the ability to detect small defects and subsurface defects, as it is strictly a near-surface investigation method.

Surface Hardness Methods

Essentially, the surface hardness methods for nondestructive testing of concrete consist of impact type tests based on the rebound principle. Some of these methods have been effectively used to test concrete since the 1930's. Due to the complexity of concrete as a material and the disparity between the concrete surface and the inner structure, surface methods are inherently limited in their results. However, surface methods have been proven to give an effective evaluation of the uniformity of a concrete member and in comparing concrete specimens in a relative sense.

The most widely used surface hardness methods are the testing pistol by Williams, the pendulum hammer by Einbeck, the spring hammer by Frank and the rebound hammer by Schmidt. The Schmidt rebound hammer has become the industry favorite in the use of surface hardness measurements today. The Schmidt hammer is basically a hand-held spring plunger that is suitable for lab or field-testing. The capabilities of the Schmidt hammer have been extensively tested, and there are over 50,000 Schmidt hammers in use world-wide (Malhotra & Carino 1991).

The basic rebound principle consists of a spring-driven mass that is driven against the surface of a concrete specimen with a known energy. The rebound distance of the mass is measured and the "hardness" of the concrete surface is estimated from this value. A harder surface results in a longer rebound distance due to the increase in energy reflected back to the impinging mass. However, despite its apparent simplicity, the rebound hammer test involves complex problems of impact and the associated stress wave propagation (Neville 1995). The energy absorbed by a concrete sample is related to both its strength and its stiffness. Therefore, it is the combination of concrete strength and stiffness that influences the rebound number.

There is no unique relation between surface hardness and in-situ strength of concrete. This relationship is dependent upon any factor affecting the concrete surface, such as surface finish, degree of saturation, and surface preparation. The concrete mix design, including the type of aggregate, water/cementitious materials ratio and cement type can also affect hammer results. The method cannot accurately determine the subsurface condition of concrete. It tests only a localized area of concrete to a depth of perhaps 20 or 30mm (BSI, 1986). The condition of the concrete will further affect the rebound number. Areas of honeycombing, scaling, rough surfaces and high porosity will decrease the rebound number. Areas of carbonation will increase the rebound number. Therefore, the user must insure careful selection of a representative area of concrete and must understand the limitations inherent in the test.

The Schmidt rebound hammer is, in principle, a surface hardness tester with little apparent theoretical relationship between the strength of concrete and the rebound number of the hammer. However, within limits, empirical correlations have been established between strength properties and the rebound number (Malhotra & Carino 1991). The accuracy of the rebound hammer has been estimated between ±15-20% under laboratory testing conditions and ±25% in field-testing conditions. Such accuracy, however, requires a proper calibration of the hammer with the concrete in question.

The American Society for Testing and Materials (ASTM) has created a standard test for the Rebound Number of Hardened Concrete (ASTM C 805-97). This test specification should be referenced and strictly followed for proper testing procedures.

Penetration Resistance Methods

The basic principle behind penetration resistance methods is the application of force to a "penetrating object," and then determining the resistance of a specific concrete to such penetration by measuring the depth of penetration. Penetration resistance methods have been effectively used to test concrete since the 1960's. The limitations of penetration methods are similar to the limitations of surface hardness methods. The depth of penetration is usually only a small percentage of the full depth of the concrete member. Penetration methods have been proven to give an effective near surface evaluation of *in- situ* compressive strength, uniformity of concrete and soundness at different locations. The two most commonly used penetration resistance methods are the Pin Penetration Method and the Windsor Probe.

The Pin Penetration method uses a spring-driven mechanism to drive a 30 mm long, 3.6 mm diameter steel pin into the concrete surface. The pin is subsequently removed and the depth of the resulting hole is measured. The Windsor Probe test uses the same principle, although larger diameter steel probe is used. Table 2-1 contains a schedule of probe sizes for each test. The Windsor Probe test requires a larger driving force and employs a gunpowder charge to develop the necessary impetus. ASTM has approved a standard test for the Penetration Resistance of Hardened Concrete (ASTM C 803-97), which covers both tests. This test specification should be referenced for proper testing procedures.

Table 2.1: Standard sizes of pin and probe used for penetration tests.

	Pin Penetration Method	Windsor Probe Test
Size of Penetration:	30 mm length 3.6 mm diameter	80mm length 6.3/7.9mm diameter
Usable Range of Concrete Strength:	450 – 4000 psi 3-28 MPa	450 – 6000psi 3 – 40 MPa

The ASTM standard requires three firmly embedded test probes in a given test area to constitute as one test for both penetration test methods (ASTM C803-97)The penetration methods are still near-surface tests but do offer reliable empirical relationships between concrete strength and penetration resistance. Consistent empirical correlations have been successfully established between strength and penetration resistance. The penetration methods have been estimated to be within ±5% accuracy under both laboratory and field-testing conditions when the test procedure is performed properly and a valid correlation has been developed.

The primary limitation of penetration methods is that they do not offer a full-depth appraisal of the concrete that they are testing. They are considered to be surface-testing methods only and they do not yield absolute values for the strength of concrete in a structure. They are effective at estimating *in situ* concrete strength only when the proper correlations are performed subsequent to testing. Penetration methods are not purely nondestructive in nature since they induce some damage to the tested specimen. It is more accurate to consider penetration tests as semi-destructive.

Pullout Test

The basic purpose of the pullout test is to estimate the *in situ* strength of a concrete structure. Pullout tests consist of measuring the force required to extract a mechanical insert embedded in a concrete structure. The measured pullout force can then be used to estimate the compressive, tensile and shear strength of the concrete. The pullout test was originally developed in the former Soviet Union in the 1930's and later independently developed in the United States in the early 1940's. Further research has led to several modifications since then. The test that is most commonly used in industry today is the pullout test as modified by Kaindl in the 1970's.

The pullout test, illustrated in Figure 2.9, uses a metal insert that is inserted into fresh concrete or mechanically installed into hardened concrete. The tensile or "pullout" force required to extract the embedded insert, and the core of concrete between the insert and the surface, can give accurate estimates of the concrete's compressive, tensile and shear strengths. The pullout test has become a proven method for the evaluation of the *in situ* compressive strength of concrete and has several industry applications. The pullout test is used to determine whether the strength of the concrete has reached a sufficient level such that post-tensioning may commence; cold weather curing of concrete may be terminated or forms and shores may be removed.

Consistent empirical correlations can be established between strength properties and pullout test methods. Pullout test results have been estimated to be within ±8% accuracy for laboratory and field-testing conditions when the test procedure has been performed properly and a proper correlation has been developed.

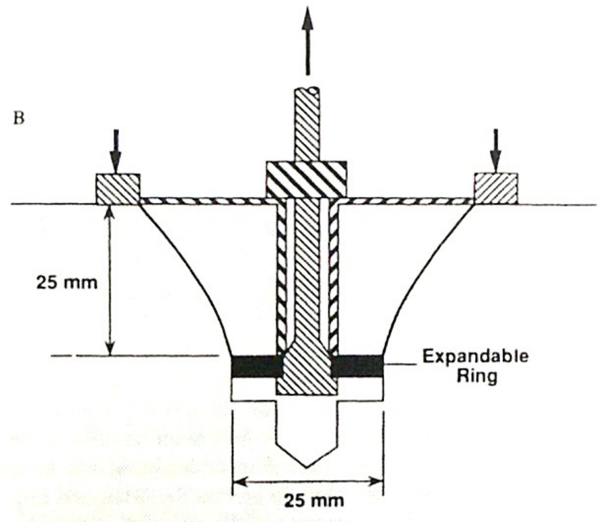

Figure 2.9: Illustration of typical pullout test (Malhotra & Carino 1991)

The pullout test method does not provide a full-depth appraisal of the concrete structure that is being tested. It is not truly nondestructive in nature since it induces significant damage to the tested member. It is more accurate to consider the pullout test as semi-destructive. The damage incurred during pullout testing is usually more significant than most other "NDT" methods and patching of the tested structure is usually required. Figure 2.9 shows a schematic of the pullout test. ASTM has created a standard test for the Pullout Strength of Hardened Concrete (ASTM C 900-99). This test specification should be referenced for proper testing procedures.

Break-Off Test

The primary purpose of the break-off test is to estimate the strength of a concrete structure. This test involves the breaking off of an internal cylindrical piece of the *in situ* concrete at a failure plane parallel to the surface of the concrete component. The measured break-off force can then be used to estimate the compressive and tensile strength of the concrete. The break-off test was originally developed in Norway in 1976. It was later introduced into the United States in the early 1980's. The test procedure used today is essentially the same as when the test was originally introduced.

The break-off test can use a cylindrical sleeve that is inserted into fresh concrete to create the embedded cylinder. Alternatively, the embedded concrete cylinder can be drilled into hardened concrete using a core drill bit. The embedded cylinder size is usually 55mm in diameter and 70mm in height. Figure 2.10 illustrates a typical cross section of the breakoff test.

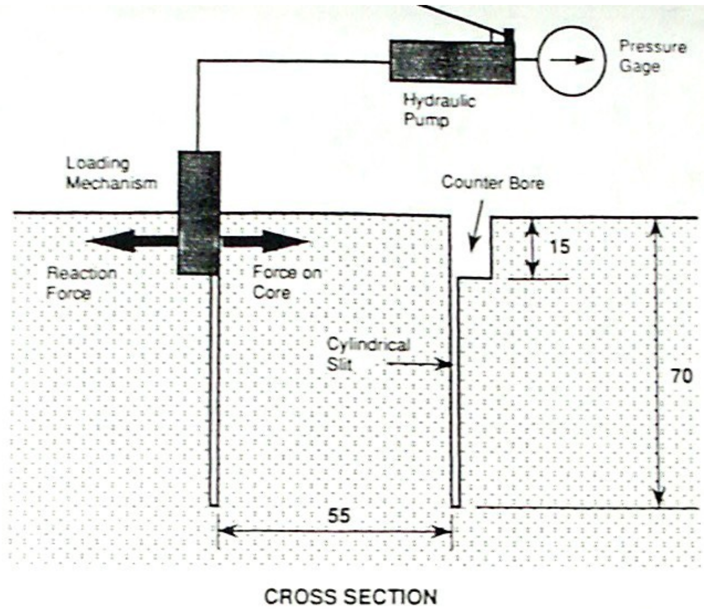

Figure 2.10: Schematic of breakoff test, dimensions in mm (Malhotra & Carino 1991)

The actual test method involves the application of a horizontal force to the upper edge of the embedded concrete cylinder, which is slowly increased until failure. The force required to break the embedded cylinder is then used to estimate the concrete compressive and tensile strength. The break-off test is a proven method of evaluation of the *in situ* compressive strength of concrete and has several industry uses. Like the pullout test (described later) it is used to determine whether the strength of the concrete has reached a specified value so that post-tensioning of a bridge structure may commence, cold weather curing of concrete may be terminated, or forms and shores can be removed.

Consistent empirical correlations have been established between strength properties and break-off test methods. The break-off test results have been estimated to be within ±7% accuracy for laboratory and field-testing conditions when the test procedure has been performed properly and sufficient data is available to formulate a proper correlation.

The primary limitation of the break-off test is that it is not truly nondestructive in nature. It induces significant damage to the tested member. Thus, it is more accurate to consider the break-off test as semi-destructive. The volume of removed material is 667 cm^3 or 41 in^3. Thus, the damage incurred during break-off testing is typically more extensive than other "NDT" methods, and patching of the tested structure is usually required.

ASTM has approved a standard test for the Break-Off Number of Hardened Concrete (ASTM C 1150-96). This test specification should be referenced for proper testing procedures.

Ultrasonic Testing

Ultrasonic testing is a NDT method that is used to obtain the properties of materials by measuring the time of travel of stress waves through a solid medium. The time of travel of a stress wave can then be used to obtain the speed of sound or acoustic velocity of a given material. The acoustic velocity of the material can enable inspectors to make judgments as to the integrity of a structure.

The term ultrasonic is defined as a sound having a frequency above the human ear's audibility limit of about 20,000 hertz. Ultrasonics are very popular in the medical industry and have been used there for over thirty years, allowing doctors to non-intrusively investigate internal organs and monitor blood flow in the human body. The materials industry has also been able to utilize ultrasonics for non-intrusive investigation of assorted materials such as metals, composites, rock, concrete, liquids and various other nonmetals.

The first studies of ultrasonics are recorded as far back as the Sixth Century B.C. when Greek philosopher, Pythagorus performed experiments on vibrating strings. Galileo Galilei is credited with performing the first of the modern studies of acoustics. He was the first scientist to correlate pitch with frequency of sound. The earliest known study of the speed of sound in a liquid medium took place in 1822 when Daniel Colladen, a Swiss physicist/engineer, and Francois Sturm, a Swiss mathematician, used flash ignition and a bell to successfully estimate the speed of sound in Lake Geneva, Switzerland. In 1915, Paul Langevin pioneered the study of high-frequency acoustic waves for submarine detection during the outbreak of World War I (Guenther 1999).

The age of ultrasonic testing of materials was establised in 1928 by Sergei Y. Sokolov, a scientist at the Lenin Electrotechnical Institute in Leningrad, Russia. Sokolov proposed and demonstrated that he could translate ultrasonic waves or sound pressures into visual images. In the 1920’s he advanced the idea of creating a microscope using high frequency sound waves. He then applied his ideas to detect abnormalities in metals and other solid materials. As technologies have developed over the twentieth century, the knowledge gained through the use of the high frequency microscope has been applied to other ultrasonic systems (e.g. radar) (Guenther 1999).

In the United States, the development of the ultrasonic test is attributed to Dr. Floyd Firestone, who, in 1942, introduced what is now called the pulse echo technique (described later) as a method of nondestructive testing. Dr. Firestone successfully used the pulse echo technique for ultrasonic flaw detection. Ultrasonics have since been used to evaluate the quality of concrete for approximately 60 years. The method can be used for non-intrusively detecting internal defects, damage, and deterioration in concrete. These flaws include deterioration due to sulfate and other chemical attacks, cracking, and changes due to freeze-thaw cycling.

Theory

Ultrasonic testing of materials utilizes the vibrations of the particles that comprise a given medium. Sound waves and ultrasonic waves are simply the vibrations of the particles that make up a solid, liquid, or gas. As an energy form, the waves are an example of mechanical energy.

The motion of vibration is described as a periodic motion of the particles of an elastic body or medium, in alternately opposite directions from the position of equilibrium when that equilibrium was disturbed. However, vibration can also be described as an oscillation, which is the act of swinging back and fourth between points. An elastic oscillation is one in which the driving force behind the oscillation (e.g. a spring) is proportional to the displacement of the object. Figure 2.11 illustrates the basic sinusoidal oscillation of a free body on a loaded spring and the resulting sine curve that can be achieved when the motion is plotted with respect to time.

The sinusoidal waveform that is created by sound waves is a convenient characteristic of the wave motion that allows scientists to quantify sound in terms of amplitude and frequency. The frequency of these waves differentiates sonic from ultrasonic waves. The unit of frequency is the hertz or Hz, and is defined as one cycle of vibration per second. Sounds below approximately 16 Hz are below the lower limit of human audibility, whereas sounds of 20,000 Hz are above the upper limit of human audibility.

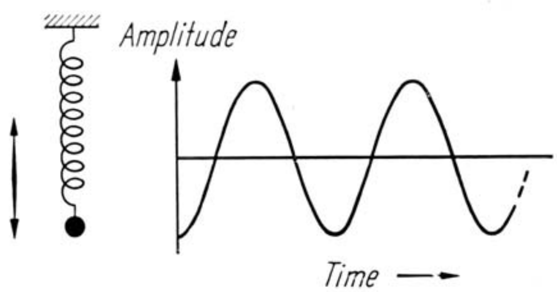

Figure 2.11: Sinusoidal oscillation of a loaded spring (Krautkramer 1979)

The basis of ultrasonic testing is particle vibration within a medium upon the application of mechanical energy. Figure 2.11 shows the free body motion of a single mass and its interaction with a single spring. Considering the mass from the diagram in Figure 2.11 to be a particle, and the spring to be the connection of particles, the simple principle of free body motion to fit a particle interaction model can be expanded as seen in Figure 2.12.

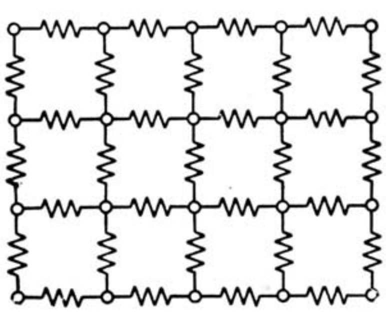

Figure 2.12: Model of an elastic body (Krautkramer 1979)

The model depicted in Figure 2.12 is the basic model used in wave science. Mechanical waves propagate through materials by means of particle motion. Wave propagation is largely dependent upon the type of excitation or energy input, the mass of the individual particles, and the spring stiffness of their internal connections. A wave initiated by an external event such as normal or shear force, travels by vibratory movement transmitted from particle to particle. If the springs that connect the particles were infinitely stiff, all particles of the material would start to oscillate at the same instant and the wave would be transmitted at an infinite speed. Hence, the material's elasticity and density play an important role in wave propagation (Kaiser & Karbhari 2002). Internal friction and other forces resist particle motion upon excitation, and wave propagation occurs at a finite rate. This rate is referred to as its wave velocity and is dependent upon material composition.

Although sound waves can propagate through all three forms of matter (solids, liquids and gases), the type of waveform able to move though a material is dependent on the material phase. For materials in the gaseous or liquid phase, dilatational waves are typically the only form that travels well. Dilatational waves are also referred to as compression or longitudinal waves and are the primary stress waves produced by material excitation. The particle motion in a longitudinal wave is parallel to the direction of propagation. The result is a compressive or tensile stress wave.

Distortional waves are the secondary stress waves that are produced upon forced contact. These waves are also called shear or transverse waves. In shear waves, the particle motion of the wave front is normal to the direction of propagation, resulting in shear stress.

Rayleigh waves, also called surface waves, differ from longitudinal and shear waves because they do not propagate through a solid. Rayleigh waves propagate along the surface in an elliptical motion.

Lamb waves are similar to Rayleigh waves because they also do not travel through a material and are also considered surface waves. Lamb waves, however, occur only in solids that are a few wavelengths in thickness and have a uniform thickness. Common objects subject to the development of lamb waves are plates, pipes, tubes, and wires.

The behavior of waves at material interfaces

The term *interface* is defined as a surface forming a common boundary of two bodies, spaces, densities or phases. One of the most common interfaces people are familiar with is the oil-water interface. In materials science, an interface is usually defined as a fringe between two materials, which have different properties such as density or phase. Another possible difference in material properties is acoustic impedance, which is defined as a material's density multiplied by its wave speed. When stress waves collide with material interfaces, portions of the waves are reflected and refracted. The principle of refraction is best described by Snell's law, which relates the angle of refraction and the wave velocity to the refraction angle of two materials.

$$\frac{\sin i^o}{V_1} = \frac{\sin R^o}{V_2} \qquad \text{-------- [1]}$$

where: i^o = angle of incidence
R^o = angle of refraction
V_2 = wave velocity in Medium 2

Figure 2.13 shows a typical example of the refraction angle of an ultrasonic wave as it enters a different material. The concrete-air and the concrete-steel interfaces are the two most common interfaces encountered in nondestructive testing of civil engineering structures.

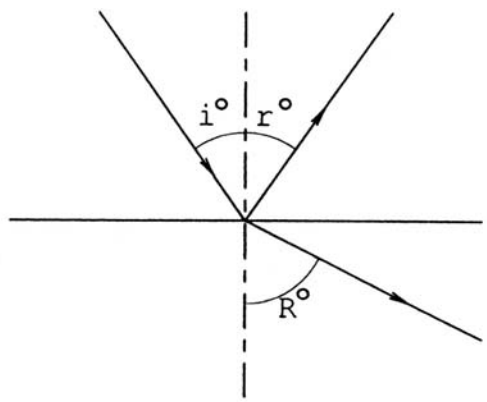

Figure 2.13: Graphical illustration of Snell's law (Hellier 2001)

Most of the illustrations used to describe the characteristics of ultrasonics consider the sound or ultrasound as a two-dimensional ray, which is somewhat simplified for the study of ultrasonics and nondestructive testing. A more accurate representation of the sound energy is a three dimensional beam. The study of a sound beam is more complicated than a sound ray. As the complexity of the physical characteristics in a material increases, different mechanical mechanisms become factors in their analysis.

Scientists define attenuation as the gradual loss of sound wave energy through a medium. Attenuation can be more accurately described as the combined effect of a number of parameters:

- Interference from diffraction effects
- Interference adsorption (friction and heat)
- Interference scatter
- Interference beam spread (Hellier 2001)

The combination of these effects can create disturbances and erratic signals within a material. One of the early challenges of scientists using ultrasonic equipment was deciphering and filtering the interference signals created by material properties.

Instrumentation

Commercial ultrasonic equipment has been under development since World War II. The first equipment available to the materials engineering industry was produced in the 1950's. Since then, a variety of ultrasonic detection devices have become available. Most of the ultrasonic devices used for material inspection and flaw detection are portable and battery powered. A portable ultrasonic testing device is illustrated in 2.14. Portability enables material inspection in the field and a high degree of user flexibility.

Figure 2.14: A portable ultrasonic testing device used at the University of Florida.

The typical testing apparatus used for ultrasonic testing consists of the following:

- Transducer
- Time Measuring Circuit
- Receiver/Amplifier
- Display
- Reference Bar
- Coupling Agent

Transducer

A transducer is used for transforming electrical pulses into bursts of mechanical energy. A typical pulse velocity apparatus consists of a transmitting transducer and a receiving transducer. The transmitting transducer generates an ultrasonic pulse through the test specimen, and the receiving transducer receives the pulse. The generation and reception of ultrasonic waves is accomplished using piezoelectric crystals. Piezoelectric elements are reciprocal, which means an applied voltage generates a deformation, or an impinging stress generates a voltage. This physical property makes piezoelectric elements ideal as transducers (Papadakis 1999).

Time measuring circuit

The time measuring circuit or clock is an essential component of the ultrasonic pulse velocity equipment. It controls the frequency output of the pulse by signaling the pulser to provide a high-voltage pulse to the transducer. The time measuring circuit measures the time of travel of a pulse or stress wave through the test specimen. Since the primary function of the time measuring circuit is to regulate pulse generation, it is commonly referred to as a pulser. It provides an output to the display when the receiving transducer receives a pulse. The time measuring circuit is capable of producing an overall time-measurement resolution of 1 microsecond (μs). ASTM C597-97 requires a constant signal with a varying voltage of ±15% at a temperature range of 0°C - 40°C.

Receiver/amplifier

The receiver is the term applied to all of the circuit functions that amplify the weak echoes and determine their amplitude. It has four basic components, the preamplifier, the logarithmic amplifier, the rectifier and the low pass amplifier.

The function of the preamplifier is to ensure that any signal from the receiving transducer arrives at the time measuring circuit. Since electrical outputs from the transducer are relatively small, signal amplification is necessary to overcome the resistance in the transducer cable, which can be relatively long. The function of the logarithmic amplifier is to process weak echo signals. Once the weak signals are amplified, the rectifier and the low pass filter process the signals. After processing by the receiver/amplifier, a useable signal can be sent to the display. A schematic of a typical ultrasonic pulse velocity meter is shown in Figure 2.15.

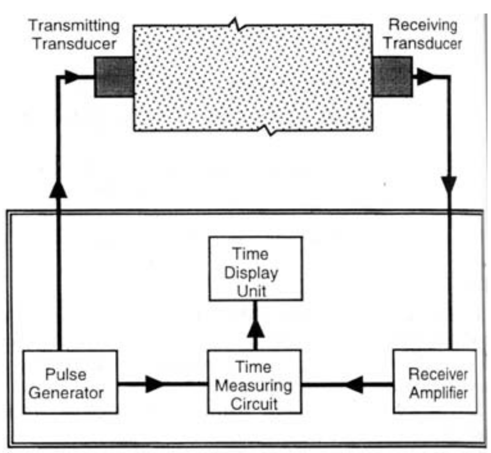

Figure 2.15: Schematic of a pulse velocity apparatus (ASTM C597-97 2001).

Display

The signal received by the ultrasonic test equipment is typically displayed digitally with modern equipment. The results consist of a direct reading of display time on an x-y coordinate system.

The x-axis becomes the time trigger and the y-axis represents the mechanical energy received. The display units can also illustrate defect or anomaly locations and sizes, depending on the type of data requested by the user.

The information obtained in the ultrasonic test is referred to as a scan. Currently there are three types of scans that are applicable to ultrasonic testing: A-scans, B-scans, and C scans. The A-scan is the simplest scan form. It is a spot scan of the material and results in the most basic form of displayed information. The resulting scan is a waveform where regions of high frequency sound waves are recorded and displayed as peaks on the screen. B-scans are a bit more sophisticated. They incorporate a linear scan instead of a point or spot scan. B-scans are essentially the summation of a series of A-scans that are produced by "sweeping" the transducer over the material specimen. C-scans are even more complicated than B-scans because they incorporate a two dimensional grid system. C-scans are comprehensive scans that are most applicable to nondestructive testing of materials. Figure 2.16 illustrates the differences between these three types of scans.

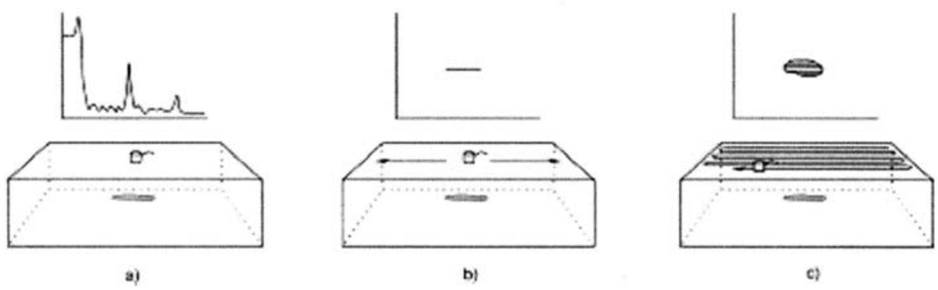

Figure 2.16: Idealized scans of a material defect:
a) A-scan, b) B-scan, c) C-scan. (Kaiser & Karbhari 2002)

Reference bar

The reference bar is a piece of material that is used to calibrate the ultrasonic apparatus. Ultrasonic instruments, which use a microprocessor to record delay time, do not require a reference bar. These instruments can be calibrated by compressing both transducer together to obtain a zero reading. Otherwise, ASTM C597-97 requires that a bar of metal or some other material for which the transit time of compressional waves is known. The reference bar is used as a functional check of ultrasonic equipment prior to testing.

Coupling agent

A coupling agent is usually required to ensure the efficient transfer of mechanical energy between the transducer and the tested material. The purpose of placing the coupling material between the transducer and test specimen is to eliminate air between the respective surfaces. Typically, coupling agents consist of viscous liquids such as grease, petroleum jelly, or water-soluble jelly. Ponded surface water is also considered an acceptable couple. Water is considered as an acceptable couple for underwater ultrasonic testing.

Acoustic velocity calculation

The acoustic velocity wave speed of a given concrete specimen can easily be obtained with the travel time of a stress wave and the length of the specimen. The pulse is sent from the sending transducer to the receiving transducer through the concrete specimen as see in Figure 2.17. The relationship of a specimen's acoustic velocity is simply calculated from a time and a length measurement. It should be noted that cracks, flaws, voids and other anomalies within a material specimen could increase time of travel therefore decreasing the materials acoustic velocity. However, assuming the specimen in Figure 2.17 is free of anomalies, its acoustic velocity can be calculated simply by. The length of the specimen is 200 mm.

Figure 2.17: Typical ultrasonic pulse velocity test procedure.

$$V = L/T; \qquad V = 0.2\text{m}/47.5\mu\text{s} = 4210 \text{ m/s} \qquad \text{-------- [2]}$$

The experiment shown in Figure 2.17 provides the user with a quantitative result. The pulse velocity acoustic velocity, V, of stress waves through a concrete mass is related to its physical properties (ASTM C597-97). is a function of Young's Modulus of Elasticity E, the mass density ρ, and Poisson's Ratio ν. The relevant equation for wave speed is:

$$V = \sqrt{\frac{E(1-\nu)}{\rho(1+\nu)(1-2\nu)}} \qquad \text{-------- [3]}$$

The acoustic velocity of a solid varies given its composition. Therefore, different materials have different acoustic velocities. The acoustic velocities of common materials are shown in Table 2.2 (Krautkramer 1991).

Flaw detection

The immersion testing method involves typical ultrasonic equipment, though the test specimen is completely submerged in water. The water acts as a coupling agent, which aids in the transfer of a clear signal from the transducer to the material being tested. Immersion testing is usually performed in a laboratory on relatively small test specimens, but can be applied to structures in the field. It is possible to perform immersion testing on structures using a technique called ponding. This technique involves the creation of a layer of water or pond between the specimen and the transducer and thus is only applicable to the upper surface of structures or submerged sections of underwater structures.

Table 2.2: Acoustic velocities of common materials used in construction

Material	Acoustic Velocity (m/s)
Aluminum	6320
Cast Iron	3500-5800
Concrete	2000-5500
Glass	4260-5660
Iron	5900
Steel	5900
Water	1483
Ice (water)	3980

Contact methods are the most commonly used methods in the ultrasonic nondestructive testing of materials. Contact methods require the use of a coupling agent, as described in the Coupling Agent section. The development of contact methods allow more versatility in the ultrasonic testing of specimens, since they enable inspectors to test structures and components regardless of orientation. The ultrasonic pulse velocity testing method, as described in ASTM C597-97, is a contact method.

As illustrated in Figure 2.18, there are three possible transducer arrangements in ultrasonic pulse velocity testing. These variations include through or direct transmission, semidirect transmission, and surface or indirect transmission.

The through transmission arrangement is considered to be the preferred approach. It is the most energy efficient arrangement because the pulse receiver is directly opposite the pulse transmitter. Since the distance between the two transducers is minimized, the amount of pulse energy lost through material friction is also minimized.

The semidirect arrangement is less energy efficient than the through transmission arrangement due to the geometry of the transducer arrangement. The angles involved cause signal interference and therefore are more likely to produce errors. The semidirect arrangement is still useful for inspections where through transmission testing is not due to unfavorable structure configuration. The method is also useful for testing of composite columns that contain heavy reinforcing steel within their core. The semidirect transducer arrangement facilitates ultrasonic testing of the concrete in the column while avoiding interference from the embedded steel.

The surface method is the least efficient of the three ultrasonic pulse velocity configurations. This is due to the nature of the waves that travel through the surfaces of materials. The amplitudes of waves received via the receiving transducer are typically less than 5% of waves received by the direct transmission method. Such a small amount of wave energy obtained by the receiving transducer can result in errors in the measurement and analysis of a wave signal. Although the arrangement is the least efficient of the three methods, it is useful in situations where only one surface of a structure or specimen is accessible, such as a floor slab. Surface wave speed and surface crack depth are acquirable through the surface method as well. These methods are explained in the impact echo section of this chapter. Impact-echo and ultrasonics utilize the same principle for crack depth measurement.

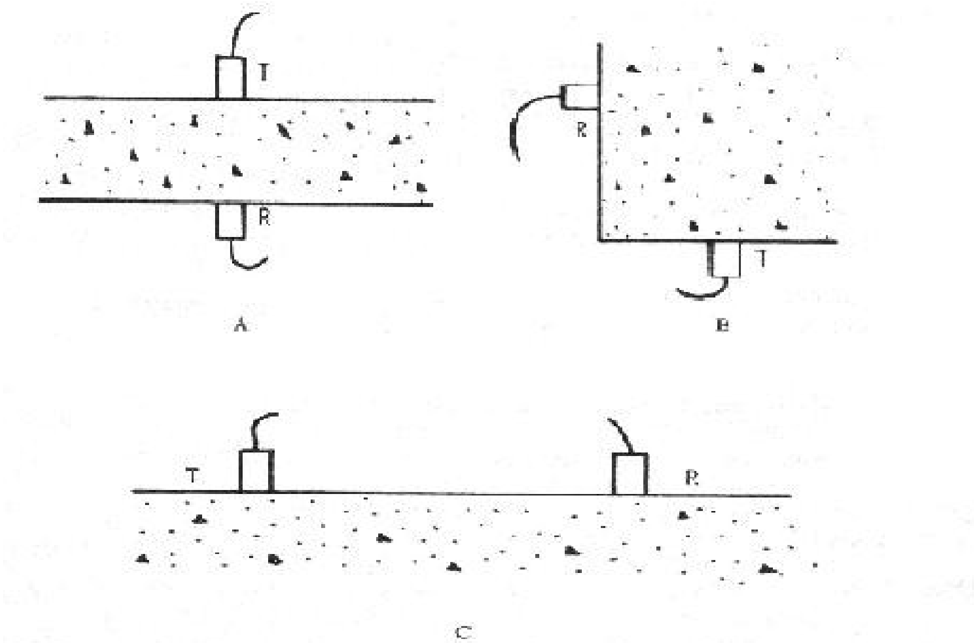

Figure 2.18: Methods of pulse velocity measurements:
a) direct method, b) indirect method, c) surface method.
(Malhotra & Carino 1991)

Noncontact methods of ultrasonic testing are under continuous research. This field of study has many desirable attributes and similar fields of study include acoustic levitation and transportation.

At the present time, there are several noncontact acoustical techniques being developed for the nondestructive testing of materials and structures. New acoustical techniques are now available as a result of the development of the piezoelectric transducer. Three techniques exist: electromagnetic transducers (EMATs), laser beam optical generators, and air or gas-coupled transducers (Bergander 2003).

Most contact ultrasonic testing requires the use of a piezoelectric transducer to send and receive the stress wave signals. The signals are introduced into and received from the test specimen through physical contact of the transducers coupled to the test surface. EMATS are composed of an RF coil and a permanent magnet. The RF coil is excited by an electric pulse which sends an electromagnetic wave along the surface. The EMATS technique requires the test surface to be magnetically conductive. (Green 2002).

Laser ultrasound facilitates the non-contact ultrasonic testing of materials regardless of the materials' electrical conductivity. It provides the opportunity to make truly non-contact ultrasonic measurements in both electrically conducting and electrically nonconducting materials, in materials at elevated temperatures, in corrosive and other hostile environments, and in locations generally difficult to reach, all at relatively large distances from the test surface (Green 2002). Laser ultrasound techniques are able to produce compression, shear, Rayleigh and Lamb waveforms, increasing the test's versatility and serviceability. Laser generated and air coupled ultrasonics have been successful in the characterization of materials which are non-electrically conducting but are not yet serviceable for flaw detection and material investigation. However, the contemporary non-contact ultrasonic methods have been proven to be scientifically applicable in the aeronautics and metallurgical disciplines. A schematic representation of contact transducers vs. non-contact transducers is illustrated in Figure 2.19

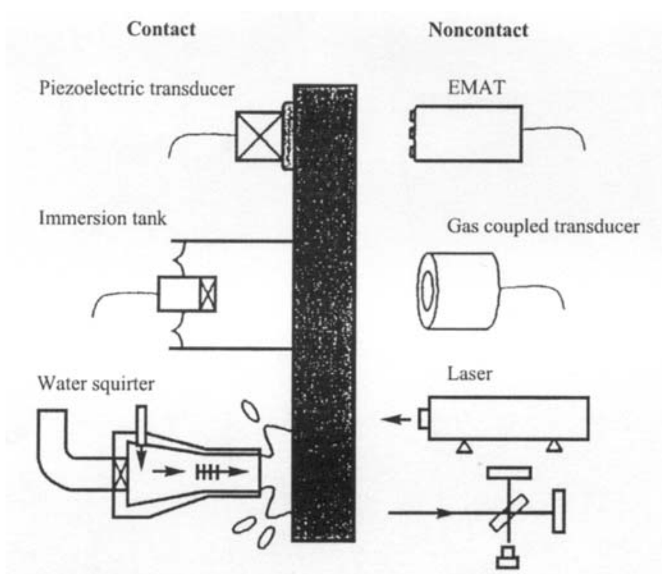

Figure 2.19: Illustration of contact and noncontact techniques. (Green 2002)

Pulse-echo testing

The pulse-echo test is based upon stress wave propagation. It uses the same principles and concepts as the impact-echo method (described later). The basic principle behind both methods is referred to as the "pitch and catch" technique. In pulse-echo testing, a stress wave or pulse is created by a transmitting transducer, just as it is with ultrasonic pulse velocity method. Some types of pulse-echo equipment utilize the same transducer to receive while others require separate sending and receiving transducers. This latter type of arrangement is often termed as "pitch and catch." However, the receiver and transmitter need not necessarily be separate transducers placed at different points on the test specimen but can be combined to a single transducer. This type of testing is referred to as “true pulse echo.” Figure 2.20 provides a schematic of the pulse echo principle.

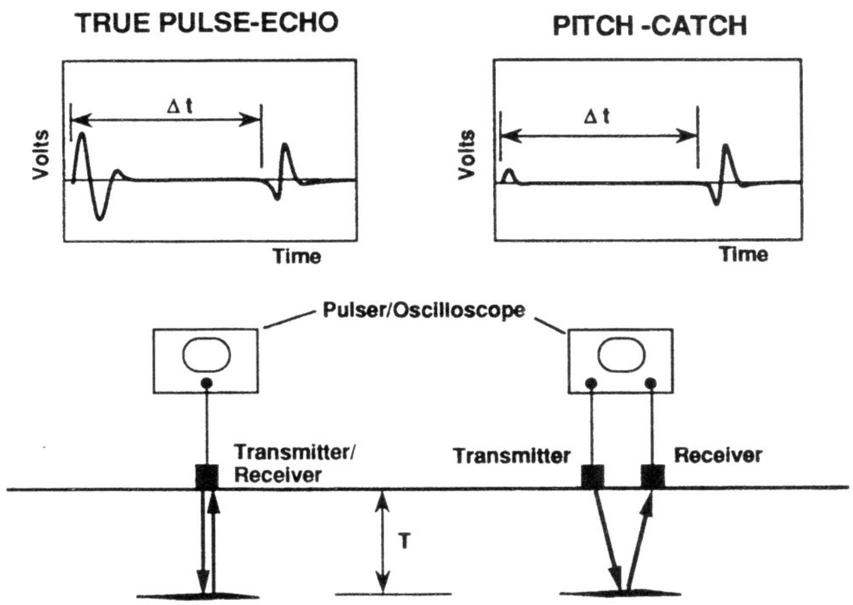

Figure 2.20: Schematic of pulse-echo and pitch and catch techniques. (Malhotra & Carino 1991)

The echo wave coming from the flaw is described by its transit time from the transmitter to the flaw and back to the receiver. Later, the reflected wave from the back side of the specimen, for example the back echo or bottom echo, arrives after a correspondingly longer delay. Both echoes are indicated according to the intensity, or rather amplitude, which is referred to as echo height because of their usual presentation as peaks above the horizontal zero line. (Krautkramer 1990). Figures 2.21 a and b provides a schematic of the typical setup and results from pulse echo scans.

The primary difference between the pulse-echo method and the impact-echo method is that the former technique utilizes a transmitting transducer while the latter employs a mechanical impactor. Both methods use a receiving transducer, which is used to detect the reflected waveform. The difference between the transmitting transducer and the mechanical impactor is the waveform created. The mechanical impact creates a spherical wave front, whereas the transmitting transducer creates a pulse wave beam, resulting in a much smaller material examination area.

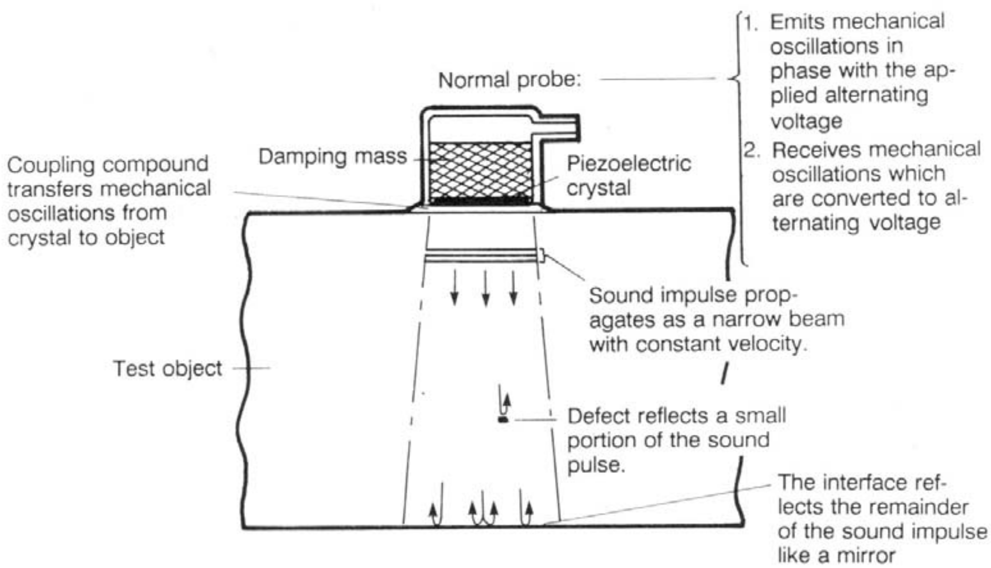

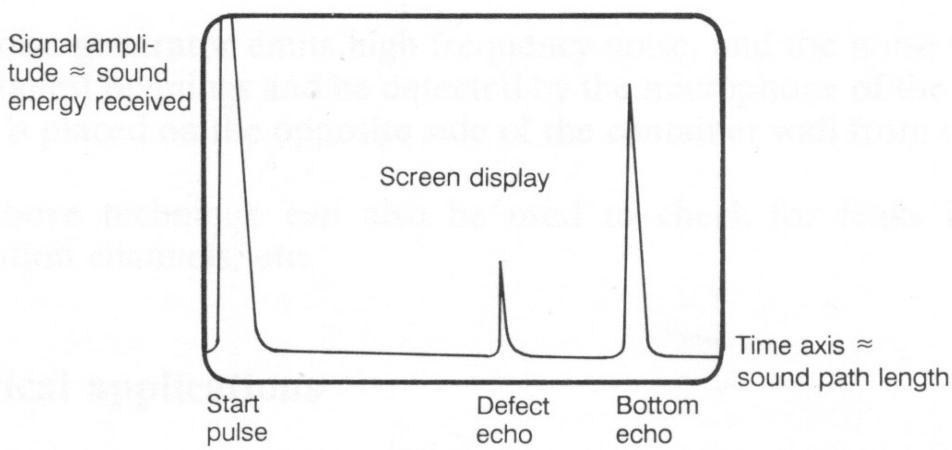

Figure 2.21: Pulse echo schematic:
(a)Typical test setup, and (b) resulting display. (Boving 1989)

The biggest limitation to the pulse-echo method can be attributed to the geometry of the specimen. The reflections of internal anomalies are dependent upon their orientation. In cases where discontinuities, and opposite surfaces, are oriented unfavorably or parallel to the ultrasonic ray path, it may be unable to receive reflected pulse wave signals. The orientation of anomalies and defects is equally important to size in the pulse echo method. The most favorable orientation for an anomaly is perpendicular to the ultrasonic ray path. Figure 2.22 provides an illustration of the signal response due to the orientation of an anomaly. Reflections due to uneven surface morphology can cause *signal scatter*, as shown in Figure 2.23, resulting in the test missing the backwall echoes. This phenomenon can make it difficult to determine anomaly location.

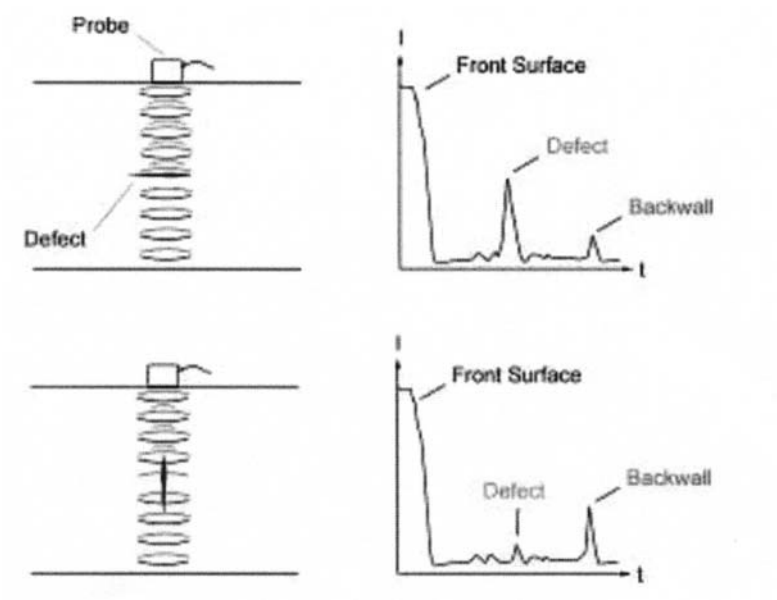

Figure 2.22: Reflections of stress waves from internal discontinuities.
(Kaiser & Karbhari 2002)

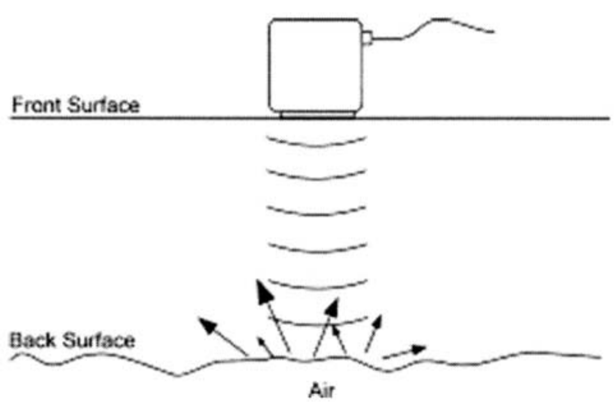

Figure 2.23: Signal scatter due to uneven reflecting surface morphology.
(Kaiser & Karbhari 2002)

Applications of ultrasonics

Ultrasound has been used to determine the integrity of various materials including metal and alloys, welds, forgings and castings. Ultrasound has also been applied to concrete in an attempt to nondestructively determine *in situ* concrete features such as:

- Compressive strength
- Defect location
- Surface crack measurement
- Corrosion damage

Strength determination

The material properties of concrete are variable, and strength determination is a difficult and complicated process. The basic ingredients of concrete are hydrated cement paste, aggregates, water and air. The hydrated cement paste is a highly complex multiphase material. The mineral aggregates are porous composite materials differing greatly from the cement paste matrix. The interface between paste and aggregate particles has its own special properties. Concrete can aptly be considered a composite of composites, heterogeneous at both the microscopic and macroscopic levels (Popovics 2001). Concrete, unique in its placement, is one of the only materials used in construction that is usually batched and transported to a construction site for placement in the form of a viscous liquid. The concrete liquid is then formed and left to form a hardened paste. It is this hardened concrete for which material properties can be estimated in construction practice.

Minimum concrete strengths can be accurately predicted and estimated. However, the most commonly accepted method of measuring the compressive strength of *in situ* concrete is through core testing. Many studies have shown that there is no particular correlation between the strength of concrete defined by ASTM standards and the strength of concrete actually in a structure (Mindess et al. 2003). Since some of the material properties of concrete, like strength, change with time and exposure, determining the strength of *in situ* concrete nondestructively is a valuable ability. Concrete is the only engineering material in which strength determination is attempted by ultrasonic measurements. The demand to test ultrasonically has been created by industry needs. Using NDT methods to achieve a reliable conclusion regarding the condition of a structure allows engineers to more efficiently plan repairs.

At the present time, there is no theoretical relationship between ultrasonic pulse velocity, or wave velocity and the compressive strength of concrete. However, in infinitely elastic solids, the P-Wave C_p is a function of Young's Modulus of Elasticity E, the mass density ρ, and Poisson's Ratio ν. The relevant equation for wave speed is:

$$C_p = \sqrt{\frac{E(1-\nu)}{\rho(1+\nu)(1-2\nu)}} \qquad \text{-------- [4]}$$

Using this formula, it is possible to use the wave speed from ultrasonic testing to obtain other physical properties of concrete, such as compressive strength. However, most prior studies have been laboratory controlled and were performed on concretes with consistent mix parameters. These studies tend to neglect the effects of age and weathering on hardened concrete, which is a limiting factor when considering ultrasonic testing for strength determination in older structures (Lemming 1996, Popovics et al.1999, 2000, Popovics 2001, Gudra & Stawiski 2000, Lane 1998, Krautkramer 1990, Malhotra 1984, 1994, Malhotra & Carino1991).

The ultrasonic determination of concrete strength has been intensively researched. Although some studies have shown positive results (Lemming 1998, Popovics et al.1999, 2000, Popovics 2001, Gudra & Stawiski 2000, Lane 1998, Krautkramer 1990, Malhotra 1984, 1994, Malhotra & Carino1991), there is no completely acceptable method for the determination of concrete strength using ultrasonics. This is due to the complexities of the material, the generated waveform, and the structure. Thus, continued research toward the development of a concrete strength versus ultrasonic pulse velocity relationship is justified (Popovics 2001).

Defect detection

The most successful application of ultrasonics has been in the detection and location of the presence of discontinuities in concrete specimens and structures. Ultrasonic testing has been proven to be capable of detecting various anomalies including rebar, prestressed tendons, conduit delaminations, voids, and cracks. The reliability of ultrasonic tests has been confirmed when applied to the testing of concrete and masonry structures.

Ultrasonics are useful in the evaluation of construction and in the rehabilitation of structures. The sonic test is a reliable technique used to evaluate the effectiveness of grout injection. Investigations, repeated before and after repair, allow for control of the distribution of the grout in the masonry. Nevertheless, in the tested case, it was impossible to distinguish between the effects of each grout, the materials being injected having similar modalities (Binda 2001).

Recent research has been conducted using array systems and ultrasonic tomography to evaluate concrete specimens and structures. Tomography is defined as a method of producing a three-dimensional image of the internal structure of a solid object by the observation and recording of the differences in the effects on the passage of waves of energy impinging on those structures. Ultrasonic tomography can be performed by measuring the times-of-flight of a series of stress pulses along different paths of a specimen. The basic concept is that the stress pulse on each projection travels through the specimen and interacts with its internal construction. Figure 2.24 illustrates the basic concept behind ultrasonic tomography. Variations of the internal conditions result in different times of flight being measured (Martin et al. 2001).

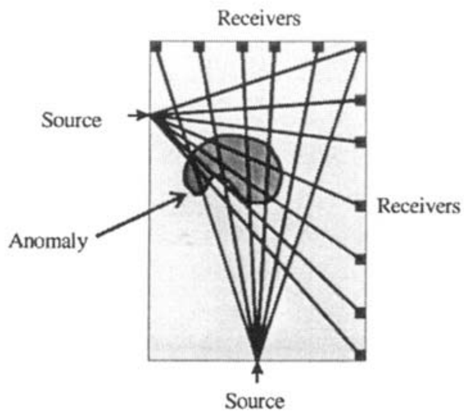

Figure 2.24: Setup of ultrasonic tomographic ray paths. (Martin et al. 2001)

Field research has revealed that ultrasonic tomography constitutes a reliable method for investigating concrete structures. However, it is time consuming, and thus the practicality of using this method for global inspection of structures is limited.

Ultrasonic imaging and tomography methods have incorporated the use of array systems for transducer arrangements to be utilized for the inspection and defect detection. The practical application of the system shows that it is possible to measure the concrete cover of large construction elements, even behind dense reinforcing bars. The data is evaluated by means of time-of-flight corrected superposition. The array system together with a three-dimensional reconstruction calculation can be used for the examination of transversal prestressing ducts. The system has already been used successfully on site (Krause et al. 2001).

The most recent research in ultrasonics and its uses in nondestructive testing has been the automated interpretation of data. The interpretation of NDT data is a difficult task, and those who do so must be trained and skilled in the NDT discipline. However, when large engineering structures are inspected, the amount of data produced can be enormous and a bottle neck can arise at the manual interpretation stage. Boredom and operator fatigue can lead to unreliable, inconsistent results where significant defects are not reported. Therefore, there is great potential for the use of computer systems to aid such interpretation (Cornwell & Mc Nab 1999). At present, the automated data analysis systems are unreliable for industry use. However, the value of automated flaw analysis has been successfully demonstrated on examples of real defects and made correct flaw diagnoses (Cornwell & McNab 1999). It appears as though the biggest limiting factor of the automated interpretation of NDT data is a general lack of knowledge involving defect and flaw detection. The information obtained via the use of ultrasonics and other NDT methods requires the interpretation of an experienced technician or engineer. Scientists have yet to find the simple answers with respect to ultrasonic data that allow computers and computer programs to be utilized for interpretation.

Surface crack measurement

Surface crack measurement has been studied by several researchers and the results are considered to be reliable when the testing procedure is properly performed. In a concrete specimen with a known wave speed, a crack that is present will cause the path length of the ultrasonic pulse to become larger. Using simple geometric calculations, it is possible to obtain the depth of a surface initiated crack within a specimen, as long as that crack represents significant void space (i.e. is wide enough to eliminate contact of the sides). The limitation of this method is smaller cracks that lack large void space. In such cases, the pulse may be able to cross the crack due to the small discontinuity in the concrete, thus shortening the path length. Figure 2.25 illustrates the concept of crack depth measurement.

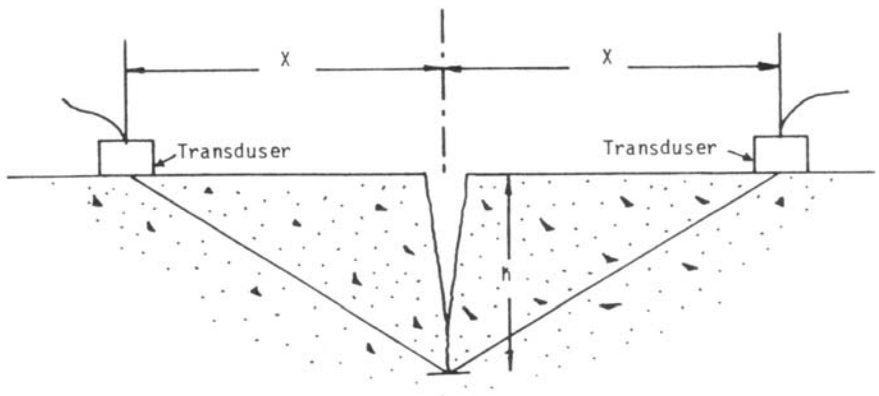

Figure 2.25: Measurement of crack depth. (Malhotra 1991)

Detection of corrosion damage

Corrosion of reinforcing steel is one of the most prevalent problems plaguing concrete structures. The most commonly used methods of corrosion detection are electrochemical methods, such as the DC polarization method, the AC impedance method, and the open circuit potential method. Such electrochemical methods can only obtain overall information theoretically. However, pitting corrosion often occurs in reinforcing steel in reinforced-concrete members. The local environment surrounding the metal surface is not uniform, and inappropriate loading may induce cracks in concrete that allow, or even draw, chloride ions from the environment. These ions can penetrate the concrete along the cracks faster than at other, uncracked areas. Electrochemical measurements for the detection of corrosion damage in reinforced concrete members may underestimate the local pitting corrosion rate because the electrochemical parameters represent global information obtained by taking an average of the total amount of local corrosion on the whole metal surface area (Yeih & Huang 1998).

Laboratory research has been performed that has correlated ultrasonic wave amplitude attenuation to corrosion damage in reinforced concrete specimens. Some of the limitations of this approach include the test control conditions. Most of the research involving corrosion degradation in reinforced concrete specimens has involved the corrosion of steel in intact concrete specimens. However, structures observed in the field typically exhibit corrosion damage as a result of material deficiencies in the concrete that encases it, usually a result of both the concrete and the steel. This problem requires further analysis of the combined effect of both materials for field applications. Laboratory studies have yet to incorporate both materials. The ultrasonic investigation of a deteriorated reinforced concrete specimen essentially requires the comprehension of ultrasonic wave forms that account for dissimilar material effects from the steel and complex multiphase heterogeneous material that is concrete. Ultrasonic testing analysis of the resulting damage of such complex conditions is difficult to perform. Further research and testing is needed before ultrasonic testing can be reasonably applied in field use for the detection of corrosion effects in reinforcing steel. Engineers need to understand the shortcomings of nondestructive testing tests so that they can make proper determinations and accurate evaluations of structures (Boyd et al. 2002).

Structural health monitoring

Structural health monitoring is at the forefront of structural and materials research. Structural health monitoring systems enable inspectors and engineers to gather material data of structures and structural elements used for analysis. Ultrasonics can be applied to structural monitoring programs to obtain such data, which would be especially valuable since the wave properties could be used to obtain material properties. There is scarce literature available on the monitoring of in-place concrete structures and structural elements.

Current research in structural monitoring relates to the performance of fiber reinforced polymer composites and other structural strengthening methods. Fiber optics have given rise to remote structural health monitoring, remote sensing, and nondestructive load testing. Ultrasound has been applied to concrete strength, crack detection, thickness measurements, and wave speeds of concrete structures.

The concept behind using ultrasonics for structural health monitoring is observing changes in the structure's wave speed over time. As previously discussed, the wave speed is a function of Young's Modulus of Elasticity E, the mass density ρ and Poisson's Ratio ν. The overall quality of the concrete is associated with the ultrasonic wave speed (Ryall 2001).

Table 2.3: Relationship between pulse velocity and concrete quality.

Longitudinal Pulse Velocity (m/s)	Quality of Concrete
> 4500	Excellent
3500-4500	Good
3000-3500	Doubtful
2000-3000	Poor
< 2000	Very poor

This testing approach may be used to assess the uniformity and relative quality of the concrete, to indicate the presence of voids and cracks, and to evaluate the effectiveness of crack repairs. It may also be used to indicate changes in the properties of concrete, and in the survey of structures, to estimate the severity of deterioration or cracking. When used to monitor changes in the condition over time, tests are repeated at the same positions (ASTM C597-97). Decreases in ultrasonic waves speeds over time can reveal the onset of damage before visible deficiencies become evident. This allows inspectors and engineers to implement repair recommendations before minor deficiencies become safety hazards.

Impact Echo

The term "ultrasonic" refers to sound waves having a frequency above the human ear's audibility limit, which is about 20,000 Hz. Ultrasonic testing has been used to successfully evaluate the quality of concrete for approximately 60 years. This method can be used for non-intrusively detecting internal defects in concrete. Some of these flaws include deterioration due to sulfates or other mineral attack, and cracking and changes due to freeze-thaw cycling. One type of ultrasonic testing is the impact-echo method.

Development of method

Nicholas Carino of the National Bureau of Standards (NBS) developed the impact-echo method in the 1970's and 1980's for assessment of buildings and bridges that failed during construction (Sansalone & Streett, 1997). Mary Sansalone focused her research on the refinement and application of the impact-echo method for her Ph. D thesis at Cornell University. Their research comprises the majority of impact-echo research and development performed in the United States applicable to concrete and concrete structures.

Early research focused on laboratory studies involved the location of defects and voids in concrete. There have been four key research breakthroughs since research began to successfully develop impact echo as an NDT method (Sansalone & Streett, 1997). The concerns utilization of the numerical simulation of stress waves in solids using finite element computer models. This method was implemented to help facilitate the interpretation of early experimental results. The models created were two-dimensional finite element models based on Green's functions, which simulate stress wave propagation in plates. Green's functions are widely used in determining responses in solids to an applied unit force. These functions can be used to obtain the propagation of elastic waves in solids. This mathematical formulation was essential in the interpretation of results obtained through experimentation.

The second key research breakthrough relates to the use of steel ball bearings to produce impact generated stress waves. The impacting of objects on the surface of a given solid produces stress waves that facilitate signal acquisition. This elastic impact results in a force-time function that is defined and mathematically applicable. The impact-echo method does not use a pulse-generating transducer to generate stress waves, rather, the impacting of an object, typically a small steel ball, provides the stress wave. The development of the impact method overcame the need for a pulse generating transducer. Typical steel balls range from 4 to15 mm in diameter but can be larger or smaller depending on the desired waveform needed for the test. Typical impact speeds are 2 to 10 meters per second but can also vary depending upon the desired waveform. The contact time typically ranges from 15 to 80 μs. Proper selection of steel ball diameter and impact speed is essential in flaw detection to create the correct wave frequency, which is typically less than 80 kHz. This range can vary depending on the properties and dimensions of the test sample.

The third key research advancement was the development of a transducer that can acquire impact generated stress waves. The development of the correct receiving transducer was an integral phase in the advancement of the impact-echo method. The receiving transducer was developed by T.M. Proctor (Hamstad and Fortunko, 1995). The intended use for the receiving transducer was the acoustic emission testing of metals. However, it was discovered that the transducer was compatible with impact-echo testing of concrete. The receiving transducer is composed of a small conical piezoelectric element bonded to a larger brass block. For protection of the transducer tip, a lead element is fitted between the transducer tip and the material to be tested. Some tests use coupling materials such as gels to provide an effective test surface. In areas where a smooth concrete surface is not available, the concrete is usually grinded to a smooth surface to ensure proper transducer-to-surface coupling. Figure 2.26 is a schematic of a typical piezoelectric transducer.

The final key research advance pertains to the use of frequency domain analysis for signal interpretation. Waveform analysis is the determining component in the use of NDT. In many cases the operator has difficulty in interpreting the wave signals received in the time-domain by the piezoelectric transducer. Using a Fourier transform on the time-domain signals, it is possible to graph the wave's frequency-domain signal. The result is a frequency vs. amplitude plot, also called an amplitude spectrum.

Recent research advances

Much of the research and development of the impact-echo method has been carried out at Cornell University. This research primarily involves the relevant application of impact-echo to the evaluation and inspection of concrete and masonry materials (Sansalone & Streett, 1997). Through this research, the methods for determining wave speeds in concrete, grout, and masonry were improved for industry use. The research also helped develop applicable methods for locating and determining flaws in concrete and masonry. Some of the flaw types that have been accurately detected using the impact-echo method include cracks, voids, bonding voids, honeycombing, and concrete damage. The method can also be used to obtain the thickness of a material such as concrete or asphalt pavement.

The advances in the impact-echo method made at Cornell University used a combination of research techniques. These techniques include numerical models, finite-element analysis, eigenvalue analysis, resonant frequency analysis and laboratory testing. The first portable impact-echo system was developed by Mary Sansalone and Donald Pratt and was patented by Cornell University. The patented system has five basic components including spring-mounted impactors (ball bearings), a receiving transducer, a high-speed digital-to-analog data-acquisition system, a rugged and powerful laptop-size computer, and software for transferring analyzing and storing test data (Sansalone & Streett, 1997). Figure 2.27 is an illustration of a typical impact-echo equipment system.

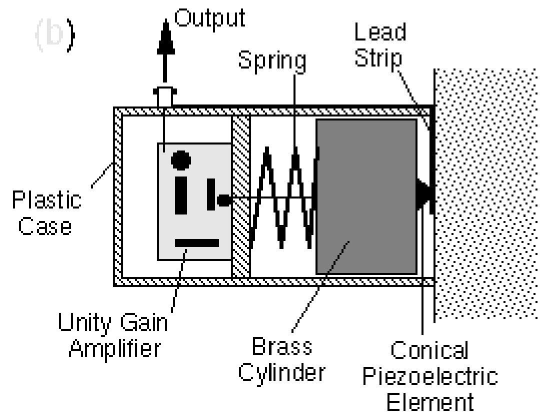

Figure 2.26: Schematic of a typical piezoelectric transducer used for impact echo testing. (Carino 2001)

The portable impact-echo system has been successfully developed as a commercial product and is available for retail purchase. Most portable impact-echo systems that are available for consumer use are purchased with four components, with the laptop computer being omitted.

Stress wave theory

The effective use of the impact-echo system requires that the user have a basic understanding of the properties and fundamentals of stress waves. In solid mechanics, when any two objects collide local disturbances take place within a given material. The disturbances can cause deformations that may be plastic or elastic in nature. A plastic deformation is defined as a deformation in which the material is permanently deformed. Elastic deformations are the type in which the material is temporarily deformed but then returns to its original shape. When an elastic collision occurs between objects, a disturbance is generated that travels through the solid in the form of stress waves. There are three primary modes of stress wave propagation through elastic media: dilatational, distortional, and Rayleigh waves (Sansalone & Carino, 1989).

Figure 2.27: View of a typical impact-echo equipment system.

Dilatational waves are the primary stress waves produced upon impact. They are also referred to as primary waves, P-waves, or compression waves. The particle motion of the wavefront of P-waves is parallel to the direction of impact propagation. The result is a compressive or tensile stress wave (Sansalone & Streett 1997). The P-wave velocity is the fastest of the three stress waves produced from the impact. Typical P-wave speeds for concrete ranges from approximately 3000 m/s to 5500 m/s. For normal strength concrete, P-wave speed usually ranges from 3500 m/s-4500 m/s.

Distortional waves are the secondary stress waves that are produced upon forced contact. These waves are also called shear waves or S-waves. In S-waves, the particle motion of the wave front is normal to the direction of propagation producing shear stress. (Sansalone & Streett 1997). S-wave speed in normal concrete is usually about 62 percent of the P-wave speed.

Rayleigh waves are also called R-waves or surface waves. Rayleigh waves, unlike P-waves and S-waves, do not propagate through the solid. Rayleigh waves propagate along the surface of a given concrete specimen in an elliptical motion. P-waves and S-waves propagate through a concrete specimen in spherical wavefronts. Rayleigh wave speed is usually 56 percent of P-wave speed. Figures 2.28 and 2.29 illustrate the typical relationship between stress wave types.

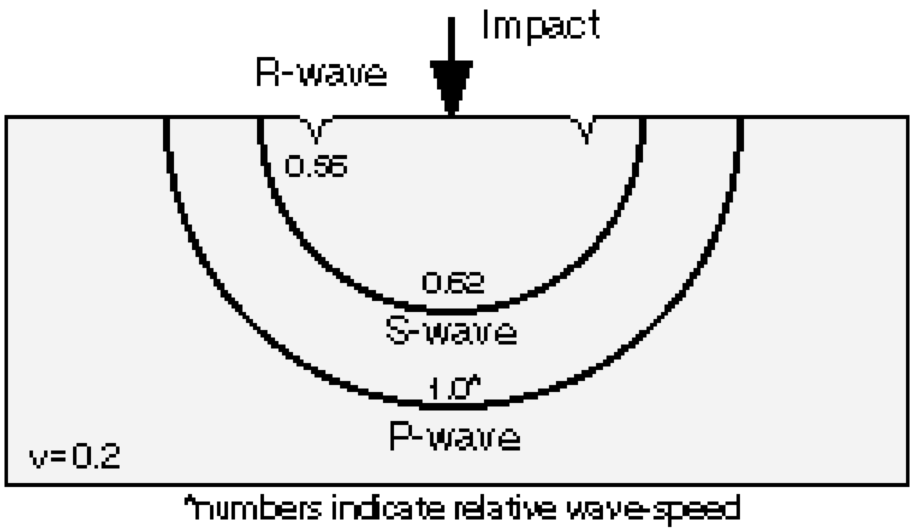

Figure 2.28: Illustration of typical wave propagation through a solid. (Carino 2001)

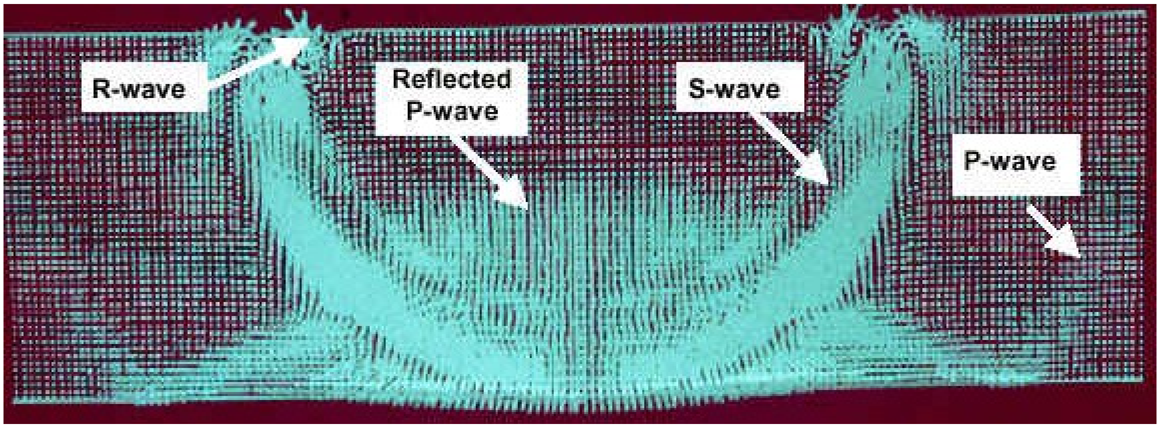

Figure 2.29: Model of wave propagation through a solid. (Carino 2001)

The wave speeds in elastic solids are related to Young's Modulus of Elasticity E, Poisson's ratio ν, and the density ρ (Sansalone & Streett, 1997). In the equations below C_p, C_s and C_r, describe the P-wave, S-wave and R-wave speeds respectively.

$$C_p = \sqrt{\frac{E(1-\nu)}{\rho(1+\nu)(1-2\nu)}} \qquad \text{--------} \; [5]$$

$$C_S = \sqrt{\frac{G}{\rho}} \quad ; \quad C_S = \sqrt{\frac{1-2\nu}{2\rho(1+\nu)}} \qquad \text{--------} \; [6]$$

$$C_R = \left(\frac{0.87+1.12\nu}{1+\nu}\right) C_S \qquad \text{--------} \; [7]$$

Where: G = Shear Modulus of Elasticity.

The typical range of values for Poisson's ratio "ν" is typically 0.17-0.22. Inserting this value for ν into the above equations, along with the typical density and modulus of elasticity values, will give typical wave speeds found in concrete. The modulus of elasticity of a concrete specimen, the compressive strength, and the appropriate wave speed of the concrete can be obtained. Equation 5 can be used as an example obtain a typical wave. P-wave speed for a concrete sample as follows:

Using: $E=30x10^9$ Pa, ρ = 2400 kg/m3, and ν = 0.18

$$C_p = \sqrt{\frac{E(1-\nu)}{\rho(1+\nu)(1-2\nu)}} \quad C_p = \sqrt{\frac{30x10^9(1-.18)}{2400(1+.18)(1-2(.18))}} = 3700\text{m/s}$$

As discussed previously, 3700 m/s is an acceptable P-wave speed for concrete.

Force-time function of impact

Stress waves can be produced by several different instruments. The ultrasonic pulse velocity method uses a stress wave transmitting piezoelectric transducer. The impact-echo method applies the collision of a steel sphere generating stress waves. The parameters that characterize the duration of the impact or contact time are sphere size, and the kinetic energy of the sphere at the point of impact. The variation of impact force with time is called the force-time function, accurately represented by a half sine curve (Sansalone & Streett 1997). The contact time duration between a small steel sphere and a concrete surface is relatively short, ranging from 30 μs to 100+ μs. Figure 2.30 illustrates the typical force-time relationship.

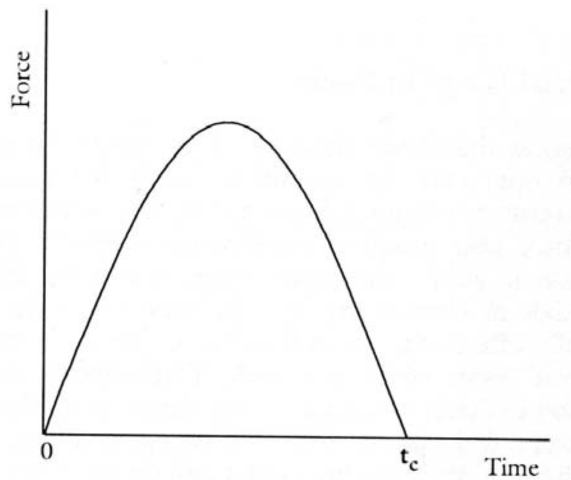

Figure 2.30: Typical force-time function for the elastic impact of a sphere on a solid. (Sansalone & Streett 1997)

One result of the impact of a steel sphere on a concrete specimen is the transfer of kinetic energy from the sphere to the concrete. The energy transfer takes place in the form of particle displacements resulting in stress waves on the impacted solid. The maximum force is proportional to the kinetic energy of the moving sphere at impact, and the particle displacements are proportional to this force (Sansalone & Streett 1997). The time of contact, however, has a faint reliance on the kinetic energy of the sphere, being a linear function of sphere diameter.

The stress waves generated by the impact contain a wide distribution of frequencies. The frequency distribution is influenced by the force-time function of the collision. The objective of frequency analysis is to determine the dominant frequency components in the digital waveform. The optimum technique used to create the amplitude spectrum is the fast Fourier transform (FFT) technique. The FFT technique assumes that any waveform, no matter how complex, can be represented by a series of sine waves added together. The FFT displays the amplitudes of the various frequency components in the waveform. The amplitude spectrum obtained by the FFT contains half as many points as the time domain waveform. The maximum frequency in the spectrum is one-half the sampling rate. This shows the initial portion of the computed amplitude spectrum. Each of the peaks corresponds to one of the component sine curves (Carino 2001).

Figure 2.31a illustrates a typical group of sine waves which is transformed into a typical frequency spectrum in Figure 2.31b.

The linear relationship between time of contact and sphere diameter can be described as:

$$t_c = 0.0043D \quad \text{--------} \; [8]$$

where D is the sphere diameter in meters and t_c is the contact time in seconds. For an impact using a sphere of a given diameter, a maximum frequency of useful energy is created. This relationship, like the sphere diameter and contact time relationship, can also be described as a linear function.

$$f_{max} = \frac{291}{D} \quad \text{--------} \; [9]$$

Where f_{max} is the maximum frequency of useful energy in hertz and D is the sphere diameter in meters.

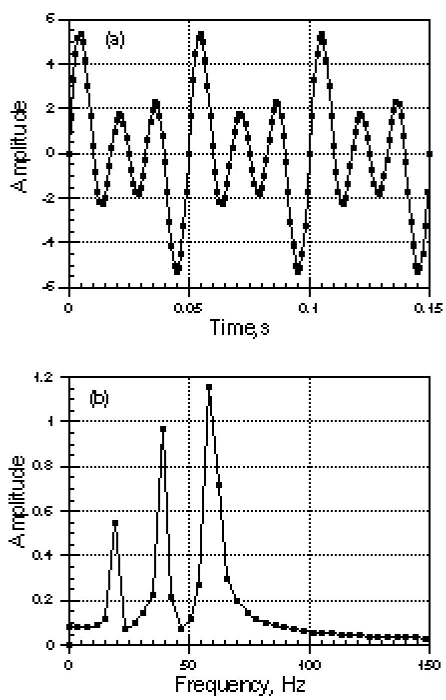

Figure 2.31: Example of frequency analysis using FFT:
(a) represents the frequency distribution,
(b) represents the corresponding amplitude spectrum. (Carino 2001)

The interesting concept behind Equation 9 is that maximum usable frequencies are smaller when larger diameter spheres produce impacts. However, larger spheres produce larger forces and larger maximum stress wave amplitudes. The contact time decreases with decreasing sphere diameter but the range of useful frequencies increases with a smaller diameter sphere. However, using smaller spheres increases the likelihood that the higher frequency stress will be scattered by the natural inhomogenities inherent in concrete. In practice, it has been found that the smallest sphere useful in impact-echo testing has a diameter of approximately 3mm (Sansalone & Streett 1997).

Behavior of stress waves at material interfaces

The term interface is defined as a surface forming a common boundary of two bodies, spaces, or phases. One of the most common interfaces people are familiar with is the oil-water interface. In material science, an interface is usually defined as a fringe between two materials which have different properties, such as density and phase. Other differences in material properties are acoustic properties (such as acoustic impedance). Acoustic impedance is defined as the material density multiplied by the materials stress wave velocity. When stress waves collide with material interfaces, portions of the waves are reflected and refracted. In obtaining the depth of a flawless concrete specimen, users assume stress waves are being reflected at the concrete/air interface as seen in Figure 2.32.

In the development of the impact echo method, the use of finite element models (FEMs) was prominent in the study of particle motion and stress wave propagation through a concrete medium. The use of FEMs permitted the developers of the impact-echo technique to study waveforms at projected instantaneous phases in the wave's displacement. The model studies provided necessary information concerning the reflection of stress waves in a concrete media. Figure 2.33, illustrates the ray paths of typical P-wave propagation in a solid.

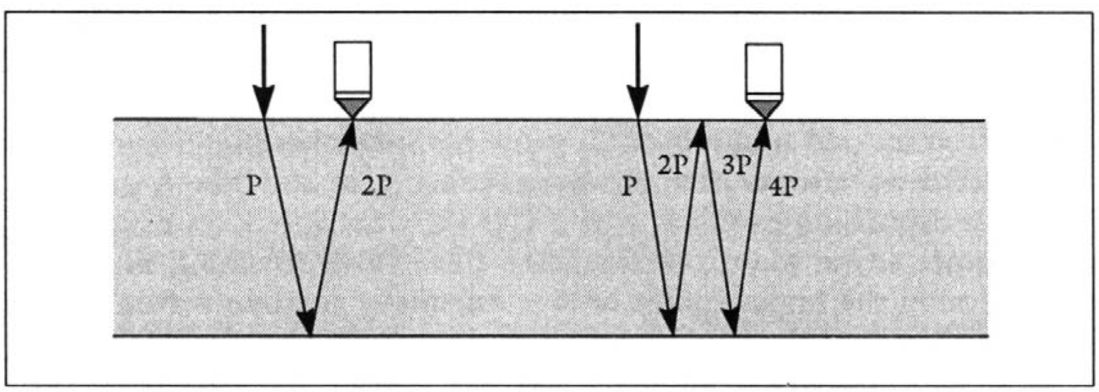

Figure 2.32: Plots of P, S and R-waves at various times after an impact: (a) 125 μs, (b)150 μs, (c)200 μs and (d) 250μs. (Sansalone & Streett 1997)

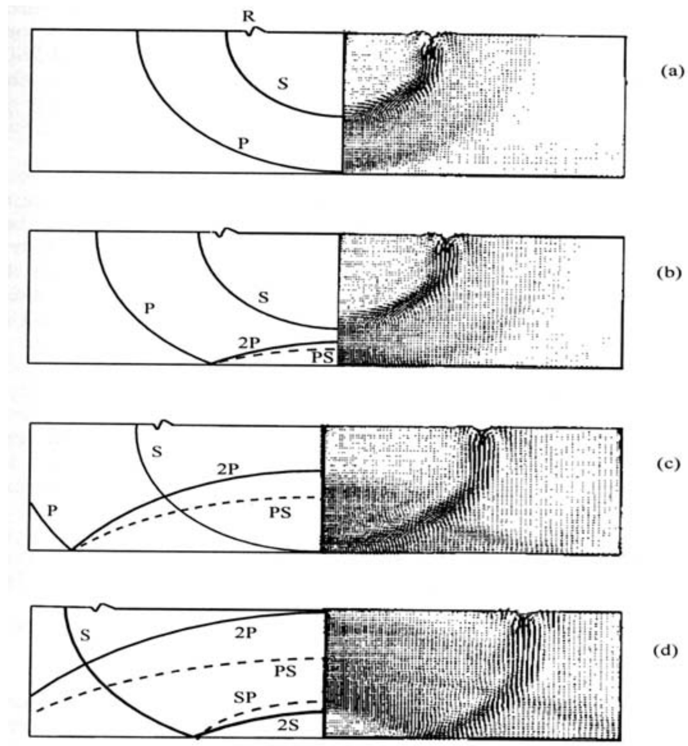

Figure 2.33: The ray path of typical P-wave propagation through a solid media. (Sansalone & Streett 1997)

Stress wave behavior between interfaces of solids is more complicated than the stress wave behavior between a solid-gas interface. Upon collision with a solid-gas interface, most of the P-wave energy is reflected back into the solid media. However, in a stress wave collision with a solid-solid interface, the P-wave energy is partially reflected and partially refracted. The amount of energy that is allowed to pass through or refract the second solid medium depends upon its acoustic impedance. It is possible to get a coefficient of refraction if the acoustic impedance of the materials involved is known and the amplitude of the particle motion is obtained for the initial P-wave.

$$R = \frac{A_{reflected}}{A_i} = \frac{Z_2 - Z_1}{Z_2 + Z_1} \qquad \text{-------- [10]}$$

$$R = \frac{A_{refracted}}{A_i} = \frac{2Z_2}{Z_2 + Z_1} \qquad \text{-------- [11]}$$

Where R is the coefficient of refraction, $A_{reflected}$ & $A_{refracted}$ are the reflected and refracted P-wave amplitudes; A_i is the amplitude of the initial P-wave; Z_1 is the acoustic impedance of the initial medium; and Z_2 is the acoustic impedance of the medium beyond the interface.

There are three basic relationships between Z_1 and Z_2. The first relationship exists when Z_1 is notably greater than Z_2. Due to this relationship, the Z_1/Z_2 relationship is comparable to the solid-gas interface in which the P-wave is completely reflected and virtually no refraction takes place. This situation is common in the application because most defects in concrete are related to void space in the concrete matrix.

A second relationship between solid-solid interfaces is when the Z_2 is much greater than Z_1. Consider Z_1 to approach zero and consider Equation 11 above, then $A_{refracted}$ approaches $2A_i$. When this condition exists, the amplitude of the wave is equal to that of the incident wave, while the amplitude of the refracted wave is twice that of the incident wave. There is no phase change in the reflected or refracted wave. In impact-echo testing, the no phase change case occurs, for example, when the first region is concrete and the second region is steel or rock, as the acoustic impedances of those materials are several times grater than that of concrete (Sansalone & Streett 1997).

The third relationship between solid-solid interfaces exists when Z_2 is approximately equal to Z_1. When a value of 1 is used for both Z_1 and Z_2, $A_{reflected}$ becomes zero and $A_{reflected}$ becomes one. In this situation, most of the stress wave energy is transmitted through the interface to the second solid. This situation is possible when a concrete specimen is bonded to another concrete structure or a concrete structure has been properly patched.

Inserting Z_1 and Z_2, into Equation 10 and Z_1 is greater than Z_2, a negative value is obtained coefficient of friction "R". The negative R value denotes a phase change in the stress wave at the point of reflection. Since impact induced P-waves are compression waves, a phase change indicates the waves will become tension waves upon reflection. This phenomenon is important to consider because when P-waves are reflected and Z_1 is less than Z_2, as in a case when steel is the solid behind the interface, the reflected waves do not undergo phase change. Figure 2.34 below illustrates the phase changes that take place in stress waves upon reflection.

As seen in figure 2.34a illustrates the return of a tension wave in each reflection. In 2.34b, the return of a compression wave is alternated with the return of a tension wave for each stress wave reflection. The arrival of a tension wave causes an inward displacement of the surface, while the arrival of a compression wave causes an outward displacement on the material surface. The reason stress waves do not change phase when reflected on a solid medium with a higher acoustic impedance is because the stress wave "bounces" off the second material and returns to the impact source. The "bouncing" takes place because materials with higher acoustic impedances have higher densities and the small surface displacements that usually take place at solid/gas interfaces, do not take place at boundaries more dense than the original medium.

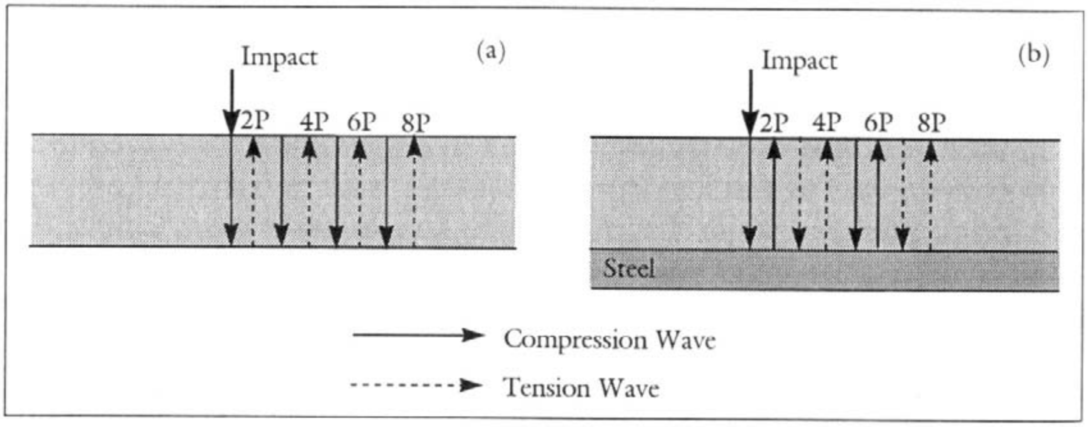

Figure 2.34: Impact echo ray paths; (a) phase change at both boundaries, (b) phase change at upper boundary only. (Sansalone & Streett 1997)

Waveform analysis - idealized case

As stated in the introduction to stress waves section, such waves are the particle motion caused by the energy of an impact. When wavefronts reach the surface, the particle motion causes small displacements, which are detected by the receiving transducer. The transducer converts the surface displacement into a proportional voltage signal. The voltage signal becomes the primary output to the testing software. The output produced requires proper understanding of waveform analysis. For each test, the operator must properly interpret the waveform in order to ascertain the quality of the data obtained.

A common scenario in impact-echo testing is the testing of a solid plate with solid/gas interfaces at both concrete surfaces. As seen in Figure 2.35, the principle features of the idealized waveform detected by the transducer are those produced by the P-wave, which travels into the structure and undergoes multiple refractions between the two surfaces, and the R-wave, which travels outward across the surface (Sansalone & Streett 1997).

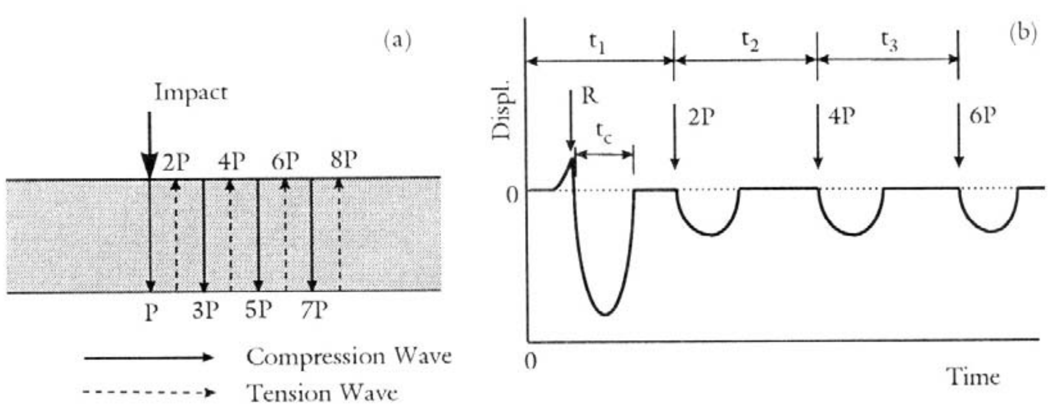

Figure 2.35: Schematic representations of; (a) P-wave ray reflections, and (b) the resulting idealized waveform. (Sansalone & Streett 1997)

The typical elapsed time for the above waveform recorded is less than four milliseconds. As previously noted, R-waves propagate through a solid as surface waves and reflections of R-waves will not be recorded unless the distance between the receiving transducer and the horizontal solid-gas interface is less than the specimen depth. However, since the impact between the steel ball and the concrete specimen does not occur at a point directly below the transducer, the R-wave causes a negative displacement at the receiving transducer. As shown in the Figure 2.35, the amplitude of the R-wave is larger than any other feature in the wave spectrum. Figure 2.35 also illustrates that the time elapsed for the R-wave to return back to zero in the displacement spectrum is the time of contact "t_c" of the impacting sphere. In this event, the point of the impacting sphere is relatively far from the receiving transducer, the arrival of the P-wave reflection may occur before the arrival of the R-wave. To avoid this phenomenon, the operator must ensure that the impact point of the sphere is relatively close to the transducer. Since the P-wave and S-wave speeds are greater than the R-wave speed, there is a small displacement just prior to the arrival of the R-wave. This small displacement is due to the arrival of the P and S wavefronts.

The reflections of the P-wave with the solid-gas interface shown in Figure 2.35, illustrate the expected phase change. The arrival of the tension wave at the impacting surface causes a small inward displacement causing the wave reflections shown at times t_1, t_2 and t_3. The elapsed time t_1, between the impact and arrival of the 2P wave at the surface is the distance the wave has traveled, being twice the solid thickness. The P-wave arrivals at the upper surface cause displacements that are periodic in nature. This periodicity is the dominant feature of the waveform after the passage of the R-wave. The period of the waveform in Figure 2.35 is t_1 and its frequency is $1/t_1$, the reciprocal of the period. This yields a simple relationship shown in Figure 2.33, which is at the heart of the impact-echo method (Sansalone & Streett 1997).

$$f = \frac{C_p}{2T} \qquad \text{--------} \; [12]$$

Waveform analysis - actual case

The technique presented in the previous paragraph is an accurate description of waveform analysis, but it illustrates waveform circumstances under idealized conditions. One difference between the idealized case and the actual case is that the reactions of the transducer to the material displacements is caused by stress waves. As the stress waves reflect due to the solid-gas interface, the receiving transducer experiences its own particle motions. This additional movement is referred to as "overshoot". Overshoot causes the waveform displayed by the digital analysis software to have only the negative portion of each wave. This wave analysis software phenomenon is illustrated in Figure 2.36.

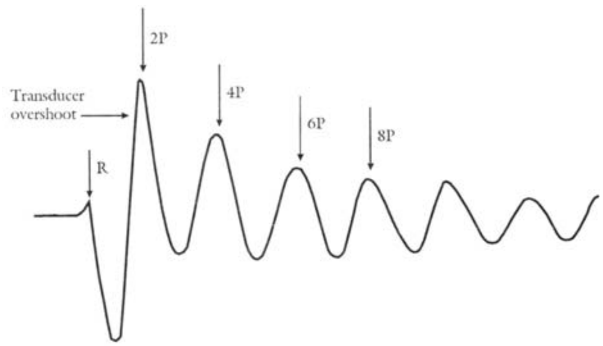

Figure 2.36: Actual waveform on an impact-echo test plate. (Sansalone & Street 1997)

Figure 2.36 shows the actual waveform as it would be received and displayed by impact-echo software in field-testing. Another phenomenon that this figure illustrates is the decay of the spectral amplitude with the increasing number of wave reflections. This decay is a result of energy losses due to friction as the wave propagates within the solid matrix.

Through rigorous testing in the development of impact echo, it was observed that the frequencies obtained in laboratory testing of concrete specimens were not equal to the frequencies calculated in Equation 12. The use of finite element models and laboratory testing revealed a deviation of approximately 5% between the observed laboratory data and the expected results obtained by Equation 12. After considering the geometry of the specimen, the developers found that it was necessary to include a shape factor in the frequency equation. In the case of a solid plate, the characteristic dimension is the thickness T, and the shape factor β is 0.96 (Sansalone & Streett 1997).

$$f = \frac{\beta \cdot C_p}{2T} = \frac{0.96 \cdot C_p}{2T} \qquad \text{-------- [13]}$$

Field measurement of material stress wave speed

In field-testing, it is crucial to establish the wave speed of the solid before specimen dimensions and qualities are to be tested. The most common method for directly measuring the wave speed of a solid is through the use of two receiving transducers. The transducers are commonly placed in a spacer device, at a known fixed length from each other. Once the transducers are properly spaced and fixed to the concrete specimen, a single P-wave can be used to measure the wave speed of the concrete. Figure 2.37 illustrates the typical test set up behind the measurement of wave speed. Figure 2.38 is an example of a typical output obtained in acquisition of the wave speed.

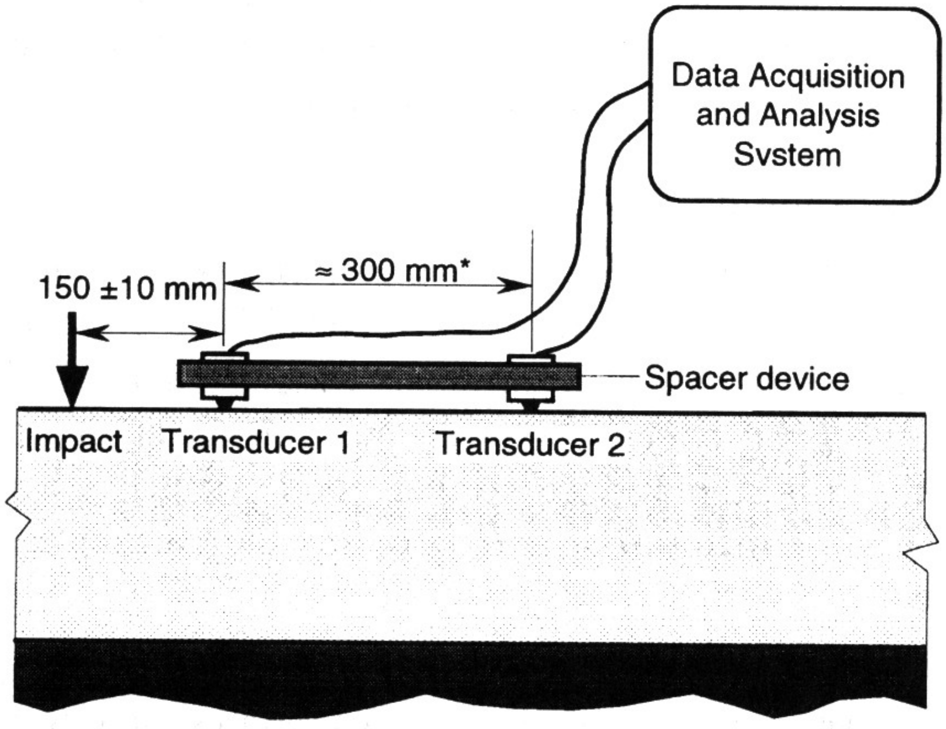

Figure 2.37: Schematic representation of the test set up for wave speed measurements. (ASTMC 1383-R98a 2001)

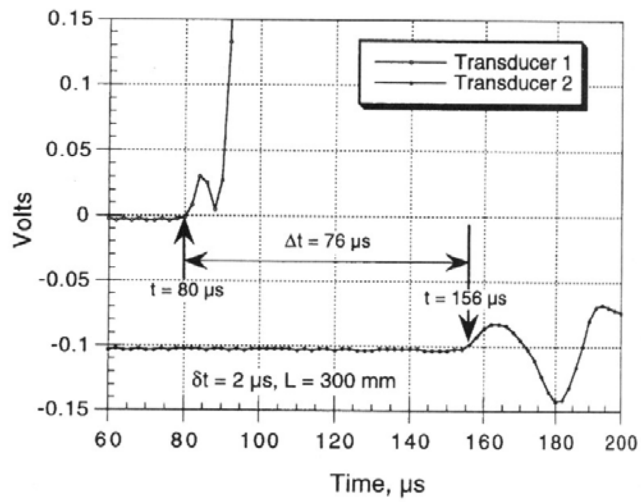

Figure 2.38: Example waveform obtained in wave speed measurements. (ASTM 2001)

When the test is performed, the output would simply record the time at which the P-wave is received by each transducer. The wave speed would then be:

$$Cp = \frac{L}{t_2 - t_1} \qquad \text{-------- [14]}$$

However, it is important to create the impact far enough from the initial transducer to allow for P-wave separation from the S and R-waves. This is the basis for having the minimum distance between the impact of the sphere and the first transducer set to ½L. For the example of output illustrated in Figure 2.38, the results are t_2 = 156 μs, t_1 = 80 μs and L=300 mm. Using Equation 14, the wave velocity of the sample is obtained by the following:

$$C_P = \frac{300\,\text{mm}}{156\,\mu\text{s} - 80\,\mu\text{s}} = 3950 \text{ m/s}$$

Once the wave speed has been established for the concrete specimen, then testing for the specimen's thickness, concrete quality, flaw and anomaly detection may be performed.

The effect of flaws on impact-echo response

Impact-echo was developed to nondestructively investigate concrete. One of the advantages of impact-echo testing is the versatile equipment and the relatively brief duration of the testing procedure. This allows inspectors to efficiently and accurately investigate structures and concrete specimens for condition assessment. The impact echo responses of materials can be classified according to the type, depth, and size of flaw.

For the purposes of impact-echo testing, a crack is defined as an interface or separation where the minimum opening is 0.08 mm or larger. Stress waves are able to propagate across voids that are smaller than 0.08 mm, hence there is not enough wave reflection to detect these smaller deficiencies. Since water has a coefficient of reflection of approximately 0.7, the majority of the stress wave energy at a solid-water interface is reflected and water filled voids can also be detected using the impact-echo method.

As the depth of a void from the surface increases, the smallest size that can be detected also increases. Based on analytical and laboratory studies, it has been suggested that if the lateral dimensions of a planar crack or void exceed 1/3 of its depth, the flaw depth can be measured. If the lateral dimensions exceed 1.5 times the flaw depth, the flaw behaves as an infinite boundary and the response is that of a plate with thickness equal to the flaw depth (Carino 2001). Figure 2.39 illustrates the relationship between crack depth and detectability.

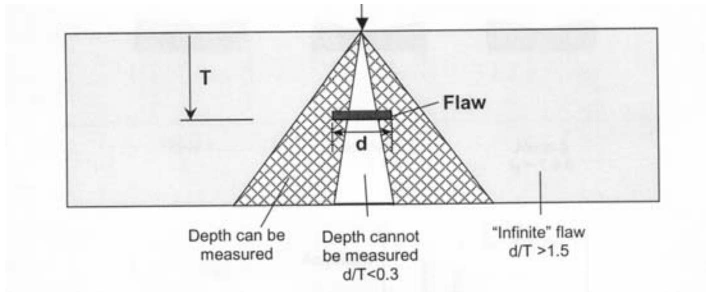

Figure 2.39: Illustration of the smallest detectable crack and its dependency on depth.

If the flaw is located entirely within the white area, the crack depth cannot be measured (Carino 2001) When larger cracks or voids are present, the impact-echo response will be essentially the same as if there was a solid/gas boundary at that interface. The test will produce results that represent the termination of the material at the depth of the flaw. A crack or void within a concrete structure forms a concrete/air interface. Laboratory experiments have shown that cracks with a minimum width (crack opening) of about 0.08mm (0.003 inches) cause almost total reflection of a P-wave. The responses from cracks and voids are similar, since stress waves are reflected from the first concrete/air interface encountered. Thus a crack at a depth **d** will give the same response as a void whose upper surface (nearest to the impact surface) is at the same depth (Figure 2.40).

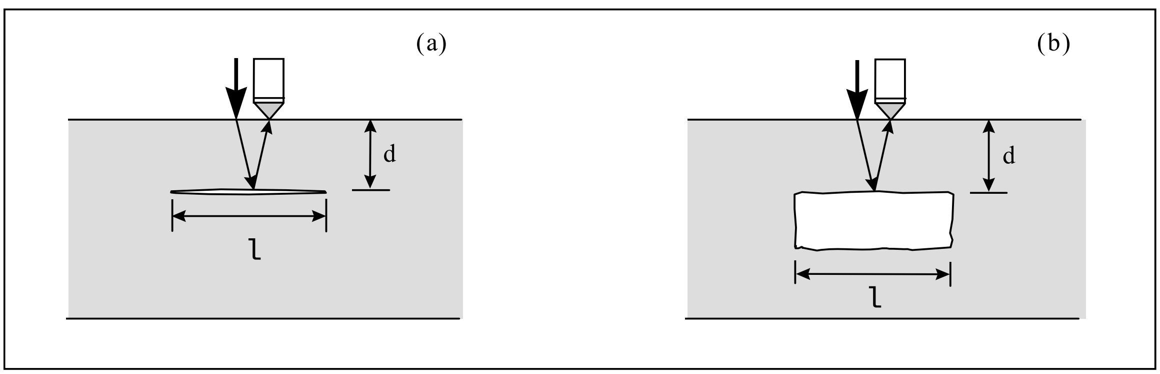

Figure 2.40: A crack at depth "d" gives the same response as a void at that depth. (Sansalone & Streett 1997)

In cases where the lateral dimensions of the crack are about equal or less than the depth of the crack, propagating stress waves are both reflected and refracted from the surface. Hence, they are diffracted around the edges of the crack (Sansalone & Streett 1997). For similar cases where more complicated waveforms exist, the frequency spectrums are affected accordingly.

Applications

When properly used, the impact-echo method has achieved unparalleled success in locating flaws and defects in highway pavements, bridges, buildings, tunnels, dams, piers, sea walls and many other types of structures. It can also be used to measure the thickness of concrete slabs (pavements, floors, walls, etc.) with an accuracy of 3 percent or better. Impact-echo is not a "black-box" system that can perform blind tests on concrete and masonry structures and always tell what is inside. The method is used most successfully to identify and quantify suspected problems within a structure, in quality control applications (such as measuring the thickness of highway pavements) and in preventive maintenance programs (such as routine evaluation of bridge decks to detect delaminations). In each of these situations, impact-echo testing has a focused objective, such as locating cracks, voids or delaminations, determining the thickness of concrete slabs or checking a post-tensioned structure for voids in the grouted tendon ducts.

Determining the depth of surface-opening cracks

A surface-opening crack is any crack that is visible at the surface. Such cracks can be perpendicular, inclined to the surface, or curved, as shown in Figure 2.41. The two waveforms, labeled 1 and 2, in Figure 2.42(b), are the signals from transducers 1 and 2 in Figure 2.42(a). The arrival of the direct P-wave, a compression wave, at transducer 1 causes an upward surface displacement and a positive voltage (time t_1), while the diffracted wave that first reaches transducer 2 is a tension wave, which causes a downward displacement and a sudden voltage drop (time t_2). The elapsed time between t_1 and t_2, the wave speed, and the known distances H_1, H_2 and H_3, are used to calculate the depth D.

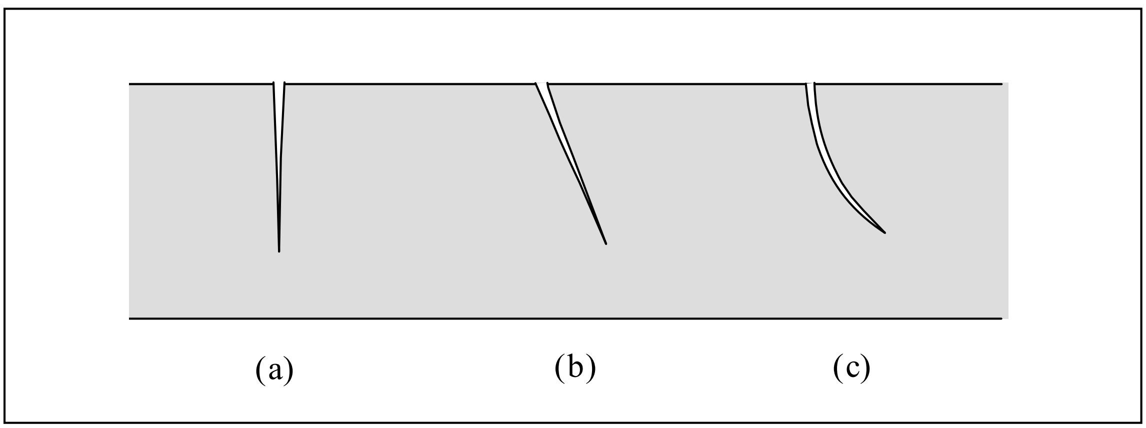

Figure 2.41: Surface-opening cracks; (a) perpendicular, (b) inclined, and (c) curved. (Sansalone & Street 1997)

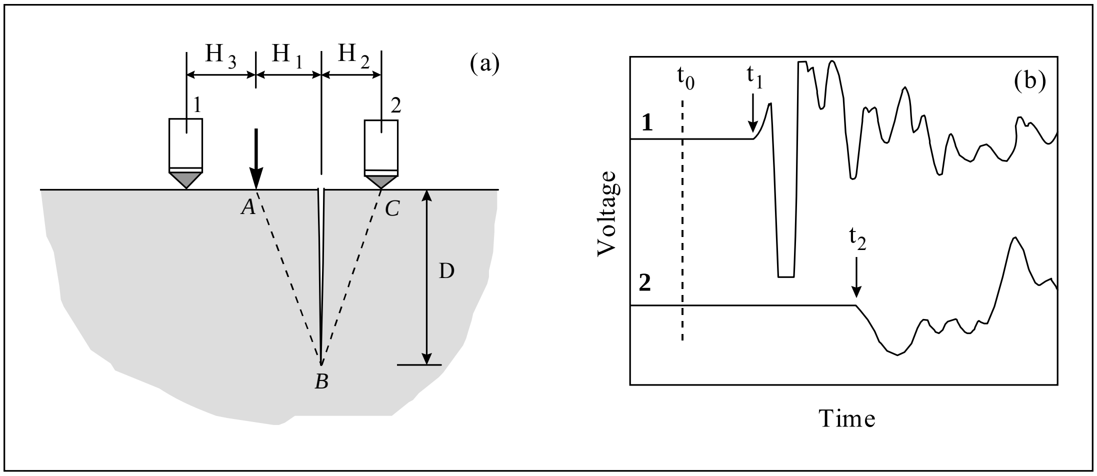

Figure 2.42: Measuring the depth of a surface-opening crack: (a) schematic of experimental test setup, and (b) sample waveforms. (Sansalone & Street 1997)

Voids under plates

Detecting voids under concrete plates is one of the simplest applications of the impact-echo method. It relies on the clear and easily recognizable difference between waveforms and spectra obtained from plates in contact with soil, on the one hand, and plates in contact with air (a void under the slab) on the other.

Figure 2.42 shows a typical set of results obtained from an impact-echo test on a concrete plate in contact with soil. The waveform shows periodic displacements caused by P-wave reflections within the concrete plate, but because energy is lost to the soil each time a P-wave is incident on the concrete/soil interface, the amplitude of the displacements (indicated by the signal voltage) decays rapidly. The corresponding spectrum shows a single peak corresponding to the frequency of P-wave reflections from the concrete/soil interface. Note however, that the peak is somewhat rounded and is broader than those obtained from plates in contact with air. In Figure 2.43 only a few wave reflections were recorded before the signal decayed to an undetectable level.

For comparison, Figure 2.44 shows a typical result obtained from an impact-echo test on the same plate at a location where a void exists in the soil just below the plate. In this case P-wave reflections occur from a concrete/air interface at the bottom of the plate. Because virtually all of the wave energy is reflected at a concrete/air interface, surface displacements caused by the arrival of reflected P-waves decay more slowly compared to those reflected from a concrete/soil interface. The response is essentially the same as that obtained from a simple concrete plate in contact with air. The spectrum exhibits a very sharp, high amplitude peak corresponding to the P-wave thickness frequency. If the concrete slab is relatively thin (about 150mm or less) a lower frequency, lower amplitude peak, labeled f_{flex} in Figure 2.44(c), may also be present, as a result of flexural vibrations of the unsupported portion of the plate above the void. Flexural vibrations occur because the unsupported section above the void is restrained at its edges where it contacts the soil. The response is similar to that produced by an impact above a shallow delamination. However, because the thickness of the slab is relatively large, the amplitude of the flexural vibrations is smaller relative to the P-wave thickness response.

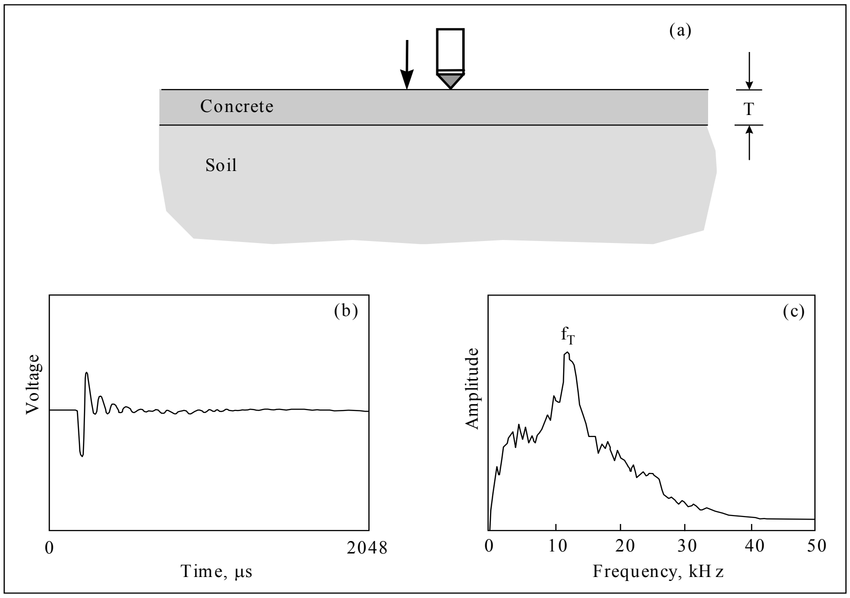

Figure 2.43: The impact-echo response of a concrete slab on soil subgrade; (a) cross-section, (b) waveform, and (c) frequency spectrum. (Sansalone & Streett, 1997)

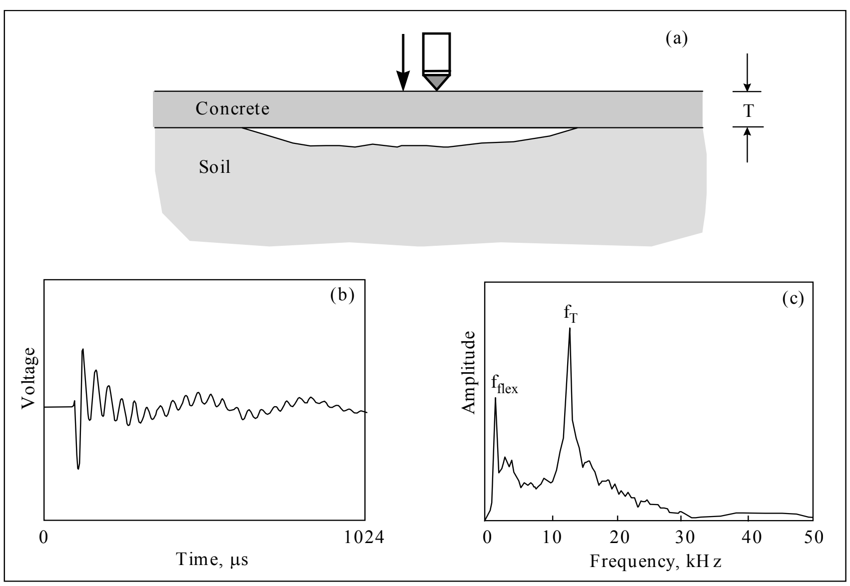

Figure 2.44: The impact-echo response obtained from a concrete slab at a location where a void exists in the soil subgrade; (a) cross-section; (b) waveform; and (c) frequency spectrum. (Sansalone & Streett, 1997)

Steel reinforcing bars

Impact-echo is primary used to locate flaws in, or thickness of, concrete structures. Impact-echo may also be used to determine the location of steel reinforcing, though magnetic or eddy current meters are better suited to this purpose. The acoustical impedance of steel is 5 times that of the concrete. If the sizes of reinforcement bars are known the impact-echo response can be estimated. If information is not known the reinforcing size can be estimated from a cover meter. Impact echo can be applied to evaluate the corrosion of reinforcing bars. The response is similar to solid plates, with single large amplitude peak P-wave thickness frequency. Waves travel around the corroding bar, instead of propagating through it, since the corrosion forms an acoustically soft layer around the bar. Short duration impacts result in peaks at higher frequencies, corresponding to reflections from the corroding surfaces. This method has been able to identify corrosion on reinforcement bars and has proven to be cost-efficient in identifying wall repair locations.

Voids in the tendon ducts of post-tensioned structures

The impact-echo method can be used to detect voids in grouted tendon ducts in many, but not all, situations. The method's applicability depends on the geometry of a structure and the locations and arrangement of tendon ducts. Small voids in tendon ducts cannot be detected if the ratio of the size of the void to its depth beneath the surface is less than about 0.25. In addition, complicated arrangements of multiple ducts, such as often occur in the flanges of concrete I-beams, can preclude detection of voids in some or all of the ducts. In other cases, portions of structures can be successfully tested and information can be gained that permits an engineer to draw conclusions about the condition of the grouting along the length of the duct. The simplest case is that of post-tensioned ducts in a plate structure, such as a bridge deck or the web of a large girder, in which there is only one duct directly beneath the surface at any point. In all cases, the impact- echo method is restricted to situations where the walls of the ducts are metal rather than plastic. Effective use of the impact-echo method for detecting voids in grouted tendon ducts requires knowledge of the location of the ducts within the structure. This information is typically obtained from plans and/or the use of magnetic or eddy-current cover meters to locate the centerlines of the metal ducts. Once the duct locations are known, impact-echo tests can be performed to search for voids.

Metal ducts

Tendon ducts in post-tensioned structures are typically made of steel with a wall thickness of about 1mm (0.04 inches). The space not occupied by tendons inside the duct is (or should be) filled with grout, which has acoustic impedance similar to that of concrete. Because the wall thickness of a duct is small relative to the wavelengths of the stress waves used in impact-echo testing, and because a steel duct is a thin layer of higher acoustic impedance between two materials of lower acoustic impedance (concrete and grout), it is transparent to propagating stress waves. Therefore, the walls of thin metal ducts are not detected by impact-echo tests. (In contrast, plastic ducts have a lower acoustic impedance than concrete or grout, and they are not transparent, complicating attempts to detect voids within plastic ducts)

Benefits to using impact-echo

Applications of the IE method include quality control programs (such as measuring pavement thickness or assessing pile integrity), routine maintenance evaluations to detect cracks, voids, or delaminations in concrete slabs, delineating areas of damage and corrosion in walls, canals, and other concrete structures. Impact echo can be used to assess quality of bonding and condition of tunnel liners, the interface of a concrete overlay on a concrete slab, concrete with asphalt overlay, mineshaft and tunnel liner thickness.

Concrete pavements and structures can be tested in less time, and at lower cost, meaning more pavements and structures can be tested. No damage is done to the concrete and highway workers spend less time in temporary work zones, reducing the chance of injury and minimizing downtime for the traveling public. Impact-echo, according to ASTM, may substitute for core drilling to determine thickness of slabs, pavements, walks, or other plate structures.

Acoustic Emission

Acoustic emission (AE) is defined as a transient elastic wave generated by the rapid release of energy within a material. These deformations can come from plastic deformation such as grain boundary slip, phase transformations, and crack growth. (Davis 1997). Unlike most nondestructive testing techniques, acoustic emission is completely passive in nature. In fact, acoustic emission cannot truly be considered nondestructive, since acoustic signals are only emitted if a permanent, nonreversible deformation occurs inside a material. As such, only nonreversible processes that are often linked to a gradually processing material degradation can be detected (Kaiser & Karbhari 2002). Acoustic emission is used to monitor cracking, slip between concrete and steel reinforcement, failure of strands in prestressing tendons, and fracture or debonding of fibers in fiber reinforced concrete.

Theory

There are two types of acoustic emission signals: continuous signals and burst signals. A continuous emission is a sustained signal level, produced by rapidly occurring emission events such as plastic deformation. A burst emission is a discrete signal related to an individual emission event occurring in a material, such as a crack in concrete. An acoustic emission burst signal is shown in Figure 2.45.

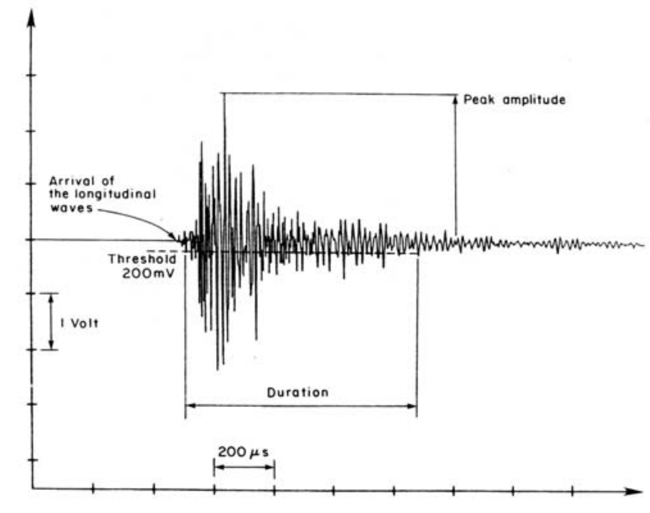

Figure 2.45: Burst acoustic emission signal with properties. (Malhotra 1991)

The term "Acoustic emission signal" is often used interchangeably with acoustic emission. An AE signal is defined as the electrical signal received by the sensor in response to an acoustic wave propogating through the material. The emission is received by the sensor and transformed into a signal, then analyzed by acoustic emission instrumentation, resulting in information about the material that generated the emission.

An acoustic emission system setup is shown in Figure 2.46.

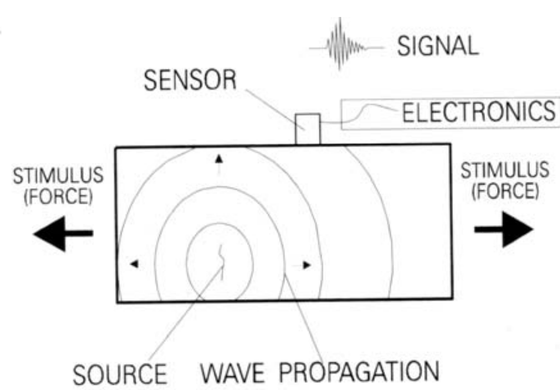

Figure 2.46: Acoustic emission process. (Hellier 2001)

Method development

Acoustic emission testing is used to obtain noise sounds produced by material deformation and fracture. Early terminology for acoustic emission testing was "microseismic activity." AE signals occur when micro or small fractures are detected within the material. The first documented observations of Acoustic Emission activities occurred in 1936 by two men, Forster and Scheil, who detected clicks occurring during the formation of martensite in high-nickel steel. In 1941, research by Obert, who used subaudible noise for prediction of rock bursts, noted that noise rate increased as a structure's load increased. In 1950, Kaiser submitted a PhD thesis entitled "Results and Conclusions of Sound in Metallic Materials Under Tensile Stress" (Scott 1991).

Kaiser's research is considered to be the beginning of acoustic emission as it is known today. In 1954 Schofield became aware of Kaiser's early work, and initiated the first research program in the United States related to materials engineering applications of acoustic emission (Scott 1991).

During the early developmental testing for AE, several correlations were formed. Acoustic emission readings in materials of high toughness differed in amount and size from low toughness material. This was attributed to the differences in failure modes (Scott, 1991). Early acoustic emission testing signals were small and required a relatively calm environment for proper testing. With the use of an additional sensor, background noise could be isolated, which enabled testing to be carried out in a relatively noisy environment. The preliminary results of acoustic emission testing required massive data calculations due to the extensive numerical output the acoustic emission signals produced. This phenomenon distracted scientists, diverting too much of their attention to signal analysis instead of evaluation of the signal itself. Acoustic emission testing proved to be a highly sensitive indicator of crack formation and propagation.

Early use of acoustic emission testing proved to be valuable, but the first acoustic emission signals acquired contained large amounts of noise signals. This made it difficult as scientists were unable to develop AE as a quantitative technique. The material sensitivity and initial research results gave birth to a successful future for acoustic emission as a reliable nondestructive test.

Kaiser effect

One of the most common uses of acoustic emission is in load testing of a structure or specimen. The generation of the acoustic emission signals usually requires the application of a stress to the test object. However, acoustic emissions were found not to occur in concrete that had been unloaded until the previously applied maximum stress was exceeded during reloading (Malhotra 1991). This phenomenon takes place for stress levels below 75 – 85% of ultimate strength and is found to be only temporary. Therefore, it cannot be used to determine the stress history of a structural specimen. Additional theory can be found in several references (Ohtsu et al. 2002; Hearn 1997; Tam & Weng 1995; Yuyama et al. 1992; Malhotra 1991; Scott 1991; Lew et al. 1988).

Equipment and instrumentation

An acoustic emission system has the same basic configuration as seen in ultrasonic testing systems. The typical testing apparatus used for acoustic emission (shown in Figure 2.47 consists of the following:

- Transducer
- Reveiver/Amplifier
- Signal Processors
- Transient Digitizers
- Display
- Calibration Block
- Coupling Agent

Transducer

The acoustic emission transducer is more commonly referred to as a sensor. It is the most important part of the instrumentation. Sensors must be properly mounted to assure the proper configuration to attain the desired signal. Sensors are calibrated using test methods stated by societies. An array of different sensors is shown in Figure 2.48.

An important factor in acoustic monitoring is the location of sensors. For monitoring cases in which the location of a crack or deficiency is known, a single sensor is sufficient for monitoring. However, for the detection of deficiencies in a two dimensional plane or three dimensional solid, the geometric configuration of the sensors is vital to the location of the deficiencies. ASTM Standard Guide for Mounting Piezoelectric Acoustic Emission Sensors specifies guidelines for mounting piezoelectric acoustic emission sensors. The performance of sensors relies heavily upon the methods and procedures used in mounting. Detection of acoustic emission signals requires both appropriate sensor–mounting fixtures and consistent sensor–mounting procedures (ASTM E-650-97).

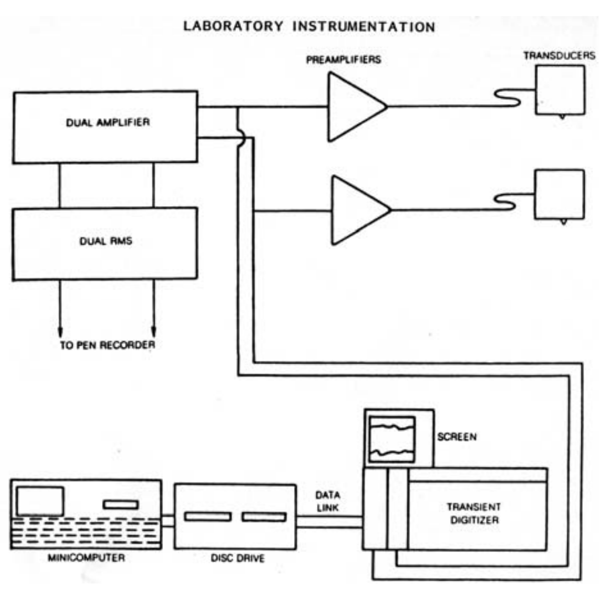

Figure 2.47: Basic setup of acoustic emission equipment. (Miller 1985)

Figure 2.48: Various acoustic emission sensors. (Miller 1985)

Receiver/amplifier

"Receiver" is the term applied to all of the circuit functions that amplify the weak signals and prevent loss in sensor activity. The receiver has four basic components: the preamplifier, the logarithmic amplifier, the rectifier and the low pass amplifier.

The function of the preamplifier is to ensure that any signal from the transducers arrives at the time measuring circuit. Since electrical outputs from the transducer are relatively small, signal amplification is necessary to overcome the resistance from the transducer cable, which can be relatively long. The function of the logarithmic amplifier is to process weak echo signals. Once the echo signals are amplified, the low pass filter processes the signals. After the signal has been processed by the receiver/amplifier, a useable signal can be transmitted to the display. Microprocessor-based systems have become more widely used in recent years. Such units perform single channel analysis, along with source location, for up to eight AE channels.

Signal processors

Signal processors are designed to allow data collection only on certain portions of a load cycle. Envelope processors attempt to filter out the high frequencies, leaving only the signal envelope to be counted. Logarithmic converters allow the output of the signal analyzer electronics to be plotted in logarithmic form. A unit allows combination of several preamplifier outputs so that several sensors can be monitored by one channel of electronics (Reese 1993).

Transient digitizers

Transient digitizers (also called transient recorders) are used to study individual AE burst signals. A signal is digitized in real time and then stored into memory. A transient digitizer is used in sequence with an oscilloscope or spectrum analyzer to display AE signals at visible speeds. Digital rates vary on transient digitizers. The fastest sampling rate becomes the limiting rate, with some instruments sampling up to 1 pulse/ns. Sampling rates can be modified for testing purposes. One advantage of transient digitizers is an additional mode of triggering, the pretriggering mode, where the input signal is continuously being digitized and the data fed into the memory (Reese 1993). This configuration allows a digitized picture of the signal to be displayed as received. More advanced digitizers allow recording of multiple signals simultaneously. The recording of more than one acoustic emission signal is shown in Figure 2.49.

Display

The signal received by acoustic emission test equipment is typically displayed digitally. The display uses an interval timer and a direct reading of display time on an x-y coordinate system. The x-axis displays the time trigger and the y-axis represents the mechanical energy received. The display units can also illustrate defect and anomaly locations and sizes depending on the type of scan request by the user. Older acoustic emission systems used monitors to display received acoustic emission signals, however, most current acoustic emission systems use computer software and monitors to display results.

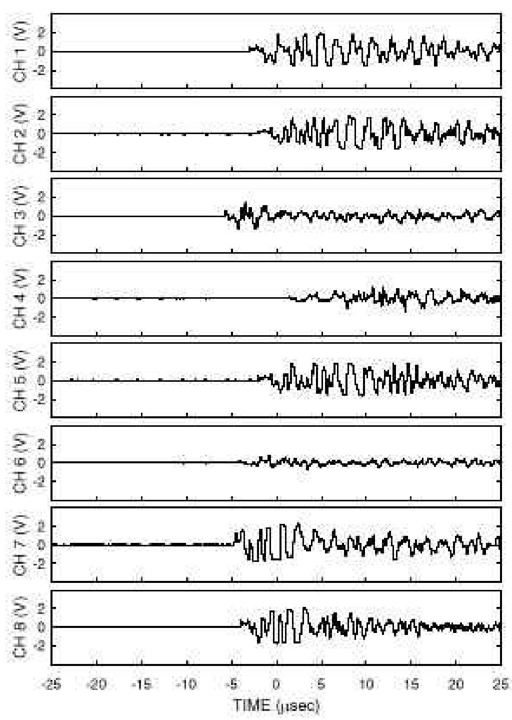

Figure 2.49: Transient recorder with multiple output acoustic emission signals. (Sypeck 1996)

Calibration block

ASTM states that annual calibration and verification of pressure transducers, AE sensors, preamplifiers (if applicable), signal processors, (particularly the signal processor time reference), and AE electronic simulators (waveform generators) should be performed. Equipment should conform to manufacturer's specifications. Instruments should be calibrated to National Institute for Standards and Technology (NIST) (ASTM E 1932-97). An AE electronic simulator, used in making evaluations, must have each channel respond with a peak amplitude reading within ± 2dBV of the electronic waveform output. (ASTM E 1932-97) Figure 2.50 is a photograph of a typical calibration block.

A system performance check should be done immediately before and after an acoustic emission examination. The preferred technique is the pencil lead break test. A description of the test procedure is described in ASTM E 750-98.

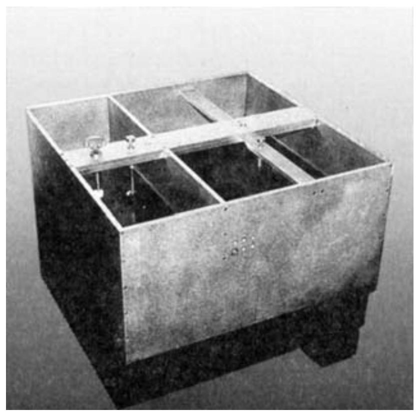

Figure 2.50: Acoustic emission calibration block.

Acoustic emission signals are introduced into the structure and examined on an oscilloscope or with an AE system used in the test. If any doubt occurs in the sensor's response, it should be remounted. Three sources of the acoustic signal are the Hsu–pencil source, the gas–jet, and the electrical pulse to another sensor mounted on the structure. A description of the sources can be found in ASTM E-976. Two types of verification are periodic verification and post verification. ASTM defines periodic verification as the verification of the sensors periodically during the test. Post verification is defined as verifying the condition of the sensors to be in working condition at the end of the test.

Coupling agent

A coupling agent is usually required to ensure the efficient transfer of mechanical energy between the tested material and the transducer. The purpose of placing the coupling material between the transducer and test specimen is to eliminate air between the contact surfaces. Typical coupling agents are viscous liquids such as grease, petroleum jelly, and water-soluble jelly.

In acoustic emission testing it is common to bond the sensors to the test specimen. This setup is used for tong term testing or monitoring of structures and specimens. When applying bonds, it is possible to damage the sensor or the surface of the structure during sensor removal.

Evaluation of acoustic emission activity

Acoustic emission activity may be determined as the cumulative acoustic emission or as an event count. Analysis techniques should be uniform and repeatable. Techniques of evaluation include event counting, rise time, signal duration, frequency analysis and energy analysis. Field and laboratory evaluations include damage analysis and proof loading. The measurement of the acoustic emission count rate is one of the easiest and most applicable methods of analyzing acoustic emission data (Reese 1993). Acoustic emission count indicates the occurrence of acoustic emission and gives a rough estimate of the rate and amount of emission. The amplified signal is fed into an electronic counter. The counter output is often transformed by a digital-to-analog converter so that it can be plotted on a X-Y recorder (Reese 1993).

An event count will result in the number of burst emissions signals that are produced during an event. An acoustic emission event is defined as a detected acoustic emission burst. This means that an acoustic emission event describes the acoustic emission signal and not the acoustic emission. For the event count to be correct, the decay constants of the AE signals must be the same. A mixture of decay constants will often confuse the event-counting circuitry (Reese 1993).

For most experiments, the count or the energy per event will give about the same results (Reese, 1993). Acoustic emission bursts are larger when a loaded specimen is approaching failure. It is only when there is a change in either the damping factor or the frequency that the energy per event is the better parameter (Reese, 1993). The energy released per event will result in the amount of AE signals received.

Signal rise time

The signal rise time can be defined as the interval between the time when the AE signal is first detectable above the noise level and the time when the peak amplitude occurs (Reese 1993). Rise depends on the distance between the acoustic emission source and the sensor. It can help to determine the type of damage mechanism.

Signal duration

Signal duration is defined as the length of time that the burst emission signal is detectable It is dependent upon the preamplifier noise level and detection of the signal. A trigger circuit is used to stop and start a separate counter that counts clock pulses. The signal duration is independent of the frequency content of the burst signal. The signal duration method is useful when repeating the same test. A change in either the average signal duration or the distribution of durations can indicate either a change in the signal path to the sensor or a change in the generating mechanism (Reese, 1993

Sensor location

Determination of the number of sensors required for the test, their placement strategy and location on the part to be monitored is needed. Placement of sensors on a concrete specimen during a fiber pull-out test is shown in Figure 2.51.

A single sensor used near the expected source of AE is sufficient when background noise can be controlled or does not exist. When background noise is limited, the use of a single AE data sensor near the expected source plus guard sensors near any background source will suffice. ASTM defines a guard sensor as one whose primary function is the elimination of extraneous noise based on arrival sequences. The guard sensors will effectively block noises that emanate from a region closer to the guard sensors than to the AE data sensor. Another technique involves the placement of two or more sensors to perform spatial discrimination of background noise and allow AE events to occur. ASTM defines *spatial discrimination* as the process of using one or more guard and data sensors to eliminate extraneous noise. In situations where irrelevant noise cannot be controlled during testing and could be emanating from any and all directions, a multiple sensor location strategy should be considered. Using a linear or planar location strategy will allow for an accurate source location of the acoustic emission. Applications of spatial filtering and/or spatial discrimination will only allow data emanating from the region of interest to be processed as relevant AE data.

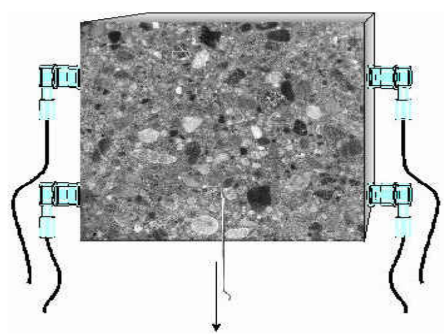

Figure 2.51: Placement of sensors on a concrete cube.

Applications of acoustic emission

Acoustic emission has been used to determine the integrity of various materials, including metal and alloys, welds, forgings and castings. Acoustic emission has been applied to concrete in an effort to nondestructively evaluate in situ concrete for load testing and structural monitoring.

Load testing

The most successful application of acoustic emission is detecting the presence of discontinuities or cracks, and their location, in concrete specimens and structures. Perhaps the most researched application of acoustic emission testing has been used in the load testing of concrete structures and specimens. Since acoustic emission is a passive nondestructive testing technique, acoustic signals are only emitted if a permanent, nonreversible deformation occurs inside a material. Therefore, acoustic emission is extremely useful for detecting the formation of cracks and microcracks occurring in concrete structures.

Consideration of the load intensity in relation to the integrity of the test object results in the success of an acoustic emission examination. Applied load is defined by ASTM as the controlled or known force or stress that is applied to an object under test for the purpose of analyzing the object's reaction by means of acoustic emission monitoring of that stress. If the load is not of sufficient intensity, the tested object will not undergo sufficient stress and will not produce acoustic emissions. If the applied load is part of the monitoring process, a suitable time for acoustic emission examination is when process noise is low and the applied load at a maximum. Appropriate stress levels are used to excite the "latent defects" without damaging the object (ASTM E-1932-97).

A reinforced concrete slab under fatigue loading from the initial loading to final failure in the laboratory was compared to the acoustic emission monitoring of reinforced concrete slabs under traffic loading by comparing visual observations of cracking processes and acoustic emission source location (Yuyama et al. 1992). The experiment concluded that, by comparing crack density history and acoustic emission activity history, cracking processes under fatigue loading can be predicted and evaluated by monitoring the acoustic emission signals. The research paper also revealed that the damaged area due to cracking can be roughly identified by the acoustic emission source location.

One valuable conclusion from laboratory testing is that the area of reinforced concrete near the initial emanation of acoustic emission signals will result in the cracking area during the final load. The fatigue process in reinforced concrete structures can be evaluated by periodically monitoring these structures under service loads (Yuyama et al. 1992).

A fundamental study was made of acoustic emissions generated in the joint of rigid frames of reinforced concrete under cyclic loading. The test concluded that different acoustic emission sources, such as tensile cracks or shear cracks, could be clearly discriminated by comparing the results of the visual observation and the crack width measurement (Yuyama et al. 1992).

Studies have been performed on fiber reinforced concrete specimens to observe the response of fiber reinforced concrete to loading. Based on the experiment, several conclusions can be drawn. The examination of acoustic emission activities and source location maps reveal that the microscopic fracture response recorded by acoustic emission monitoring is consistent with the macroscopic deformation of the material. Steel fibers are more efficient than PVA fibers in blunting microcrack nucleation (Li & Li 2000).

Structural monitoring

Most highway bridge inspection is performed via visual inspection. When deficiencies are observed, the action taken usually involves increased inspection of the defective area. Given that the rate of deterioration is usually unknown, the frequency of inspection is increased without a reasonable forecast of the behavior of the defect. Acoustic emission testing utilizes the induced stress waves that are released when microstructural damage occurs. This passive NDT technique is commonly referred to as structural health monitoring.

At present, portable AE sensors are available for the continuous monitoring of known flaws. Research to date has provided a reasonable scientific base upon which to build an application of acoustic emission as part of a bridge management program (Sison et al. 1996). This technique could be best utilized by implementing a continuous monitoring system with an array of sensors on newly constructed bridges. The technology is available for instrumentation configured with portable data acquisition and transfer systems, making it possible for engineers to continuously monitor bridge condition. Engineers could use the information gained via AE systems to decrease the frequency of inspection on sound structures and monitor profound AE events to determine the need for essential inspections.

Other successful uses of AE have been applied to leak detection in tanks, pipelines, and conduits. It has also been used to monitor the integrity of dams and other mass concrete construction.

Impulse Response

The impulse response (IR) test has several applications relating to civil engineering and to the condition assessment of structures. Researchers originally developed it in the 1960's for evaluating the integrity of concrete drilled shafts. Engineers are less familiar with its widespread capabilities in relation to testing of reinforced concrete structural components such as floors, pavement slabs, bridge decks and other structures. The impulse response technique is similar to the impact-echo test method previously discussed in this chapter. Though the two methods are quite similar in theory, they differ in several respects, such as having different uses.

In essence, the IR method is a fast, coarse method of evaluating structures while the alternative methods are for more detailed investigations. The IR method is likened to a vague diagnosis made by a family doctor and subsequently referred to a medical specialist for further diagnosis.

Testing equipment

The impulse response method uses a low-strain impact to propagate stress waves through an element. Most testing apparatuses are comprised of a one-kilogram sledgehammer with a load cell in the head. The hammer has a fifty-millimeter diameter double-sided head. One end is rubber-tipped for low stress level impacts, typically around 700 psi, while the other is aluminum-tipped for impacts that can reach stress levels of more than 7000 psi.

A structure's response to the impact is measured by a geophone. Both the geophone and the instrumented hammer are linked to a portable computer for data acquisition. Figure 2.52 is a photograph of a hammer and geophone. Figure 2.53 is a schematic of the typical equipment setup.

Principles of the impulse response method

Most acoustic testing techniques are based on stress-wave propagation theory and monitor the behavior of such waves as they travel through a material. The impulse response method differs from this approach; it instead measures the response of the tested material to the impact itself.

Figure 2.52: The instrumented sledgehammer and geophone used in the IR method. (Davis 2003)

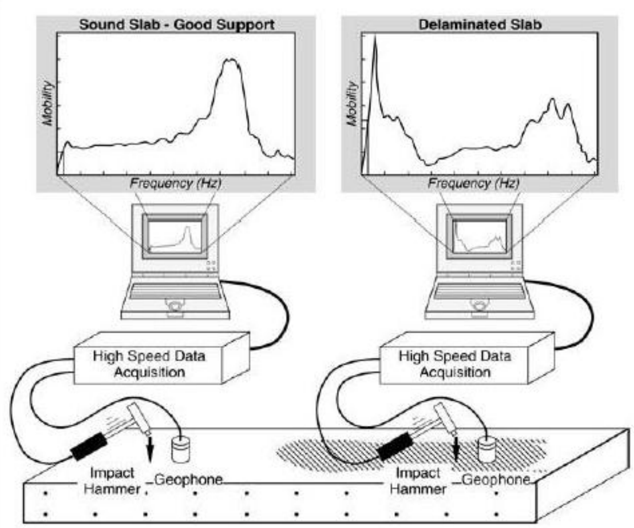

Figure 2.53: Schematic of the impulse response technique. (Davis 2003)

Since the stress that is applied to a structure in the IR test is quite large, the structure responds to the impact in a bending mode over a relatively low frequency range (0 – 1000 Hz). This differs from structures being evaluated with the impact-echo method, which would respond to the generated stress waves in a reflective mode over a higher frequency range.

When testing a structure using the impulse response method, a geophone is placed upon the surface that is then struck with the instrumented sledgehammer. The geophone is usually attached to the surface of the concrete so that it can act in the same plane as the hammer blow. The time records for the hammer force and the velocity response from the transducer are received by the computer as voltage-time signals and then processed using the Fast Fourier Transform (FFT) algorithm. At that point, velocity and force spectra are generated, and the velocity spectrum is divided by the force spectrum, yielding a transfer function more commonly known as the mobility of the structure. A plot of mobility versus frequency can be generated. This plot represents velocity per unit force versus frequency and provides information regarding the condition of the structure being tested. Additional material properties that can be obtained include dynamic stiffness, mobility and damping, and the peak/mean mobility ratio.

The transfer function

When an IR test is performed, the data gathered can be used to generate force and velocity spectra. The velocity spectrum is divided by the force spectrum to produce a transfer function more commonly referred to as the mobility of the structure. A theoretical impulse response spectrum is shown below in Figure 2.54.

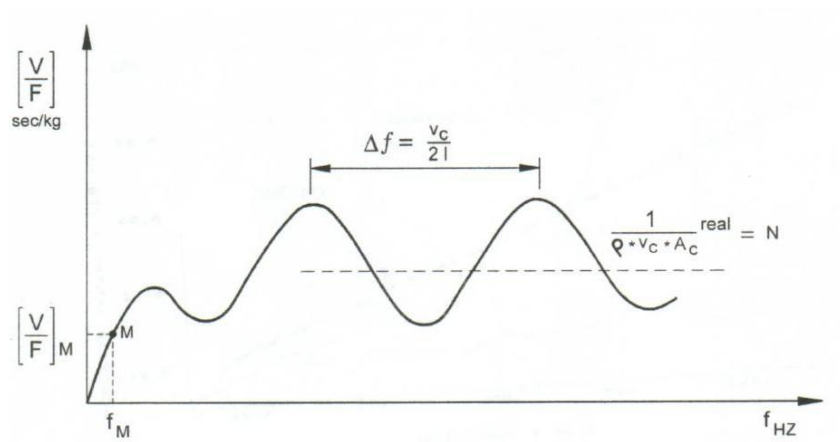

Figure 2.54: Theoretical impulse response mobility spectrum.

The first portion of the transfer function is the dynamic stiffness portion (usually in the range of 0 – 100 Hz), which has a linear slope. This linear slope quantifies the flexibility of the area around the test point for a normalized force input. The dynamic stiffness of the material is the inverse of this flexibility.

The mobility of the structure being tested is the quotient of the velocity spectrum divided by the force spectrum, typically expressed in units of seconds per kilogram. The average mobility value over the frequency range of 100 - 1000 Hz is related to the thickness and the density of the specimen. Above a frequency level of approximately 100 Hz the measured mobility value oscillates around an average mobility value, *N*, which is a function of the specimen's thickness and its elastic properties. A reduction in thickness of the specimen correlates to an increase in average mobility. Figure 2.55 is a schematic of a typical mobility plot.

When a material is impacted, an elastic wave is generated. The decay of the spectral amplitude is due to the energy losses attributed to friction as the wave propagates through the solid matrix. When cracking, honeycombing or consolidation voids are present in the concrete, there will be an associated reduction in the damping and stability of the mobility plots over the frequency range that is evaluated.

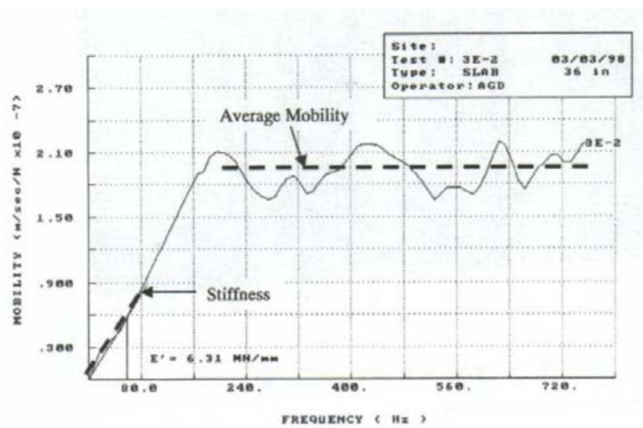

Figure 2.55: Typical mobility plot for sound concrete. (Davis 2003)

Peak/mean mobility ratio

When there is an area below a slab on grade that has been undermined, or there are debonding or delaminations present within a concrete sample, the response behavior of the uppermost layer controls the results of the IR test. There will be a noticeable increase in average mobility between the frequency range of 100 to 1000 Hz, and the dynamic stiffness will be considerably reduced. The ratio of this peak to the mean mobility is an indicator of loss of support below a slab on grade or the presence and degree of debonding within the sample. This concept is illustrated in Figure 2.56. Notice that the mobility of the concrete in the upper curve is considerably more than the mobility of the sound concrete shown in the lower curve.

The impulse response test is capable of detecting delaminations up to nine inches below the surface of a structure. Traditional methods, such as acoustic sounding, are able to detect concrete deficiencies up to approximately two to three inches below the surface. The impulse response method is able to test for delaminations through asphalt overlays when ambient temperatures are low enough to preserve relatively high asphalt stiffness. Figure 2.57 depicts typical mobility plots for sound and delaminated concrete.

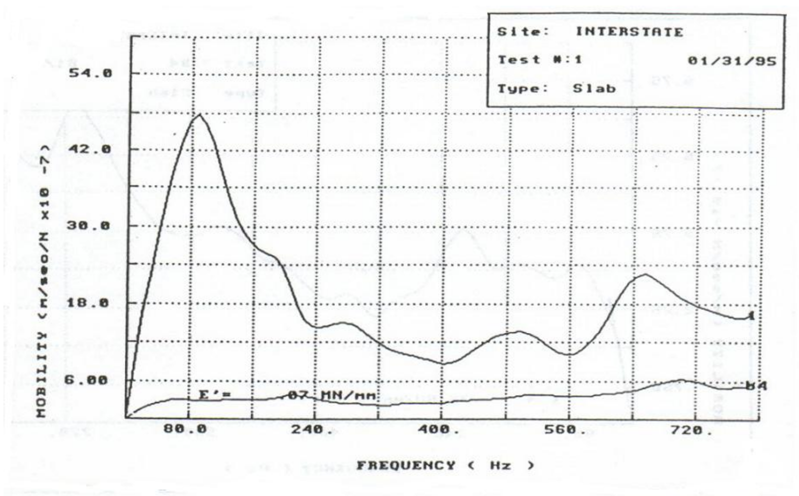

Figure 2.56: Mobility plots for sound and debonded concrete. (Davis et al. 2001)

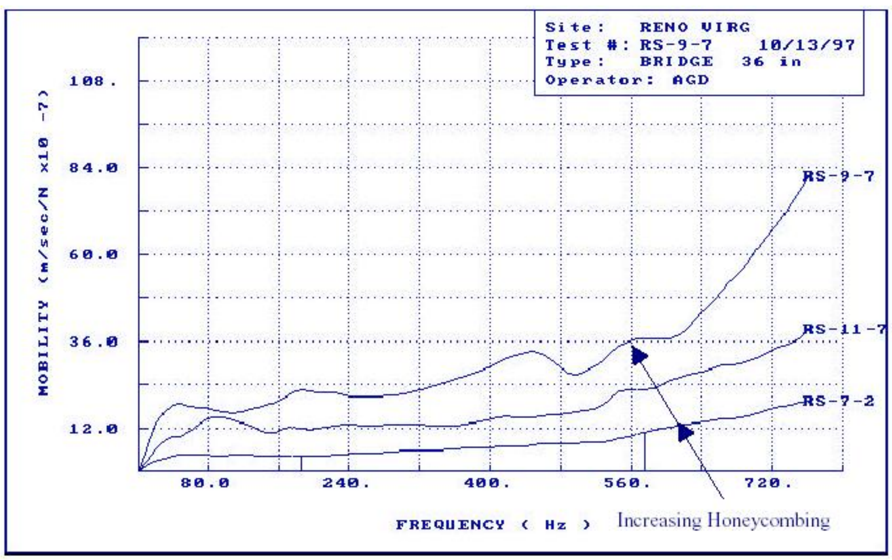

Figure 2.57: Mobility plots for sound and delaminated concrete. (Davis et al. 2001)

Further development for concrete applications

The inspection industry has focused on the practicality of this testing method, which has resulted in the development of more efficient testing procedures. Improvements have focused mainly on more rapid data acquisition and the storage of data from testing of large concrete surfaces, with computer extraction of the IR stiffness and mobility parameters for each test result. The time required for the impulse response method to perform the "family doctor" version of testing is approximately five percent of the time it would take for the impact-echo method to assess the same area.

In the early 1990's, the Federal Highways Administration (FHWA) published a report regarding the evaluation of bored concrete piles; the IR method was a less reliable test method than the cross-hole sonic logging method. Although the IR method has not been used in North America for evaluation of pile integrity, it is still applicable for material testing in other capacitates.

Magnetic Methods

Materials containing iron, nickel, cobalt, gadolinium and dysprosium have a high degree of magnetic alignment to each other and to themselves when they are magnetized. Therefore, they are called ferromagnetic materials. Other materials such as oxygen are faintly attracted or repelled by a magnetic field. These materials are referred to as paramagnetic materials. Diamagnetic materials have the magnetic equivalent of induced electric dipole moments, which are present in all substances. However, this is such a weak effect that its presence is masked in substances made of atoms that have a permanent fixed magnetic dipole moment.

The idea of using magnetic techniques for nondestructive testing and evaluation of ferromagnetic materials originated in 1905. In 1922, E.W Hoke was granted the first United States patent on a particular ferromagnetic inspection method. In recent history, this inspection technique has been used in the petroleum, aerospace and automotive industries, as well as in other industries that require quality control of ferromagnetic materials.

Magnetic fields

A magnetic field is a volume of space containing energy that magnetizes a ferromagnetic material. The magnetic field is created by the introduction of electric current and perturbates outward in a radial pattern. Figure 2.58 is a schematic of a typical magnetic field induced by an electrical current. The density of the magnetic lines, referred to as the flux density, increases when the field strength and the magnetic permeability increase.

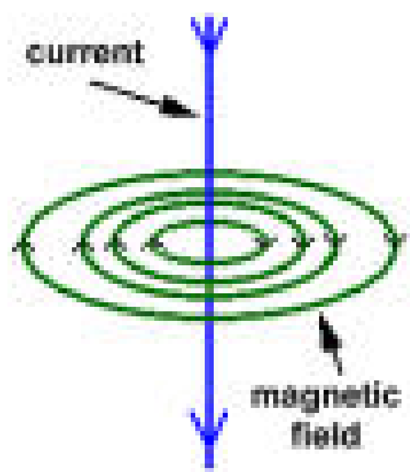

Figure 2.58: Schematic of a typical magnetic field induced by an electric current.

Types of magnetizing energy

Two sources of magnetizing energy used in magnetic testing are permanent magnets and electric currents. Permanent magnets usually consist of bar or horseshoe configurations. They are inexpensive methods of magnetization but are limited by a lack of control of field strength and the difficulty of removing strong permanent magnets from the tested specimens. The horseshoe type of magnet forms a uniform longitudinal field between the poles. It provides low levels of magnetization. Electric currents characterize the second category of magnetizing energy. Longitudinal or circular fields can be formed by the correct implementation of electric currents. Direct current (DC), alternating current (AC), and rectified alternating current are used to magnetize test materials. DC and rectified AC penetrate deeper into a material than AC, primarily due to a phenomenon called the "skin effect". The skin effect is more defined in ferromagnetic materials than in nonmagnetic types of materials. Thus, DC or rectified AC is used when test requirements include the detection of deep flaws.

Magnetization classifications

The most common magnetization techniques are classified as direct or indirect. Direct magnetization involves the passage of an electric current through a material. Indirect magnetization is caused by an adjacent magnetic field, which is excited by current flow through a portion of the material.

Magnetic flux leakage

Magnetic flux leakage (MFL), formerly referred to as magnetic field perturbation testing (MFP), consists of subjecting a magnetically permeable material to a magnetic field. The field strength requirements depend on the permeability of the material and the sensitivity of the test probes.
The principles of magneto-statics demonstrate that when a homogeneous magnetically permeable material is immersed in a static, uniform, external magnetic field, the magnetic field within the material approaches the same magnitude as the magnetic field in which it is immersed. These perturbed fields are called leakage fields due to the "leakage" of magnetic flux out of the material and into the air. Leakage is caused by the reduction in cross-sectional area of the magnetic material due to the anomaly.

Inspections using magnetic flux leakage techniques

The preferred characteristic of the MFL technique is that mechanical contact with the test specimen is not necessary. In many cases, both the exciting coil and the sensing coil may be operated without directly contacting the material. This advantage has particular importance in the structural concrete industry. Another benefit of MFL is that it requires no specific surface preparation other than cleaning. This method is easily automated for high-speed, detailed testing. It is also useful for identifying surface cracks, near-surface inclusions, and nonmagnetic coating thickness on a permeable base, as well as in monitoring physical and mechanical properties that cause changes in magnetic permeability. Sensitivity is limited by ambient noise and magnetic fields. The test specimen must be magnetically saturated, thereby limiting demagnetization concerns. The extreme sensitivity of the method has been utilized to detect surface cracks and subsurface inclusions on the order of 0.3 mm.

The magnetic flux leakage method has been applied to the determination of nonmagnetic coating thickness, the depth of case hardening, and the carbon content of a material. Another major application has been in testing steel bearing raceways and gear teeth. In its most refined form, MFL is one of the most sensitive methods for the detection of surface and near-surface cracks and flaws in ferromagnetic materials.

Electric current injection

The Electric Current Injection (ECI) technique, also called the eddy current method, is an extension of the magnetic field perturbation method. It is used in materials that are electrically conductive but not magnetically permeable. ECI is classified as a non-particulate magnetic field method. The parameter sensed is the magnetic field perturbation near the surface of the test object. This testing method is carried out by inducing an electric current between two points of an electric current. Defects and flaws are obtained by recording the magnetic field signals in a manner similar to the MFP method.

Applications to concrete

Currently, magnetic testing methods have no relevant use in the nondestructive testing of concrete itself. Concrete is nonmagnetic in nature, so the use of magnetic flux leakage for the detection of flaws and anomalies in concrete devoid of reinforcing steel is insignificant. However, the use of magnetic methods for the inspection of ferromagnetic materials embedded within concrete structures has proven to be extremely valuable. Magnetic methods have been applied to detect defects in prestressing tendons and steel rebar within concrete structures. They have proven effective in the detection and location of embedded steel.

Covermeter

The concrete covermeter, also referred to as the pacometer, was developed in 1951 in England. Since its original development, the covermeter has gone through several generations of revisions. Presently available, systems are reasonably priced for use in inspection. A photograph of a typical covermeter shown in Figure 2.59.

Figure 2.59: Covermeter used by the Civil Engineering Dept at the University of Florida

The principle operation of the covermeter is based on ferromagnetic principles. The covermeter detects a bar by briefly magnetizing it, then registering the magnetic field as it tapers off. The typical configuration of the covermeter testing technique is depicted in Figure 2.60. The covermeter utilizes the eddy current method of magnetic testing. This method induces "eddy-currents" to flow around the circumference of the bar, producing a magnetic field. The head of the device picks up the magnetic signal. Pulse techniques separate the received signal from the transmitted one. Therefore, no signal is produced in the absence of a metallic material. The strength of the induced magnetic field primarily depends on the depth of the ferromagnetic element beneath the probe and the size of the element being detected. The concrete industry primarily uses covermeters to detect the presence, size, and depth of rebars.

Figure 2.60: Typical configuration of covermeter testing apparatus.

Applications of magnetic flux leakage

Magnetic flux leakage has been effectively applied to the detection of deficiencies in steel members within concrete structures. The use of an array system has successfully identified ruptures of steel in prestressed tendons and rebar cracks in bridge decks (Krause et al. 2002).

Due to the extreme sensitivity of magnetic flux leakage sensors, the system is well suited for condition monitoring of the steel components in bridge decks. Slight changes in the metallic structure of embedded steel and tendons can be detected in order to monitor the onset of damage in the metallic components of bridge structures.

Ground Penetrating Radar

The ground penetrating radar (GPR) method uses reflected waves to construct an image of the subsurface, in much the same way as seismic-reflection profiling. The source consists of a transmitter loop, which emits a short pulse of high-frequency (10 - 1000 MHz) electromagnetic energy into the ground. The reflection response is measured using a receiver loop, which is generally kept at a fixed distance from the transmitter. GPR is used in a variety of applications including soil stratigraphy, groundwater flow studies, mapping bedrock fractures, determining depth to the water table, and measuring the thickness of glaciers (Malhorta & Carino 1991).

Theory

Both the GPR and ultrasonic pulse velocity techniques involve pulsing waves into a solid material. GPR differs from ultrasonics since it uses radar waves rather than stress waves. Radar waves and stress waves behave in a similar manner when introduced into a solid. GPR is governed by the reflection of the wavefronts in the host material in the same manner as the stress waves produced during impact-echo and ultrasonic testing. The basic theory behind GPR is analogous to the theory discussed in the impact echo section of this paper and will not be restated here.

In principle, the propagation of radar waves, or signals, is affected by the dielectric properties of the media, so that the attenuation and reflected components vary accordingly (Colla & Brunside 1998). Concrete is a low loss dielectric material, with the exception of any metal which may be present within the concrete. When an electromagnetic signal passes through a dielectric medium, the amplitude will be attenuated (Casas et al. 1996). The main parameter which controls the subsurface response is the dielectric constant, K^*, which is a dimensionless and complex number. The velocity at which radar signals propagate is given by:

$$v = \frac{c}{K^{1/2}} \qquad \text{--------} \ [15]$$

where the speed of light $c = 3\times10^8$ m/s, and K is the real part of K^*. Reflections occur when a radar pulse strikes a boundary where there is an abrupt change in the dielectric constant. The reflection coefficient, which represents the ratio of reflected-wave amplitude to the incident wave, is given by:

$$R = \frac{K_2^{1/2} - K_1^{1/2}}{K_1^{1/2} + K_2^{1/2}} \qquad \text{-------- [16]}$$

Equations 15 and 16 are the principle equations upon which the theory of GPR is based. The wave velocity and reflection coefficient of dissimilar materials within the same medium can be distinguished subsequent to signal processing.

Instrumentation

The use of ground penetrating radar is fairly popular within the geological and geophysical fields throughout the world. Although GPR is becoming increasingly popular for the nondestructive testing of concrete structures, it is a highly specialized system. The primary components in a radar system are a waveform generator, an antenna, a signal processing unit and a display unit.

Generator

Waveform generators are used to transmit a signal to the antenna. The signal can be a continuous or a pulsed excitation signal, which is then transmitted into the test material. Generators are capable of emitting varying or continuous frequencies of signals depending on the type of testing being performed.

Antenna

Antennas for GPR radiate and receive electromagnetic waves. The GPR antenna performs basically the same functions as the "head" of the covermeter device. However, instead of using magnetic fields, it sends and receives an electromagnetic beam. The beam is usually driven at 1 GHz for use in concrete and is much more focused than the excitation fields utilized in the covermeter device. The dipole antenna is most commonly used today. It is a contact based antenna that provides a diverging beam. Alternatively, the horn antenna employs a more focused beam and has found use in vehicle-mounted surveying of highway and bridge decks, where the antenna is usually located 30cm above the surface of inspection (Kaiser & Karbhari 2002).

Display

Most of the GPR systems in service today employ a visual display that instantaneously produces an image of the scan. An oscilloscope produces the image after the antenna receives it. Internal discontinuities are produced by the reflected signal and are visualized through the use of grayscale or color. Figure 2.61 shows a typical GPR scan.

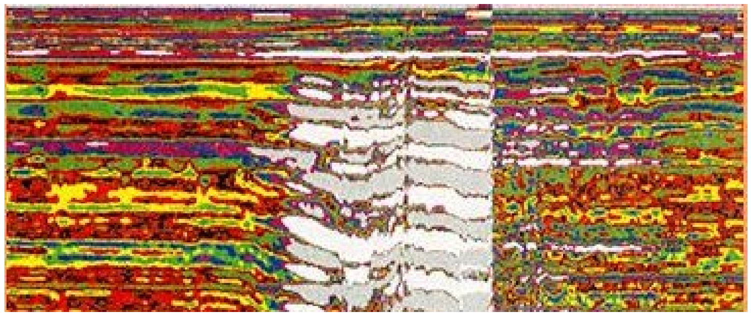

Figure 2.61: Typical display of a GPR Scan. The white portion denotes an anomaly.

Applications

GPR has been studied and applied to the nondestructive testing of materials for the past several decades. Several successful applications of GPR in the concrete industry include (Casas et al. 1996):

- the identification of reinforcing bars in concrete
- the identification of large cracks and voids in concrete
- concrete quality and appraisal
- duct location in post-tensioned bridges
- void identification in post-tensioned ducts

A logical classification for GPR would be to include it as a qualitative NDT technique that can effectively be used to aid in structural condition assessment and evaluation. Its performance in the rapid detection of anomalies embedded in concrete structures is an extremely valuable tool for inspectors, especially when identifying problems with post-tensioned ducts. The proper grouting of post-tensioned bridge structures has been a prevalent problem throughout the state of Florida for the past several decades. GPR offers an immediate inspection method that would enable owners of bridges to inspect the quality of post-tensioned structures before closing future contracts.

Resonant Frequency

Powers originally developed the resonant frequency method in 1938. He discovered that the resonant frequency of a material can be matched with a harmonic tone produced by materials when tapped with a hammer (Malhorta & Carino 1991). Since then, the method has evolved and incorporated the use of electrical equipment for measurement.

Theory

An important property of any elastic material is its natural frequency of vibration. A material's natural frequency of vibration can be related to its density and dynamic modulus of elasticity. Durability studies of concrete materials have been performed indirectly using resonant frequency as an indicator of strength and static modulus of elasticity. These relationships for resonant frequency were originally derived for homogenous and elastic materials. However, the method also applies to concrete specimens if the specimens are large in relation to their constituent materials. (Malhorta & Carino 1991).

The study of physics has determined resonant frequencies for many shapes, including slender rods, cylinders, cubes, prisms and various other regular three-dimensional objects. Young's dynamic modulus of elasticity of a specimen can be calculated from the fundamental frequency of vibration of a specimen according to Equation 17 (Malhorta & Carino 1991).

$$E = \frac{4\pi^2 L^4 N^2 d}{m^4 k^2} \qquad \text{-------- [17]}$$

Where:

E = Young's dynamic modulus of elasticity
d = density of the material
L = length of the specimen
N = fundamental flexural frequency
k = the radius of gyration about the bending axis
m = a constant (4.73)

Testing

ASTM has created a standard test that covers measurement of the fundamental transverse, longitudinal and torsional resonant frequencies of concrete specimens for the purpose of calculating dynamic Young's Modulus of elasticity. (C-215-97, 2001) This test method calculates the resonant frequencies using two types of procedures, the forced resonance method or the impact resonance method.

The forced resonance method is more commonly used than the impact resonance method due to the ease of testing and interpretation of results. The forced vibration method uses a vibration generator to induce vibration in the test specimen while the vibration pickup transducer is coupled to the specimen. The driving frequency is varied until the pickup signal reaches a peak voltage. The specimen's maximum response to the induced vibration occurs at the resonant frequency. Figure 2.62 illustrates the typical setup of a resonant frequency device. The vibration generator is coupled to the right side of the specimen while the pickup is coupled to the left.

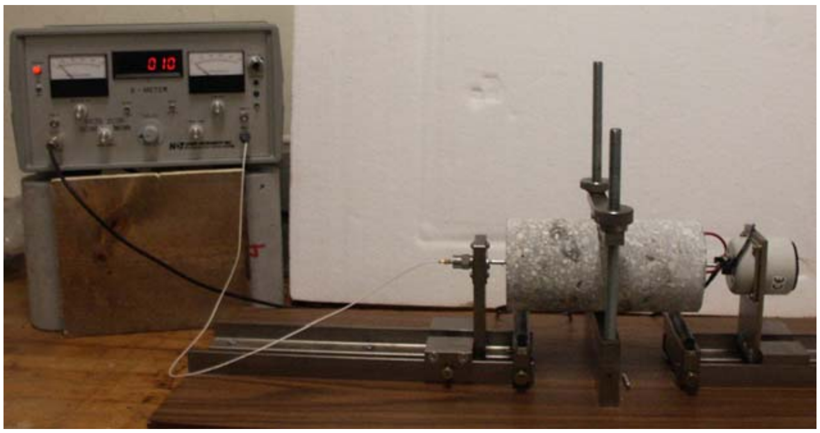

Figure 2.62: Typical forced resonant frequency setup.

The impact resonance method is similar to the impact-echo and impulse response methods. The impact resonance method employs a small impactor to induce a stress wave into the specimen. However, the forced resonant frequency method uses a lightweight accelerometer to measure the output signal. The signal is then processed to isolate the fundamental frequency of vibration.

The standard test method is limited to the testing of laboratory specimens (i.e. cylinders or prisms), and at present there is no standardized method applying the use of resonant frequency to larger specimens or to specimens of irregular shape.

Limitations

The resonant frequency method has been successfully applied to the nondestructive testing of laboratory specimens. The test is somewhat limited by a number of inherent problems in the method. Resonant frequency testing is usually performed on test specimens to non-destructively calculate cylinder compressive strength. However, the test actually calculates the dynamic modulus of elasticity. Extensive laboratory testing has revealed that cylinder compressive strength and dynamic modulus of elasticity are not an exact correlation. Thus, when concrete strength is extrapolated from resonant frequency testing, two sources of error exist. The first source of error is experimental error, which can be fairly significant when performing the resonant frequency test. “Limited data are available on the reproducibility of the dynamic modulus of elasticity based on resonance tests” (Malhorta & Carino 1991, p155). The second source of error is the assumption that has to be made when converting dynamic modulus to compressive strength. Since the correlation between the two properties is not absolute, sources of error will be present in any modulus to strength conversion. Figure 2.63 graphically displays the experimental results obtained relating cylinder compressive strength with dynamic modulus of elasticity. The experimental data can be predicted within ±10% assuming the results from a given resonant frequency test have zero error. In reality, converting dynamic elasticity to compressive strength would yield an uncertainty greater than ±10%.

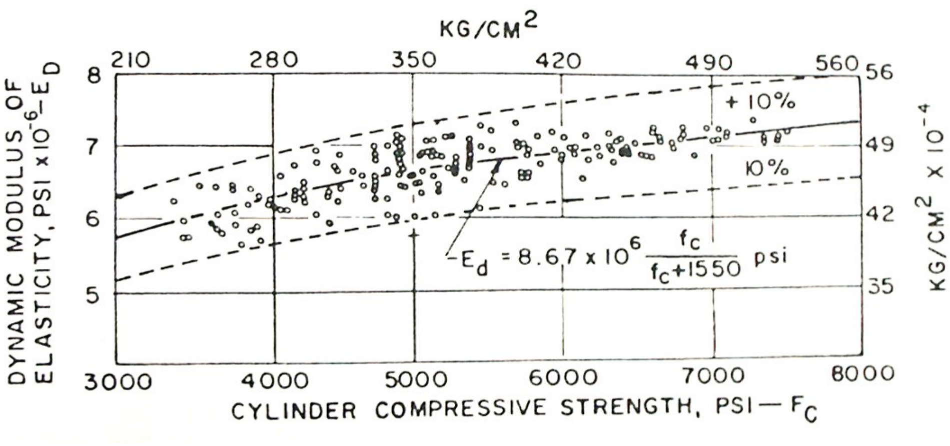

Figure 2.63: Dynamic modulus of elasticity vs. cylinder compressive strength. (Malhorta & Carino 1991)

Applications

Resonant frequency can be a useful tool for detecting material changes regardless of whether an actual dynamic modulus or compressive strength can be calculated. Resonant frequency can be used to measure qualitative changes in a material property if used as a monitoring technique. The existence of structural damage in an engineering system leads to a modification of the modal parameters, one of which is resonant frequency.

It is possible to monitor a given complex structural element with shape parameters that prohibit an accurate calculation of geometric parameters such as radius of gyration or density. Complex structures are often too large or have immeasurable properties, such as the exact location of internal steel members, to extract relatively simple material properties that are easily calculated in the laboratory setting. However, when used as a quantitative technique resonant frequency can detect material changes between tests. A review of methods of damage detection using natural frequencies has shown that the approach is potentially practical for the routine integrity assessment of concrete structures (Salawu 1997). Using the natural frequency changes of a structure may not be useful for identifying the location and assessment of specific cracks and anomalies within a structure. The technique can detect changes in a structure or structural element, if an acceptable baseline is established at the time of construction.

Infrared Thermography

Infrared thermography (IRT) is a non-destructive evaluation (NDE) technique that characterizes the properties of a material by monitoring its response to thermal loading. The term "*thermal loading*" is commonly used to describe the transfer of energy from a heat source to a solid object. This technique is currently being used on an array of structures and materials ranging from carbon fiber reinforced polymers (CFRP) to human teeth. Due to this widespread applicability, the field of IRT has grown considerably in recent years. Recently, IR has been used for the nondestructive examination of concrete structures and structural repairs.

Theory

The term "infrared" refers to a specific portion of the electromagnetic spectrum containing waves with frequencies just less than those of red visible light, *infra*red means less than red. Figure 2.64 illustrates the electromagnetic spectrum, depicting where infrared waves are classified.

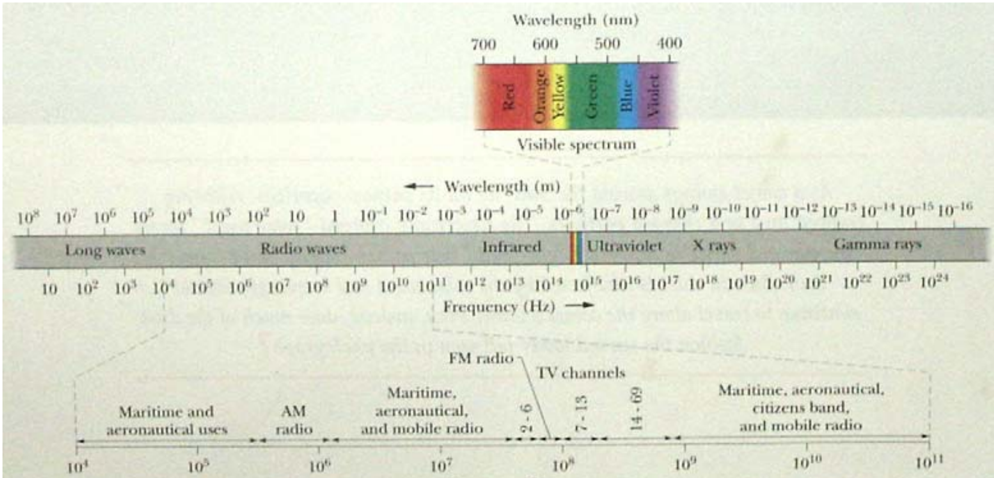

Figure 2.64: The electromagnetic spectrum. (Halliday et al. 1997)

Sir Isaac Newton (1642-1727) was the first person to perform an experiment revealing the presence of IR waves. The relationship between visible light and heat had long been recognized, since sunlight had an obvious effect on the temperature of an object. The important observation in Newton's experiment was that objects could still be heated if they were placed outside of the visible spectrum observed when a beam of light passes through a prism. Newton knew something was responsible for generating the heat, but it could not be observed with the naked eye (Maldague 2001).

The first person to formally quantify a thermal image was Max Planck. Planck's theory of radiation can be summarized as follows:

- All objects emit quantities of electromagnetic radiation
- Higher temperature objects emit greater quantities of radiation.
- The electromagnetic radiation emitted from a body consists of a "broadband" signal in that it contains radiation with a spectrum of wavelengths.

Since IR waves are essentially the same as visible light waves, it is important to understand how they interact with the surface being measured. For IR thermography images to contain the desired temperature data, it is important to distinguish between the radiation emitted from an object (which is related to its temperature) and radiation that is reflected off of the object from other sources. Emissivity (ε) is the quantity used to describe a particular surface's ability to absorb and emit radiation. For the case of a "blackbody", the emissivity is assumed to be 1. This means that all of the incident radiation falling on the surface is absorbed and results in an increase in temperature of the object. This increase in temperature then results in increased radiation by the object. For the case of a mirrored surface (a perfect reflector), the emissivity is assumed to be zero. This implies that none of the radiation being emitted by the surface was actually generated by the object.

Emissivites for common engineering materials are provided in Table 2.4. Note that materials with a low emissivity are not particularly well suited for inspection by IR thermography. However, it is possible to increase the emissivity of shiny objects by treating the surface with flat paint.

Table 2.4: Emissivities of common engineering materials.

Material	Emissivity
Steel Buffed	.16
Oxidized	.80
Concrete	.92
Graphite	.98
Wood	.95
Window Glass	.94

Another interesting phenomenon is the emissivity of glass. The relatively high value of 0.94 indicates that glass is essentially opaque to IR waves. As a result, an IR camera pointed at a glass window will provide temperature information for the glass surface as opposed to the temperature of any visible objects on the other side. This phenomenon is of significant importance when considering which materials are suitable for use in IR camera lenses and associated optics.

IR thermography and material assessment

The fundamental concept behind using IR thermography as a non-destructive evaluation technique is that sound and unsound materials have different thermal conductivity properties. If a constant heat flux is applied to the surface of a uniform homogeneous material, the increase in temperature on the surface of the object should be uniform. If, however, the material is non-homogeneous, the temperature along the surface will vary (see Figure 2.65).

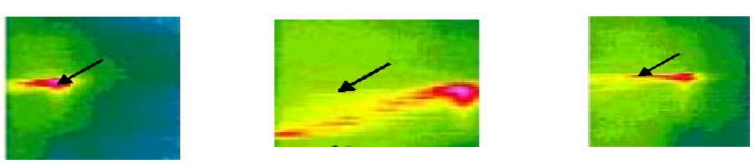

Figure 2.65: Typical thermograph revealing defects.

Passive thermography

The passive approach to IR thermography is simple and involves collecting temperature data from a scene without applying an external heat source. This method provides qualitative information about a situation and can be used to quickly determine if a problem exists. In the construction industry, passive IR thermography has been used for many years to evaluate thermal insulation in buildings and moisture infiltration in roofs. Passive thermography is also used to detect delaminations in reinforced concrete bridge decks (ASTM D4788-88). The following sections contain detailed descriptions of each test standard and special considerations for each case are noted.

ASTM D4788-88: delaminations in RC bridge decks

In this test, a vehicle mounted IR imaging scanner is driven slowly over the bridge deck under consideration. If the evaluation is performed during daylight hours, the delaminated areas will appear as "hot spots". During the evening time as the bridge is cooling down, the delaminated areas will appear "cooler" relative to the sound bridge deck. The IR scanner can also be incorporated with an electronic distance-measuring device so the resulting thermographs can be overlaid onto scaled CAD drawings. If any areas of concern appear in the thermographs, a more detailed inspection of the suspect area can be performed (usually by coring or ultrasonic evaluation).

For delaminations to be detected, there must be a minimum temperature difference of 0.5 °C between the delaminated area and sound areas. The test standard indicates that roughly three hours of direct sunshine is sufficient to develop this temperature differential.

It is also specified that the bridge deck should be dry for at least 24 hours prior to testing. Windy conditions should also be avoided and care must be taken when interpreting results in areas where shade may have influenced the surface temperature distribution.

Passive thermography is a non-destructive testing technique that provides qualitative information about a situation. Once potential problem areas have been identified, further testing (usually destructive in nature) can be conducted in the suspect areas. The primary advantage of this technique is that large areas can be surveyed relatively quickly and without disruption to the users of a structure.

Active thermography

In active thermography, heat is applied (by the inspector) to the surface of the object under investigation while an IR camera monitors the temperature variations on the surface. The advantage of active thermography over passive is that a quantitative analysis of the data collected can reveal important defect characteristics (size and depth). This type of IR thermography is not usually employed in civil engineering structures for overall NDE since the required energy inputs would be large. However, thermal input from the sun or a building's heating/cooling system and subsequent IR measurements is a form of active thermography.

Since IR thermography is only capable of monitoring the surface temperature of an object, the technique is usually limited to situations where defects are located near the surface. As defect depth increases and defect size decreases, assessment becomes more difficult. Active IR involves more elaborate test setups than are encountered in passive thermography. The required minimum resolvable temperature difference (MRTD) of IR camera equipment is smaller and heating of the specimen surface must be carefully controlled. As a result, most applications of active IR thermography are performed in a laboratory or well controlled manufacturing environment.

Equipment

Scanning radiometers are devices capable of generating 320 x 240 pixel digital images containing the exact temperature data for each pixel. The precise temperature data is obtained by comparing the IR image signal to the signal generated by an internal reference object. Depending on the data acquisition system employed, thermal images containing 76,800 unique temperature values can be obtained at a rate of 50 to 60 frames per second (see Figure 2.66).

Applications

Current applications of IRT include the evaluation of concrete and composite structures for delaminations, coating thickness, and the integrity of coating-substrate bonds. With the increased use of advanced composites in civil engineering structures, IRT becomes a potential means of evaluating the quality of installation and long-term durability of the composite strengthening system.

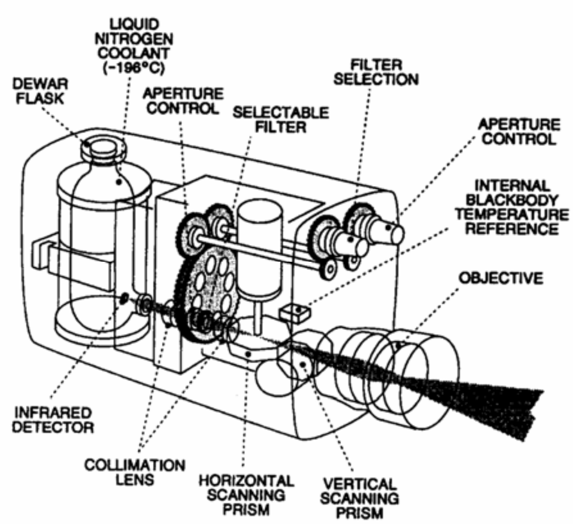

Figure 2.66: Schematic of a scanning radiometer IR camera. (Maldague, 2001)

In an experiment performed at the University of Florida (Hamilton & Levar 2003), reinforced concrete beams were bonded with CFRP composites and tested to failure. During the test procedure, the beams were periodically IR inspected for initial bond quality and bond failure under load testing. The use of acoustic sounding to detect unbonded or disbonded CFRP laminates can leave as much as 25% of voids undetected. The use of IR thermography for the inspection of concrete structures strengthened with CFRP laminates is the most efficient method of qualitative inspection for structures with this type of repair.

IRT was proven to be effective as a qualitative NDT technique for the inspection and repair of the concrete roof shell at the Seattle Kingdome prior to its demolition. “In 1992, ceiling tiles attached to the roof underside fell approximately 300ft onto the seating area prior to the venue opening for a baseball game. The safety problem initiated a major rehabilitation program for the concrete shell roof of the almost 25 year old structure” (Weil & Rowe 1998, p389). IRT was used as the primary NDT method to locate subsurface anomalies in the roof structure. Delaminated or voided areas of concrete will prevent solar energy from passing through the roof structure causing a “hot spot” to form when the roof is thermally loaded. Unbonded areas in concrete repaired with CFRP are detected in the same manner. Figure 2.67. provides an illustration of the effect that delaminations and voids in concrete have on the conduction of heat the through the roof structure.

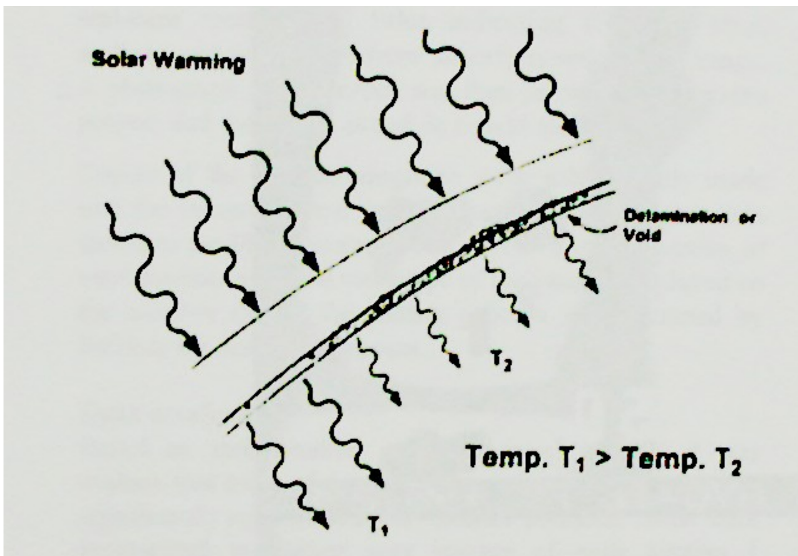

Figure 2.67: Schematic description of thermographic void detection process. (Weil & Rowe 1998)

The inspectors were able to thermographically survey the entire roof structure, which was 360,000 ft^2 in area, in three days of testing using a single camera. Inspectors performed a more detailed inspection at each anomaly with sounding techniques and impact-echo for quantitative material analysis. Repairs to the roof shell were made according to test results and inspector recommendations.

Radioactive Testing

Radioactive testing dates back to the discovery of X-rays by Ivan Pului and Wilhelm Roentgen in the late 1880’s and 90’s. While Pului published material relating to X-ray experiments in the "Notes" of the [Austrian] Imperial Academy of Sciences in 1883 several years before Roentgen’s first publication on X-ray technology, Roentgen is credited as the discoverer of X-ray technology and won the 1901 Nobel Prize based on his achievements (Kulynak 2000).

The contributions by Marie and Pierre Curie are the most profound advances regarding radioactivity, a term they coined. The Curies discovered gamma rays in the late 1800's while working with several different elements including bismuth, barium and uranium. They discovered polonium and radium, and the experiments the Curies conducted with radium and its radioactive effects were presented in Marie's doctoral thesis in 1903. As a result, Marie won the Nobel Prize in 1903 (Hellier 2001).

Radiography

A radiograph is a picture produced on a sensitive surface by a form of radiation other than visible light, typically an X-ray or a gamma ray. Radiography is the NDT technique that employs the use of radiographs for material inspection. X-rays are a form of electromagnetic radiation with a relatively short wavelength, about 1/10,000 the wavelength of visible light. Gamma rays are 1/1,000,000 that of visible light. It is this extremely short wavelength that enables X-rays or gamma rays to penetrate through most materials (Reese 2003). Structural radiography is very similar to the X-ray technique people experience during a doctor's visit. The method involves a wave source, usually X-rays or radioisotopes, and a detector, which is most commonly photographic film. Figure 2.68 depicts a typical radiography setup.

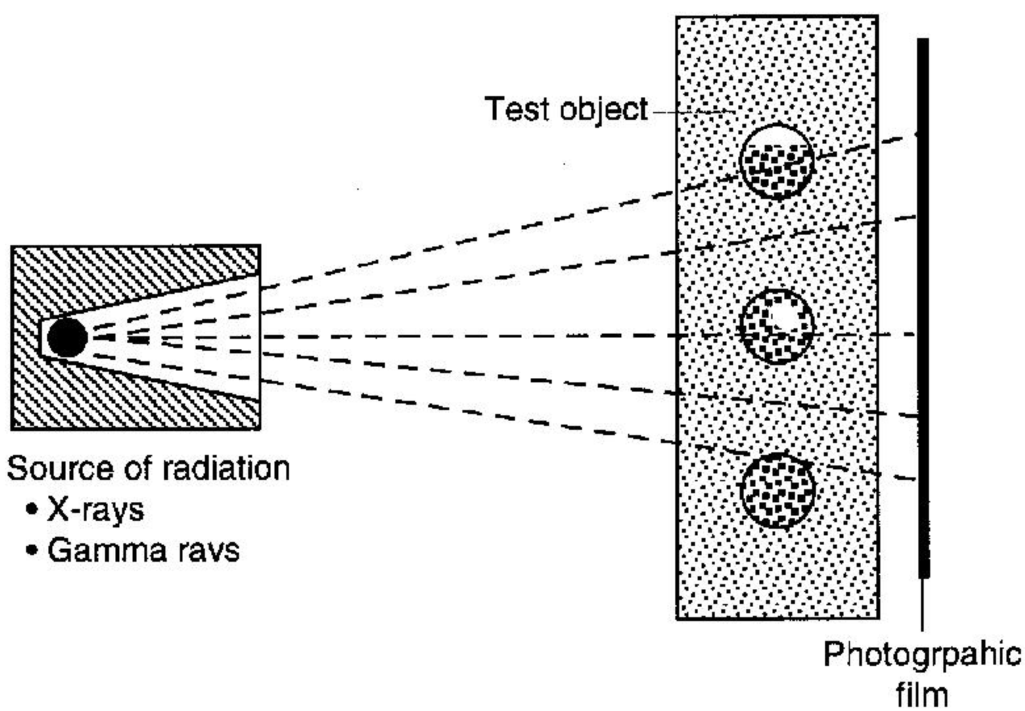

Figure 2.68: Radiography schematic. (Lew et al. 1998)

A limitation of radiography as an NDT technique is that both sides of the material to be tested must be accessible for inspection. Therefore, structural elements like slabs and foundation walls are not typically accessible for testing with radiography. ASTM has developed a testing standard covering the practices to be employed in the radiographic examination of materials and components. The standard outlines a guide for the production of neutron radiographs that possess consistent quality characteristics, as well as a guide for the applicability of radiography (ASTM E 748-02).

Radiometry

Often the terms radiometry and radiography are used interchangeably despite the fact that the tests are different. While radiography produces a visible image, radiometry is more quantitative in nature and is used to ascertain material properties. While both NDT techniques implement the use of radiation energy to analyze material properties, some radiometry techniques require only one side of a material to perform testing. The backscatter mode and certain aspects of the direct transmission mode (for both radiometry techniques) can send and receive radiation signals from a single side of the material.

The direct transmission mode of radiometry uses the same principles as the radiography test, though the radioisotope source can be oriented in several configurations to enable personnel to perform surface testing of a material. The direct transmission mode of radiometry uses the same theory as radiography, the main difference being that the equipment is configured differently. The direct transmission mode of radiometry usually has one or two probes that penetrate into the test material. A radioisotope source emits pulses, which are received by the detector. The rate of arrival of the pulses is related to the density of the material. This technique is commonly used in geotechnical engineering for the rapid calculation of soil composition, water content and density. Figure 2.69a illustrates a direct radiometry configuration with an internal signal detector and external source. Figure 2.69b is a schematic of a direct radiometry device with both an external signal detector and source (Malhorta & Carino 1991).

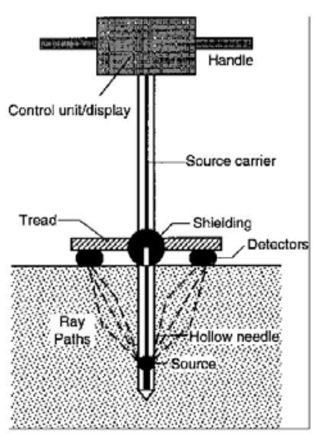

Figure 2.69a

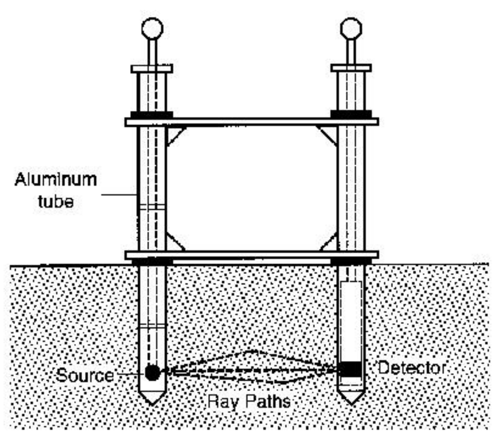

Figure 2.69b

Figure 2.69: Schematics of direct radiometry; (a) internal signal detector and external source, (b) external signal detector and source. (Lew et al. 1998)

In the backscatter measurement of radiometry, the source and the detector are adjacent to each other, but are separated by a lead radiation shield. The backscatter method is basically the same test as direct transmission and measures the same material properties. The only difference between the two tests is equipment configuration. Figure 2.70 illustrates a backscatter radiometry configuration.

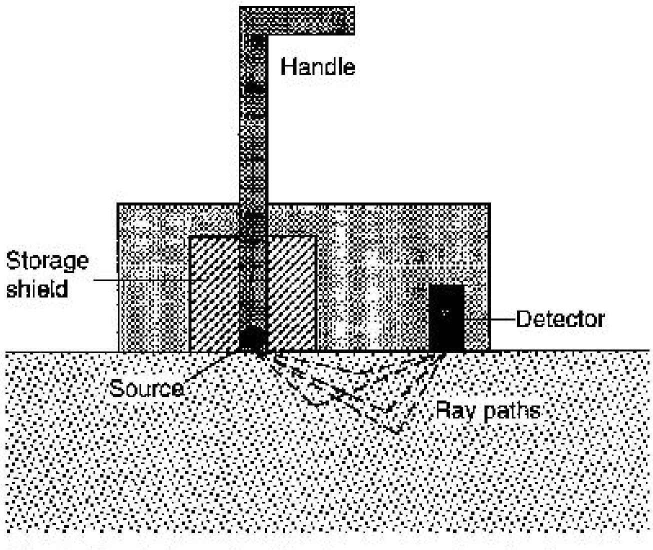

Figure 2.70: Schematic of backscatter radiometry. (Lew et al. 1998)

Applications

Radioactive methods have various applications in the nondestructive testing and monitoring of structures. Radiography may be the most powerful qualitative means of NDT since it offers inspectors a view of the internal structural elements unrivaled by any other nondestructive inspection technique. One example of the enhanced capabilities of radiography compared to any other NDT method is illustrated in Figures 2.71a and 2.71b.

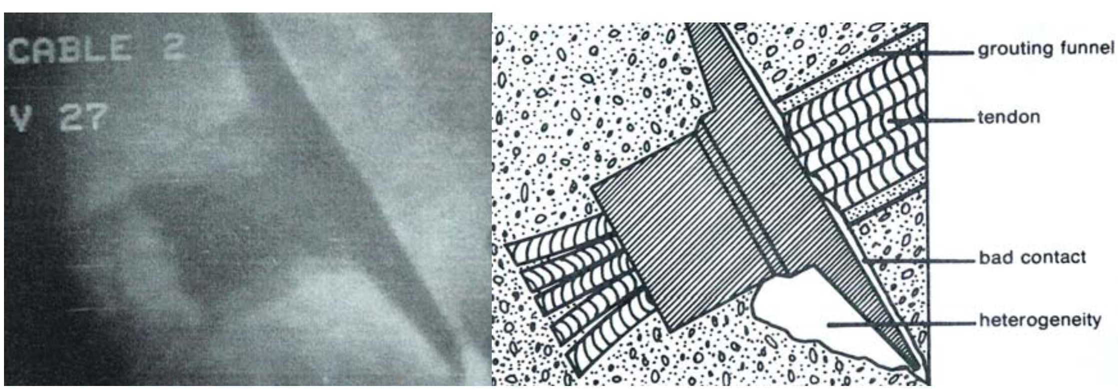

Figure 2.71a Figure 2.71b

Figure 2.71: Image of prestressing cable anchorage in concrete (a) X-radioscopic image of a prestressing cable anchorage embedded in a concrete, (b) schematic and brief explanation of the radiographic image. (Malhorta & Carino 1991)

Radiography can be applied to virtually any structural element in which two opposite sides are accessible. The method permits inspectors to assess every component on a visual basis, comparable to a medical doctor's ability to examine internal organs non-intrusively. Radiometry has been successfully used to quantitatively determine properties of concrete such as density, porosity, water content and thickness. The techniques used for determining material properties and integrity using radiation waves is comparable to the techniques used in determining material properties via stress waves. However, stress waves are of a lower energy and less versatile for material inspection than radiation waves.

Limitations

Although radiation testing is among the most powerful methods used in nondestructive testing today, it has several limitations that prevent it from becoming the most widely used NDT technique. Radiation testing techniques are the most expensive of NDT methods available for the testing of concrete materials. The technique is so much more expensive than the other techniques in service today, that many inspectors don't consider it to be practical from a cost-benefit standpoint.

Radiation testing presents many safety concerns that are not easily addressed in the field. It is usually feasible to protect operating personnel while conducting testing. However, it is not always practical to use radiographic testing due to public safety concerns. An example of this problem was demonstrated by the FDOT in February of 2002. Before the removal of an abandoned bridge adjacent to the Ft. Lauderdale airport, the FDOT contracted several consultants to demonstrate the capabilities of different NDT systems on the bridge deck. Among the techniques demonstrated on the bridge were impact-echo testing, GPR, magnetic flux leakage and radiography. The radiographic method was the only method that required the bridge structure and the roadway beneath it to be completely free of personnel for testing, and that both roadways were completely closed to traffic. In most urban areas it is not feasible for such roadway closures since bridge structures are usually built in high traffic volume areas. The same types of problems arise when performing radiographic testing of buildings and building components.

Conclusions

There are a large number of NDT techniques currently available for the evaluation of concrete structures, though many are designed for specific problems and not relevant to the application being formulated in this research. In general, it has been concluded that quantitative techniques are more applicable to this application than are qualitative techniques. The ability to produce a numerical measurement or rating will be necessary for future service life modeling or maintenance planning.

Due to the findings in the literature review, several test techniques were eliminated from inclusion in the laboratory and field testing portions of the project. The most promising techniques identified for the monitoring of new structures in order to detect the onset of deterioration in concrete include impact echo, ultrasonic pulse velocity, resonant frequency and acoustic emission.

CHAPTER 3
SURVEY OF RELEVANT BRIDGE STRUCTURES IN FLORIDA

The National Bridge Inventory (NBI) covers 600,000 bridges on the nation's interstate highways, U.S. highways, state and county roads, and other routes of national significance. The NBI is maintained by the Federal Highway Administration using data provided by the state and local transportation departments (Bhide 2001). The FDOT's "Pontis" Bridge Management System (BMS) is the client run server application used to inventory the bridge structures for the state.

The majority of bridges in the state of Florida are constructed of concrete. These bridges are classified in the 25-50 year age range. Deterioration rate studies suggest that structures in this category deteriorate slowly during the first few decades of their design life (typically 50 years), followed by a rapid decline. (NBI 2003) If these predictions are correct, Florida, as well as the U.S. will incur extensive rehabilitation and reconstruction costs over the next two decades. The Department of Civil Engineering at University of Florida conducted a survey of bridge structures within the Pontis system in an attempt to categorize prevalent bridge deficiencies occurring throughout the state.

Currently, the FDOT's Pontis system has inventoried a total of 12,573 bridge structures and sign structures. Of the 12,573 bridge structures, 9,585 were constructed with concrete. The survey conducted by the University of Florida, inventoried and categorized relevant concrete bridge structures. In addition, personnel from the FDOT's State Maintenance Office, Materials Office and District Offices were interviewed to ascertain any prevalent problems within concrete bridges throughout the state.

Definition of Sufficiency Rating

A bridge sufficiency rating is a numerical value assigned to a bridge structure subsequent to inspection, based on its condition. The major factors used to determine sufficiency rating are structural adequacy, serviceability and essentiality for public use. Therefore, the structural condition of a bridge and its sufficiency rating are not completely dependent upon each other. Figure 3.1: is a summary the factors used for calculating sufficiency rating.

Figure 3.1 illustrates the percentages of each factor used in the calculation of bridge sufficiency rating. Structural adequacy and safety comprise 55 percent of the total bridge rating. Since there are several components that affect a bridges sufficiency rating, it is not completely accurate to use the sufficiency rating as part of the methodology for a materials or structural survey. Interviews with FDOT personnel confirmed that presently the sufficiency rating is the best way to query bridge structures based for structural deficiencies.

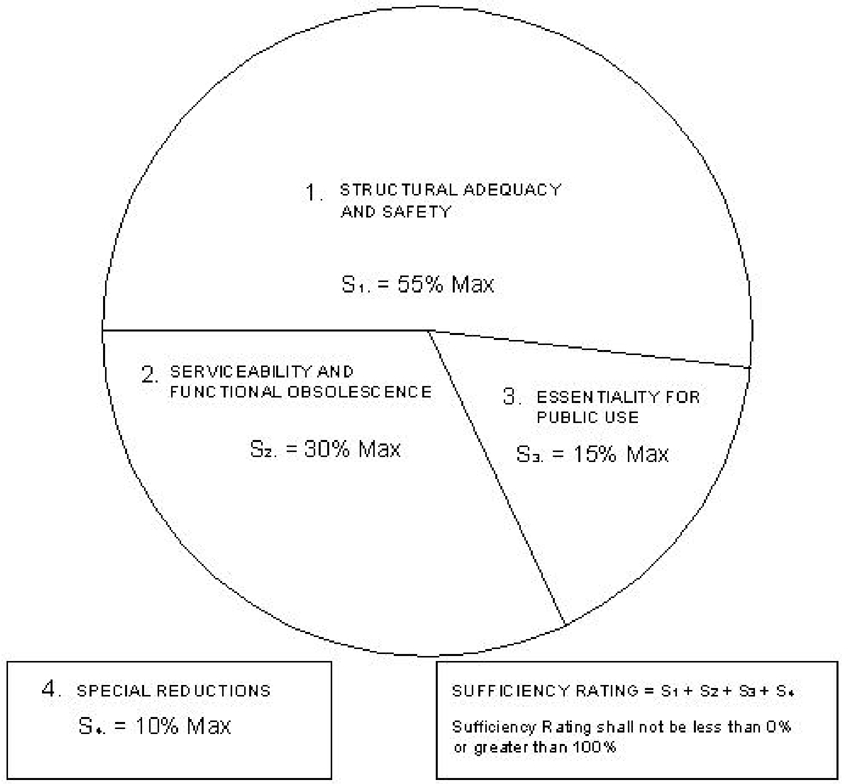

Figure 3.1: Summary of sufficiency rating factors (FHWA 1995)

Methodology

Originally, the purpose of the bridge survey was to identify prevalent bridge deficiencies that were typical among concrete structures throughout the state. However, the Pontis system is limited in its querying abilities and does not allow for specific problems, deficiencies, or inspector recommendations. Presently, the Pontis system can execute queries based on bridge ID number, structure name, name of the feature intersected, county, age, length and sufficiency rating. Another limitation of Pontis is that it lacks the ability to form more than one query at a time. Therefore, without printing, reading, and manually categorizing each of the 12,573 bridge reports, it was not possible to determine prevalent material or structural problems.

Pontis lacks the ability to make queries of specific bridge structure deficiencies. Therefore, the bridge queries were based solely on sufficiency rating. However, the structural condition of a bridge and its sufficiency rating are not completely dependent upon each other.

The Pontis system was used to query the bridges by sufficiency rating. A typical query is illustrated in Figure 3.2. Since the Pontis system cannot query by more than one item, all of the relevant bridges queried had to be categorized by hand. As an attempt to create a baseline of structure performance, the bridges were categorized by condition, age and feature intersected.

All bridges that were 40 years of age and older with a sufficiency rating of 85 or above set the baseline for durable structures. All bridges 20 years or younger with a sufficiency rating of 75 or below were considered to be less durable and should be monitored for material and structural problems.

Bridge ID	Feature Intersected	Dist	Cnty	Length (ft)	Built	Deck	Super	Sub	Culv	Suff Rate
034065	COCOHATCHEE CANAL	D1 - Bartow	(03)Collier	37	2002	N	N	N	8	100
080038	CR 578 COUNTY LINE RD	D8 - Turnpike	(08)Hernando	181	1999	9	9	8	N	100
100410	RAMP I75 NB TO SR582 WB	D7 - Tampa	(10)Hillsborough	148	1985	7	8	8	N	100
094043	PLATTS BRANCH	D1 - Bartow	(09)Highlands	57	1988	N	N	N	7	99.9
040012	HOG BAY CREEK	D1 - Bartow	(04)De Soto	43	1955	N	N	N	7	99.9
064094	OAK CREEK	D1 - Bartow	(06)Hardee	82	1990	7	7	7	N	99.9
064117	HORSE CREEK	D1 - Bartow	(06)Hardee	162	1998	7	7	7	N	99.9
094030	CATFISH CREEK	D1 - Bartow	(09)Highlands	37	1960	N	N	N	7	99.8
024047	APOPKA CANAL	D7 - Tampa	(02)Citrus	58	1987	7	7	7	N	99.8
050050	FISHEATING CRK OVERFLOW	D1 - Bartow	(05)Glades	252	1974	7	7	8	N	99.8
044038	HAMPTON BROOK	Central Office	(04)De Soto	25	1900	N	N	N	6	99.8
064097	OAK CREEK	D1 - Bartow	(06)Hardee	70	1990	7	7	7	N	99.8
010014	ALLIGATOR CREEK	D1 - Bartow	(01)Charlotte	49	1967	N	N	N	6	99.8
010097	BROAD CREEK	D1 - Bartow	(01)Charlotte	24	1981	N	N	N	7	99.8
024048	APOPKA CANAL	D7 - Tampa	(02)Citrus	72	1987	7	7	7	N	99.8
070062	GRANDMAS GROVE CREEK	D1 - Bartow	(07)Hendry	75	1999	8	8	8	N	99.7
094045	S.C.F.E. RAILROAD	D1 - Bartow	(09)Highlands	64	1999	8	8	8	N	99.7

Figure 3.2: The result of a typical bridge query by sufficiency rating

The FDOT uses visual inspection the primary method of gathering data that is imputed into the Pontis system. As discussed in Chapter 2 visual inspection is often subjective and is dependent upon 'human factor' that is often encountered during structural inspection. The susceptibility to human misinterpretation and the requirement for establishing a baseline for defects in general, especially under poor conditions, can lead to inconsistent identification of anomalies, resulting contradicting evaluations (Quaswari 2000).

Another limitation of using the Pontis system is that a bridge sufficiency rating is calculated by quantifying the results from visual inspections. Contradicting evaluations can alter a bridge sufficiency rating drastically. Interviews with FDOT personnel corroborated with the indication that discrepancies in evaluation ratings, as a result of inconsistencies in visual inspection results affect the value bridge sufficiency rating when inputted into the Pontis system.

According to the FHWA's recording and coding guide for bridges, the deck, superstructure, and substructure are given a general condition code based on a scale of a 0-9, 0-code represents a bridge closed and a 9-code is superior to present desirable criteria. Rigorous attempts to classify data using the general condition codes were unsuccessful because the bridge sufficiency rating is dependent of the general condition code. Figure 3.3 shows examples of bridges that are approximately the same age, and the same structural code classifications but have different sufficiency ratings.

Feature Intrsected	Cnty	Length (ft)	Built	Deck	Super	Sub	Culv	Suff Rate
LITTLE TROUT R/ER	(72)Duval	132	1939	7	7	7	N	99.5
SANTA FE RIVEI	(26)Alachua	256	1994	7	7	7	N	99.5
MID-PRONG ST MARYS RIVER	(27)Baker	260	1992	7	7	7	N	99.5
SANTA FE RIVEI	(26)Alachua	256	1994	7	7	7	N	99.5
PETERS CREEK	(71)Clay	193	1993	7	7	7	N	99.5
SANTA FE RIVEI	(26)Alachua	256	1994	7	7	7	N	99.5
ST. JOHNS BLUF RD.	(72)Duval	220	1972	7	7	7	N	99.3
BLACK CREEK	(71)Clay	1,465	1973	7	7	7	N	99.3
LITTLE BLACK CEEK	(71)Clay	350	1985	7	7	7	N	99.2
BLACK CREEK	(71)Clay	1,465	1973	7	7	7	N	99.4
Canal	(73)Flagler	51	1949	7	7	7	N	61
Canal	(75)Orange	56	2003	7	7	7	N	60.8
JUMPER CREEK CANAL	(18)Sumter	100	1957	7	7	7	N	60.8
CANAL C-4	(75)Orange	80	1969	7	7	7	N	60.4
South Fork of New River	(86)Broward	410	1960	7	7	7	N	60.1
Sassagoula River	(75)Orange	90	1990	7	7	7	N	58.3
PANAMA CANAL	(86)Broward	40	1964	7	7	7	N	58
RIO ARAGON CANAL	(86)Broward	98	1968	7	7	7	N	58

Figure 3.3: Examples of Pontis codes vs. sufficiency ratings.

The inability of the Pontis system to sort and classify bridges with regard to structural or material integrity is the most limiting feature of the system. Due to the lack of such a feature, a statically significant data analysis based on structural sufficiency cannot be performed.

Results

Pontis Data Analysis

Currently the Pontis system has 12,573 bridge structures inventoried. However, the report published by the FHWA in 2002 has a total of 11,526 bridge structures inventoried. There are several reasons for the discrepancy between the current count and the 2002 published count.

The first reason is that as new bridges are constructed on an annual basis, the number of bridges in the Pontis system will rise accordingly. Another reason for the inconsistency among the figures is that the NBI publishes the number of bridges that are completely constructed. While the Pontis system has an inventory of all bridges that are completely constructed, as well as bridges currently under construction. A third reason for the difference in numbers is due to errors in the inputs of the bridge data. The FDOT has downsized a large percentage of its staff. Private consultants are now performing the majority of the bridge inspection and data entering into to the Pontis system. Recently, there are instances in which bridges are mistakenly entered or duplicated within Pontis. For the purposes of this survey, we will use the numbers published from the 2002, NBI for overall quantities. However, the categorized figures were obtained through an analysis of data performed by the University of Florida.

Of the 11,526 bridge structures in the state, 9,585 were constructed with concrete. The concrete bridges were analyzed and 686 of them fit into the two durability categories previously stated. Of the 686 bridges, 202 bridges fit into the deficient new structure (DNS) category (i.e. 20 years or younger with a sufficiency rating of 75.0 or less). However, 41 of the DNS 202 bridges are made of concrete. The majority of the deficient bridges are steel or wood structures, accounting for 161 of the 202 bridges. Of the 41 DNS bridges made of concrete, 21 are functionally obsolete. Accordingly, 19 of the 21 DNS bridges, were functionally obsolete and had sufficiency ratings above 60.0. These 19 functionally obsolete bridges were considered to have a low deficiency rating based on the “S3” sufficiency rating input parameter from the equation in Figure 3.2. For the uses of this survey, they are considered to be structurally sufficient. Therefore, 22 of the 9,585 concrete bridges throughout the state can be classified as newly constructed and structurally deficient.

Over 90% of the concrete bridge structures within the state employ slab design and multi beam/girder design. Consequently, the 17 of the 22 newly constructed deficient bridges are slab and beam/girder design. Upon review of the individual bridge reports, it was found that the most prevalent deficiency in these structures is deterioration of the bridge deck. According to the FHWA’s recording and coding guide for bridges, the bridge deck average general code is 6.73 out of 10, for the 22 newly constructed deficient bridges (Where 7 is considered to be good condition and 6 is satisfactory condition.) Again, we see some inconsistency when trying to deduce a structural condition based on sufficiency rating.

Conclusions

The Pontis system is a very effective database system for monitoring long term data from the inspection of bridge structures. There are, however, a number of issues that could be improved. There is a need for more quality control regarding interpretation of structural deficiencies and disposition of the data within the system. Private consultants rather than FDOT personnel performed most of the bridge inspections. As a result, consistency in the interpretations of bridge conditions is being compromised. It appears as though a more exact definition of conditions is needed to regain the necessary quality control of inspection reports.

The system appears to lack a protocol to maintain the consistency among units of physical properties (i.e. some reports use the English system of measurement, where others use SI units). Since the system lacks user consistency between such simple parameters, it is difficult to rely on the quality control of sufficiency ratings to draw any statistical conclusions based on the data within the system. Consequently, a statistical analysis was not performed on the bridge data within the Pontis system. Deductive arguments made from the data available would be insufficient to infer reliable conclusions.

Limitations of Pontis system include:

- The inability to process data sorts of more than one data field within the system for a single data query
- The inability to perform data sorts based on material type

The expansion of the Pontis system to include multiple data sorts would allow for more complicated data analyses to be undertaken. The addition of a sorting material based query would enable users to perform statistically significant data analysis on bridge structures based on material type.

As a result of our survey, it has been determined that 22 newly constructed concrete bridge structures were classified as deficient. Since 17 of the 22 deficient bridge structures are typical designs, they provide a good baseline for testing. Upon plan review, these bridges should be considered for condition monitoring. The use of several qualitative and quantitative NDT methods should be employed to further assess the material integrity of each bridge.

Personnel Survey

Screening was performed for each of the seven FDOT districts. It was concluded that the information available from the PONTIS database, though helpful, is not sufficient for the purposes of this research project. The PONTIS data provides details on damage and deficiencies to FDOT bridge structures but, in most cases, does not include causes of this damage. As a result, six of bridges were chosen for direct inspection by the researchers in order to ascertain the missing information.

The PONTIS system does not have the capacity to act as a stand alone system for these purposes. Therefore, it was essential to incorporate FDOT personnel interviews to establish a sample of bridges that were suitable for NDT testing and field inspection.

As a result of the PONTIS survey and FDOT personnel interviews, the following bridges were visited:

- Bahia Honda Bridge
- Niles Channel Bridge
- Sebastian River Bridge
- Sebastian Inlet Bridge (Robert W. Graves Bridge)
- Wabasso Bridge

Each bridge was examined to locate typical deficiencies and to assess the overall quality of concrete used for construction. The literature review reported in Chapter 2 served as an evaluation of NDT technology currently available today. The NDT techniques most suitable for use in concrete materials inspection are: visual inspection, acoustic sounding, rebound hammer, impact-echo and ultrasonic pulse velocity. The penetration resistance methods and the breakoff test were considered suitable for material inspection but due to their partially destructive nature they were not permitted by the FDOT for use. Inspections were thus limited to non-intrusive testing techniques.

Findings

Each of the five bridges was inspected using the sounding, impact echo, ultrasonic pulse velocity, and rebound hammer methods. Each bridge had at least one unique feature that provided information useful to the application of NDT methods in the field. The applications of the NDT techniques applied to the field revealed the condition of overall material properties and structural deficiencies. Without the use of NDT techniques the deficiencies and material properties could not have been established.

The use of nondestructive testing techniques enabled the field inspection personnel to discover the onset of material deficiencies within the bridge structures visited. Through the use of impact-echo, ultrasonic pulse velocity and sounding, the following discoveries were made:

- The onset of surface deterioration due to exposure at each of the bridge structures.
- Delaminations and poor repair work on the strut and pile jackets on the Niles Channel bridge.
- Visible and hidden torsional cracking at the column-pier connection on the Bahia-Honda and Sebastian Inlet bridges.
- Poor quality repairs made on the Sebastian River Bridge.
- Atypical coarse aggregate in the Wabasso bridge that is not typically used in bridge construction.

The field evaluations confirmed that the selected nondestructive testing methods are able to detect the onset of damage to concrete materials not yet visible to the human eye. When properly used, combinations of nondestructive techniques can identify certain types of damage observed in the field. Material sampling can be greatly reduced by implementation of a proper nondestructive testing regimen. Additionally, the research revealed that indications of material type and properties can be ascertained via the use of NDT.

CHAPTER 4
LABORATORY TESTING PROGRAM

From the information acquired in the literature review task, it has been concluded that nondestructive testing results are directly affected by changes or damage to the microstructure of concrete. This damage typically takes the form of either microstructural cracking and/or changes to the chemical makeup of the hydrated cement paste. Its effect on the NDT techniques in question should be relatively consistent from one type of damage to another. Thus, it was decided that the sulfate attack mechanism could be used to induce damage in concrete specimens in order to relate the progressive damage to NDT results.

Concrete Parameters

The primary property affecting sulfate resistance of concretes is water/cement ratio. The proposed research will examine two water/cement ratios, the ACI 318 requirement for severe sulfate exposure (0.45) and a “worst case scenario” (0.65). Mixture designs are shown in Table 4.1 below.

Table 4.1: Concrete Mix Designs

W/C Ratio	Proportions (lb/ft^3)			
	Cement	Water	Coarse Aggregate	Fine Aggregate
0.45	507.0	228.6	682.9	855.1
0.65	350.3	228.6	717.0	958.7

Materials

Cement – Type 10 Ordinary Portland Cement, manufactured by Rinker Materials.

Water – potable tap water as supplied by Gainesville Regional Utilities.

Fine Aggregate – standard “Concrete Sand” provided by Rinker Materials. The fine aggregate was introduced into concrete mixer in oven-dried state (as per FDOT standard practice). The batch water was adjusted to account for a 1.9% absorption.

Coarse Aggregate – 89 stone provided by Rinker Materials from their Ocala depot. The coarse aggregate was pre-soaked in water permeable bags for a minimum of 7 days and then allowed to drip-dry (as per FDOT standard practice) prior to being introduced into the concrete mixer. Moisture content tests indicated an average free water content (in addition to SSD) of 5.1% (with very little variation). The batch water was adjusted accordingly.

Admixtures – a water reducer (Adva 100 manufactured by Grace Construction Products) was used to adjust slump of 0.45 W/C mixes to match that of the 0.65 W/C mixes. No air entrainers or permeability reducing agents were used.

Exposure Conditions

It was essential that the exposure of concrete to sulfates be conducted in an appropriate manner. One of the primary considerations that must be made when deciding upon exposure conditions is reproduction of the sulfate attack processes that occur in the field.

- Blocks were removed from their exposure (and destructively tested) at successively longer ages in order to provide a time line of sulfate attack degradation. Relatively large scale specimens (36 in x 20 in x 10 in) were used that essentially simulate real-world concrete exposed to a sulfate environment (see Figure 4.1). Destructive test specimens consist of cores taken from these blocks at varying ages.

- Partial immersion has been implemented to simulate the partially buried or immersed condition of typical footings or bridge piers. This is actually a more severe exposure than complete immersion because of the higher rate of sulfate movement through the concrete, due to an induced evaporation cycle.

- Specimens were exposed to sulfates immediately after demolding, simulating the backfilling of footings with sulfate bearing soils or the removal of cofferdams in seawater environments. The ends of the blocks were coated with an impermeable barrier to prevent 3-dimensional penetration of sulfates, thus representing a section of footing within a longer structure.

- Cores were removed from each of the blocks at three different elevations, relative to the immersion line. The lowest set was taken from the completely submerged section, the middle from just above the immersion line, and the uppermost set from 11 inches above the immersion line. Since the majority of evaporation occurs just above the immersion line, the latter set was well above the sulfate exposure region.

- Blocks were cored at varying ages in order to provide a time line of sulfate attack degradation. Due to the number of cores needed from each block (and the mass of the resulting block) a pair of blocks was cast for each testing age so that the entire blocks could be removed from the sulfate solution immediately prior to coring.

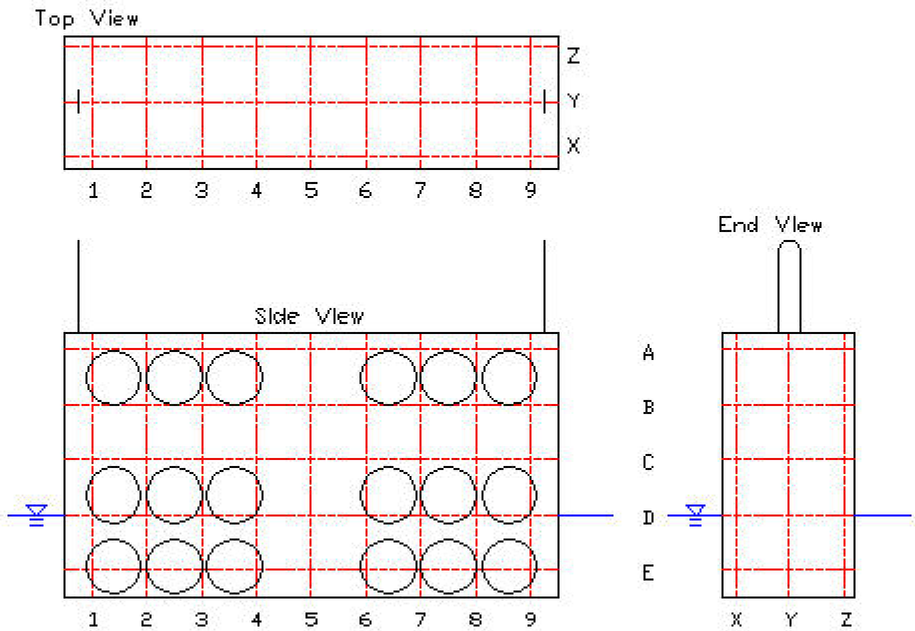

Figure 4.1: Sulfate exposure block details.

Half of the blocks were exposed to a 5% sodium sulfate solution (as described in ASTM C 1012) in order to accelerate deterioration without changing the mechanisms of sulfate attack process. The other half of the specimens were exposed, under identical conditions, to lime-saturated water in order to establish a base-line for damage evaluation. Companion cylinders were also cast and completely submerged in each of the two exposure solutions. These cylinders allowed comparison of the partial immersion condition of the large scale blocks with the complete immersion condition specified in ASTM C 1012.

In order to generate a timeline of data, several specimens were cast so that destructive testing results could be obtained at various ages. Table 4.2 indicates the time line for each of the blocks, showing the casting date and the end date whereupon coring was carried out.

Table 4.2: Casting and Maturity Dates for Exposure Blocks

Block Type	Casting Date	Maturity Date
1 Month	May 2003	June 2003
3 Month	January 2003	May 2003
12 Month	January 2003	January 2004
24 Month	June 2003	June 2005
36 Month	July 2003	July 2006

Note: The 24 and 36 month blocks have not yet been tested and extend beyond the finish date of this research contract.

Tables 4.3 and 4.4 list all of the blocks cast for sulfate exposure and limewater exposure, respectively, and provide details concerning the relevant water to cement ratio and age variables for each specimen.

Table 4.3: Blocks Exposed to Sulfate Solution

Block #	W/C	Date Cast	Age at Coring (mth)
1, 2	0.45	1/28/2003	12
5, 6	0.45	2/6/2003	3
9, 10	0.45	5/20/2003	1
13, 14	0.45	6/17/2003	24
19, 20	0.65	1/21/2003	12
23, 24	0.65	2/13/2003	3
25, 26	0.65	6/12/2003	1
29, 30	0.65	7/10/2003	24
33, 34	0.45	7/16/2003	36
37, 38	0.65	7/23/2003	36

Table 4.4: Blocks Exposed to Lime-Saturated Solution

Block #	W/C	Date Cast	Age at Coring (mth)
3, 4	0.45	1/28/2003	12
7, 8	0.45	2/6/2003	3
11, 12	0.45	5/20/2003	1
15, 16	0.45	6/17/2003	24
17, 18	0.65	1/21/2003	12
21, 22	0.65	2/13/2003	3
27, 28	0.65	6/12/2003	1
31, 32	0.65	7/10/2003	24
35, 36	0.45	7/16/2003	36
39, 40	0.65	7/23/2003	36

Specimen Evaluation

A summary of the testing procedures to be performed on each specimen is indicated below in Table 4.5 below.

Table 4.5: Specimen Test Procedures

Specimen Type	Nondestructive			Destructive		
	UPV	IE	RH	CS	ST	PT
Blocks	✓	✓	✓			
Cores	✓	✓		✓	✓	✓
Cylinders				✓	✓	✓

Note: UPV = ultrasonic pulse velocity, IE = impact echo, RH = rebound hammer, CS = compressive strength, ST = splitting tension, PT = pressure tension

Nondestructive Evaluation

The large block specimens were monitored at regular intervals until reaching their final exposure limit (i.e. 1, 3, 12, 24, or 36 months). The testing regime consisted of regular nondestructive evaluation of the concrete samples approximately every week until the specimens were six weeks old, and every two weeks thereafter.

Figure 4.2: Ultrasonic pulse velocity testing of exposure blocks.

Figure 4.3: Impact-echo testing of exposure blocks.

Nondestructive tests were performed using a James Instruments V-Meter Mark II Ultrasonic Pulse Velocity meter and a Germann Instruments Docter-1000 Impact-Echo testing apparatus. Figures 4.2 and 4.3 consist of photographs of both tests being performed on the block specimens.

Each block was tested at fifteen locations. Measurements were taken through the concrete blocks at heights of 75 mm (center of the submerged concrete), 240 mm (slightly above the immersion line), and 405 mm (well above the immersion line). Five locations at each height were tested, four through the block's width and one through the length. Figure 4.4 indicates the ultrasonic pulse velocity testing locations.

Thirty-seven weeks into the monitoring, salt crystallization and scaling became visually apparent on the specimens exposed to sulfate solution. It was decided that the pulse velocity at this location was of interest as well. However, it was impossible to measure the pulse velocity in the scaled area due to an inability to form an effective couple between the concrete and the pulse velocity transducers. In an effort to measure the velocity through the concrete at this location, diagonal measurements were made by placing the transducers above and below the scaled area and taking diagonal readings through the section (see Figure 4.4). The average time from the two tests was then calculated and the width corrected for the geometry of the length measurements. From these results, the pulse velocity through the damaged area was estimated.

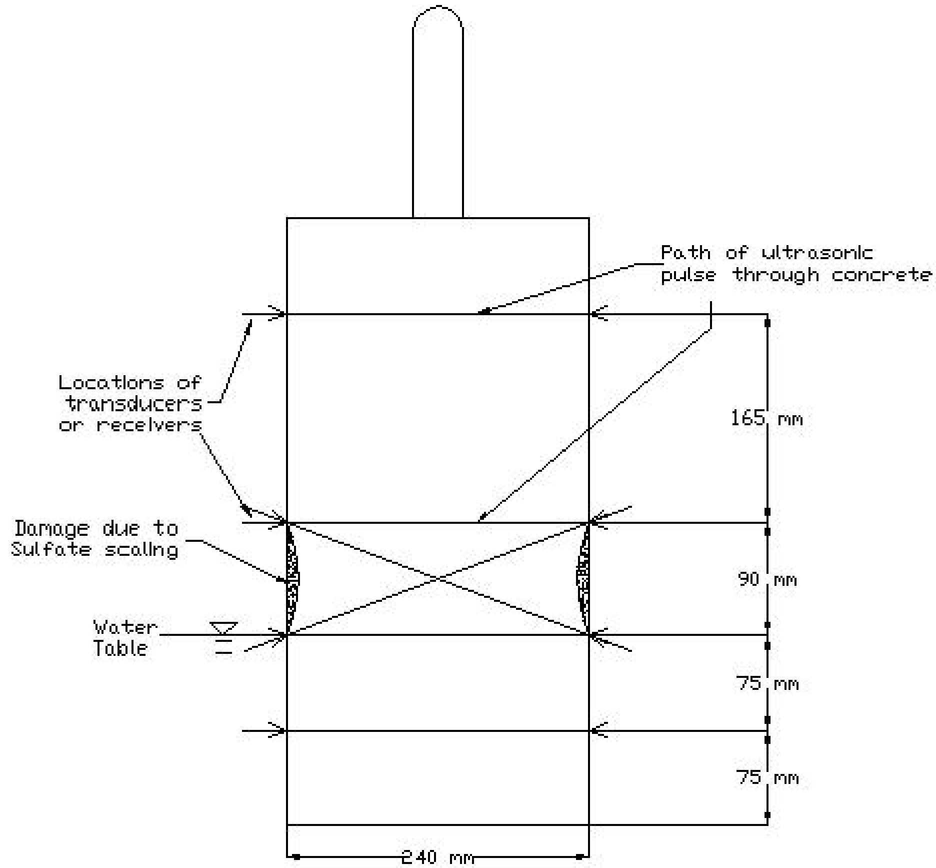

Figure 4.4: Location of ultrasonic pulse velocity tests on concrete block specimens.

Impact-echo surface wave velocity tests were performed at the same heights as the pulse velocity tests. Six tests were performed per block, two at each level. Only one face was tested per block. At the age of thirty-seven weeks, an additional line of testing was added to the testing regime right at the immersion line at a height of 150 mm.

Destructive Testing

Of the ten cores taken at each elevation (five from each block in a pair), three were tested in compression, three in splitting tension, and three in pressure tension. These cores were used to establish the effect of sulfate attack on the standard mechanical properties of the concrete. The final core was used to provide samples for investigation of microstructural cracking. Analysis of the physical changes in the microstructure, induced by sulfate exposure, were performed using a Variable Pressure Scanning Electron Microscope (VP SEM) equipped with an energy dispersive X-ray spectrometer (EDS).

Results - *Nondestructive Evaluation*

Velocity Measurements

Once the velocity data were collected, average values for each testing height of each specimen were calculated and plotted against time for each of the 3-month and 12-month blocks. Due to the shear number of graphs produced, these figures have been included in Appendix A, with an example of each exposure solution provide in Figures 4.5 and 4.6.

As indicated in the legends, dashed lines (labels beginning with 'UPV') represent through thickness UPV readings taken with the ultrasonic pulse velocity meter. Solid lines (labels beginning with 'IE') refer to near surface p-wave velocity readings obtained using the impact echo technique. For each of the two techniques, three lines are shown, representing the three different testing heights, as described previously.

Examining the graphical data reveals a number of general trends consistent throughout all of the specimens. Firstly, the figures indicate that all wave velocities increased at successively lower points on the specimen. This phenomenon is to be expected due to segregation during casting. As large samples of concrete are poured, the larger aggregates and denser materials within the matrix tend to migrate toward the bottom, whereas the water and less dense materials tend to migrate upward. Since denser materials tend to exhibit higher wave velocities, a trend develops wherein the measured values increase proportionally to the inverse of their distance from the bottom of the specimen.

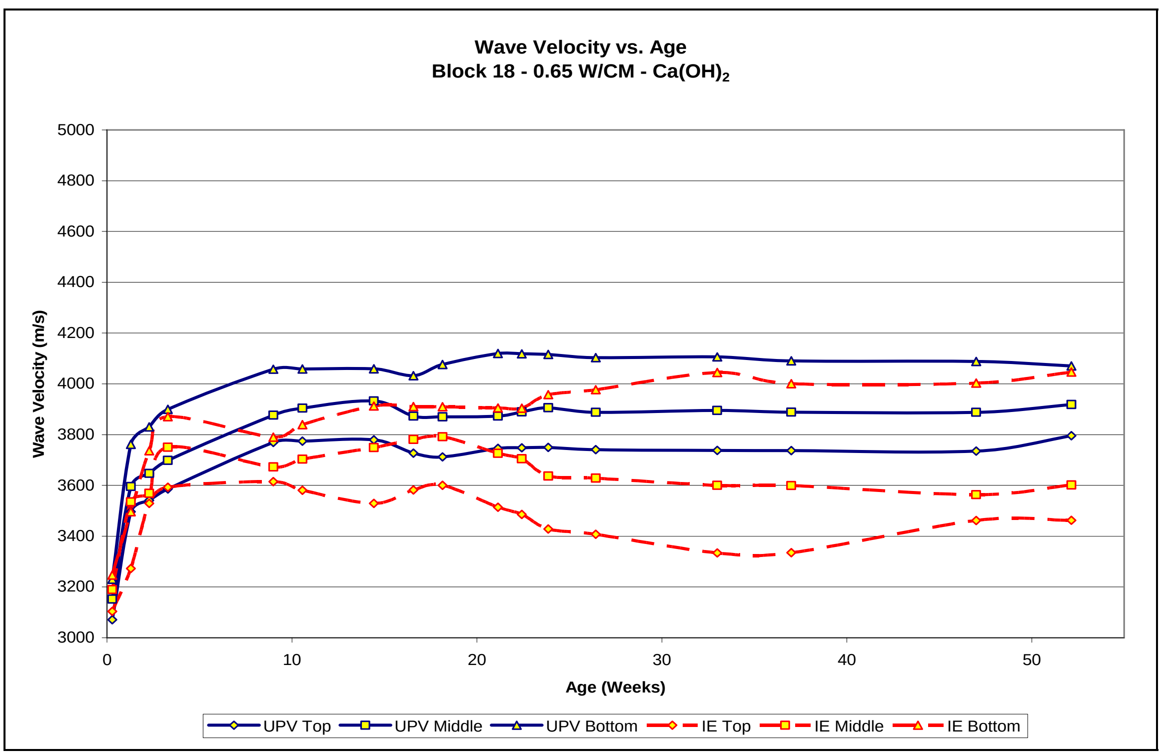

Figure 4.5: Wave velocities for a one-year sample exposed to lime water (A14).

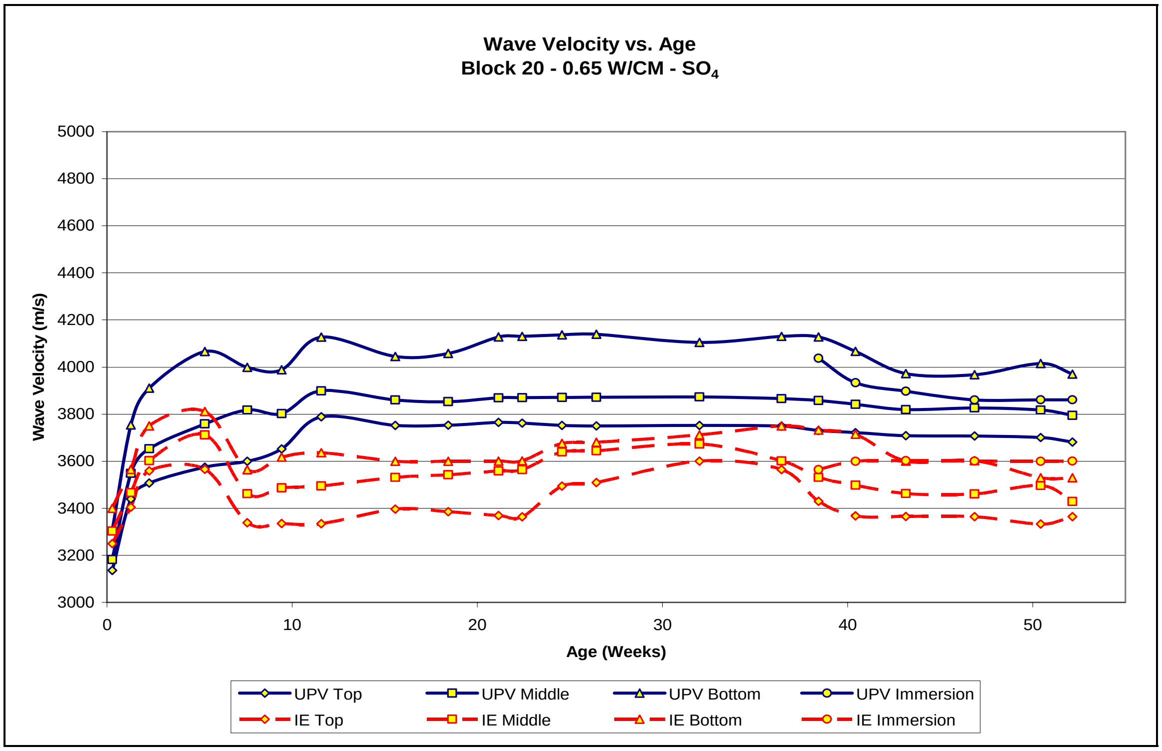

Figure 4.6: Wave velocities for a one-year sample exposed to sulfate solution (A16).

Additionally, as the specimens cure the difference becomes greater since the lower regions are in direct contact with water and the upper exposed portion is not. Eventually, this reaches equilibrium and the differences become relatively constant.

Secondly, near surface p-wave velocities initially tended to be lower than the corresponding through thickness UPV values at the same location. This was true in virtually every case, though the proportional relationship between the two changed over time. This change was dependent upon exposure conditions.

There was a definitive trend evident in wave velocity increase over time. The portions of the concrete samples that were continuously immersed in either liquid (limewater or sulfate solution) tended to exhibit a more rapid gain in wave velocity for both surface and through thickness measurements. This can again be attributed to the extended curing of the lower portions of the samples, as they were continuously immersed in their respective solutions. This ongoing improvement due to curing is a near surface effect caused by direct contact with the surrounding solution and has a continuously decreasing influence relative to distance from the surface. As a result, the near surface p-wave values increased faster than the through thickness UPV values and their plots converged in the immersed portions of the blocks exposed to lime saturated water.

Finally, as expected, the wave velocity values for the 0.45 w/c specimens were significantly higher than the corresponding values for the 0.65 w/c blocks. Again, a denser material will exhibit higher wave velocities. In this case, the lower water-to-cement ratio resulted in a denser microstructure.

The near surface p-wave velocities for the higher w/c blocks exposed to sulfate solution began to exhibit an obvious decay near the end of their 12-month exposure period for the immersed portion of the block. By comparison, the same portion of the companion block exposed to lime water exhibited no significant change in p-wave velocity. The decay in wave velocity in the lower level of the blocks exposed to sulfate solution is due to the onset of damage caused by the sulfate attack.

Evidence of the evaporation cycle was easily seen in the samples exposed to sulfate solution. A band of salt crystals formed in a region approximately 75 mm above the immersion line (Figures 4.7). These crystals were a result of evaporation of the sulfate solution from the surface of the blocks, whereupon the sodium sulfate precipitated out upon the surface. Eventually, surface scaling became evident (Figure 4.8) as the sulfate crystal growth began to induce damage within the surface layer of the concrete. A similar, less extensive, effect was observed on the blocks exposed to lime water, as the evaporation cycle resulted in the formation of a lime precipitate on the surface of the block. In this case, however, scaling of the surface material did not occur.

The results of the nondestructive testing on the block specimens demonstrated that there are significant differences between the surface wave velocities and through wave velocities of large-scale concrete samples under different exposure conditions. The study also revealed that it is possible to detect the onset of damage due to sulfate attack on concrete specimens.

The study confirmed that the water / cement ratio does have a dramatic effect on the penetrability of deleterious substances into concrete laboratory samples which, in turn, has an effect on the durability of the concrete.

Figure 4.7: Efflorescence at the immersion line on blocks exposed to sulfate solution.

Figure 4.8: Surface scaling due to sulfate crystallization.

Rebound Hammer Testing

Rebound hammer testing was performed on the front face of each block immediately prior to coring. Tests were performed at one-inch intervals between gridlines 1-9 along gridlines A-E (see Figure 4.1). A total of 33 tests were performed on each of gridlines A through E and an average value for each gridline was calculated. A photograph of rebound hammer testing is shown in Figure 4.9.

Figure 4.9: Rebound hammer testing.

Since the cores from the top of the block and at the immersion line were centered between gridlines, rebound hammer values for the cores taken at the top of the block and at the immersion line of the blocks were taken as the average values for gridlines A and B, and gridlines C and D respectively. The cores from the bottom of the block were centered on gridline E, so the average rebound number value from gridline E was matched with these cores. All rebound hammer data is presented in Appendix B.

Results - *Destructive Testing*

At the conclusion of their respective exposure cycles, the blocks were removed from their respective conditioning solutions. Eighteen core samples were then taken from each block, six at each testing height. Figure 4.10 illustrates coring operation, while Figure 4.11 shows a block with the cores removed.

One set of cores was taken as close to the bottom of the block as possible to ensure the entire core came from beneath the immersion line. Another set was taken right at the immersion line and the last set was taken as close as possible to the top of the block, well above the immersion line. The resulting cores were approximately 100 mm in diameter and 240 mm in length, too long for standard compressive strength testing, which requires a length-to-diameter ratio of 2.0. To compensate for this, approximately 20 mm was trimmed off each end of the cores using a diamond concrete saw. Doing this also removed any scaling damage at the surface of the concrete. Both ends of the specimens that were to be tested in compression were then ground so that they were completely flat and normal to the longitudinal axis of the core, thus preventing any loading eccentricities.

Figure 4.10: Coring technique for destructive testing of exposure blocks.

Figure 4.11: Fully cored block.

After preparation, the samples were immersed in lime-saturated water for a minimum of five days to ensure complete saturation prior to testing. All destructive tests were performed within two hours of removal from the lime-saturated water.

Compressive Strength

All compressive strength testing was performed using an MTS 810 220 kip Materials Test System in compliance with ASTM C 39. All tested specimens had nominal dimensions of 101.6 mm diameter x 203.2 mm long. A constant load rate of 14.5 MPa per minute was used. Graphs of compressive strength results as a function of exposure age are shown in Figures 4.12 and 4.13 for the limewater and sulfate-exposed specimens, respectively. Tables 4.6 and 4.7 summarize the numerical data for compressive strength testing that is presented graphically in Figures 4.12 and 4.13. Full core testing data is included in Appendix C.

When comparing Figures 4.12 and 4.13, a few things are apparent. For similar specimens, the average compressive strength for the specimens from the lime-saturated blocks is higher than the sulfate exposed blocks at all points in time. Over the course of one year, the average compressive strength of the 0.65 W/C concrete decreased when compared to specimens tested at 91 days of age, while the average compressive strength of the 0.45 W/C ratio specimens actually increased. This is indicative that concrete with a higher water-to-cement ratio is more susceptible to damage due to sulfate attack than a concrete with a lower water-to-cement ratio. The strength of cores from the top of the block did not increase at as high a rate as cores from the bottom of the blocks. This suggests that the hydration effects near the top of the block (and far from the curing solution) were not nearly as prominent as at the bottom of the block.

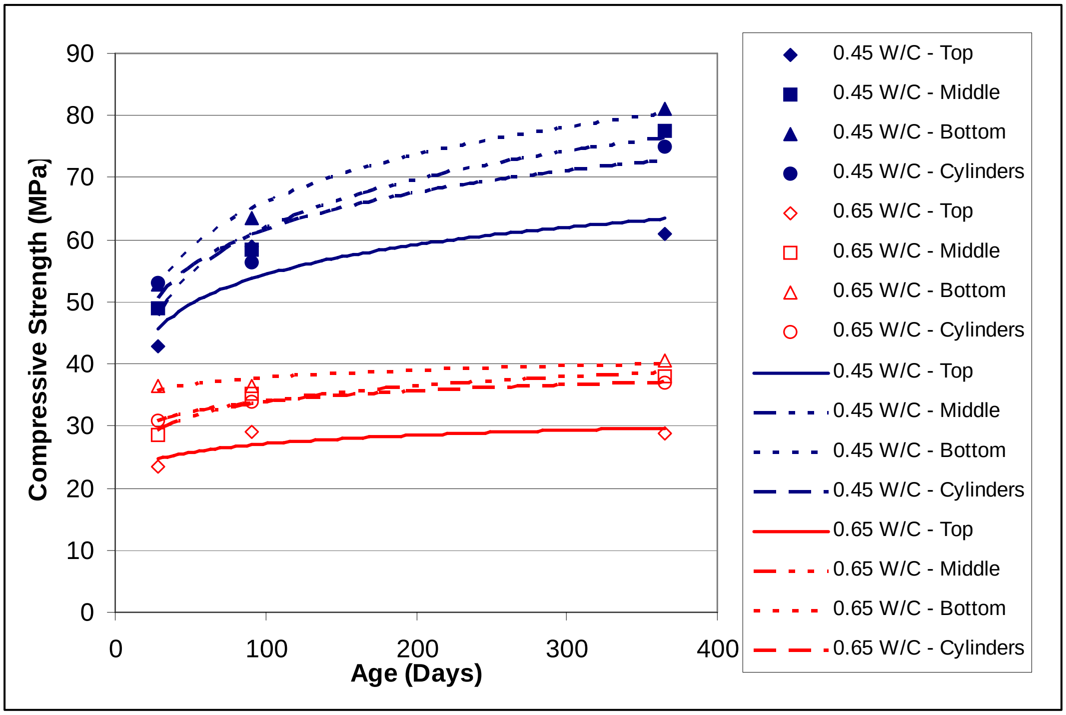

Figure 4.12: Compressive strength for specimens exposed to lime-saturated water.

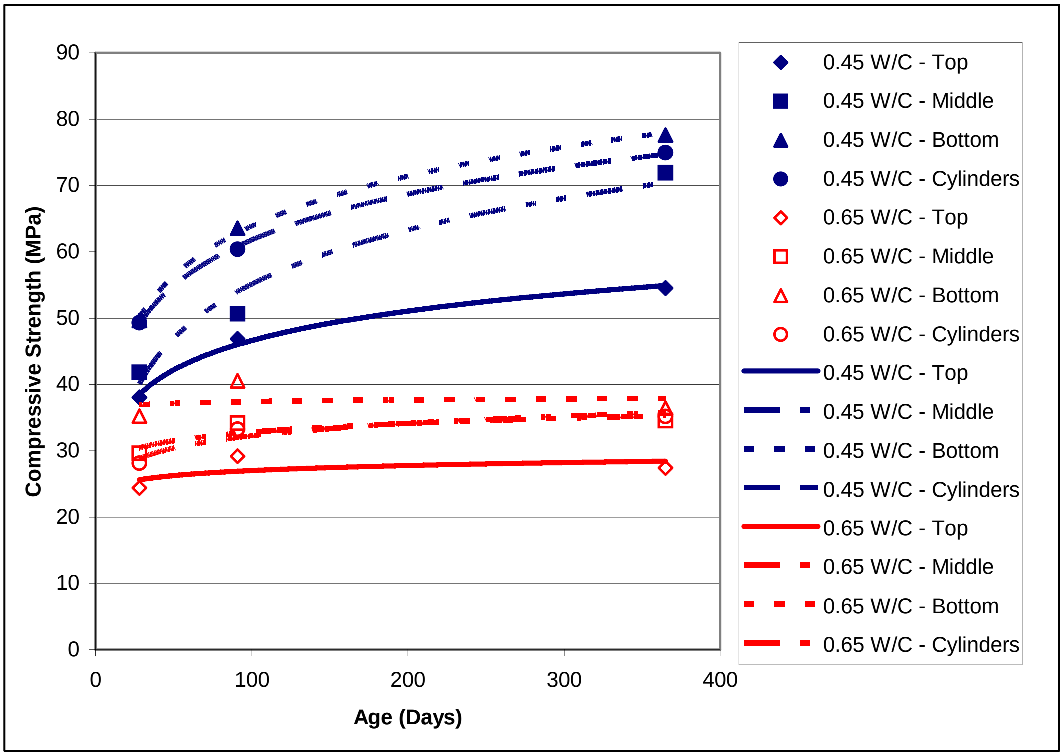

Figure 4.13: Compressive strength for specimens exposed to sulfate solution.

Table 4.6: Average compressive strength data for 0.45 W/C mixture (MPa).

Age	Limewater			Sulfate Solution		
	28 Days	91 Days	365 Days	28 Days	91 Days	365 Days
Top	42.7	59.0	61.0	38.0	46.8	54.5
Middle	49.1	58.4	77.6	41.9	50.7	71.9
Bottom	52.8	63.4	81.1	49.6	63.5	77.6
Cylinders	53.0	56.3	74.9	49.3	60.4	74.9

Table 4.7: Average compressive strength data for 0.65 W/C mixture (MPa).

Age	Limewater			Sulfate Solution		
	28 Days	91 Days	365 Days	28 Days	91 Days	365 Days
Top	23.5	29.1	28.7	24.4	29.2	27.4
Middle	28.5	35.2	38.0	29.6	34.2	34.6
Bottom	36.4	36.3	40.6	35.2	40.6	36.4
Cylinders	30.8	34.0	37.0	28.1	33.2	35.2

The strength of cylinders that were subjected to complete submersion in sulfate solution increased for both mixtures. However, the sulfate exposed cores from all locations of the blocks for the 0.65 W/C ratio decreased in strength. This phenomenon is due to the difference in transport mechanisms involved in the two cases. The evaporation front above the immersion line in the partially immersed blocks resulted in a much faster transport rate than in the completely submerged cylinders, where the ingress of sulfate is entirely controlled by diffusion alone.

Specimens from the 0.65 W/C ratio mixtures showed another general trend. Cores and cylinders that were kept immersed in sulfate solution showed a more rapid strength loss than cores from above the immersion line. This implies that the formation of ettringite and gypsum is more damaging to the concrete than the evaporation, crystallization, and scaling damage that was evident above the immersion line.

Splitting Tensile Test Results

All splitting tension testing was performed in compliance with ASTM C 496. All specimens tested had the nominal dimension of 101.6 mm x 203.2 mm. A constant load rate of 33 kN per minute was used. A photograph of a typical splitting tension test is shown in Figure 4.14.

Figures 4.15 and 4.16 show graphs of the average splitting tensile strength development for both the limewater specimens and sulfate solution specimens, respectively. Tables 4.8 and 4.9 summarize the numerical data for splitting tensile strength testing that is presented graphically in Figures 4.15 and 4.16. Complete splitting tensile strength data is included in Appendix C.

Figure 4.14: A concrete core subjected to a splitting tensile load.

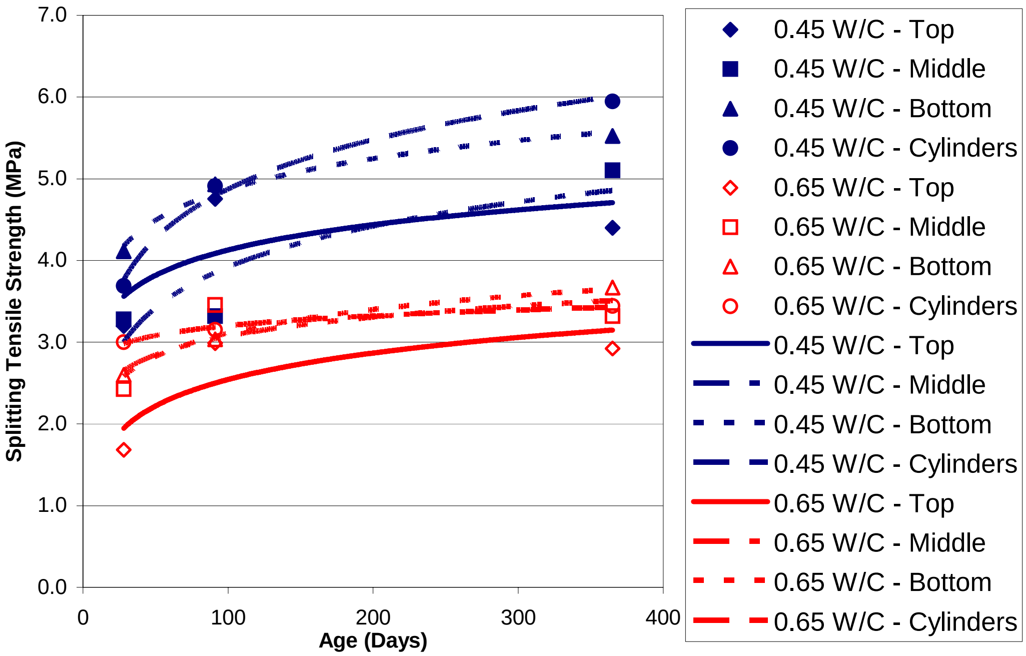

Figure 4.15: Splitting tensile strength for specimens exposed to lime-saturated water.

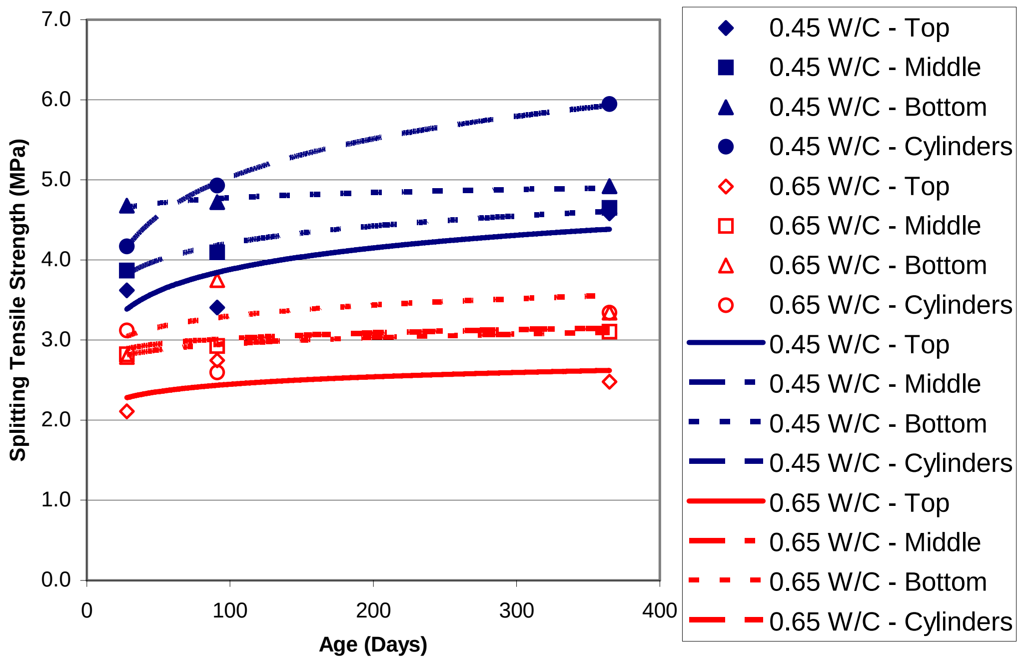

Figure 4.16: Splitting tensile strength for specimens exposed to sulfate solution.

Table 4.8: Average splitting tensile strength data for 0.45 W/C mixture (MPa).

Age	Limewater			Sulfate Solution		
	28 Days	91 Days	365 Days	28 Days	91 Days	365 Days
Top	3.2	4.8	4.4	3.6	3.4	4.6
Middle	3.3	3.3	5.1	3.9	4.1	4.6
Bottom	4.1	4.9	5.5	4.7	4.7	4.9
Cylinders	3.7	4.9	5.9	4.2	4.9	5.9

Table 4.9: Average splitting tensile strength data for 0.65 W/C mixture (MPa).

Age	Limewater			Sulfate Solution		
	28 Days	91 Days	365 Days	28 Days	91 Days	365 Days
Top	1.7	3.0	2.9	2.1	2.7	2.5
Middle	2.4	3.5	3.3	2.8	2.9	3.1
Bottom	2.6	3.0	3.7	2.8	3.7	3.3
Cylinders	3.0	3.2	3.4	3.1	2.6	3.3

When comparing the two graphed data, a few things are again apparent. For similar specimens from the 0.45 W/C mixture, the average splitting tensile strength from the blocks exposed to lime-saturated water is approximately equal to the strength of cores from the sulfate exposed blocks at all points in time. For the 0.65 W/C ratio mixtures, the average splitting tensile strength is lower for the sulfate-exposed blocks than for the blocks immersed in lime-saturated water, at all points in time.

Over the course of one year, the average splitting tensile strength of the 0.65 W/C concrete decreased when compared to the specimens tested at 91 days of age. The average splitting tensile strength of specimens from the 0.45 W/C ratio mixture actually increased, except for the cores from the bottom of the blocks, which showed very little change in strength over the one year period. This is again indicative that concrete with a higher water-to-cement ratio is more susceptible to damage due to sulfate attack than concrete with a lower water-to-cement ratio. The strength of cores from the top of the block also did not increase at as high a rate as the cores from the bottom of the blocks. This again suggests that the hydration effects near the top of the block (and far from the curing solution) were not as prominent as at the bottom of the block.

Specimens from the 0.65 W/C mixture exhibited another general trend. Cores taken from below the immersion line of the blocks exposed to sulfate solution showed a more rapid strength loss than cores from above the immersion line. Again, this implies that the formation of ettringite and gypsum is more damaging to the concrete than the evaporation, crystallization, and scaling damage that were evident above the immersion line.

The rate of strength loss for the cores tested in splitting tension was much higher than for the cores tested in compression. This is indicative that the splitting tension test is a better test than the compression test for detecting concrete damage due to sulfate attack.

Examination of the core and cylinder failure modes did not reveal any appreciable difference. All failures were along the center line of the specimen where the load was applied. In all cases the failure plane went through the aggregate. A photograph showing cores that have been failed in splitting tensile loading is shown in Figure 4.17 and a close-up of a core failed under splitting tensile load is shown in Figure 4.18.

It should also be noted that although general trends are apparent, strength values for the test results are very close. Though great care was exercised during testing to prevent any outside sources of error affecting the results, and to limit those inherent with the test itself, in many cases the coefficients of variation are high enough that when accounted for, influence the trends both up and down.

The data showed higher coefficients of variation for the splitting tensile test than for the compressive strength test. On average, the coefficients of variation for the compressive strength test were about 4.5% (with a maximum value of 9.3%) while the average coefficient of variance for the splitting tensile test was approximately 6.3% (with a maximum value of 23.6%). This higher variability is typical for tensile strength testing.

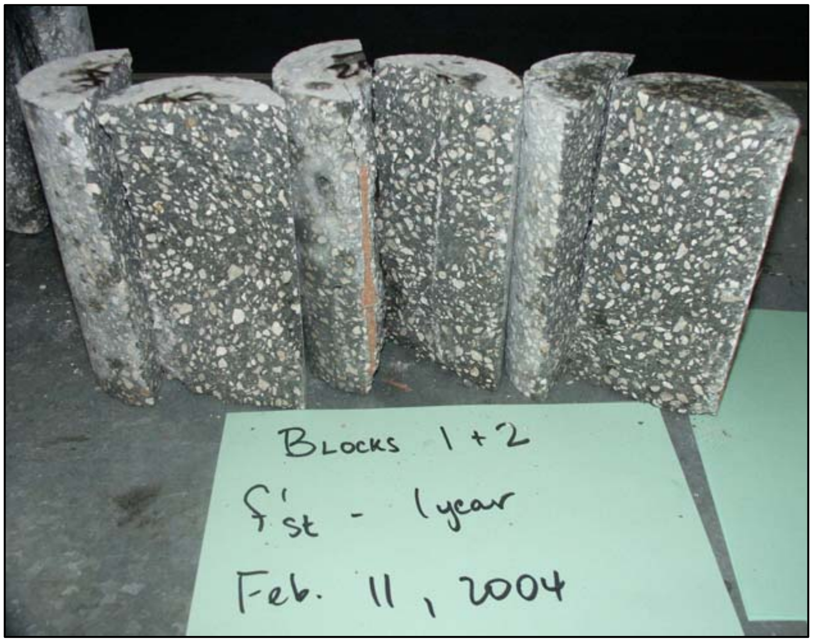

Figure 4.17: Photograph of cores failed under a splitting tensile load.

Figure 4.18: Close-up photograph of a cylinder failed under a splitting tensile load.

Pressure Tension Test Results

All pressure tensile testing was performed using a custom-built pressure sleeve. Though the test has yet to be standardized, similar research has been conducted using this test in the past. Efforts were made to duplicate the procedure used in the past research projects. All specimens tested had nominal dimensions of 101.6 mm x 203.2 mm. A photograph of a specimen being subjected to a pressure tensile load is shown in Figure 4.19.

Figure 4.19: Pressure tension testing setup.

In essence, the pressure tension test pressurizes the concrete cylinder or core by means of an externally applied gas pressure. This applied pressure acts only upon the curved surface of the specimen, which is positioned within a pressure sleeve, since the ends of the cylinder project outside the pressurized area. As long as the specimen is sufficiently saturated an internal pore pressure develops in response to this applied pressure, acting equally in all directions. Combining the applied pressure with the reacting pore pressure results in a net tensile pressure that essentially forces the ends of the cylinder apart. The peak pressure within the sleeve at failure is taken to be the ultimate tensile strength of the concrete. A constant load rate of 8.25 MPa per minute was used in this research.

The pressure tension test has been shown to be effective in detecting damage induced by various forms of concrete deterioration, of which this paper is a summary explicitly assembled to illustrate the applicability and effectiveness of the test method itself.

Figures 4.20 and 4.21 show graphs of pressure tensile strength development for both the limewater exposed specimens and the sulfate solution exposed specimens, respectively. Tables 4.10 and 4.11 summarize the numerical data for splitting tensile strength testing, with complete results included in Appendix C.

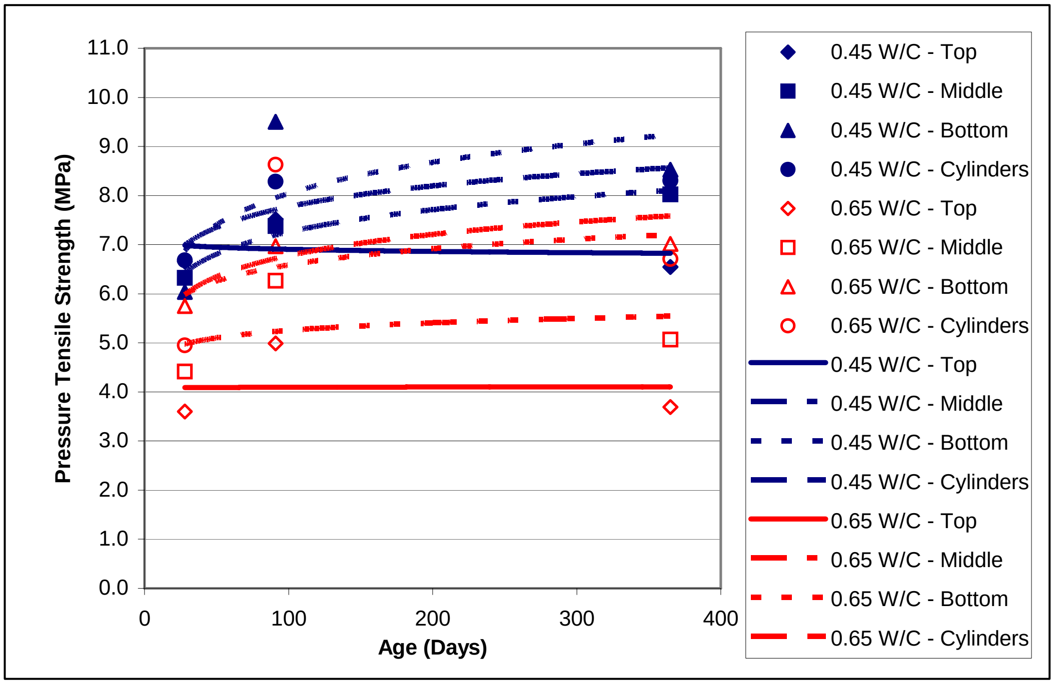

Figure 4.20: Pressure tensile strength for specimens exposed to limewater.

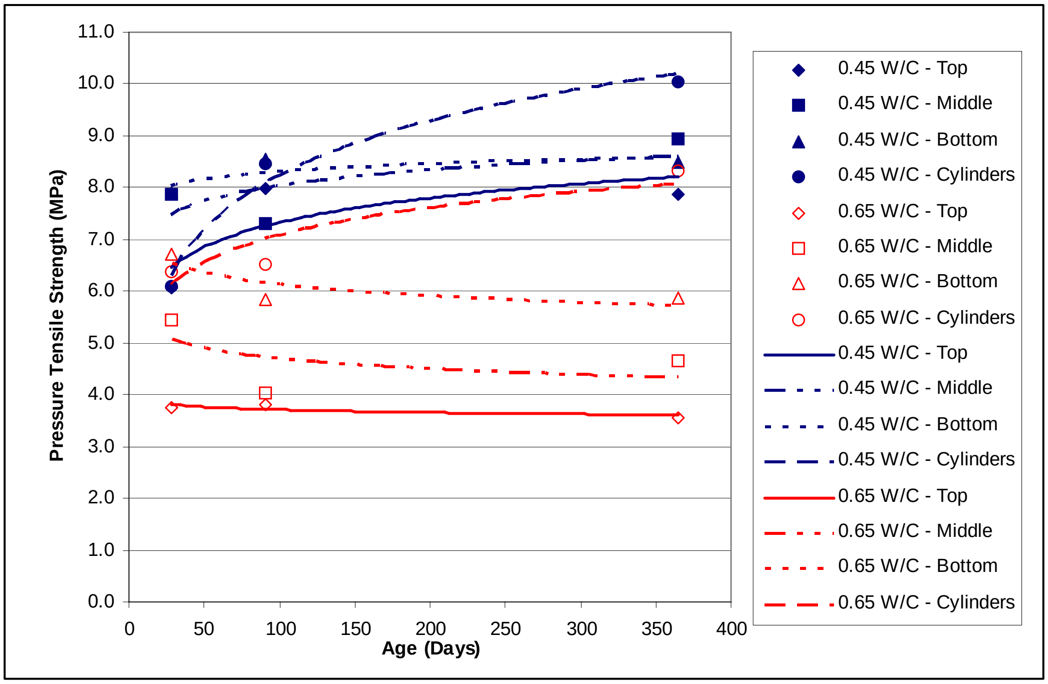

Figure 4.21: Pressure tensile strength for specimens exposed to sulfate solution.

Table 4.10: Average pressure tensile strength data for 0.45 W/C mixture (MPa).

Age	Lime			Sulfate		
	28 Days	91 Days	365 Days	28 Days	91 Days	365 Days
Top	6.7	7.5	6.5	6.1	8.0	7.9
Middle	6.3	7.4	8.0	7.9	7.3	8.9
Bottom	6.0	9.5	8.5	7.9	8.6	8.5
Cylinders	6.7	8.3	8.3	6.1	8.5	10.0

Table 4.11: Average pressure tensile strength data for 0.65 W/C mixture (MPa).

Age	Lime			Sulfate		
	28 Days	91 Days	365 Days	28 Days	91 Days	365 Days
Top	3.6	5.0	3.7	3.8	3.8	3.6
Middle	4.4	6.3	5.1	5.5	4.0	4.7
Bottom	5.7	7.0	7.0	6.7	5.8	5.9
Cylinders	4.9	8.6	6.7	6.4	6.5	8.3

Trends from these plots followed patterns similar to those from the compressive strength test results and splitting tension test results. All specimens immersed in lime-saturated water showed increasing trends. Though the data points at the age of one year showed values lower than those at 91 days, inter-batch variability of the concrete is the most probable reason for this. Close-up photographs of the 12 month specimens exposed to lime-saturated water from the 0.65 W/C mixture show a large amount of consolidation voids in the concrete compared to those exposed to sulfate solution. It is believed that the higher air content of the one-year blocks was the primary reason for the reduced strength. An example of this is shown in Figure 4.22. Improper specimen preparation is the most likely cause.

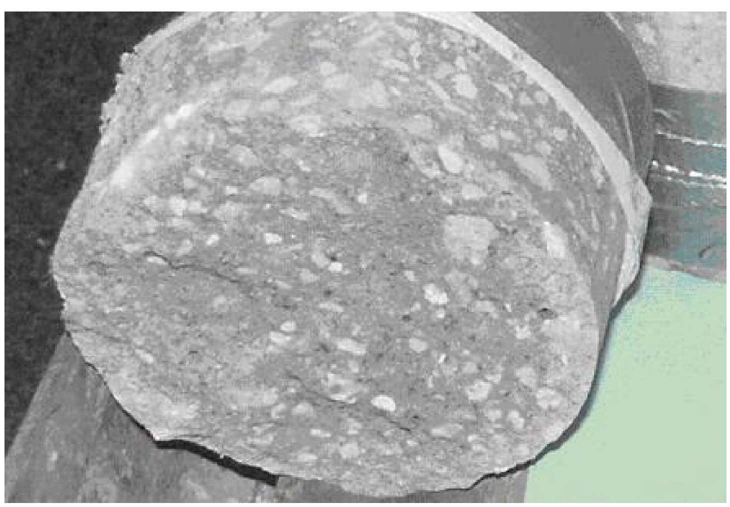

Figure 4.22: Close-up photograph of pressure tension specimen.

Cores from the 0.45 W/C mixtures that were immersed in sulfate solution showed trends of increasing strength, while specimens from the 0.65 W/C mixtures showed the opposite. This again provides evidence that a mixture with a higher water-to-cement ratio is more susceptible to damage caused by sulfate attack than a concrete with a lower water-to-cement ratio.

Cylinders from both mixtures that were immersed in sulfate solution showed similar increasing trends, again indicating that the complete immersion exposure condition results in a much slower rate of attack. The pressure tensile strength of the cores exposed to sulfates decreased over time. This contradicts the results from both the compressive strength and the splitting tensile strength tests, and suggests that the pressure tension test is the most sensitive of the three test procedures in detecting the damage inflicted on concrete due to sulfate attack.

Pressure Tension Specimen Failure Patterns

Examination of the failure plane location in the pressure tension specimens revealed an interesting phenomenon. For the cores and cylinders exposed to lime-saturated water, the location of the failure plane showed no definitive trend. However, failure of the specimens immersed in sulfate solution followed a distinct pattern.

Cores taken from the top of the blocks tended to have failure planes very close to the end of the specimens; typically failure occurred at an approximate maximum of 50 mm from the end of the cores. Cores taken from the immersion line had failure planes about one-third of the way through the specimen, and cores taken from the portion of the block that was completely immersed in the sulfate solution typically failed close to the center of the core. Cylinders also failed near the center of the specimen. Figures 4.23 through 4.26 illustrate this trend, while Figure 4.27 summarizes the failure pattern schematically.

Due to the nature of the pressure tension test, wherein the entire cylinder is evenly pressurized, failure should occur at the weakest point in the concrete specimen. This indicates that the further away from the deleterious solution the concrete is the closer to the evaporation surface the failure is. This suggests that the damage at the top of the block was close to the edge of the concrete, where evaporation and crystallization would have occurred. There would have been very little presence of sulfate near the interior portion at this location as they would have been drawn to the edge through evaporation.

For specimens taken at the immersion line, the weakest point in the matrix was deeper into the concrete, about one-third of the way through the block. Damage at this location can also be attributed to evaporation and crystallization damage. At this location, there should be more sulfates present in the interior portion of the block as they make there way up from the submerged portion.

Figure 4.23: Pressure tension cores from top of block (sulfate solution).

Figure 4.24: Pressure tension cores from immersion line (sulfate solution).

Figure 4.25: Pressure tension cores from bottom of block (sulfate solution).

Figure 4.26: Pressure tension cylinders (sulfate solution).

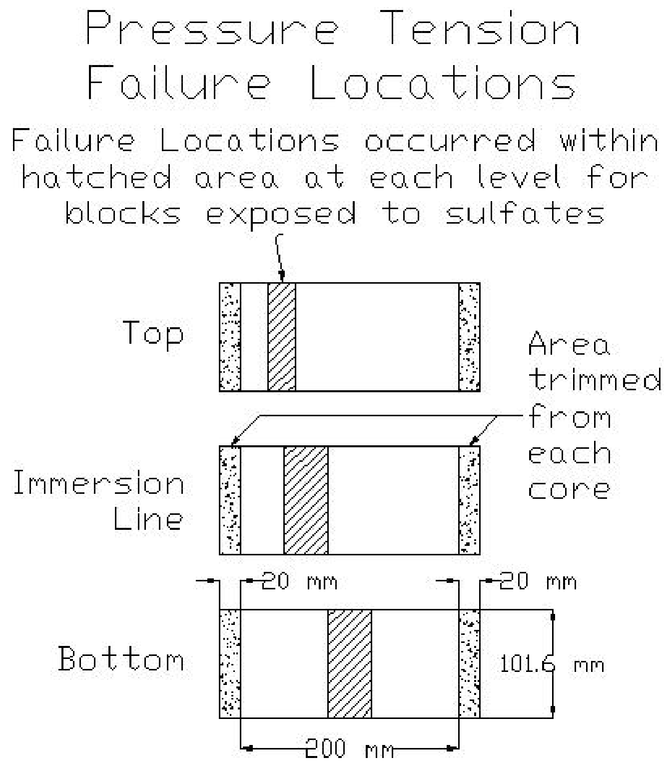

Figure 4.27: Pressure tension core failure locations.

Summary

From the destructive test results, it can be concluded that concrete with a higher water-to-cement ratio is more susceptible to sulfate attack than a concrete with a lower water-to-cement ratio (as hypothesized). For all test procedures, concrete from the 0.45 water-to-cement ratio mixture was stronger than concrete from the 0.65 water-to-cement ratio mixture. Additionally, the higher the location of the core on the block, the weaker the concrete became. The main reason for this is the higher degree of curing experienced by the concrete immersed or adjacent to the water in the respective exposure solutions.

Over time, concrete exposed to sulfates degrades, and this is confirmed by the test results. The pressure tensile test appears to be the most sensitive to detecting early-age damage caused by sulfate attack, followed by the splitting tensile test, and the compressive strength test.

Under loading, the compressive strength test acts to close up any cracks that may have formed due to the expansion of ettringite and gypsum, whereas these cracks would propagate and cause failure in the tensile test procedures. Due to this phenomenon, it takes a longer period of exposure before the damage is detectable with the compression test than with the splitting tension test or the pressure tension test. This was confirmed during testing as well. Results for concrete exposed to sulfates from the splitting tension test and the pressure tension test dropped at a faster rate, and started at an earlier age, than results from the compression tests.

Test results from all tests show that the further the concrete is from the conditioning solution, the less of an effect the solution has on the concrete. For both mixtures, the strength of the concrete immersed in lime-saturated water, increased at a higher rate for concrete below and at the immersion line than the concrete at the top of the blocks. For concrete exposed to 5% sodium sulfate solution, damage at the top of the block was not as severe as the damage below and at the immersion line.

It is believed that little could be done to reduce the degree of variance among the test results from the compressive strength and splitting tension tests. However, quite the opposite is true for the pressure tension test. Problems remain with the pressure tension test in its present state. Efforts should be made to automate the rate of loading. This would eliminate what is believed to be the main source of error inherent in the test. Special care should be taken when fabricating the specimens (as should always be the case) to ensure that the ends of the specimens are perfectly circular, thus facilitating the prevention of leaks at the end of the pressure vessel.

CHAPTER 5
ANALYSIS OF RESULTS

Correlation of Nondestructive & Destructive Results

Compressive strength versus ultrasonic pulse velocity

Prior research has found that for mature concrete, the modulus of elasticity of concrete E is proportional to the square root of compressive strength.

$$E \propto \sqrt{f'_c}$$

Further, it has been shown that the P-wave velocity C_p through elastic solids is proportional to the square root of the elastic modulus.

$$C_p \propto \sqrt{E}$$

Thus, the anticipated relationship between wave speed and compressive strength would be along the lines of Equation 6.3 (Pessiki 1988).

$$f'_c \propto (C_p)^4$$

Thus, it was anticipated that a fourth order relationship would exist between compressive strength and pulse velocity testing. The same should also hold true for surface wave speeds from impact-echo testing, as both tests measure the wave velocity through an elastic medium.

Immediately prior to coring, ultrasonic pulse velocity measurements were taken at the same elevations on the blocks at which the cores were taken. The average velocity was calculated for each elevation and then compared to the destructive test results from the cores taken at these locations.

Relationships between pulse velocity and compressive strength were developed in accordance with procedures suggested by Samarin and Meynink, and by Malhotra (Popovics 1998). Samarin and Meynink suggested a relationship of the form $Y = a \cdot X^4 + b$ (the same relationship as anticipated). Separate relationships were formed for blocks exposed to lime-saturated water, and blocks exposed to the sulfate solution. A plot of average core compressive strength versus average pulse velocity to the fourth power is shown in Figure 5.1.

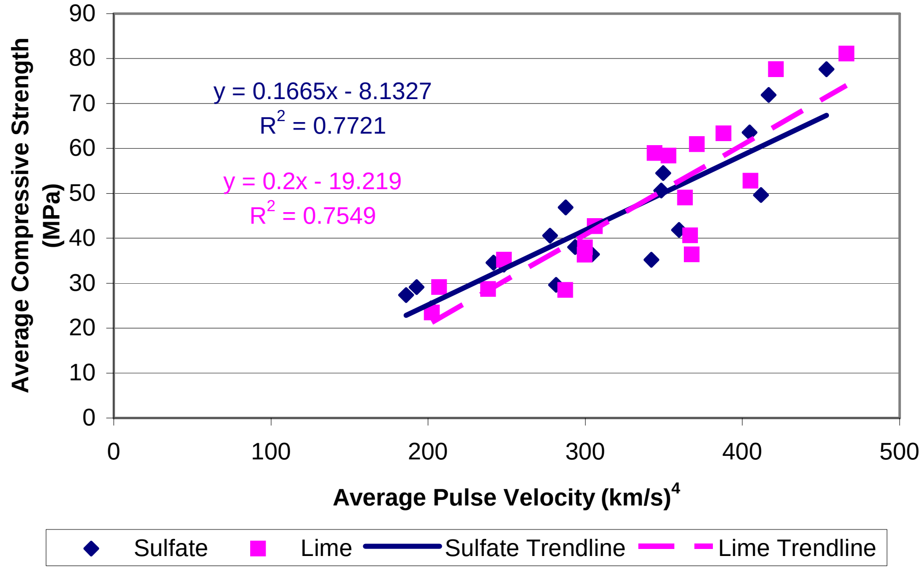

Figure 5.1: Correlation of compressive strength and pulse velocity using Samarin and Meynink relationship.

Malhotra suggested an exponential relationship of the form $Y = a \cdot e^{bx}$. Separate relationships were again derived for specimens exposed to sodium sulfate and lime-saturated water. Figure 5.2 shows a plot of these relationships.

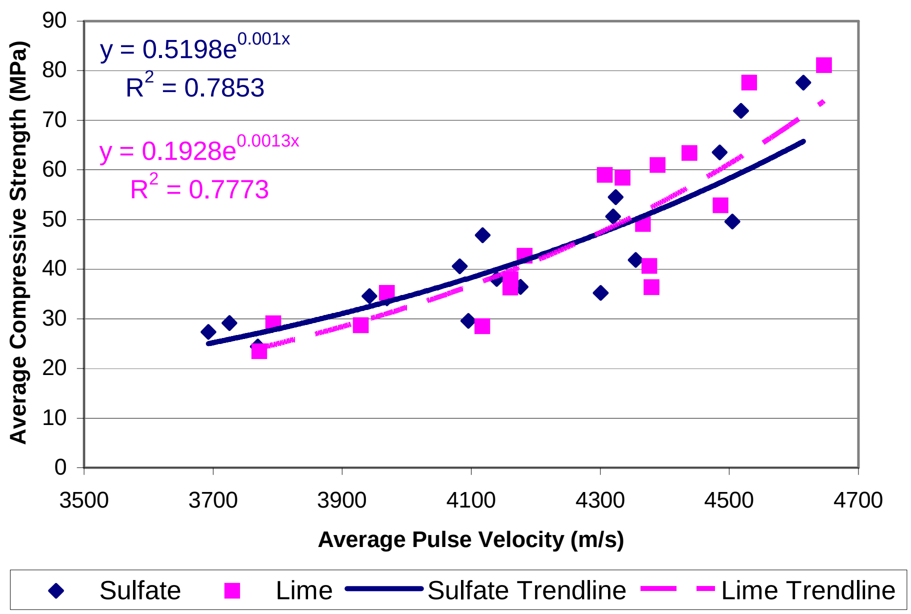

Figure 5.2: Correlation of compressive strength and pulse velocity using Malhotra relationship.

As can be seen from these plots, both methods are able to predict the compressive strength of concrete using pulse velocity testing, though the accuracy of that prediction is not very high (based on R^2 value). Malhotra's relationship appears to be slightly better than the correlation suggested by Samarin and Meynink. However, the regression values are close, and when the number of specimens tested is considered, it would not be prudent to make a decision as to which method provides a better relationship between pulse velocity and concrete compressive strength.

Pressure tension strength versus ultrasonic pulse velocity

In addition to compressive strength, correlations were also developed between ultrasonic pulse velocity and the pressure tensile strength determined from coring. Figure 5.3 shows the correlation between average ultrasonic pulse velocity and average pressure tensile strength.

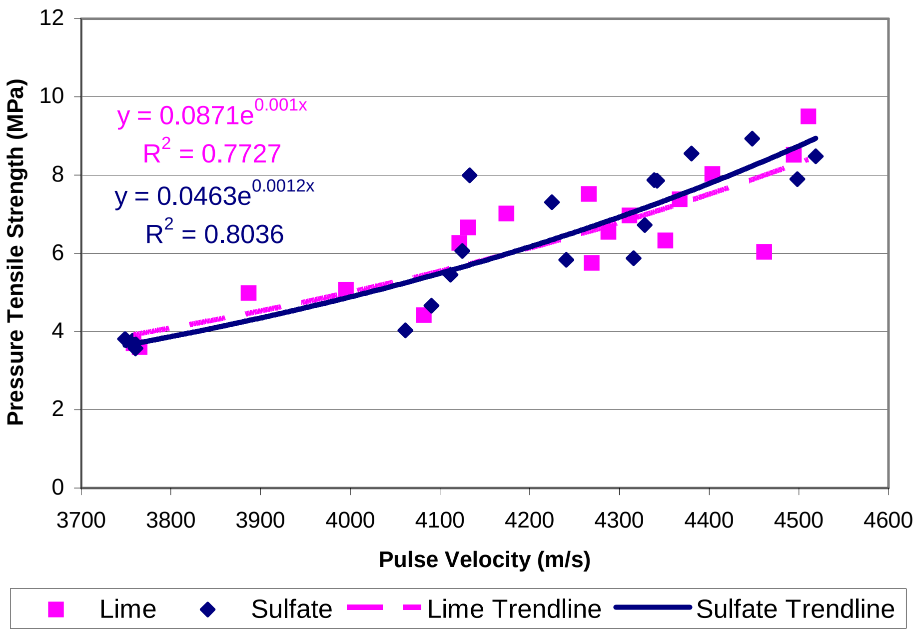

Figure 5.3: Correlation of pressure tensile strength and pulse velocity.

Curve fitting software was used to develop the relationships between pressure tensile strength and pulse velocity. It was found that exponential relationships gave the best fit for the data (as was the case with compressive strength testing as per Malhotra's suggested relationship). It is worth noting that the pulse velocity testing actually formed better relationships for prediction of pressure tensile strength than for compressive strength. This conclusion is based on the regression values for the best-fit lines, and is indicative that the pulse velocity test is sensitive to the flaws and other damage within concrete that may propagate failure under tensile load, whereas the same flaws would tend to close under a compressive load, and thus not become a source of failure.

Attempts were also made to correlate low pulse velocity results to failure locations. As discussed previously, failure locations for sulfate immersed specimens from the top row were almost always located within 50 mm of the end of the trimmed specimens, (approximately 75 mm from the original block surface), the immersion line specimens usually failed approximately one-third of the way through the specimen, and specimens below the water line almost always failed at the center of the specimen.

Pulse velocity measurements through the length of the blocks showed that at the top of the block, pulse velocities at gridlines X and Z were higher than gridline Y. At the immersion line, the differences between pulse velocities along gridlines X, Y, and Z were often indistinguishable, and for areas of the blocks that were immersed in solution, the pulse velocities at the exterior (gridlines X and Z) were almost always higher than at the center of the block (gridline Y). This may be indicative that superior curing was experienced close to the outside of the block than at the center for sections of the block immersed in solution.

For the upper and lower regions, these results correspond very well with the failure location trends reported in Chapter 4. Thus, three-dimensional tomography appears to be a feasible method for determining the damaged regions within a concrete member. In the research reported herein, this method to determine failure location is only applicable to the pressure tensile test since the failure mechanisms inherent in the other two tests (i.e. compression and splitting tension) were not capable of producing patterns showing regions of suspect concrete within the test specimens themselves. If used properly, three-dimensional tomography can be a very valuable tool for locating regions of damage within concrete structures.

Splitting tensile strength versus ultrasonic pulse velocity

Finally, correlations were developed between ultrasonic pulse velocity and the splitting tensile strength determined from coring. Figure 5.4 shows the correlation between average ultrasonic pulse velocity and average spitting tensile strength.

Curve fitting software was again used to develop the relationships between splitting tensile strength and pulse velocity and it was found that exponential relationships gave the best fit for this data as well. Based on the regression values for the best-fit lines, the pulse velocity testing formed even better relationships for predicting splitting tensile strength than compressive strength and pressure tension. Again, this is indicative that tensile strength testing is more sensitive to the flaws and other damage within concrete than is compression testing.

Compressive strength versus impact-echo P-wave speed

In addition to the wave speeds obtained from ultrasonic pulse velocity testing, a second set of values was acquired using the impact echo technique to measure wave speed along the surface of the concrete blocks. Figure 5.5 shows a correlation of compressive strength and surface wave velocity measured from impact echo testing.

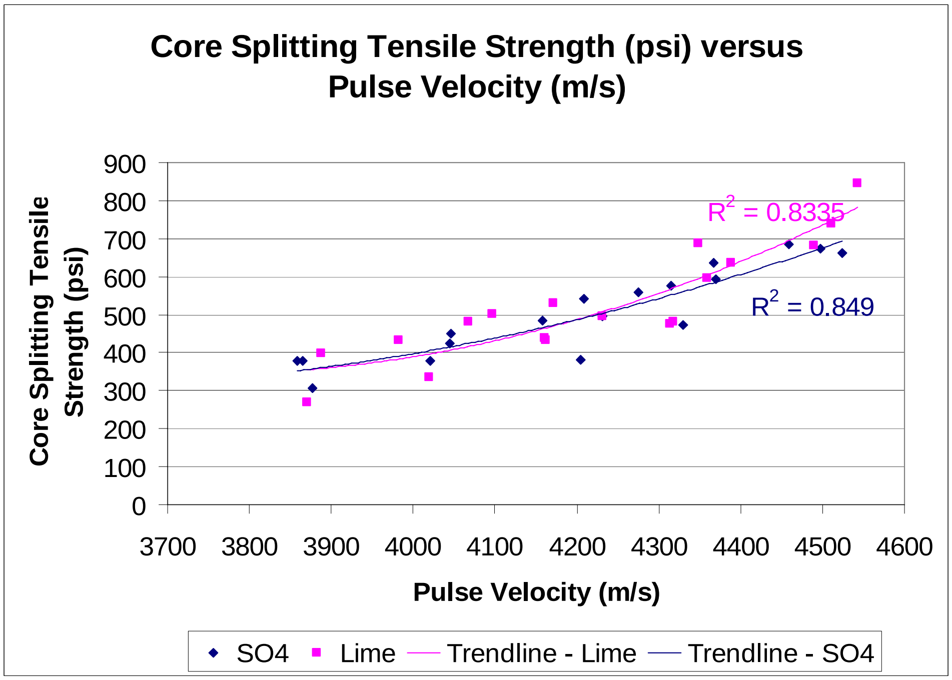

Figure 5.4: Correlation of splitting tensile strength and pulse velocity.

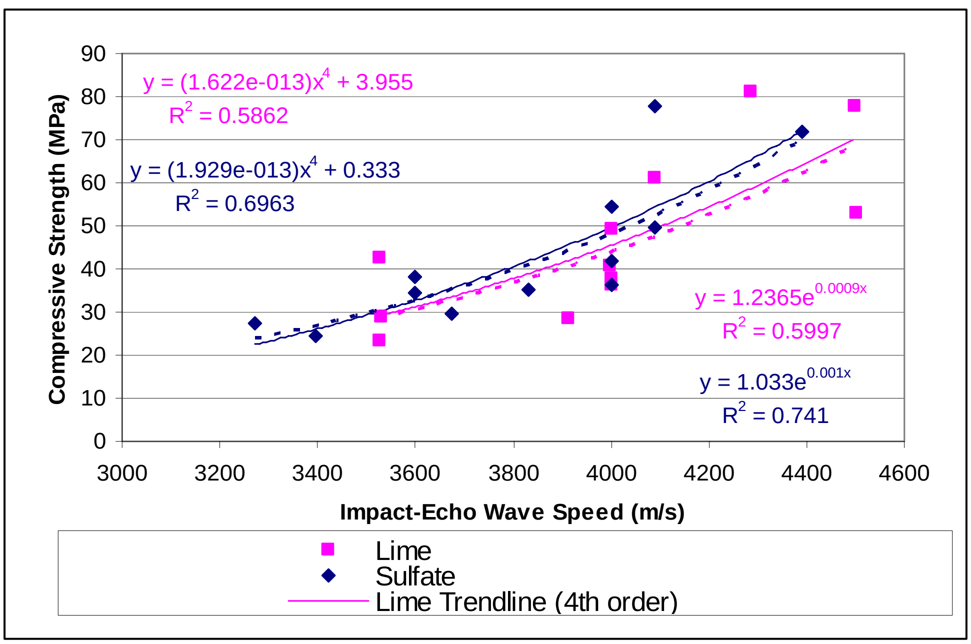

Figure 5.5: Correlation of compressive strength and surface P-wave speed from the impact echo technique.

Also shown in Figure 5.5 are exponential trend lines. Both fourth order and exponential relationships do correlate with destructive test results, with the exponential equations relating slightly better than the fourth order polynomial series. However, the regression values are far less accurate than those obtained from pulse velocity testing. This discrepancy is likely due to the fact that the surface wave measurements are passing almost entirely through the outer edge of the concrete block. In the case of external sulfate attack, this would mean that these measurements are being taken almost exclusively through damaged material while the compressive strength value is measured over the entire core, thus averaging the damaged and undamaged areas within the core.

Additionally, after the cores were taken from the blocks approximately 20 mm from each end of the cores was trimmed prior to testing. Thus, the actual region of the concrete through which the surface P-waves passed during impact echo testing was removed prior to compression testing. Also, the values used for making these relationships were average values from along each gridline. Had individual tests been performed and data obtained for each specimen, perhaps the test results may have shown a better correlation with the predicted values.

Pressure tensile strength versus impact-echo P-wave speed

There has been no prior research performed relating P-wave speed to pressure tensile strength due to the novel nature of the pressure tension test. Nevertheless, data was collected and attempts were made to relate surface wave speed to the tensile strength of concrete measured by the pressure tension method. The data was examined using curve-fitting software, and again the best-fit lines were found to be exponential in nature. Figure 5.6 shows a plot of the correlations developed for blocks immersed in lime-saturated water, and blocks exposed to sulfate solution.

The data correlated very well, with R^2 values of 0.87 and 0.88 for the limewater and sulfate solution specimens, respectively. This indicates that surface P-wave velocity from the impact echo technique may be a very reliable method for estimating the tensile strength of concrete. Also worth noting is the position of both trend lines. Blocks exposed to sulfate solution and blocks immersed in lime-saturated water showed increasing P-wave speed with time, but there is a shift in the relative positions of the trend lines for each conditioning solution. Limewater specimens on average tended to exhibit a faster P-wave speed for a given strength than did the specimens immersed in lime-saturated water. More research is necessary to validate the use of the impact-echo test as a reliable method of determining the tensile strength of concrete.

The higher degree of correlation between p-wave speed and tensile strength, as compare to that for compressive strength, is not surprising when one considers the mechanism involved. The development of internal damage due to microcracking will almost immediately affect tensile strength since an applied tensile stress will act to open such cracks, promoting propagation and failure. A compressive stress, on the other hand, will act to close such cracks, thus resisting propagation.

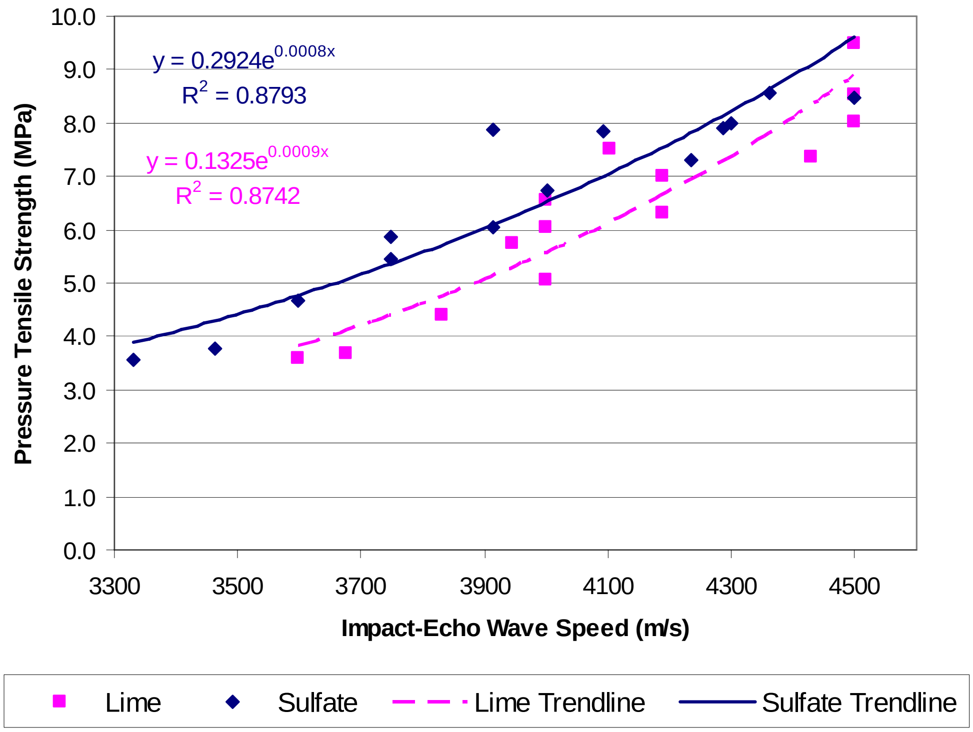

Figure 5.6: Correlation of pressure tensile strength and surface P-wave speed from the impact echo technique.

The true P-wave velocity through a solid material should not change due to the appearance of cracks within that material as long as there is a path through solid material around the cracks. However, the wave velocity calculated in both the pulse velocity and impact echo tests is based upon the gross distance between wave source and receiver, assuming a wave path that follows the shortest distance between them. Cracking within the material thus causes an increased path length through which the P-wave must travel that is not included in the measured distance, resulting in a lower calculated wave speed. In essence, then, cracking should have the same effect on both tensile strength and wave speed, a proportional reduction in both properties.

Compressive strength versus rebound number

After nondestructive testing of the cores was concluded, destructive tests were performed. Strength values were then compared to the rebound number values in an effort to form relationships between the parameters. Values for the 0.45 W/C mixtures were compared separately from those for the 0.65 W/C mixtures. It was noticed that differences between the regression values for the fit lines were almost non-existent. Thus, it was judged safe to combine the two mixtures, and instead only separate the data for blocks subjected to sulfate solution from those exposed to lime-saturated water. The values for the two groups were then combined, and again compared to see if any difference was noted.

Published literature on the topic of relating surface hardness test results to concrete compressive strength suggests that the best-fit equation for this relationship is linear, of the form Y = a + bX. As a result, linear relationships were used to develop the trend lines and corresponding equations. A plot of compressive strength versus rebound number is shown in Figure 5.7.

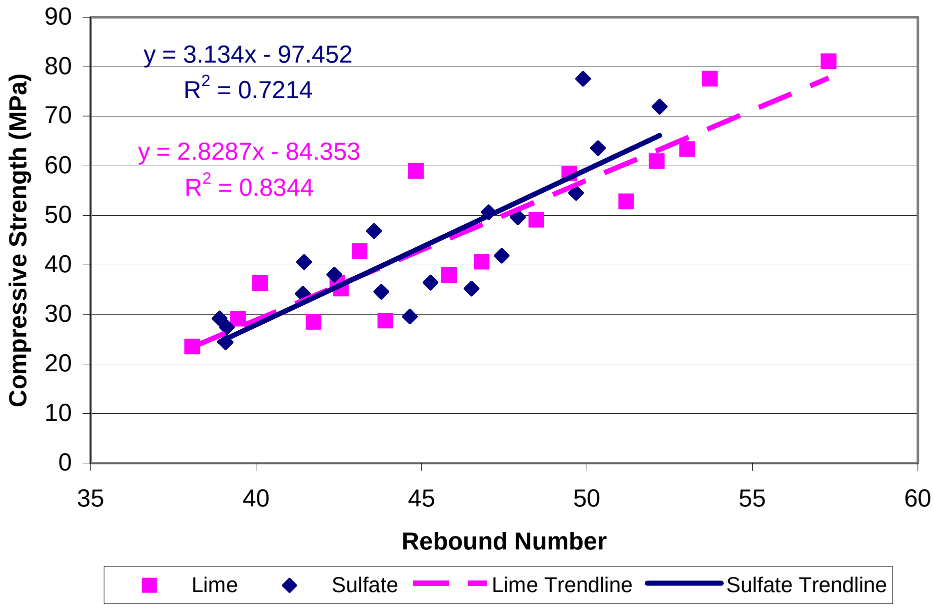

Figure 5.7: Correlation of compressive strength and rebound number.

As shown in Figure 5.7, the regression value for the sulfate samples is essentially the same as the limewater samples. However, the coefficient of determination (R^2) was considerably lower for the sulfate-exposed blocks (R^2 = 0.721 versus 0.834). Hence it can be concluded that the damage inflicted on the concrete by sulfate attack tends to affect the test results for the rebound hammer test. This can be attributed to softening of the concrete near the surface.

Visual observations during rebound hammer testing revealed that the dimples left on the concrete surface by the rebound hammer were far more noticeable on the sulfate-exposed blocks than on the limewater-exposed blocks. This was especially true for areas of the concrete that were below the immersion line, as the dimples were far more noticeable below the water line than above. This phenomenon was also observed to be worse for the 0.65 W/C ratio mixtures than for the 0.45 W/C ratio mixtures. This indicates that the sulfate solution caused surface softening of the concrete, since no such dimples were observed on blocks exposed to lime-saturated water from either mixture. It is again indicative that a high W/C ratio concrete is more susceptible to damage caused by sulfate attack than a low W/C ratio concrete. An example of these defects, from below the waterline on a 0.65 W/C block exposed to sulfates, is shown in Figure 5.8.

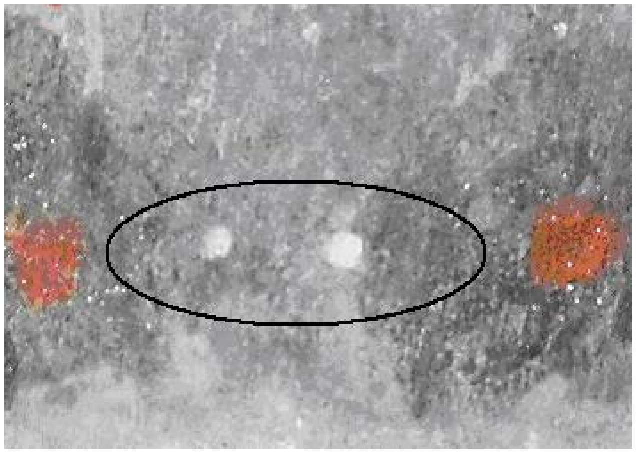

Figure 5.8: Photograph of defects induced by rebound hammer testing.

Pressure tensile strength versus rebound number

Similar to the correlation performed between compressive strength and rebound number, the pressure tensile strength values were also examined. Figure 5.9 shows the relationship between average rebound number and average pressure tensile strength.

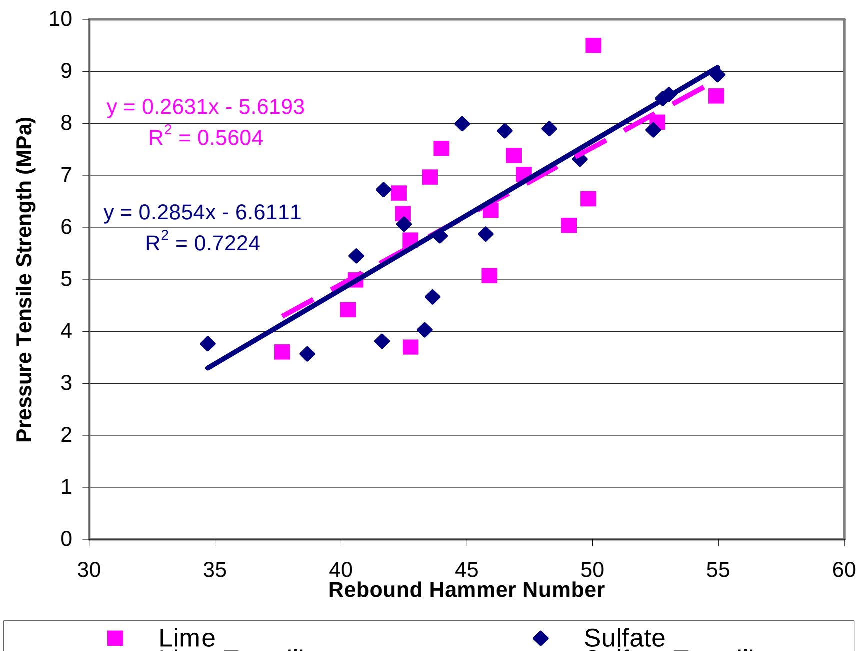

Figure 5.9: Correlation of pressure tensile strength and rebound number.

As can be seen from the Figure 5.9, a general trend does exist for the correlation between pressure tensile strength and rebound number but the accuracy of these relationships are not as high as those for compression testing (based on the comparison of R^2 values). This effect is due to the inherent nature of tensile strength testing, which tends to be more variable than compressive strength testing, especially when deteriorated concrete is evaluated.

In both correlations, compressive strength and pressure tensile strength, the correlation accuracy is lower than desired for use as a strength prediction tool. This is primarily due to the fact that the rebound hammer test is a surface hardness test, and can not detect internal damage away from the surface, whereas the strength tests are measuring a more global value through the thickness of the specimen. A deterioration mechanism that acts inward from the surface of a concrete member will show up in the rebound number results at earlier ages. Thus, the general relationships do suggest that rebound number can be used to detect the presence of damage at the surface of concrete members.

Combined Methods

The term "combined method" refers to the use of one nondestructive testing technique to improve the reliability and precision of another in predicting a property of concrete. By combining results from multiple *in situ* test methods, a multi-variable correlation can be used to estimate concrete strength. The basic idea is that if the methods are influenced in different ways by the same factor, their combined use results in a canceling effect that tends to improve the accuracy of the estimation.

Of all the nondestructive testing techniques that are used, the most common combination is that of the surface hardness method and the ultrasonic pulse velocity test. This combination has resulted in strength relationships with lower coefficients of variance than when the methods are used on their own.

Compressive Strength Prediction by Combined NDT Methods

Relationships have been formed relating concrete compressive strength to rebound number and to pulse velocity independently. However, past research has shown that when the two tests are considered simultaneously, a better estimation of compressive strength can be formed. The mathematical basis is that the accuracy of an approximation using one variable can be improved by a suitable second independent variable (Popovics 1998). The SONREB method published by RILEM outlines the methodology of making this correlation.

Data from rebound hammer tests and pulse velocity tests were combined using the relationships suggested by Samarin and Meynink, and by Malhotra (Popovics 1998). Separate correlations were again formulated for the blocks immersed in lime-saturated water and the blocks immersed in sulfate solution.

The Samarin and Meynink relationship is of the form;

$$f'_c = a \cdot R + b \cdot UPV^4 + c$$

While the Malhotra relationship is of the form;

$$\text{Log}(f'_c) = a \cdot \text{Log}(R) + b \cdot UPV + c$$

For both relationships *a*, *b*, and *c* are constants, *R* is the average rebound number, *UPV* is the average pulse velocity, and f'_c is the concrete compressive strength. Three-dimensional plots were generated of these relationships for both control and test specimens. The resulting plots for the Samarin and Meynink relationship are shown in Figures 5.10 and 5.11 while the Malhotra relationship is shown in Figures 5.12 and 5.13.

As can be seen in Figures 5.10 through 5.13, predictions made for sulfate treated specimens were not as accurate as for specimens immersed in lime-saturated water. This can likely be attributed to the effect on the rebound hammer test by the surface softening of the concrete due to sulfate exposure. In all cases, however, the estimations of concrete compressive strength improved when using the multi-variable correlation as compared to rebound hammer and pulse velocity values considered independently.

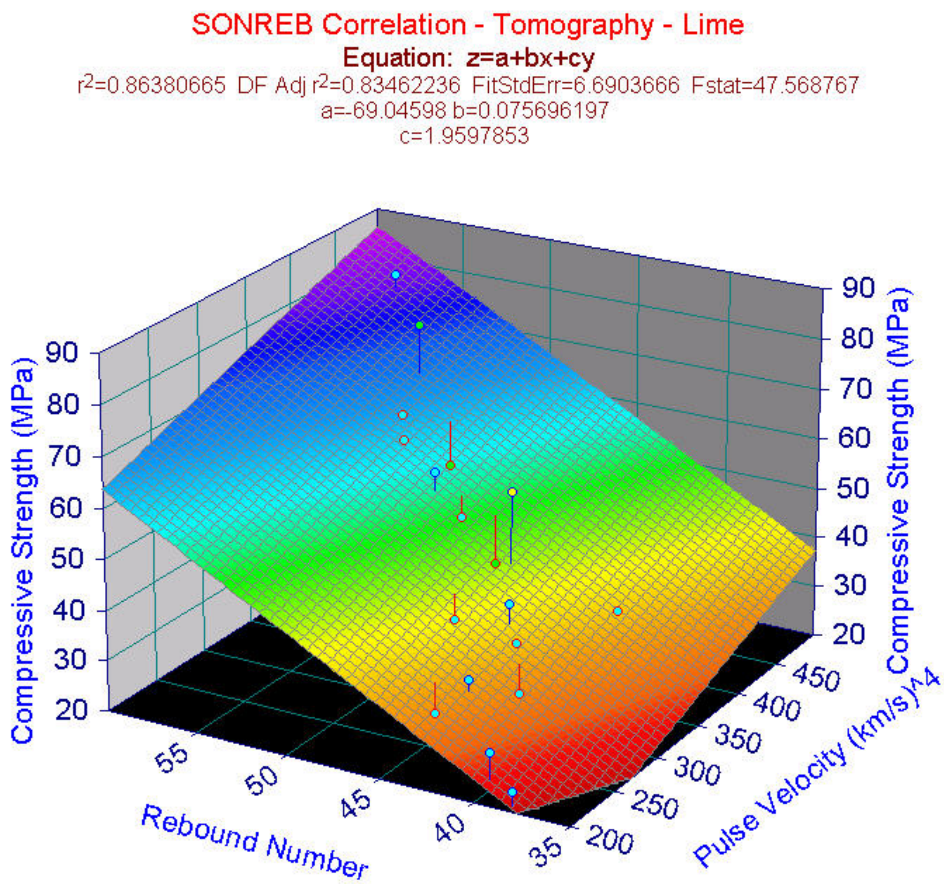

Figure 5.10: SONREB correlation for limewater specimens by Samarin and Meynink relationship.

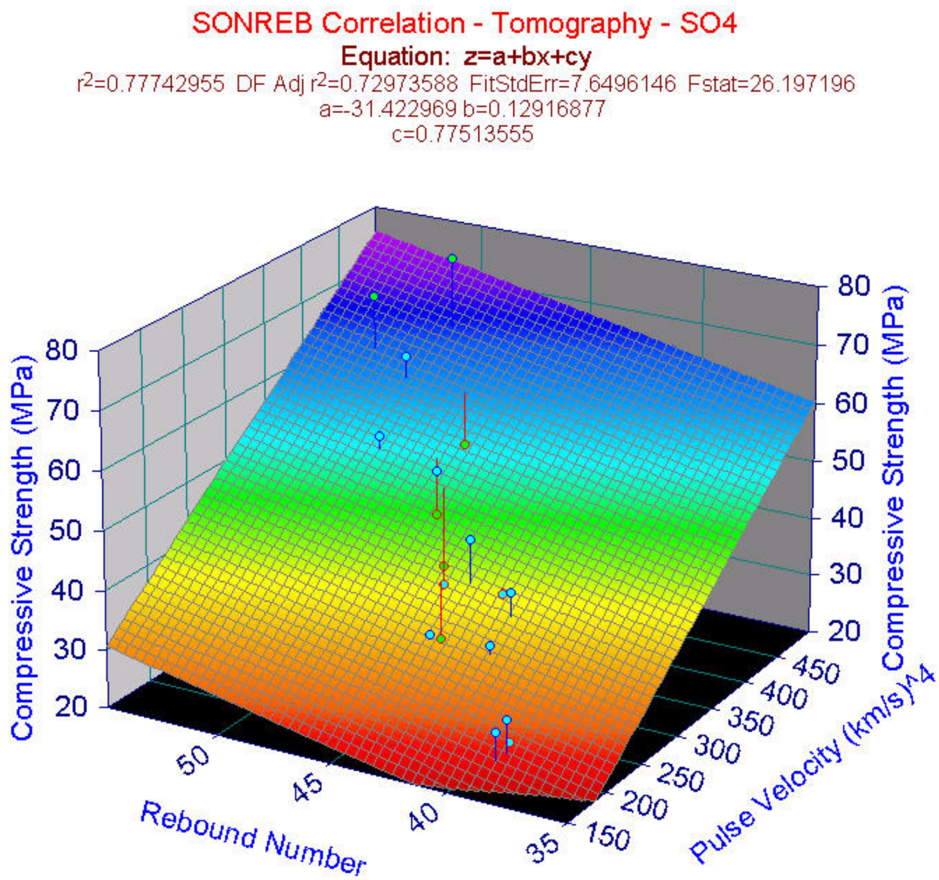

Figure 5.11: SONREB correlation for sulfate specimens by Samarin and Meynink relationship.

Again, when comparing regressions values, it would appear that the relationship suggested by Malhotra is more accurate than that presented by Samarin and Meynink. Looking at the figures, the graphs for the blocks exposed to sulfate solution appear to be less sensitive to rebound number than the blocks exposed to lime-saturated water. The slopes on the y-axes (rebound number) of the graphs are steeper for blocks exposed to lime-saturated water than for blocks immersed in sulfate solution. The opposite trend can be seen when looking at the plots for pulse velocity test results. The slopes on the x-axes (pulse velocity) of the graphs are steeper for blocks exposed to sulfate solution than the slopes for blocks immersed in lime-saturated water. These trends are indicative that the pulse velocity test is more sensitive for detecting damage in concrete than the rebound hammer test for concrete exposed to sulfate solution.

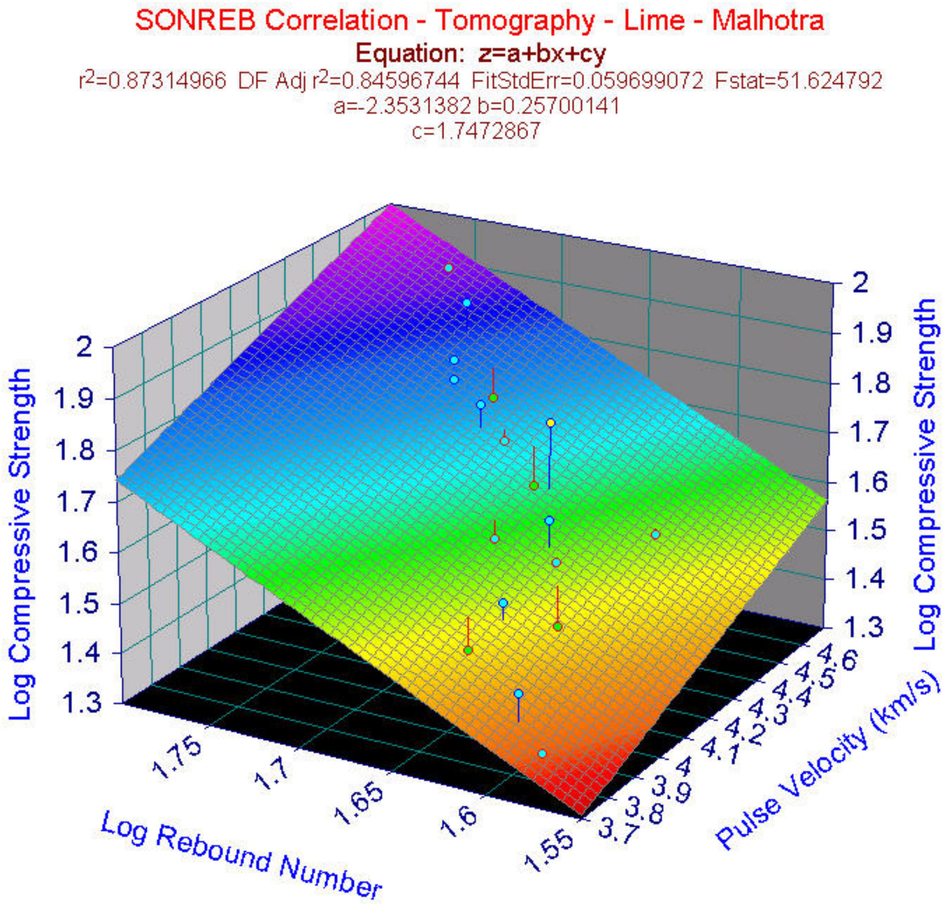

Figure 5.12: SONREB correlation for limewater specimens by Malhotra relationship.

Using the correlations generated with the SONREB method, plots showing predicted values versus actual values for compressive strength were generated. Shown in Figure 5.14 is the relationship suggested by Samarin and Meynink, while Figure 5.15 depicts the relationship suggested by Malhotra. Again, the regression values of both plots are too similar for it to be prudent to pass judgment as to which suggested relationship is the better of the two. Both relationships show reasonably good estimations of compressive strength.

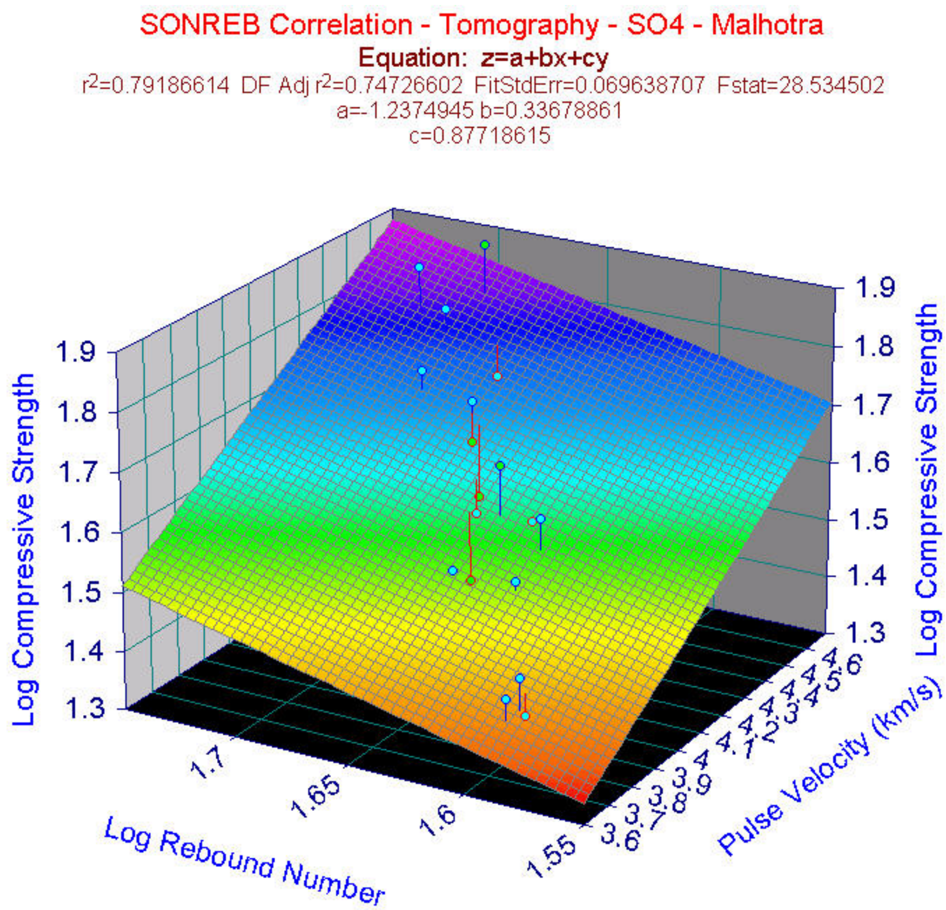

Figure 5.13: SONREB correlation for sulfate specimens by Malhotra relationship.

Resonant Frequency

Resonant frequency analysis was performed on the concrete cores in an attempt to develop relationships between compressive strength and longitudinal resonant frequency. Resonant frequencies were measured only on individual cores since the large scale blocks exceeded the capacity of the driver, and resonance could not be achieved.

Unfortunately, the data obtained from the cores showed a very wide scatter and no apparent relationships could be obtained between compressive strength and resonant frequency. The same held true for pressure tensile strength versus resonant frequency. While it has been shown that resonant frequency testing may be a suitable test to monitor specimens for changes over time (Ferraro 2003), the data reported here shows that no apparent relationship exists between resonant frequency and destructive test results.

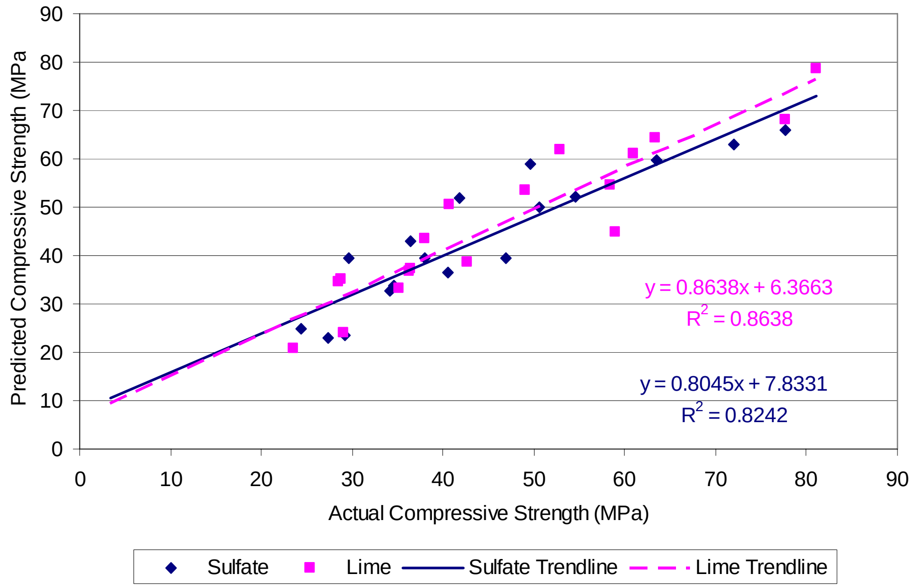

Figure 5.14: Accuracy of compressive strength predictions using the Samarin and Meynink relationship.

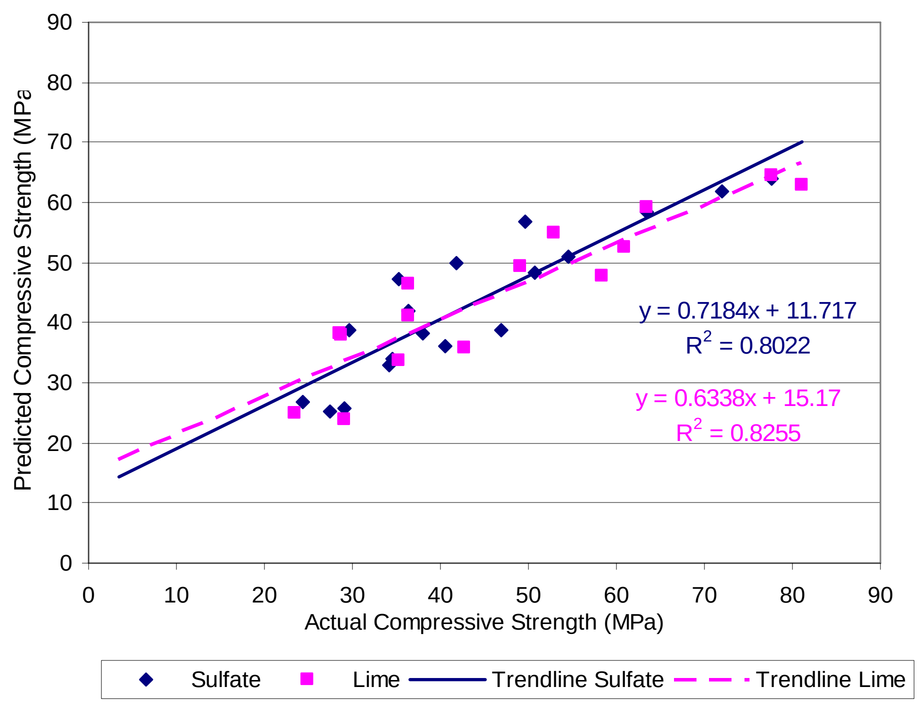

Figure 5.15: Accuracy of compressive strength predictions using the Malhotra relationship.

It should also be noted that the moisture content of the samples was not determined prior to testing. Literature has shown that moisture can have a significant effect on resonant frequency should have been accounted for during the later stages of this experiment. Figure 5.16 shows a plot of compressive strength versus resonant frequency. Figure 5.17 shows the same for pressure tensile strength. Complete resonant frequency data for all cores is included in Appendix C.

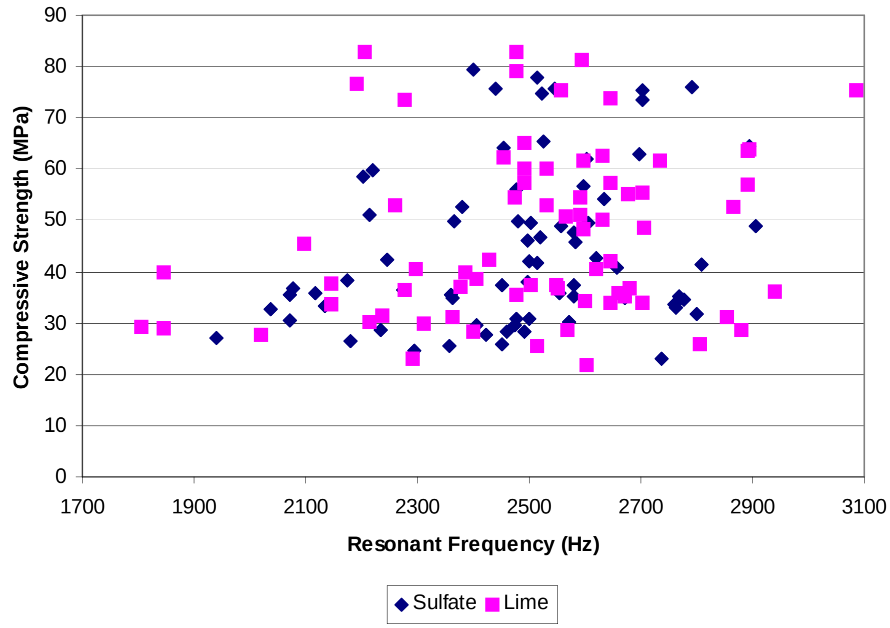

Figure 5.16: Core data for compressive strength versus resonant frequency.

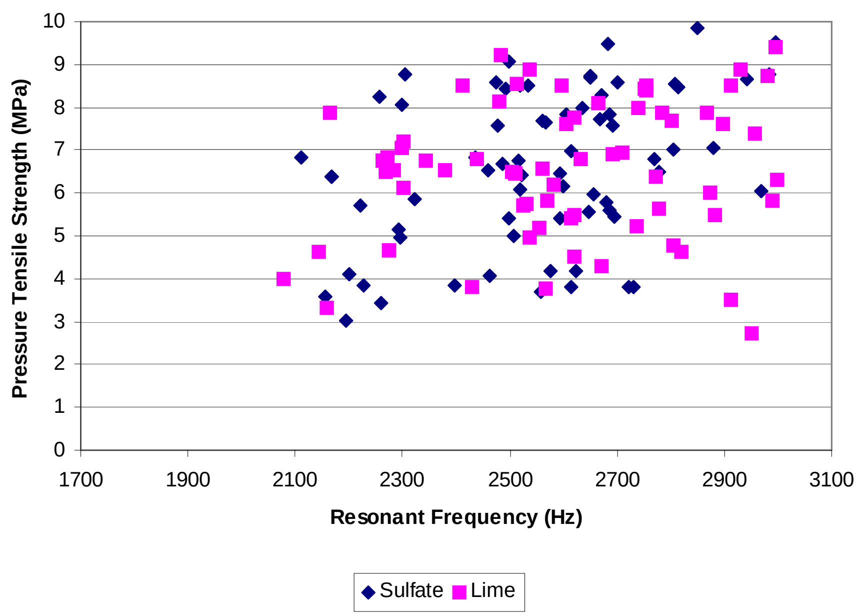

Figure 5.17: Core data for pressure tensile strength versus resonant frequency.

SEM Analysis of Microstructure

In order to evaluate the effect of microstructural cracking on the results obtained from nondestructive testing, a series of samples were removed from each of the one year blocks. Though limited in number, it was clearly evident from the samples examined that definitive trends in microstructural cracking were present in the blocks.

Samples were taken at three different locations for each block, corresponding to the location at which nondestructive testing and coring took place. One sample was taken well below the immersion line, a second right at the immersion line, and a third well above the immersion line. In each case, the sample was taken very near the outer surface, with approximately 1-2 mm of material removed during specimen preparation to ensure a smooth polished surface for SEM examination.

Figures 5.18 through 5.20 represent sample images taken from the limewater exposed blocks. The remaining images have been included in Appendix D. As expected, very little cracking is evident in any of the limewater specimens, with the minor amount present most likely due to specimen preparation.

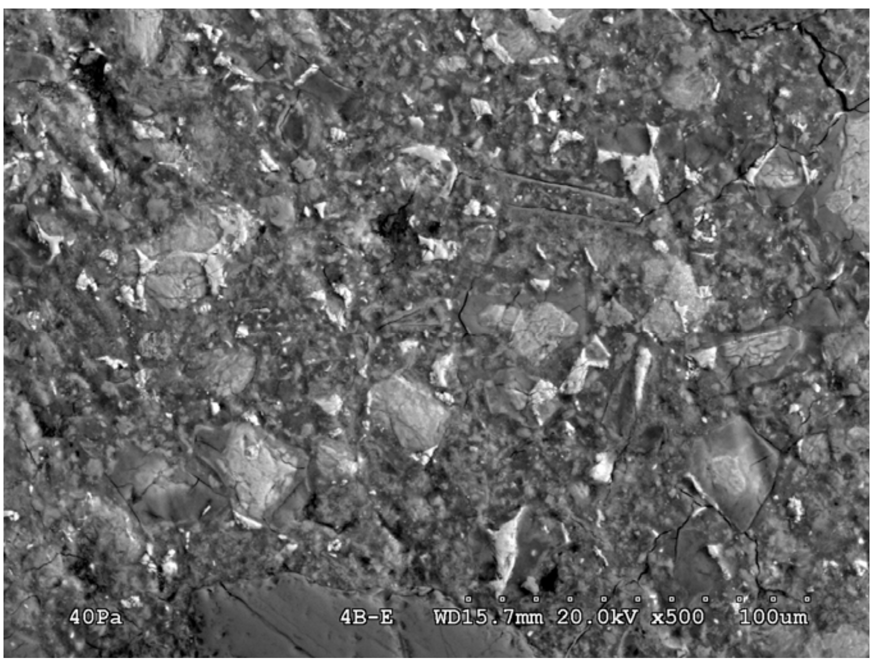

Figure 5.18: SEM image of limewater specimen below immersion line.

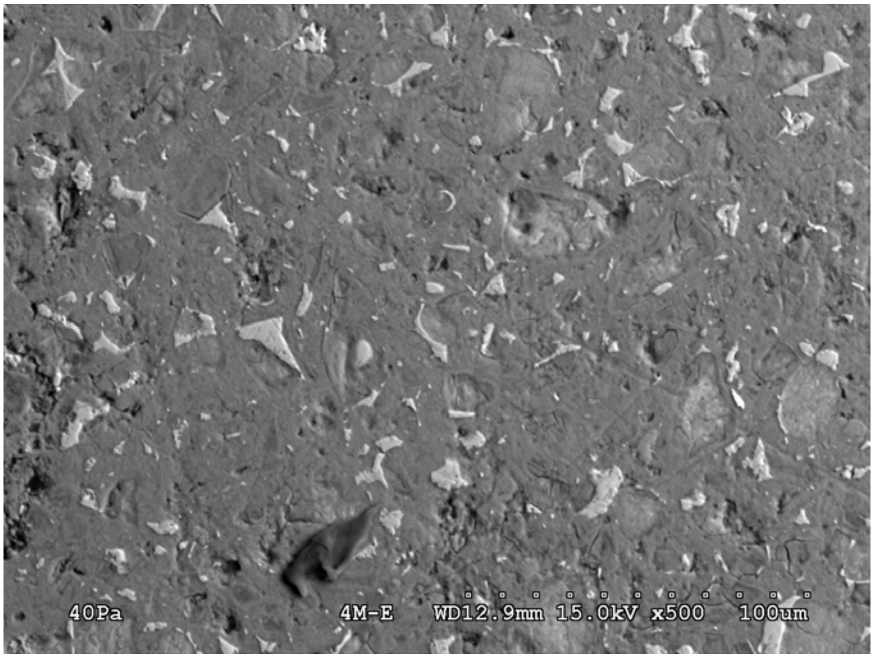

Figure 5.19: SEM image of limewater specimen at immersion line.

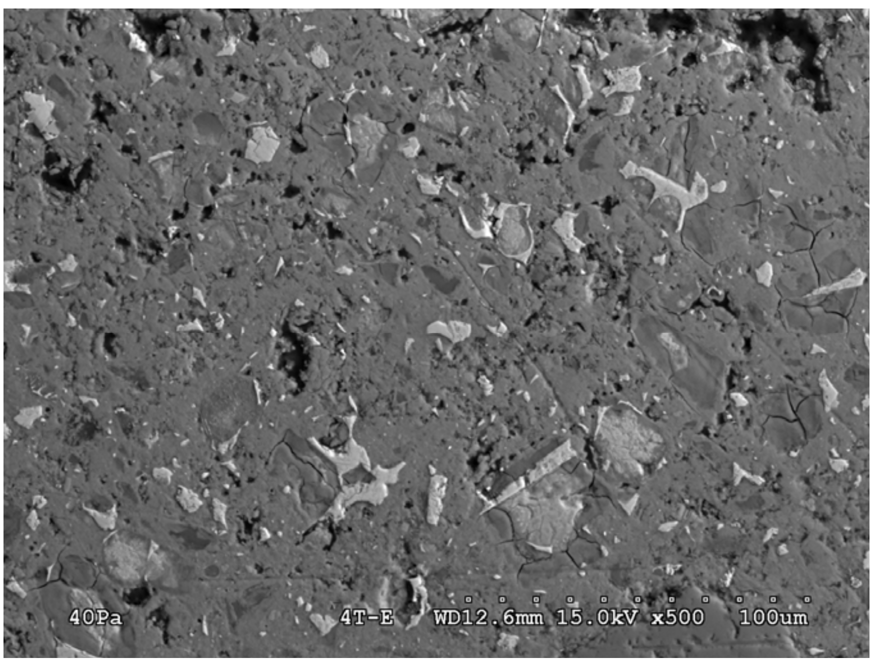

Figure 5.20: SEM image of limewater specimen above immersion line.

The sulfate exposed concrete, on the other hand, showed much more extreme evidence of microstructural damage, as shown in the example images from Figure 5.21 through 5.23. Again, the remainder of the sulfate specimen images have been included in Appendix D.

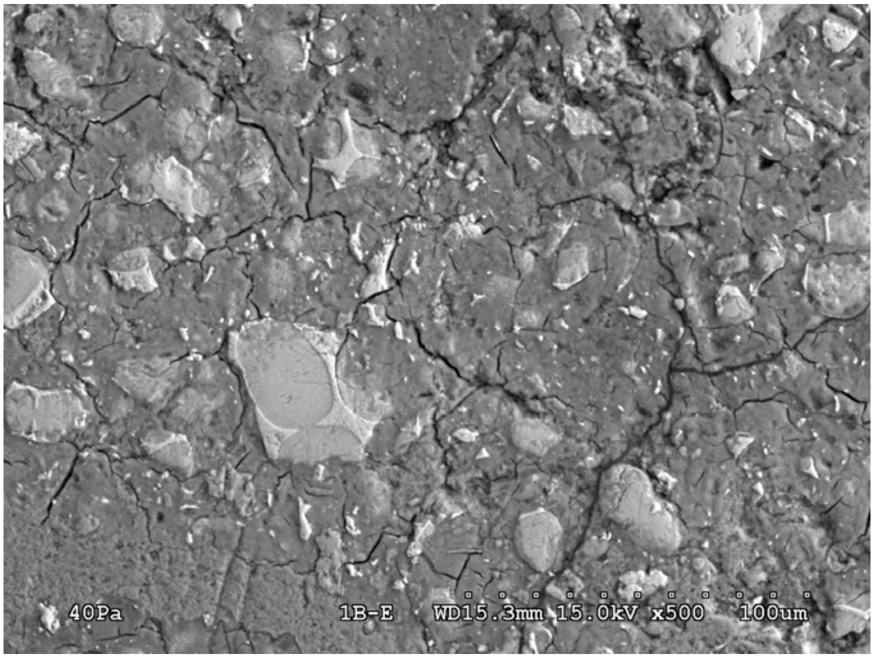

Figure 5.21: SEM image of sulfate specimen below immersion line.

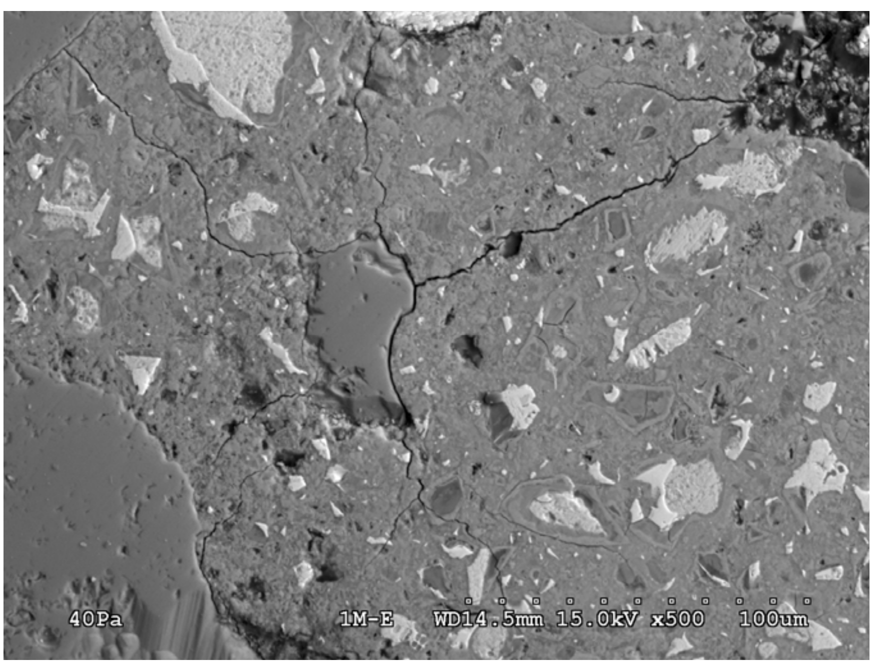

Figure 5.22: SEM image of limewater specimen at immersion line.

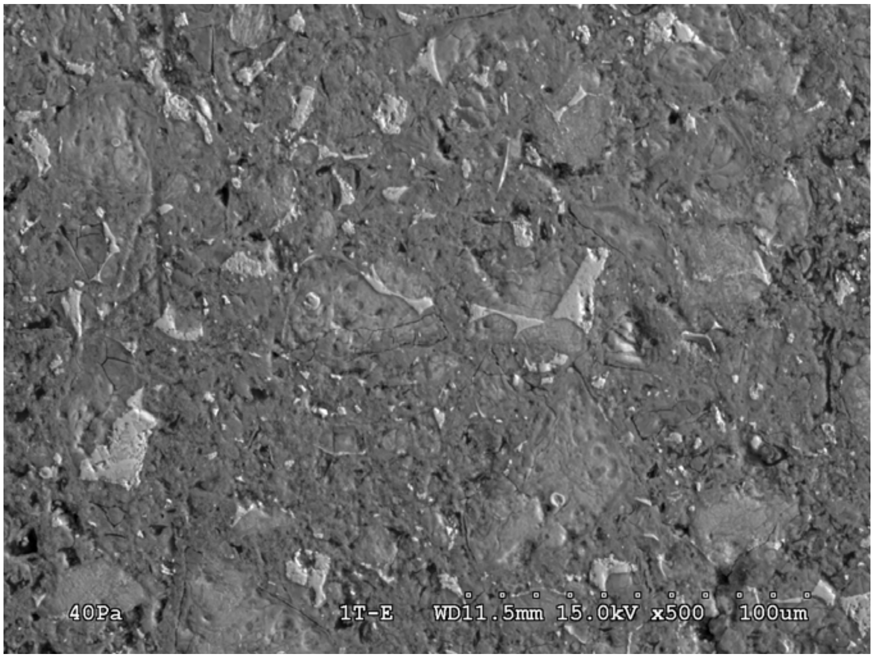

Figure 5.23: SEM image of limewater specimen above immersion line.

Of particular interest with the images taken from sulfate damaged concrete, is the variation on damage at different locations in the block. The portion below the immersion line (Figure 5.21) shows evidence of severe cracking, while the image taken at the immersion line (Figure 5.22) appears to have sustained much less extensive cracking. Finally, the sample taken well above the immersion line (Figure 5.23), and thus far removed the sulfate exposure areas, shows virtually no cracking at all.

The SEM images shown here, and in Appendix D, clearly match the results obtained from both the nondestructive and destructive test. The majority of damage in the sulfate exposure specimens has occurred in the submerged portion of the blocks where the highest degree of exposure has occurred. Above the immersion line, damage has still accumulated due to the evaporation cycle carrying sulfates through the concrete to the surface but it is less severe than in the completely immersed portion. The region of the blocks well above the immersion line, and thus above the path through which the sulfates travel to reach the surface, has sustained virtually no damage.

Though the SEM images support this data in a qualitative manner, deriving quantitative results from them would be far more beneficial. Unfortunately, such an exercise is not possible at this stage due to difficulties inherent in sample preparation. The actual process of creating a sample surface for examination, by definition, damages the material being prepared. Minimizing this damage through stabilizing techniques such as epoxy impregnation is a necessity in avoiding distortion of the results. The images included in this report show gross differences in damage due to the large differences between limewater and sulfate exposure, but cannot be used to correlate the NDT results to the destructive data until a quantification method is established.

In addition, it must be stressed that the images shown herein represent a very small region, and thus a very small proportion of the test specimens. In order to properly quantify the microstructural damage and ensure that it is representative of the entire specimen (or particular portion of the specimen), a procedure must be established that includes a larger sample size. To do this, it is necessary to scan a number of different, randomly chosen sites within the specimen and quantify the damage at each site. When done properly, this will allow a statistical representation to be formulated. Considering the large number of sites that would be necessary to effectively do this, an automated approach is required.

A technique for quantification of damage itself is also necessary, though some work in this direction has already been completed (Shah 2004). By creating a binary file from the SEM image, an analysis of empty space can be performed using image processing software. All empty space appears as black on the SEM image, meaning that it is easy to identify in the binary data. Separating voids from cracks can be accomplished by examining the aspect ratio of the black areas. Cracks have much higher aspect ratios due to their much greater length relative to their width.

The researchers are currently working on perfecting the sample preparation technique, image sampling process, and image analysis approach that will allow proper examination and evaluation of microstructural damage in an effective manner without inducing further damage during preparation

CHAPTER 6
CONCLUSIONS

A review of bridge documents, FDOT personnel, and structures in the field resulted in identification of the most prevalent defects in Florida structures. These defects include:

- Surface deterioration due to seawater exposure.
- Large scale cracking and spalling due to reinforcement corrosion.
- Visible and hidden torsional cracking.
- Other structural cracking due to various influences.
- Delamination of improperly repaired sections.

The Pontis system is a very effective database system for monitoring long term data from the inspection of bridge structures. There are, however, a number of issues that could be improved. There is a need for more quality control regarding interpretation of structural deficiencies and disposition of the data within the system. A more exact definition of conditions is needed to regain the necessary quality control of inspection reports.

There is also a need to introduce consistency among units of physical properties, since some reports use the English units where others use SI units. Other limitations include and inability to process data sorts of more than one data field within the system for a single data query and an inability to perform data sorts based on material type.

When considering factors such as effectiveness, applicability, ease of use, and cost, it appears that the most effective nondestructive testing techniques for the evaluation and monitoring of new concrete are those implementing pulse wave velocity measurements, specifically UPV and impact echo. Though not able to actually identify the type or source of damage *per se*, they are definitely capable of detecting damage and measuring severity on a relative scale over time. They are thus well suited for periodic monitoring of new structures, or even older structures once a baseline condition is assessed.

Using these techniques in a tomographic imaging strategy to create a three-dimensional “image” of a concrete member is particularly effective, not only at defining damage but also in locating and delineating the extent of that damage.

There can be a significant differences between the surface wave velocities and through wave velocities of large-scale concrete samples under different exposure conditions, especially when external deterioration mechanisms are present (i.e. sulfate attack). Additionally, in many reinforced concrete structures, it is the cover concrete that is of most interest when performing inspections for damage. The difference between using techniques that make through wave measurements (i.e. ultrasonic pulse velocity) or surface wave measurements (i.e. impact echo) can be very useful in narrowing the field of evaluation.

For example, if deterioration of the cover concrete is of interest, it is more advantageous to use the impact echo technique but if structural issues or internal flaws are the issue of interest, it may be more applicable to use the ultrasonic pulse velocity test.

For estimating the compressive strength of concrete nondestructively, the rebound hammer, ultrasonic pulse velocity, and impact-echo technique were all reliable means of predicting ultimate strength results. Combining multiple test procedures to form multivariable correlations provided more accurate predictions of ultimate strength. Resonant frequency testing was not found to be a reliable method of estimating concrete compressive strength.

The pressure tension test is still in the development stages. As such, to date there has been no prior research to relate nondestructive test results to pressure tensile strength test results. Relationships were developed to relate rebound number, ultrasonic pulse velocity, impact-echo P-wave speed, and resonant frequencies to pressure tension test results. It was concluded that ultrasonic pulse velocity and impact-echo test results provide accurate means of estimating the tensile strength of concrete. In these cases, the accuracy of prediction was higher than that for compressive strength prediction. The rebound number of the concrete was not as reliable for predicting tensile strength as it was for predicting compressive strength. Resonant frequency testing proved to be an unreliable method for prediction of strength in general.

More research is needed on the pressure tensile strength test method. Research is needed in the area of refining and automating the test procedure itself, as well as relationships between nondestructive and destructive tensile test results provided by the method. It is believed that little could be done to reduce the degree of variance among the test results from the compressive strength and splitting tension tests. However, quite the opposite is true for the pressure tension test. Problems remain with the pressure tension test in its present state. Efforts should be made to automate the rate of loading. This would eliminate what is believed to be the main source of error inherent in the test. Special care should be taken when fabricating the specimens (as should always be the case) to ensure that the ends of the specimens are perfectly circular, thus facilitating the prevention of leaks at the end of the pressure vessel.

From the destructive test results, it can be concluded that concrete with a higher water-to-cement ratio is more susceptible to sulfate attack than a concrete with a lower water-to-cement ratio (as hypothesized). For all test procedures, concrete from the 0.45 water-to-cement ratio mixture was stronger than concrete from the 0.65 water-to-cement ratio mixture. Additionally, the higher the location of the core on the block, the weaker the concrete became. The main reason for this is the higher degree of curing experienced by the concrete immersed or adjacent to the water in the respective exposure solutions.

Test results from all tests show that the further the concrete is from the conditioning solution, the less of an effect the solution has on the concrete. For both mixtures, the strength of the concrete immersed in lime-saturated water, increased at a higher rate for concrete below and at the immersion line than the concrete at the top of the blocks. For concrete exposed to 5% sodium sulfate solution, damage at the top of the block was not as severe as the damage below and at the immersion line.

The laboratory study revealed that it is possible to detect the onset of damage due to sulfate attack on concrete specimens at very early stages with wave velocity measurements. These techniques were also sensitive to other factors such as the higher inherent density and higher ultimate strength in lower W/C mixtures, localized areas of superior curing in the partially immersed specimens, and even density differences due to segregation during specimen casting.

The pressure tension test was the most effective destructive test method for evaluating the decrease in strength due to the sulfate attack mechanism. The magnitude of this loss in strength was highest in the pressure tension test and strength loss initiated at earlier ages than in the other two tests (splitting tension and compression). The pressure tension test also evidenced capabilities of locating the weakest area within the concrete cores on a consistent basis due to location of the failure plane.

Though the scanning electron microscopy images supported the laboratory testing data this data in a qualitative manner, deriving quantitative results from them would be far more beneficial. The images included in this report showed gross differences in damage due to the large differences between limewater and sulfate exposure, but can not be used to correlate the NDT results to the destructive data until a quantification method is established. A technique for quantification of damage itself is necessary.

CHAPTER 7
RECOMMENDATIONS

Much of the information garnered in this report relates to laboratory based research and must be adapted to the field. In particular, a bridge inspection program should be formulated based on the implementation of nondestructive testing for evaluating new structures. Though the work reported herein lays the foundation for this type of program, specific details such as location, extent, frequency, and statistical representation of field testing need to be addressed, much of which will be individual structure dependent.

Evaluation of damage in field structures through the use of three-dimensional ultrasonic tomography appears to be an extremely effective method for determining not only the existence of damage or deterioration, but also in physically locating the regions affected. Thus, it has the potential to be a very useful tool in the design of maintenance and repair schemes.

Improper placement of reinforcing or shifting of reinforcement during concrete placement can result in regions of unacceptably low cover. It is recommended that all critical portions of new bridge structures be surveyed immediately after completion to establish sufficient minimum cover over reinforcing steel. A covermeter or pachometer can easily determine compliance with specifications.

Of particular concern during limited field trials conducted in conjunction with this research was the discovery of torsional cracking in the pier components of a number of bridge structures in Florida. This could potentially be a recurring defect that requires further investigation. A full report on the findings thus far will be prepared separately but more extensive field testing is necessary to determine the extent of the defect and to evaluate how this problem affects bridge performance.

In addition to the baseline assessment of new structures or the determination of deterioration initiation, nondestructive testing can be applied to post-disaster evaluation of structures and service life modeling of structures. Of particular interest is the potential for dramatic improvements in service life modeling facilitated by the accumulation of long-term test results throughout the performance bond period of new structures. This type of time-line data is essential in the development of accurate predictions of service life. First, a methodology must be formulated for accumulating such data, followed by the creation of a service life model that effectively evaluates the data in predicting long term behavior.

Quantitative evaluation of microstructural damage in concrete is essential in understanding the effects of deterioration on its physical properties, whether they be determined nondestructively or destructively. An effective, accurate, and truly representative method of quantitatively evaluating cracking needs to be formulated, along with a method of preparing concrete specimens without inducing further damage that can skew results. The ability to quantify microstructural damage has wide-reaching application throughout the majority of FDOT research projects.

The pressure tension test promises to be an effective tool for destructively evaluating deterioration in concrete, especially at early ages. Further development and standardization of this test is needed before it can be fully implemented into the testing arsenal available to the FDOT.

REFERENCES

ACI (2003). *In-Place Methods to Estimate Concrete Strength.* Committee 228, American Concrete Institute, Detroit, MI.

ACI (1998). *Nondestructive Test Methods for Evaluation of Concrete in Structures.* Committee 228, American Concrete Institute, Detroit, MI.

ACI (1996). *Concrete Repair Guide*. Committee 546, American Concrete Institute, Detroit, MI.

ACI (1993). *Causes, Evaluation and Repair of Cracks in Concrete Structures*. Committee 224, American Concrete Institute, Detroit, MI.

ACI (1992). *Guide to Durable Concrete.* Committee 201, American Concrete Institute, Detroit, MI.

ASTM (2001a). *Standard Test for the Compressive Strength of Cylindrical Concrete Specimens,* C39-01. American Society for Testing and Materials, West Conshohocken, PA.

ASTM (2001b). *Standard Test for the Fundamental Transverse, Longitudinal and Torsional Resonant Frequencies of Concrete Specimens,* C215-97. American Society for Testing and Materials, West Conshohocken, PA.

ASTM (2001c). *Standard Test Method for Liquid Penetrant Examination,* E165-95. American Society for Testing and Materials, West Conshohocken, PA.

ASTM (2001d). *Standard Test for the Pulse Velocity Through Concrete*, C597-97. American Society for Testing and Materials, West Conshohocken, PA.

ASTM (2001e). *Standard Test Method for Splitting Tensile Strength of Cylindrical Concrete Specimens*, C496-96. American Society for Testing and Materials, West Conshohocken, PA.

ASTM (2001f). *Standard Test Method for Length Change of Hydraulic-Cement Mortars Exposed to a Sulfate Solution,* C1012-95a. American Society for Testing and Materials, West Conshohocken, PA.

ASTM (2001g). *Standard Test Method for Measuring the P-Wave Speed and the Thickness of Concrete Plates Using the Impact-Echo Method,* C1383-98. American Society for Testing and Materials, West Conshohocken, PA.

ASTM (2002a). *Dye Penetration of Solid Fiberglass Reinforced Pultruded Stock,* D5117-96. American Society for Testing and Materials, West Conshohocken, PA.

ASTM (2002b). *Standard Guide for Mounting Piezoelectric Acoustic Emission Sensors* E650-97. American Society for Testing and Materials, West Conshohocken, PA.

ASTM (2002c). *Standard Practice for Characterizing Acoustic Emission Instrumentation,* E750-98. American Society for Testing and Materials, West Conshohocken, PA.

ASTM (2002d). *Standard Practices for Thermal Neutron Radiography of Materials,* E748-02. American Society for Testing and Materials, West Conshohocken, PA.

ASTM (2002e). *Standard Guide for Acoustic Examination of Small Parts*, E1932-97. American Society for Testing and Materials, West Conshohocken, PA.

ASTM (2002f). *Standard Test Method for Rebound Number of Hardened Concrete*, C805-02. American Society for Testing and Materials, West Conshohocken, PA.

Benedetti, A. (1998). On the Ultrasonic Pulse Propagation into Fire Damaged Concrete. *ACI Structural Journal, 95*(3), 259-271.

Bergander, M. J. (2003). EMAT Thickness Measurement for Tubes in Coal-fired Boilers. *Applied Energy, 74*(3-4), 439-444.

Bhide, S. (2001). *Material Usage and Condition of Existing Bridges in the U.S.* Skokie, Illinois: Portland Cement Association.

Binda, L., Lenzi, G., & Saisi, A. (1998). NDE of Masonry Structures: Use of Radar Tests for the Characterization of Stone Masonries. *NDT & E International, 31*(6), 411-419.

Binda, L., Saisi, A., & Tiraboschi, C. (2001). Application of Sonic Tests to the Diagnosis of Damaged and Repaired Structures. *NDT & E International, 34*(2), 123-138.

Boving, K. G. (1989). *NDE Handbook : Non-Destructive Examination Methods for Condition Monitoring*. London: Butterworths.

Boyd, A. and Mindess, S. (2004). The use of tension testing to investigate the effects of W/C ratio and cement type on the resistance of concrete to sulfate attack *Cement and Concrete Research* 34 (3), 373-377.

Boyd, A. J., Mindess, S., & Skalny, J. (2001). Designing Concrete for Durability. *Materiales De Construccion, 51*(263-64), 37-53.

Bremner, T.W., Boyd, A.J., Holm, T.A., and Boyd, S.R., (1995). Tensile testing to evaluate the effect of alkali-aggregate reaction in concrete. Proceedings, *International Workshop on Alkali-Aggregate Reactions in Concrete.* CANMET/ACI Dartmouth, Canada, 311-326.

Brown, P.W. (1981). An evaluation of the sulfate resistance of cements in a controlled environment, *Cement and Concrete Research*, 11, 719-727.

Carino N.J. 2001, "The Impact-Echo Method: An Overview" Buildings and Fire Research Laboratory, NIST Gaithersburg, MD. Reprinted from the Proceedings of the 2001 Structures Congress and Exposition, ASCE, May 21-23 Washington D.C. Chang P.C. Editor.

Casas, J. R., Klaiber, F. W., Mari, A. R., Universidad Politecnica de Catalunya, & Iowa State University. (1996). *Recent Advances in Bridge Engineering: Evaluation, Management and Repair: Proceedings of the US-Europe Workshop on Bridge Engineering, Barcelona, 15-17 July 1996* (1st ed.). Barcelona, Spain: Artes Graficas Torres.

Casper, J. (2002). *Human-Robot Interactions During the Robot-Assisted Urban Search and Rescue Response at the World Trade Center.* Thesis (M.S.C.S.) University of South Florida.

Cawley, P., & Adams, R. D. (1988). The Mechanics of the Coin-Tap Method of Non-Destructive Testing. *Journal of Sound and Vibration, 122*(2), 299-316.

Clayton, N. and Grimer, F.J. (1979). *The diphase concept, with particular reference to concrete*, Building Research Establishment, Building Research Station, Warford, UK.

Colla, C., Burnside, C. D., Clark, M. R., Broughton, K. J., & Forde, M. C. (1998). Comparison of Laboratory and Simulated Data for Radar Image Interpretation. *NDT & E International, 31*(6), 439-444.

Cornwell, I., & McNab, A. (1999). Towards Automated Interpretation of Ultrasonic NDT Data. *NDT & E International, 32*(2), 101-107.

Davis, A. G. (1997). A Place for Nondestructive Evaluation in the Maintenance of Our Concrete Infrastructure. *Materials Evaluation, 55*(11), 1234-1237.

Davis, A. G. (1999). Review of Nondestructive Evaluation Techniques of Civil Infrastructure. *Journal of Performance of Constructed Facilities, 11*(4), 47-48.

Davis, A. G. (2003). The Nondestructive Impulse Response Test in North America: 1985-2001. *NDT & E International, 36*(4), 185-193.

Davis, A. G., Evans, J. G., & Hertlein, B. H. (1997). Nondestructive Evaluation of Concrete Radioactive Waste Tanks. *Journal of Performance of Constructed Facilities, 11*(4), 161-167.

Davis, A. G., Olson, C. A., & Michols, K. A. (2001). *Evaluation of Historic Reinforced Concrete Bridges.* Paper Presented at the Proceedings of the 2001 Structural Congress and Exposition, held May 21-23, 2001, Washington, D.C.

Facaoaru, I. (1984). Romanian achievements in nondestructive strength testing of concrete, *ACI SP-82,* Detroit, 35.

Ferarro, C. (2003). *Advanced Nondestructive Monitoring and Evaluation of Damage in Concrete Materials*, Thesis (M.E.) University of Florida, Gainesville.

FHWA, U.S. Department of Transportation. Federal Highway Administration. (1995). *Recording and Coding Guide for the Structure Inventory and Appraisal of the Nations Bridges* (No. FHWA-PD-96-001). Washington, DC: U.S. Department of Transportation.

Green, R. E. (2002). Noncontact Acoustical Techniques for Nondestructive Characterization of Materials and Structures. *International Applied Mechanics, 38*(3), 253-259.

Gudra, T., & Stawiski, B. (2000). Non-Destructive Strength Characterization of Concrete Using Surface Waves. *NDT & E International, 33*(1), 1-6.

Guenther, N. (1999). *Internship Report* (No. SS99). Soquel, California: Ultrasonic Devices, Inc.

Halliday, D., Resnick, R., & Walker, J. (1997). *Fundamentals of Physics* (5th ed.). New York: Wiley.

Hamilton, H. R., & Levar, J. M. (2003). Nondestructive Evaluation of Carbon Fiber-Reinforced Polymer-Concrete Bond Using Infrared Thermography. *ACI Materials Journal, 100*(1), 63-72.

Haynes, H., O'Neill, R. and Mehta, P.K. (1996). Concrete deterioration from physical attack by salts. *Concrete International, 18*(1), 63-68.

Hearn, S. W., & Shield, C. K. (1997). Acoustic Emission Monitoring as a Nondestructive Testing Technique in Reinforced Concrete. *ACI Materials Journal, 94*(6), 510-519.

Hellier, C. (2001). *Handbook of Nondestructive Evaluation*. New York: McGraw-Hill.

Impact-Echo Consultants, Inc. (1998). *Impact-Echo Tutorial*. Ithaca, New York: Impact-Echo Instruments, LLC.

Institute of British Standards. (1986). *Recommendations for Surface Hardness Testing by Rebound Hammer* (No. 1881 pt. 202:1986). United Kingdom: British Standards Institute.

Ju, J.W., Weng, L.S., Mindess, S., and Boyd, A.J. (1999). Damage assessment and service-life prediction of concrete subject to sulfate attack, *Material Science of Concrete Special Volume: Sulfate Attack Mechanisms*, The American Ceramic Society, Westerville, OH.

Kaiser, H., & Karbhari, V. M. (2002). *Quality and Monitoring of Structural Rehabilitation Measures* (Contract #18347): Oregon Department of Transportation.

Kearl, P. M. (1997). Observations of Particle Movement in a Monitoring Well Using the Colloidal Borescope. *Journal of Hydrology, 200*(1-4), 323-344.

Kosmatka, S.H., and Panarese, W.C. (1988). *Design and Control of Concrete Mixtures* (13th edition). Skokie, Illinois, Portland Cement Association.

Krause, H. J., Wolf, W., Glaas, W., Zimmermann, E., Faley, M. I., Sawade, G., et al. (2002). SQUID Array for Magnetic Inspection of Prestressed Concrete Bridges. *Physica C, 368*(1-4), 91-95.

Krause, M., Mielentz, F., Milman, B., Muller, W., Schmitz, V., & Wiggenhauser, H. (2001). Ultrasonic Imaging of Concrete Members Using an Array System. *NDT & E International, 34*(6), 403-408.

Krautkramer, J., & Krautkramer, H. (1990). *Ultrasonic Testing of Materials* (4th fully rev. ed.). New York: Springer-Verlag.

Kulynyak, D. (2000). Ivan Pului, the Discoverer of X-rays. *The Ukrainian Weekly, 68*(28).

Lagerbald, B. (1999). Long-term test of concrete resistance against sulfate attack. *Material Science of Concrete Special Volume: Sulfate Attack Mechanisms*, The American Ceramic Society, Westerville, OH.

Lane, D. S. (1998). *Evaluation of Concrete Characteristics for Rigid Pavements*. Charlotsville, Virginia: Virginia Transportation Research Council.

Lew, H. S., & ACI Committee 228 - Nondestructive Testing of Concrete. (1988). *Nondestructive Testing*. Detroit: American Concrete Institute.

Li, F. M., & Li, Z. J. (2000). Acoustic Emission Monitoring of Fracture of Fiber-Reinforced Concrete in Tension. *ACI Materials Journal, 97*(6), 629-636.

Maldague, X. (2001). *Theory and Practice of Infrared Technology for Nondestructive Testing*. New York: Wiley.

Malhotra, V. M. (1984). *In Situ/Nondestructive Testing of Concrete*. Detroit, Michigan: American Concrete Institute.

Malhotra, V. M., & Carino, N. J. (1991). *CRC Handbook on Nondestructive Testing of Concrete*. Boca Raton: CRC Press.

Malhotra, V. M., & Mehta, P. K. (1994). *Concrete Technology: Past, Present, and Future: Proceedings of V. Mohan Malhotra Symposium*. Detroit, Michigan: American Concrete Institute.

Martin, J., Broughton, K. J., Giannopolous, A., Hardy, M. S. A., & Forde, M. C. (2001). Ultrasonic Tomography of Grouted Duct Post-Tensioned Reinforced Concrete Bridge Beams. *NDT & E International, 34*(2), 107-113.

Miller, R. K. (1985). *Bridge Testing* (No. TR-103-68-12/85). Princeton Junction, New Jersey: Physical Acoustic Corporation.

Mindess, S., Young, J. F., & Darwin, D. (2003). *Concrete* (2nd ed.). Upper Saddle River, New Jersey: Prentice Hall.

Murphy, R. (2000). *Introduction to AI Robotics*. Cambridge, Mass achusetts: MIT Press.

NBI (2003) http://www.nationalbridgeinventory.com/new_page_1.htm Last accessed August 20, 2003

Neville, A. M. (1996). *Properties of Concrete* (4th and final ed.). New York: J. Wiley.

NOAA (2003) http://www.srh.noaa.gov/tulsa/climate/rh.html Last accessed August 20, 2003

Ohdaira, E., and Masuzawa, N. (2000). Water content and its effect on ultrasound propagation in concrete – the possibility of NDE. *Ultrasonics, 38*(1-8), 546-552.

Ohtsu, M., Uchida, M., Okamoto, T., & Yuyama, S. (2002). Damage Assessment of Reinforced Concrete Beams Qualified by Acoustic Emission. *ACI Structural Journal, 99*(4), 411-417.

Ould Naffa, S., Gouyegou, M., Piwakowski, B., and Buyle-Bodin, F. (2002). Detection of chemical damage in concrete using ultrasound. *Ultrasonics, 40*(1-8), 247-251.

Ouyang, C. (1989). A damage model for sulfate attack of concrete mortars, *Cement, Concrete and Aggregates, CCAGDP, 11*(2), 92-99

Ouyang, C., Naani, A. and Chang, W.F. (1988). Internal and external sources of sulfate ions in Portland cement mortar: two types of chemical attack, *Cement and Concrete Research*, 18, 699-709.

Papadakis, E. P. (1999). *Ultrasonic Instruments and Devices: Reference for Modern Instrumentation, Techniques, and Technology*. San Diego, California: Academic Press.

Pessiki, S. P., & Carino, N. J. (1988). Setting Time and Strength of Concrete Using the Impact-Echo Method. *ACI Materials Journal, 85*(5), 389-399.

Popovics, J. S., Achenbach, J. D., & Song, W. J. (1999). Application of New Ultrasound and Sound Generation Methods for Testing Concrete Structures. *Magazine of Concrete Research, 51*(1), 35-44.

Popovics, S. (2001). Analysis of the Concrete Strength Versus Ultrasonic Pulse Velocity Relationship. *Materials Evaluation, 59*(2), 123+.

Popovics, S., Bilgutay, N. M., Karaoguz, M., & Akgul, T. (2000). High-Frequency Ultrasound Technique for Testing Concrete. *ACI Materials Journal, 97*(1), 58-65.

Popovics, S. (1998). *Strength and Related Properties of Concrete – A Quantitative Approach.* New York: Wiley.

Qasrawi, H.Y. and Marie, I.A. (2003). The use of USPV to anticipate failure in concrete under compression. *Cement and Concrete Research, 33*(12), 2017-2021.

Qasrawi, H. Y. (2000). Concrete Strength by Combined Nondestructive Methods - Simply and Reliably Predicted. *Cement and Concrete Research, 30*(5), 739-746.

Reese, R. T., Kawahara, W. A., & Society for Experimental Mechanics (U.S.). (1993). *Handbook on Structural Testing*. Englewood Cliffs, New Jersey: Fairmont Press.

Ryall, M. J. (2001). *Bridge Management*. Boston: Butterworth-Heinemann.

Salawu, O. S. (1997). Detection of Structural Damage through Changes in Frequency: A Review. *Engineering Structures, 19*(9), 718-723.

Sansalone, M., and Carino, N.J. (1986). *Impact-Echo: A Method for Flaw Detection in Concrete Using Transient Stress Waves*. Gaithersburg, MD: U.S. Department of Commerce, National Bureau of Standards.

Sansalone, M., & Streett, W. B. (1997). *Impact-Echo: Non-Destructive Evaluation of Concrete and Masonry*. Ithaca, New York: Bullbrier Press.

Scott, I. G. (1991). *Basic Acoustic Emission*. New York: Gordon and Breach Science Publishers.

Shah, V. (2004) Detection of Microcracks in Concrete Cured at Elevated Temperature. Masters Thesis, University of Florida, School of Building Construction.

Shaw, R. E. (2002). Ultrasonic Testing Procedures, Technician Skills, and Qualifications. *Journal of Materials in Civil Engineering, 14*(1), 62-67.

Sison, M., Duke, J. C., Clemena, G., & Lozev, M. G. (1996). Acoustic Emission: A Tool for the Bridge Engineer. *Materials Evaluation, 54*(8), 888+.

Skalny, J., Marchand, J., and Odler, I. (2002). *Sulfate Attack on Concrete*. London, England: Spon Press.

Sypeck, D. J. (1996). *Damage Evolution In Titanium Matrix Composites.* Unpublished Ph.D. Dissertation, University of Virginia, Charlottesville.

Tam, M. T., & Weng, C. C. (1995). Acoustic-Emission Kaiser Effect in Fly-Ash Cement Mortar under Compression. *Journal of Materials in Civil Engineering, 7*(4), 212-217.

Thorvaldson, T., Vigfusson, V.A., and Larmour, R.K. (1927). The action of sulfates on the components of Portland cement, *Trans. Royal Soc. Canada*, 3rd Series 21, Section III.

Washer, G. A. (1998). Developments for the Non-Destructive Evaluation of Highway Bridges in the USA. *NDT & E International, 31*(4), 245-249.

Weil, G. J., & Rowe, T. J. (1998). Nondestructive Testing and Repair of the Concrete Roof Shell at the Seattle Kingdome. *NDT & E International, 31*(6), 389-400.

Wells, P. N. T. (1974). Medical Ultrasonic Diagnostics. *Electronics and Power, 20*(9), 367-370.

Wu, H. D., & Siegel, M. (2000). Correlation of Accelerometer and Microphone Data in the "Coin Tap Test". *IEEE Transactions on Instrumentation and Measurement, 49*(3), 493-497.

Wu, K., Chen, B., & Yao, W. (2000). Study on the AE Characteristics of Fracture Process of Mortar, Concrete and Steel-Fiber-Reinforced Concrete Beams. *Cement and Concrete Research, 30*(9), 1495-1500.

Yan, T Lin, Y. C.,& Lai, C. P., (2003). Prediction of Ultrasonic Pulse Velocity (UPV) in Concrete. *ACI Materials Journal, 100*(1), 21-28.

Yeih, W., & Huang, R. (1998). Detection of the Corrosion Damage in Reinforced Concrete Members by Ultrasonic Testing. *Cement and Concrete Research, 28*(7), 1071-1083.

Young, J. F., Mindess, S., Gray, R. J., & Bentur, A. (1998). *The Science and Technology of Civil Engineering Materials*: Prentice Hall.

Yuyama S., Okamoto, T., Tomita, R., Fugiwara, H., Kajio S., Ohtsu, S., & Shigeishi M. (1992). *Discrimination of Cracking Width Developed in Reinforced Concrete Structures by Acoustic Emission*. Seattle, Washington: Physical Acoustics Corporation.

Zheng, W., Kwan, A.K.H., and Lee, P.K.K. (2001). Direct tension of concrete. *ACI Materials Journal, 98*(1), 63-71.

APPENDIX A

NDT MONITORING RESULTS

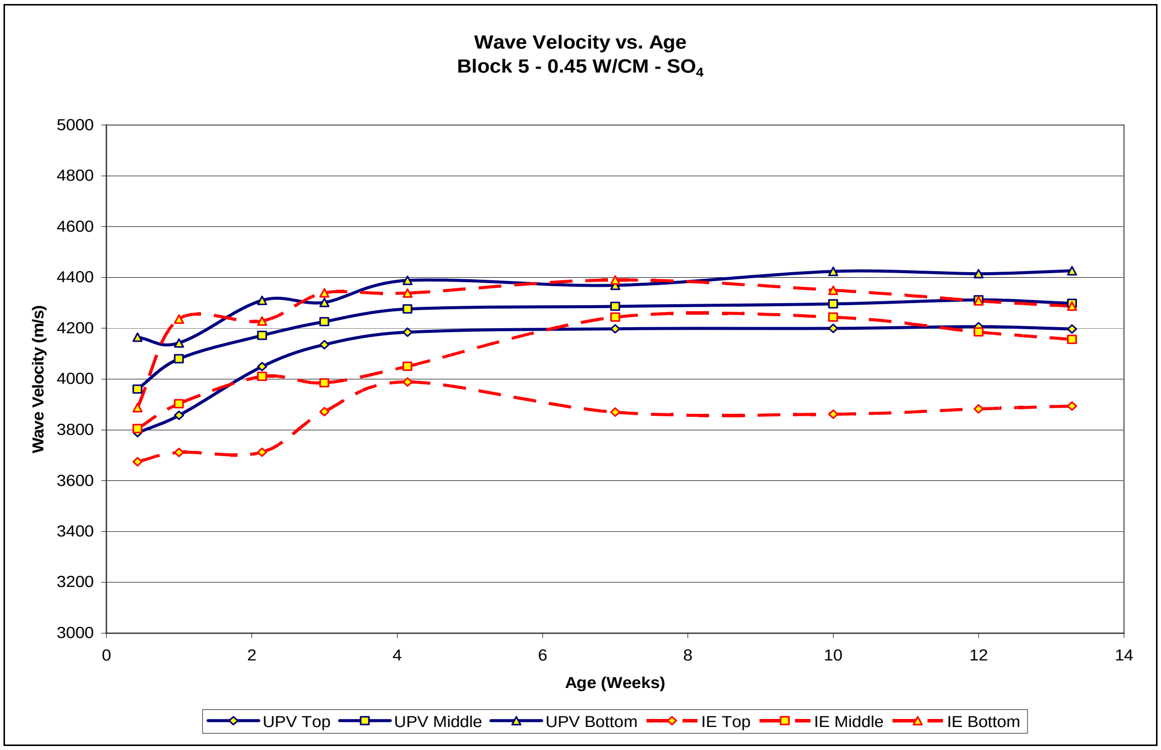

Figure A1: Graphical results for wave velocity vs. age for a three-month sample exposed to sulfate solution

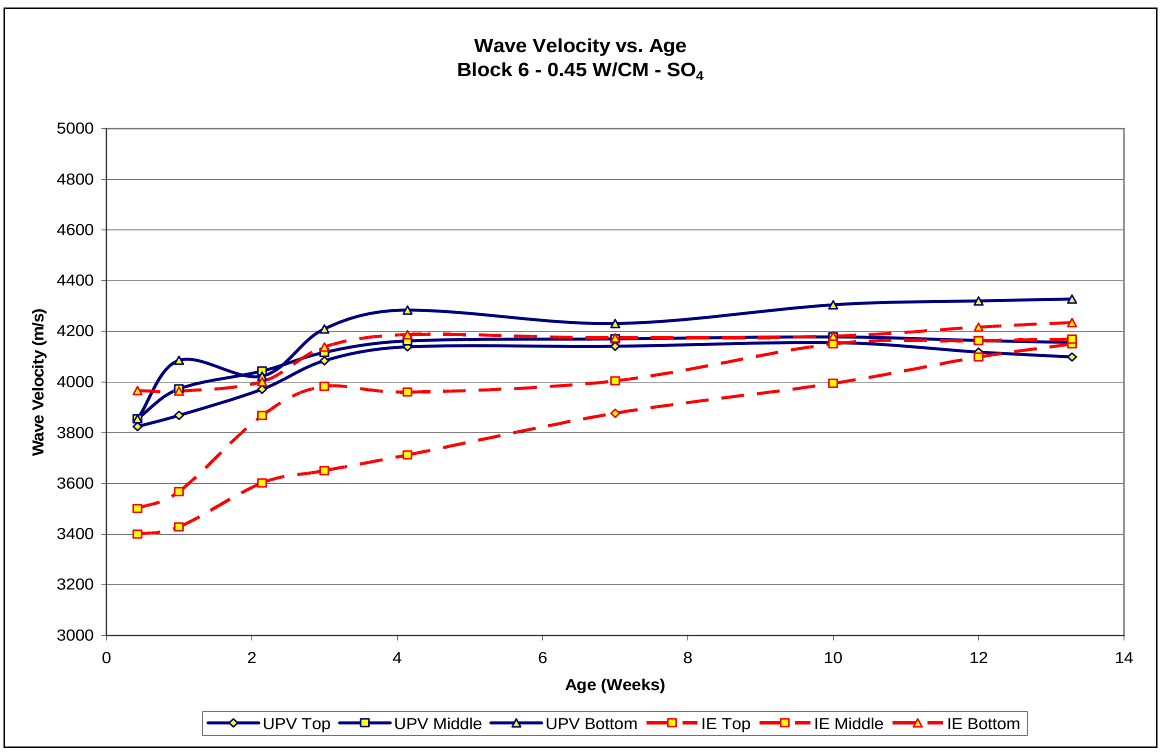

Figure A2: Graphical results for wave velocity vs. age for a three-month sample exposed to sulfate solution

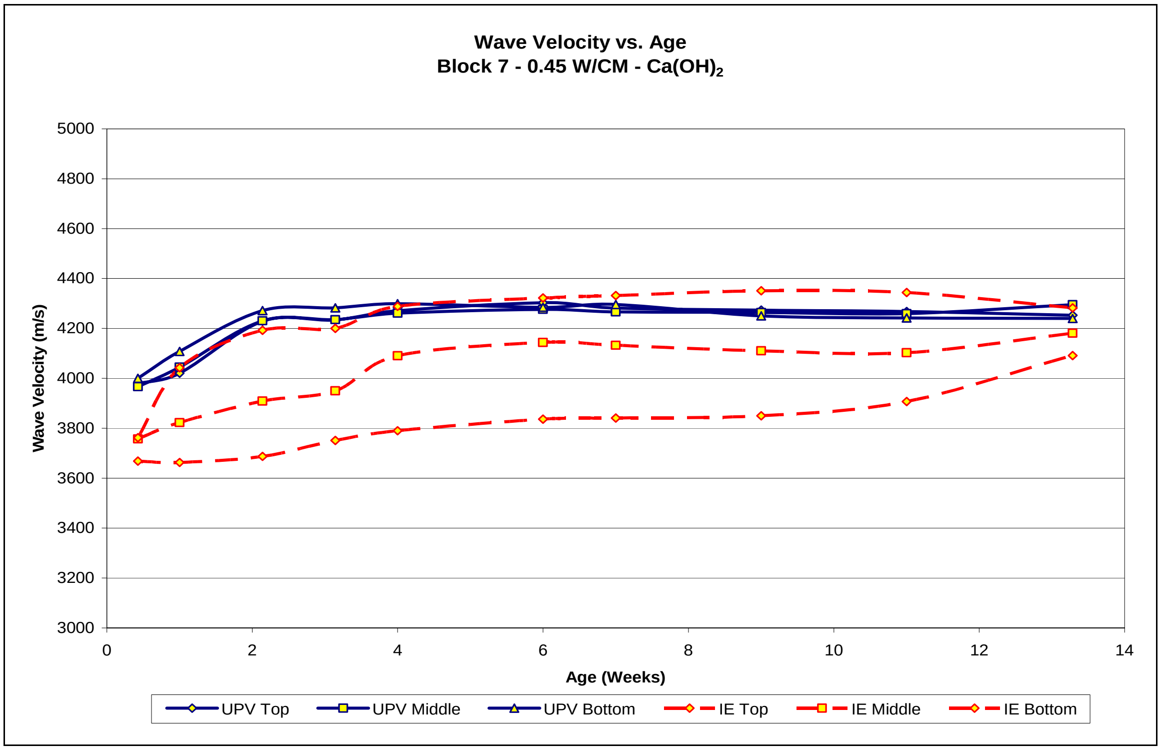

Figure A3: Graphical results for wave velocity vs. age for a three-month sample exposed to lime water solution

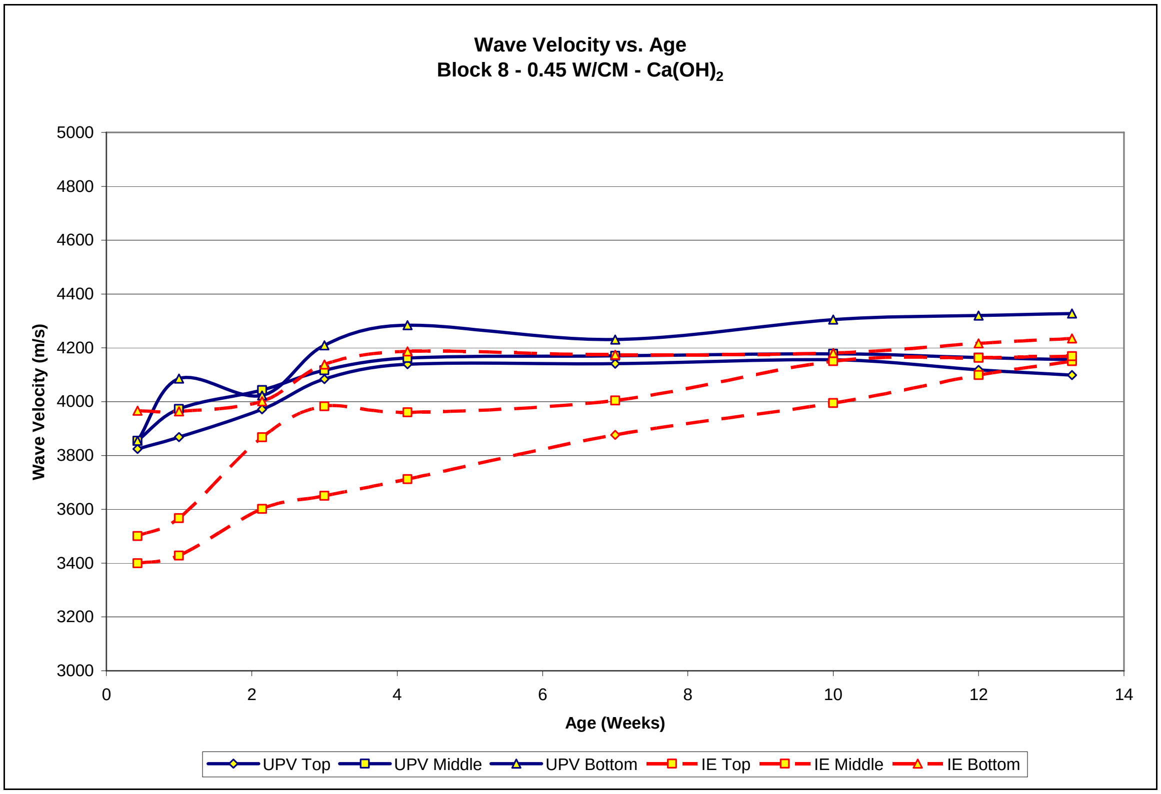

Figure A4: Graphical results for wave velocity vs. age for a three-month sample exposed to lime water solution

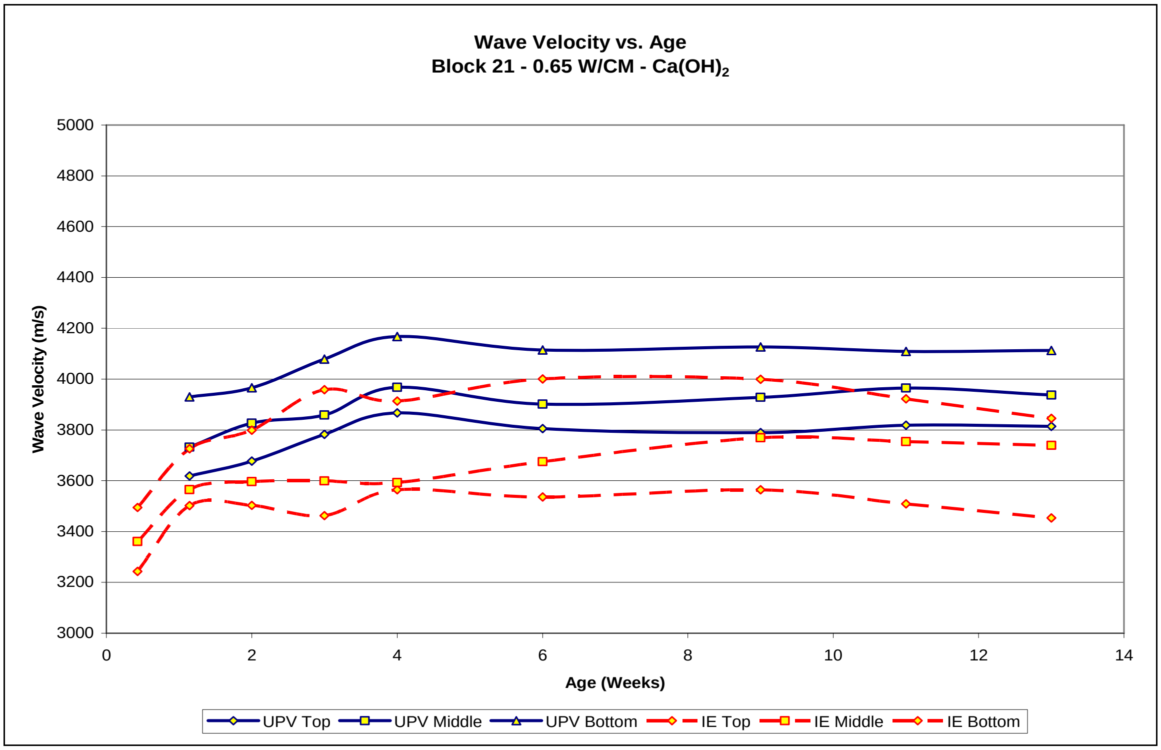

Figure A5: Graphical results for wave velocity vs. age for a three-month sample exposed to lime water solution

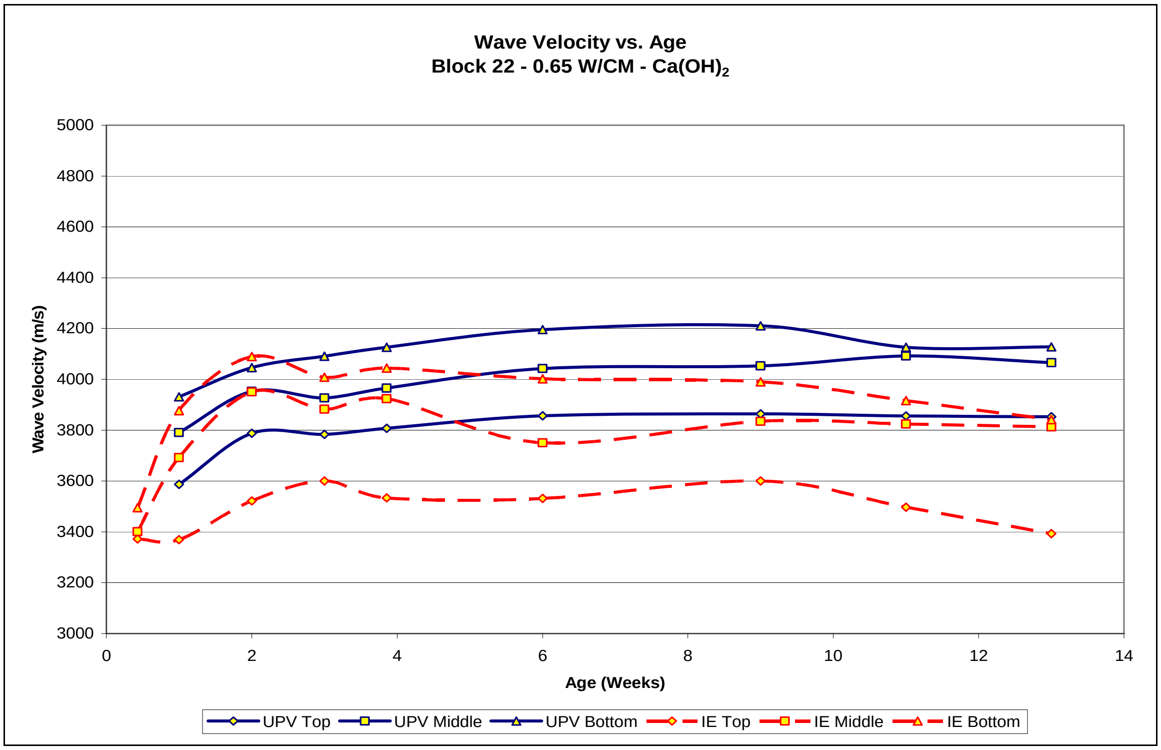

Figure A6: Graphical results for wave velocity vs. age for a three-month sample exposed to lime water solution

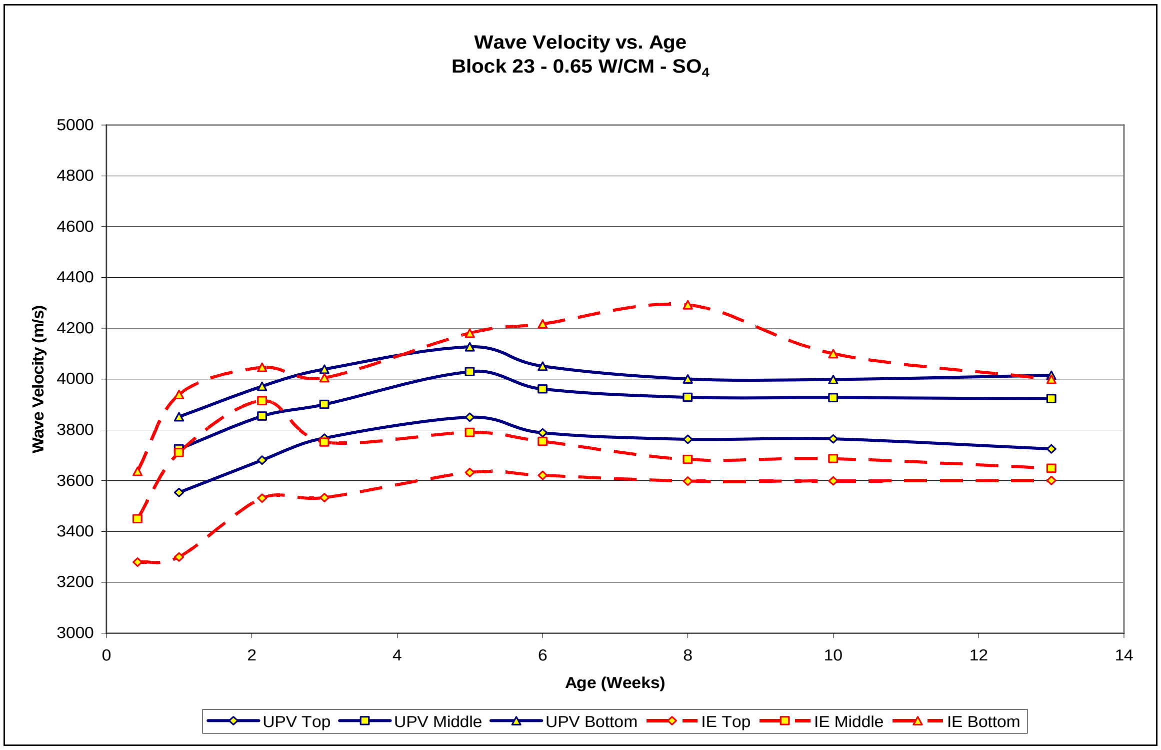

Figure A7: Graphical results for wave velocity vs. age for a three-month sample exposed to lime water solution

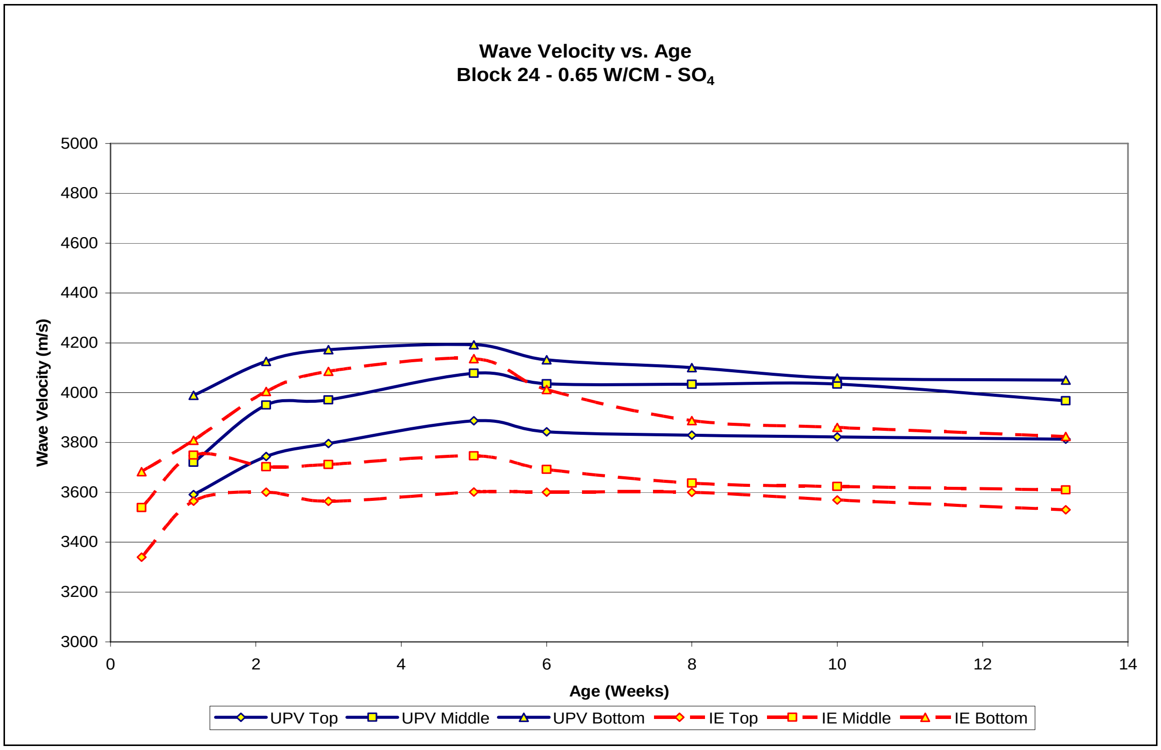

Figure A8: Graphical results for wave velocity vs. age for a three-month sample exposed to lime water solution

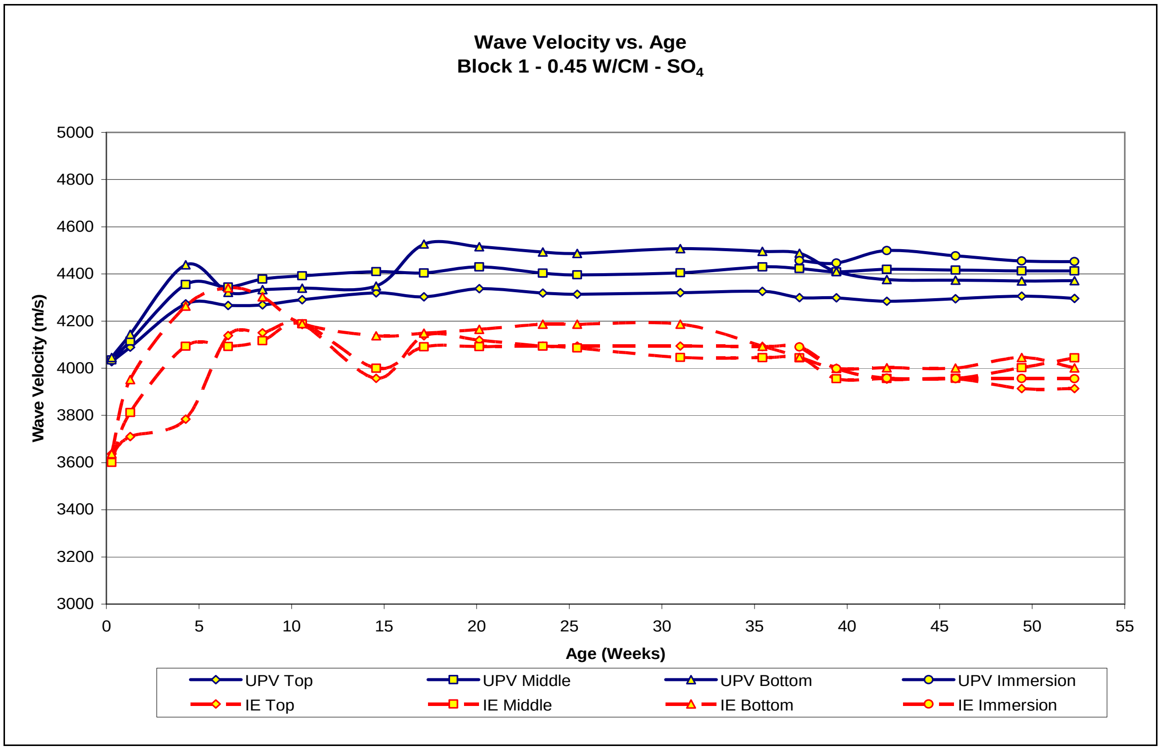

Figure A9: Graphical results for wave velocity vs. age for a one-year sample exposed to sulfate solution

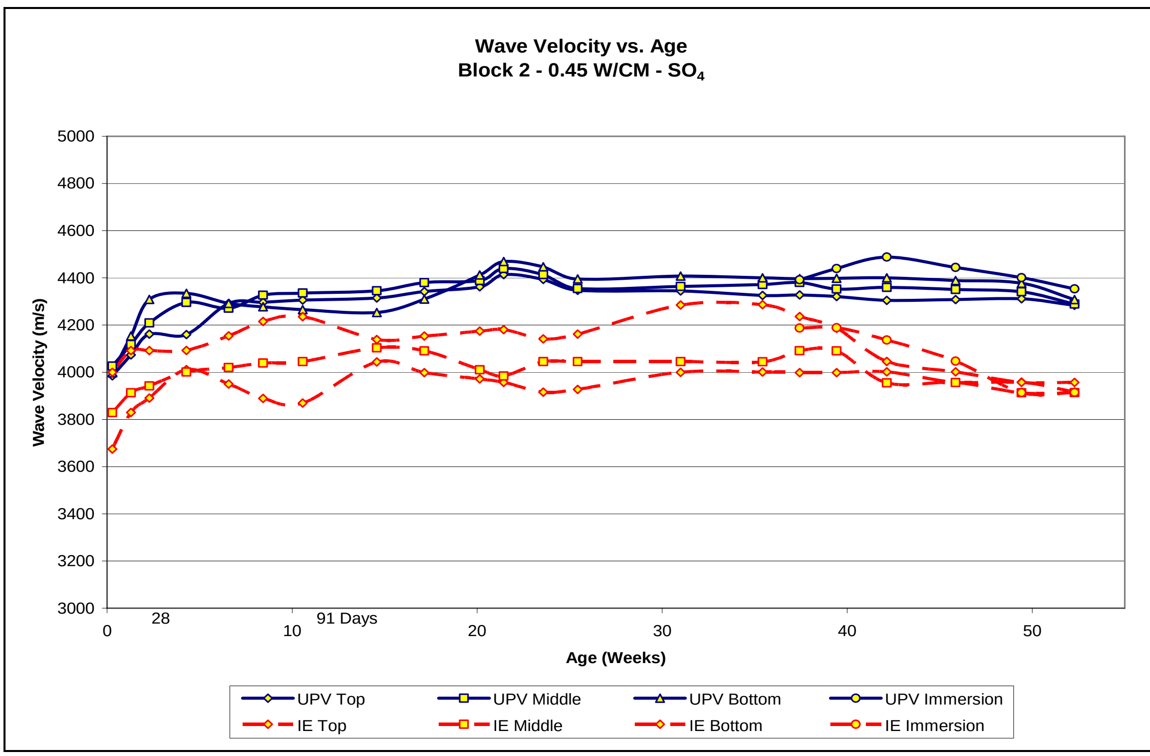

Figure A10: Graphical results for wave velocity vs. age for a one-year sample exposed to sulfate solution

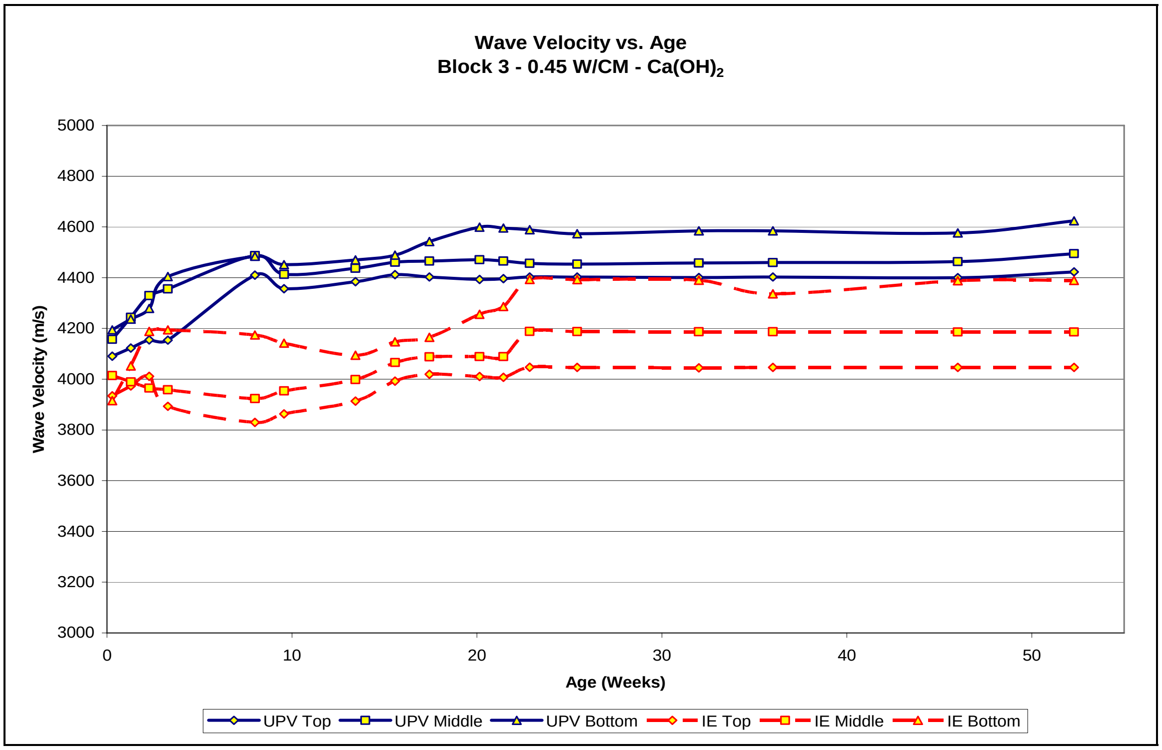

Figure A11: Graphical results for wave velocity vs. age for a one-year sample exposed to lime water solution

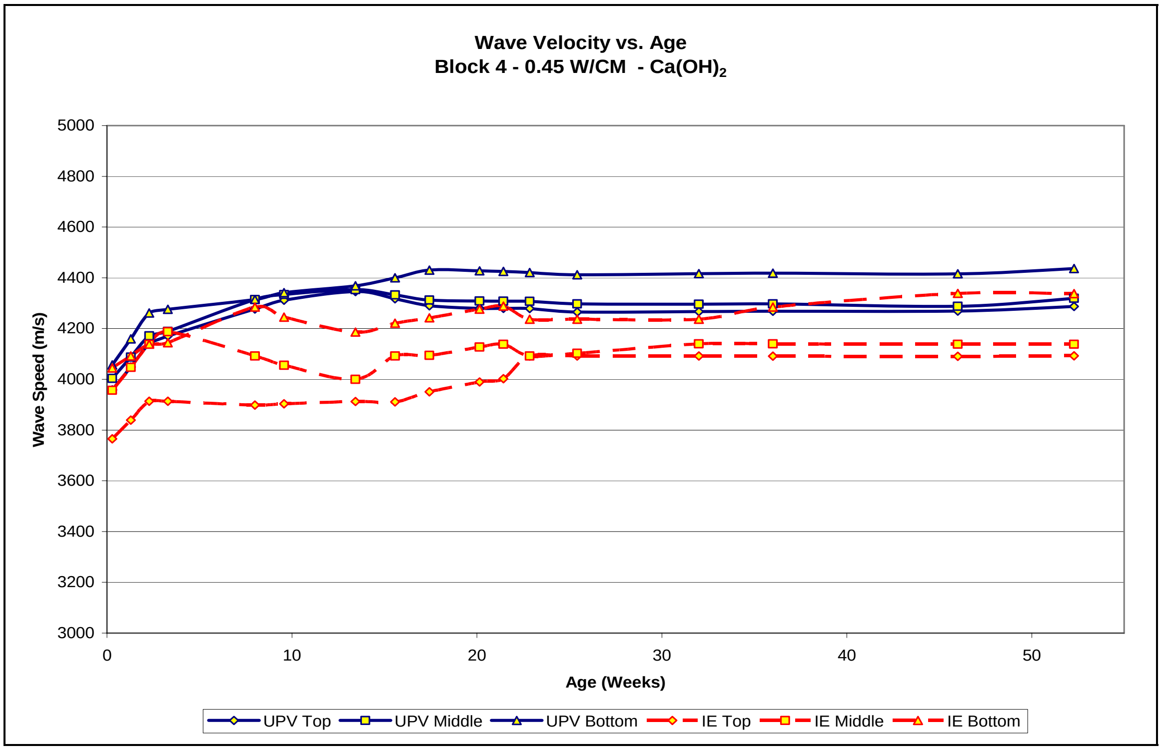

Figure A12: Graphical results for wave velocity vs. age for a one-year sample exposed to lime water solution

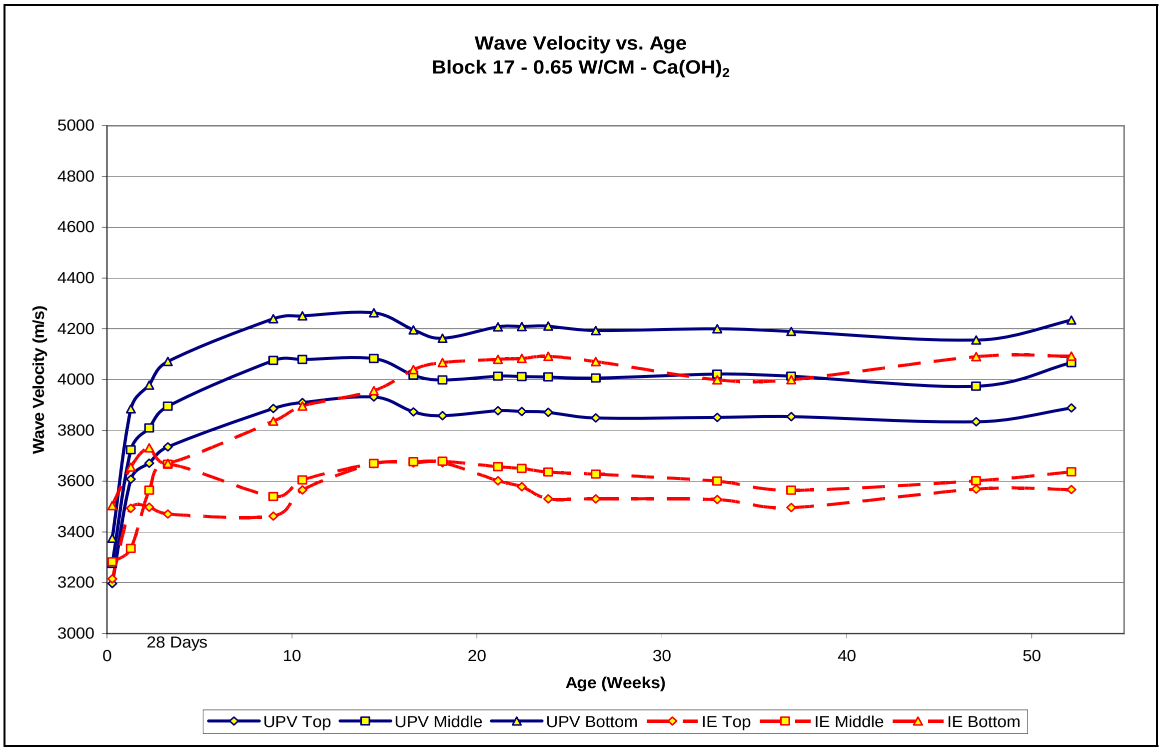

Figure A13: Graphical results for wave velocity vs. age for a one-year sample exposed to lime water solution

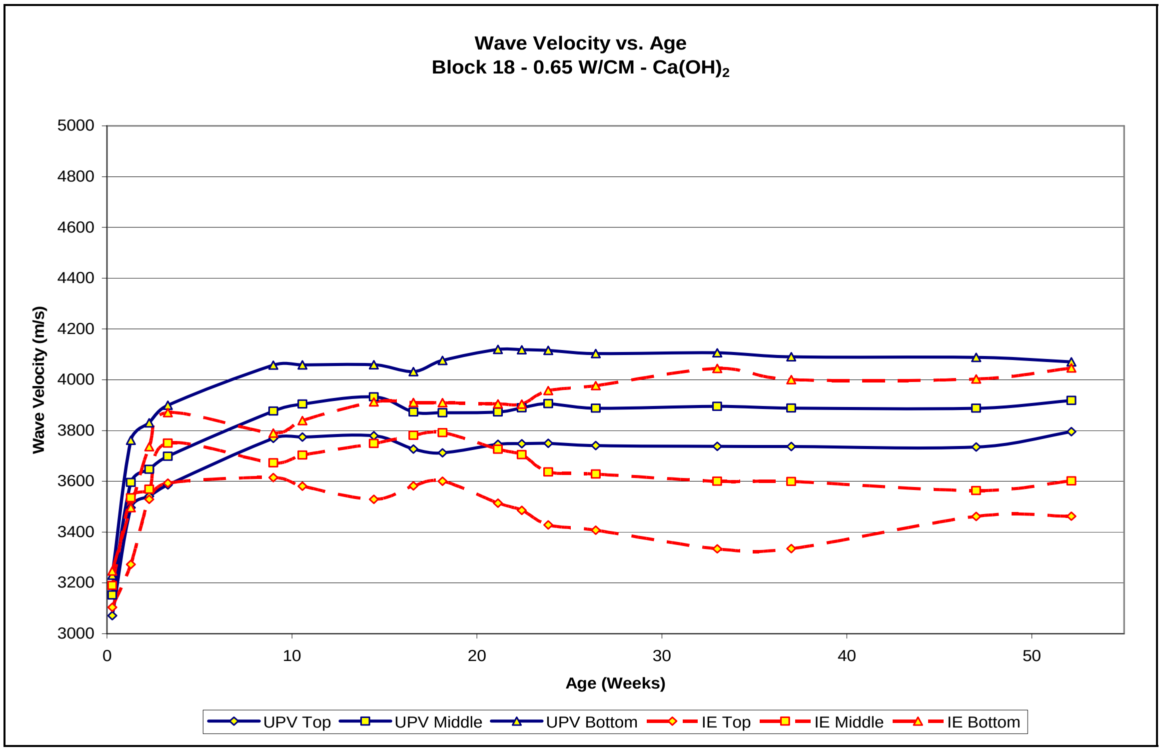

Figure A14: Graphical results for wave velocity vs. age for a one-year sample exposed to lime water solution

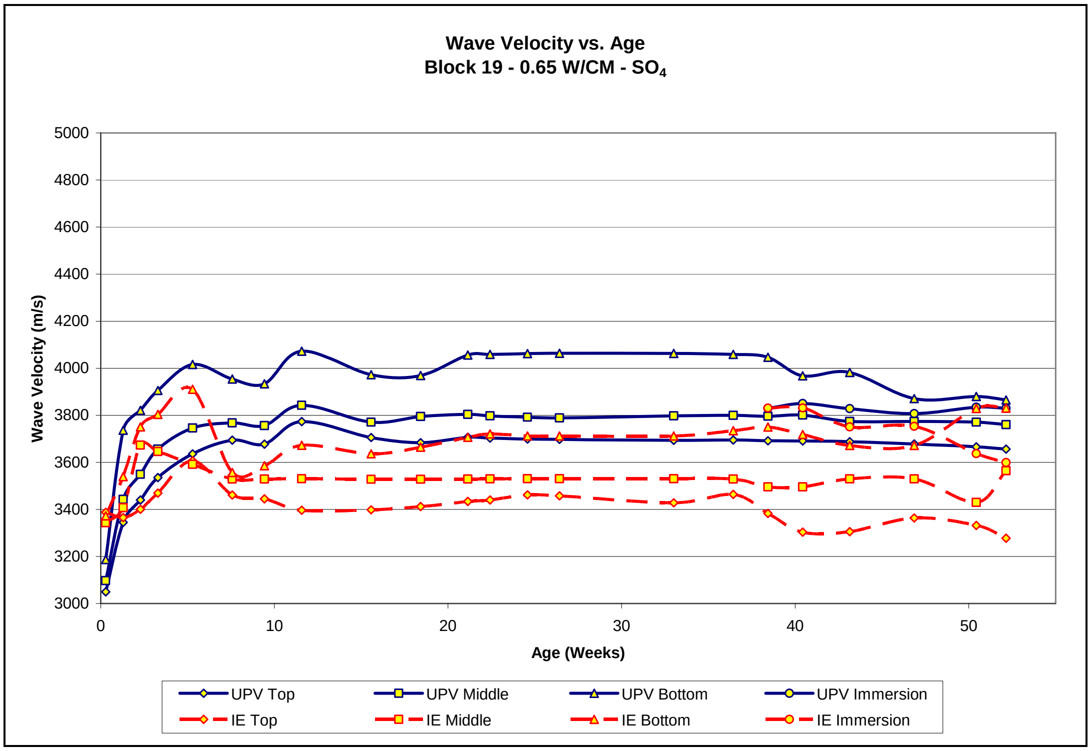

Figure A15: Graphical results for wave velocity vs. age for a one-year sample exposed sulfate solution

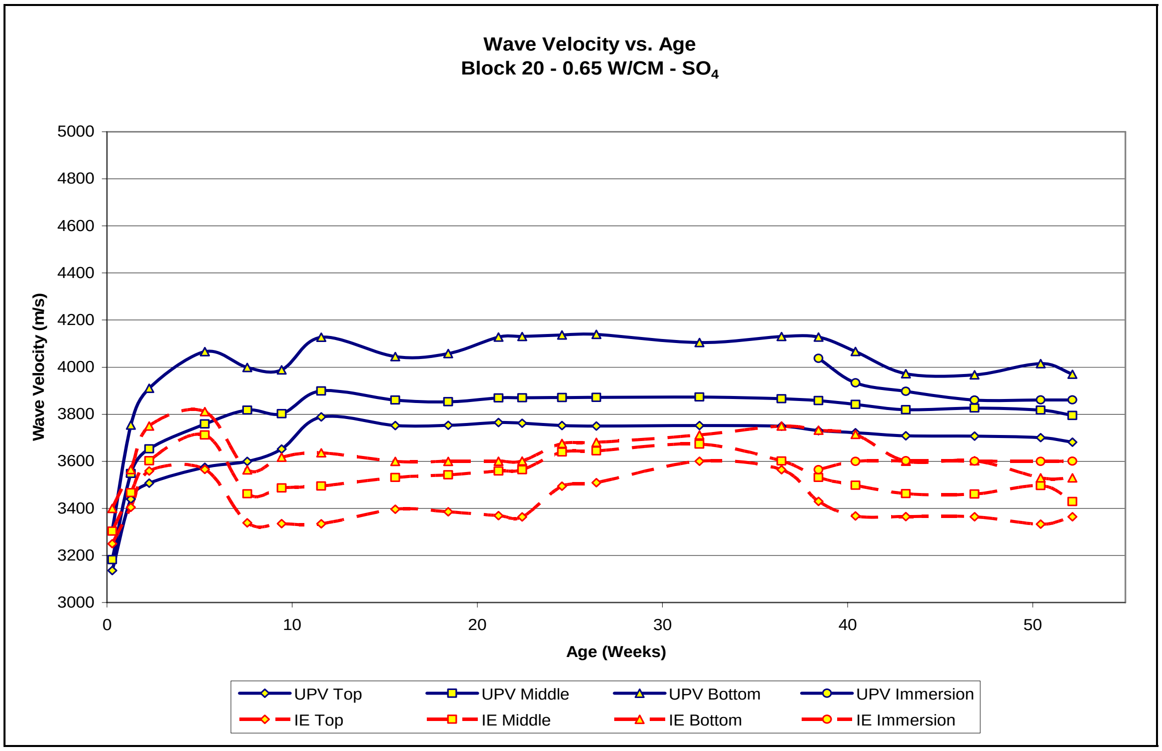

Figure A16: Graphical results for wave velocity vs. age for a one-year sample exposed to sulfate solution

APPENDIX B

REBOUND HAMMER TEST RESULTS

TABLE B.1: REBOUND HAMMER TEST RESULTS FOR BLOCK 1

Rebound Hammer Testing

Performed by: SC, BQ
Date: 1/29/2004
Block #: 1

	1	**2**	**3**	**4**	**5**	**6**	**7**	**8**	**9**	**10**	**11**
A	47	46	48	45	49	47	48	46	47	44	46
B	46	52	51	54	49	52	48	54	53	54	54
C	54	54	50	56	48	54	54	56	49	49	46
D	52	52	52	52	52	58	51	52	58	58	44
E	52	52	52	52	53	48	52	50	56	52	54

	12	**13**	**14**	**15**	**16**	**17**	**18**	**19**	**20**	**21**	**22**
A	45	48	50	47	49	48	48	53	54	49	48
B	53	54	53	47	51	56	53	52	48	50	51
C	51	50	48	49	56	56	49	56	55	56	48
D	46	46	49	49	54	50	55	55	55	54	48
E	54	45	54	50	48	48	46	48	55	53	52

	23	**24**	**25**	**26**	**27**	**28**	**29**	**30**	**31**	**32**	**33**
A	50	48	49	49	50	50	47	42	45	48	45
B	54	50	53	48	51	48	51	53	54	48	58
C	49	50	56	53	57	51	48	54	49	50	54
D	56	56	56	48	52	46	56	54	54	57	53
E	53	48	46	46	50	43	44	52	46	44	48

Table B.2: Rebound hammer test results for Block 2

Rebound Hammer Testing

Performed by: SC

Date: 1/29/2004

Block #: 2

	1	**2**	**3**	**4**	**5**	**6**	**7**	**8**	**9**	**10**	**11**
A	52	53	52	53	46	46	48	50	54	54	54
B	52	55	55	55	56	54	54	50	54	49	50
C	56	56	58	57	52	51	53	56	55	54	54
D	56	57	58	58	54	54	55	57	54	53	58
E	54	54	57	53	54	55	56	55	50	54	53

	12	**13**	**14**	**15**	**16**	**17**	**18**	**19**	**20**	**21**	**22**
A	55	49	50	56	54	55	51	50	50	53	48
B	49	50	54	52	56	57	54	50	58	57	51
C	53	53	59	56	56	52	57	57	54	54	57
D	51	47	53	56	59	56	56	56	54	56	49
E	54	54	52	55	55	57	56	52	56	47	46

	23	**24**	**25**	**26**	**27**	**28**	**29**	**30**	**31**	**32**	**33**
A	47	52	57	56	50	53	54	50	50	50	49
B	57	57	58	49	49	53	53	56	53	49	52
C	56	57	54	50	53	55	53	54	54	56	57
D	50	58	57	54	57	53	57	58	56	55	56
E	54	53	54	47	53	47	53	52	51	48	51

Table B.3: Rebound hammer test results for Block 3

Rebound Hammer Testing

Performed by: SC, BQ
Date: 1/29/2004
Block #: 3

	1	**2**	**3**	**4**	**5**	**6**	**7**	**8**	**9**	**10**	**11**
A	51	52	50	49	50	54	51	48	54	52	54
B	51	48	49	50	50	53	48	49	54	48	54
C	54	54	55	52	47	50	56	50	56	56	56
D	51	52	57	56	55	53	55	52	55	56	56
E	55	57	57	54	58	57	55	52	56	58	58

	12	**13**	**14**	**15**	**16**	**17**	**18**	**19**	**20**	**21**	**22**
A	56	53	54	54	50	52	48	52	55	52	54
B	53	53	56	50	52	51	48	54	54	55	52
C	53	51	53	50	53	49	55	50	52	52	52
D	56	56	58	52	55	56	59	59	54	58	56
E	58	58	60	59	57	60	59	58	60	58	60

	23	**24**	**25**	**26**	**27**	**28**	**29**	**30**	**31**	**32**	**33**
A	55	48	53	53	52	53	55	52	49	54	54
B	54	52	54	52	50	54	52	54	56	54	52
C	50	53	48	48	48	54	54	53	55	54	54
D	53	54	56	56	55	56	57	52	56	54	52
E	58	57	62	59	56	56	56	58	54	55	56

Table B.4: Rebound hammer test results for Block 4

Rebound Hammer Testing

Performed by: SC, BQ
Date: 1/29/2004
Block #: 4

	1	**2**	**3**	**4**	**5**	**6**	**7**	**8**	**9**	**10**	**11**
A	54	48	48	52	48	49	50	48	50	50	52
B	44	48	48	47	49	50	46	49	54	50	46
C	52	54	54	50	48	53	54	52	51	53	51
D	52	55	54	51	54	55	54	54	54	49	53
E	55	56	53	58	56	56	57	56	61	54	54

	12	**13**	**14**	**15**	**16**	**17**	**18**	**19**	**20**	**21**	**22**
A	48	42	48	46	50	52	54	48	46	52	49
B	50	52	56	53	50	56	50	56	54	54	50
C	52	53	58	53	48	55	48	51	49	52	54
D	54	54	52	54	53	54	55	57	56	59	54
E	54	52	52	54	54	53	56	56	57	56	55

	23	**24**	**25**	**26**	**27**	**28**	**29**	**30**	**31**	**32**	**33**
A	46	48	48	54	49	54	50	50	48	46	49
B	48	54	50	46	50	52	50	48	48	52	53
C	48	54	50	46	50	52	50	48	48	52	53
D	54	53	53	51	57	55	54	52	53	52	53
E	58	59	55	57	54	55	54	54	54	53	44

Table B.5: Rebound hammer test results for Block 5

Rebound Hammer Testing

Performed by: XZ, EC
Date: 5/16/2003
Block #: 5

	1	**2**	**3**	**4**	**5**	**6**	**7**	**8**	**9**	**10**	**11**
A	43	47	42	44	39	41	44	41	41	40	44
B	44	44	43	43	45	42	43	44	43	42	45
C	44	46	46	51	43	40	43	43	50	48	45
D	48	42	50	52	52	51	53	50	48	44	47
E	52	56	52	49	52	50	50	43	50	53	44

	12	**13**	**14**	**15**	**16**	**17**	**18**	**19**	**20**	**21**	**22**
A	44	44	39	45	45	39	46	44	46	42	44
B	44	44	45	45	46	44	43	45	47	46	46
C	43	47	45	48	44	45	47	46	45	46	45
D	50	54	50	52	46	48	52	46	46	50	51
E	50	48	48	45	45	44	53	52	54	48	56

	23	**24**	**25**	**26**	**27**	**28**	**29**	**30**	**31**	**32**	**33**
A	47	44	42	45	44	46	39	43	42	40	42
B	43	45	44	46	40	48	41	40	46	43	48
C	45	40	47	48	45	46	46	44	44	40	44
D	47	46	47	54	44	45	53	50	51	44	52
E	54	46	54	54	50	50	47	49	55	56	52

Table B.6: Rebound hammer test results for Block 6

Rebound Hammer Testing

Performed by: XZ, EC
Date: 5/16/2003
Block #: 6

	1	**2**	**3**	**4**	**5**	**6**	**7**	**8**	**9**	**10**	**11**
A	44	47	48	45	42	44	43	42	41	43	42
B	44	45	50	50	46	43	44	48	48	48	46
C	48	46	49	46	46	44	49	50	50	54	49
D	50	44	45	52	53	55	55	50	55	50	52
E	50	48	52	52	54	55	57	45	52	51	56

	12	**13**	**14**	**15**	**16**	**17**	**18**	**19**	**20**	**21**	**22**
A	42	42	42	43	42	44	46	48	42	42	44
B	46	36	46	49	47	41	44	46	44	42	44
C	47	47	46	46	50	49	44	44	50	48	48
D	53	53	52	52	51	50	53	53	55	54	53
E	59	59	52	54	55	56	55	58	50	52	52

	23	**24**	**25**	**26**	**27**	**28**	**29**	**30**	**31**	**32**	**33**
A	40	46	42	46	48	45	47	46	42	42	43
B	43	44	48	50	49	46	49	48	46	48	45
C	45	48	48	48	50	43	54	46	46	47	41
D	52	50	52	51	51	53	50	50	51	48	52
E	55	47	53	55	53	47	51	54	57	52	52

Table B.7: Rebound hammer test results for Block 7

Rebound Hammer Testing

Performed by: XZ, EC
Date: 5/16/2003
Block #: 7

	1	**2**	**3**	**4**	**5**	**6**	**7**	**8**	**9**	**10**	**11**
A	46	44	44	43	43	44	43	44	41	46	48
B	45	49	44	44	44	48	45	47	40	50	43
C	44	52	47	49	46	46	46	44	46	45	48
D	54	54	53	46	51	53	54	56	54	52	52
E	55	52	54	51	56	57	58	52	54	56	50

	12	**13**	**14**	**15**	**16**	**17**	**18**	**19**	**20**	**21**	**22**
A	45	41	43	47	44	43	42	46	44	42	44
B	48	48	49	46	46	42	50	46	46	48	44
C	53	46	45	53	42	50	49	44	42	40	50
D	51	55	49	53	54	52	54	48	51	52	54
E	56	51	53	48	55	52	51	53	58	52	55

	23	**24**	**25**	**26**	**27**	**28**	**29**	**30**	**31**	**32**	**33**
A	40	43	42	44	44	46	44	43	44	44	40
B	51	45	48	45	47	43	42	50	42	46	47
C	48	50	51	45	49	42	46	50	51	47	43
D	54	52	45	55	53	49	52	52	52	50	50
E	44	54	54	48	58	50	55	53	53	52	50

Table B.8: Rebound hammer test results for Block 8

Rebound Hammer Testing

Performed by: XZ, EC

Date: 5/16/2003

Block #: 8

	1	2	3	4	5	6	7	8	9	10	11
A	44	36	41	42	42	41	43	42	44	45	46
B	44	42	45	43	41	42	42	44	44	44	42
C	49	47	47	45	43	49	40	42	44	43	48
D	44	46	44	48	44	50	46	46	44	45	44
E	52	50	52	53	44	46	50	49	44	49	50

	12	13	14	15	16	17	18	19	20	21	22
A	45	43	42	43	46	42	43	45	42	43	44
B	40	44	41	46	51	51	46	46	44	45	46
C	42	43	49	50	51	45	46	44	49	46	44
D	47	50	37	51	42	50	53	50	49	53	52
E	47	52	52	46	50	46	46	52	52	52	45

	23	24	25	26	27	28	29	30	31	32	33
A	45	45	44	42	46	40	45	40	45	46	38
B	43	47	42	42	46	52	46	51	47	43	52
C	46	45	50	40	42	43	41	50	43	46	46
D	53	53	52	46	51	51	54	52	48	55	46
E	49	49	54	53	53	52	51	53	54	52	52

Table B.9: Rebound hammer test results for Block 9

Rebound Hammer Testing

Performed by: SC, XZ

Date: 6/27/2003

Block #: 9

	1	**2**	**3**	**4**	**5**	**6**	**7**	**8**	**9**	**10**	**11**
A	38	35	39	39	39	40	40	41	39	39	41
B	44	42	46	47	47	46	41	43	48	48	46
C	45	47	49	46	46	46	44	46	48	48	48
D	43	46	44	44	44	50	48	50	46	46	48
E	43	47	45	42	42	49	48	43	47	47	52

	12	**13**	**14**	**15**	**16**	**17**	**18**	**19**	**20**	**21**	**22**
A	39	41	41	41	41	41	42	34	38	40	42
B	46	44	47	44	44	46	44	44	44	42	42
C	48	48	46	48	48	46	46	43	45	45	45
D	50	52	52	52	52	44	47	48	52	53	50
E	51	48	49	51	51	50	50	48	51	51	41

	23	**24**	**25**	**26**	**27**	**28**	**29**	**30**	**31**	**32**	**33**
A	42	42	42	41	41	37	41	39	42	42	40
B	44	43	44	42	42	48	46	46	45	44	48
C	43	47	45	47	47	48	48	48	45	44	48
D	51	52	51	53	53	50	54	44	44	42	44
E	50	53	48	48	48	52	52	46	46	46	46

Table B.10: Rebound hammer test results for Block 10

Rebound Hammer Testing

Performed by: SC, XZ
Date: 6/27/2003
Block #: 10

	1	**2**	**3**	**4**	**5**	**6**	**7**	**8**	**9**	**10**	**11**
A	41	38	42	41	40	41	41	43	41	42	42
B	42	46	46	44	42	46	45	45	49	43	44
C	48	49	50	42	44	44	42	43	46	45	44
D	46	50	51	50	48	49	48	53	48	53	53
E	46	47	45	45	48	52	53	51	51	53	51

	12	**13**	**14**	**15**	**16**	**17**	**18**	**19**	**20**	**21**	**22**
A	44	42	42	41	42	40	41	40	41	42	42
B	43	44	44	44	44	44	42	43	42	44	44
C	48	44	48	44	44	42	42	42	46	44	44
D	53	49	48	50	50	48	50	53	51	50	48
E	50	46	44	51	48	48	50	50	48	47	47

	23	**24**	**25**	**26**	**27**	**28**	**29**	**30**	**31**	**32**	**33**
A	42	42	41	40	40	41	40	42	42	43	40
B	44	45	40	42	42	42	41	44	43	44	46
C	42	42	42	44	44	42	44	43	43	43	41
D	46	46	46	48	47	50	49	46	44	50	44
E	52	48	46	50	46	45	45	47	47	46	50

Table B.11: Rebound hammer test results for Block 11

Rebound Hammer Testing

Performed by: SC, XZ
Date: 6/27/2003
Block #: 11

	1	**2**	**3**	**4**	**5**	**6**	**7**	**8**	**9**	**10**	**11**
A	41	38	42	40	40	42	42	41	41	41	44
B	42	43	42	40	40	45	44	42	40	45	47
C	49	46	47	42	44	44	50	46	44	47	50
D	44	46	48	52	48	50	49	48	46	48	51
E	47	46	48	50	48	52	53	51	50	52	50

	12	**13**	**14**	**15**	**16**	**17**	**18**	**19**	**20**	**21**	**22**
A	40	42	42	43	42	42	42	44	39	41	40
B	47	45	44	44	44	48	48	48	46	45	48
C	44	48	49	52	48	48	50	49	47	47	48
D	50	46	52	47	47	45	53	53	54	50	50
E	48	51	54	54	52	53	54	56	57	53	51

	23	**24**	**25**	**26**	**27**	**28**	**29**	**30**	**31**	**32**	**33**
A	42	42	44	42	40	40	40	40	38	38	40
B	47	46	46	46	50	46	42	49	47	48	48
C	46	48	51	46	49	46	48	52	52	48	46
D	49	52	52	48	50	51	48	52	51	48	50
E	55	52	52	50	54	50	48	52	54	46	46

Table B.12: Rebound hammer test results for Block 12

Rebound Hammer Testing

Performed by: SC, XZ
Date: 6/27/2003
Block #: 12

	1	**2**	**3**	**4**	**5**	**6**	**7**	**8**	**9**	**10**	**11**
A	38	40	41	40	40	42	42	41	41	42	41
B	39	41	45	40	49	46	47	49	42	41	42
C	41	44	47	44	42	45	48	42	42	43	44
D	50	47	50	46	50	50	49	45	48	44	47
E	44	42	46	50	46	52	53	50	45	49	45

	12	**13**	**14**	**15**	**16**	**17**	**18**	**19**	**20**	**21**	**22**
A	41	40	42	42	41	38	41	37	38	42	40
B	44	43	50	48	42	44	45	40	46	49	47
C	44	46	46	44	44	49	42	41	41	42	42
D	47	46	44	46	44	50	48	49	44	46	44
E	50	52	52	52	51	49	52	51	49	49	52

	23	**24**	**25**	**26**	**27**	**28**	**29**	**30**	**31**	**32**	**33**
A	41	42	41	40	42	40	40	40	40	41	41
B	45	43	43	43	45	43	42	42	42	44	43
C	44	47	44	47	49	45	44	46	44	42	43
D	48	50	50	53	49	51	49	50	46	48	47
E	50	46	48	47	51	51	48	46	51	50	50

Table B.13: Rebound hammer test results for Block 17

Rebound Hammer Testing

Performed by: SC
Date: 1/24/2004
Block #: 17

	1	2	3	4	5	6	7	8	9	10	11
A	43	43	40	40	40	43	39	40	38	38	40
B	42	44	46	43	48	49	44	48	45	54	51
C	48	49	52	47	42	38	44	50	53	48	52
D	44	42	40	48	44	40	49	44	49	44	46
E	44	44	46	43	46	42	39	45	40	43	44

	12	13	14	15	16	17	18	19	20	21	22
A	40	38	36	39	42	40	42	40	43	41	44
B	48	54	51	49	44	43	48	46	46	46	46
C	38	42	45	52	54	55	55	38	43	45	47
D	46	46	48	43	42	48	41	45	46	46	45
E	47	47	50	50	50	47	53	46	50	50	48

	23	24	25	26	27	28	29	30	31	32	33
A	39	44	40	41	40	40	42	42	40	44	42
B	46	41	43	42	48	50	46	52	52	50	50
C	46	50	39	34	38	47	47	48	47	53	48
D	45	47	47	40	46	42	46	50	50	44	48
E	52	50	48	50	49	43	53	51	53	44	38

Table B.14: Rebound hammer test results for Block 18

Rebound Hammer Testing

Performed by: SC

Date: 1/24/2004

Block #: 18

	1	**2**	**3**	**4**	**5**	**6**	**7**	**8**	**9**	**10**	**11**
A	26	42	40	37	41	42	43	43	42	40	39
B	46	46	46	46	44	46	49	47	47	46	40
C	48	46	49	48	44	47	45	49	47	42	47
D	42	44	50	48	42	44	50	44	48	45	51
E	44	48	45	44	48	54	50	52	47	44	46

	12	**13**	**14**	**15**	**16**	**17**	**18**	**19**	**20**	**21**	**22**
A	42	44	43	43	42	43	44	40	43	41	43
B	47	48	32	47	45	43	45	45	45	45	46
C	46	44	44	48	49	47	50	46	42	38	44
D	47	49	49	43	41	48	45	48	48	48	45
E	49	50	50	46	47	48	50	50	48	50	49

	23	**24**	**25**	**26**	**27**	**28**	**29**	**30**	**31**	**32**	**33**
A	45	40	37	45	40	38	37	40	42	42	43
B	45	45	42	40	45	45	42	45	44	43	44
C	48	47	47	50	42	44	46	44	46	46	48
D	41	47	47	45	42	48	44	46	45	44	44
E	43	48	38	43	47	46	50	49	52	43	42

Table B.15: Rebound hammer test results for Block 19

Rebound Hammer Testing

Performed by: SC

Date: 1/24/2004

Block #: 19

	1	**2**	**3**	**4**	**5**	**6**	**7**	**8**	**9**	**10**	**11**
A	39	38	37	42	40	44	45	37	38	38	38
B	37	41	42	44	40	45	40	43	39	38	38
C	47	47	46	46	38	38	44	46	46	47	47
D	43	46	48	44	43	45	43	43	41	42	44
E	51	51	46	48	46	46	42	42	42	46	43

	12	**13**	**14**	**15**	**16**	**17**	**18**	**19**	**20**	**21**	**22**
A	32	38	38	38	42	38	34	38	38	36	37
B	37	42	42	40	39	38	38	40	37	44	38
C	42	40	44	44	45	44	46	38	38	44	46
D	42	44	42	42	41	42	40	45	42	45	45
E	41	38	43	45	42	43	50	46	48	40	48

	23	**24**	**25**	**26**	**27**	**28**	**29**	**30**	**31**	**32**	**33**
A	38	40	34	43	38	38	35	36	34	32	30
B	42	43	39	39	42	39	42	43	39	42	47
C	48	47	42	43	40	42	47	48	48	46	51
D	43	45	44	43	44	45	37	38	40	46	48
E	40	46	48	49	52	45	48	44	46	44	45

Table B.16: Rebound hammer test results for Block 20

Rebound Hammer Testing

Performed by: SC
Date: 1/24/2004
Block #: 20

	1	**2**	**3**	**4**	**5**	**6**	**7**	**8**	**9**	**10**	**11**
A	34	37	36	38	38	38	42	38	38	42	40
B	42	38	39	39	36	40	42	40	34	38	40
C	44	46	46	46	41	37	46	48	48	48	44
D	42	44	50	48	44	44	53	42	40	49	40
E	47	42	50	43	52	50	47	45	39	36	43

	12	**13**	**14**	**15**	**16**	**17**	**18**	**19**	**20**	**21**	**22**
A	38	36	34	35	34	33	35	34	33	37	38
B	43	40	42	42	38	34	38	40	39	44	38
C	38	38	42	44	43	45	47	44	35	40	44
D	40	41	38	44	41	42	42	45	49	46	44
E	53	44	50	44	49	48	48	46	48	47	52

	23	**24**	**25**	**26**	**27**	**28**	**29**	**30**	**31**	**32**	**33**
A	35	37	40	37	36	38	36	40	33	33	38
B	42	40	43	46	48	48	41	42	41	40	44
C	46	43	46	42	40	42	43	44	46	48	48
D	44	44	37	42	37	40	46	40	48	46	46
E	46	46	44	40	48	45	46	43	42	42	45

Table B.17: Rebound hammer test results for Block 21

Rebound Hammer Testing

Performed by: XZ, EC

Date: 5/16/2003

Block #: 21

	1	**2**	**3**	**4**	**5**	**6**	**7**	**8**	**9**	**10**	**11**
A	44	38	41	42	42	43	40	38	44	39	41
B	40	43	42	41	35	37	40	36	36	36	38
C	40	44	42	44	42	40	40	39	44	42	44
D	41	46	43	42	44	42	45	39	45	41	41
E	42	40	43	40	48	49	44	44	42	44	44

	12	**13**	**14**	**15**	**16**	**17**	**18**	**19**	**20**	**21**	**22**
A	39	45	37	39	39	41	40	40	37	36	36
B	38	42	39	44	41	39	37	38	41	41	40
C	42	39	42	42	42	37	42	45	42	39	44
D	41	46	44	48	48	48	45	45	41	46	42
E	39	40	46	41	42	44	40	41	44	45	42

	23	**24**	**25**	**26**	**27**	**28**	**29**	**30**	**31**	**32**	**33**
A	39	41	36	40	35	35	40	37	38	40	40
B	39	40	40	41	39	38	40	43	42	44	38
C	44	42	41	41	38	40	38	44	44	43	44
D	50	43	41	48	45	39	42	39	41	40	42
E	41	38	43	46	40	44	42	42	47	38	36

Table B.18: Rebound hammer test results for Block 22

Rebound Hammer Testing

Performed by: SC, EC
Date: 5/15/2003
Block #: 22

	1	**2**	**3**	**4**	**5**	**6**	**7**	**8**	**9**	**10**	**11**
A	35	39	41	38	40	37	38	39	38	41	42
B	42	46	43	41	43	44	46	40	43	44	46
C	43	41	44	42	42	38	39	38	41	40	46
D	43	42	42	46	40	45	48	48	40	42	44
E	44	42	42	42	44	43	41	46	45	46	46

	12	**13**	**14**	**15**	**16**	**17**	**18**	**19**	**20**	**21**	**22**
A	42	39	37	42	40	36	38	40	38	35	38
B	42	42	42	44	41	42	43	43	42	40	43
C	44	40	40	40	40	42	42	41	43	42	39
D	40	40	42	43	44	46	44	44	45	42	44
E	46	42	44	43	40	44	43	46	45	44	44

	23	**24**	**25**	**26**	**27**	**28**	**29**	**30**	**31**	**32**	**33**
A	38	38	36	38	39	38	40	38	36	38	38
B	42	41	42	44	41	42	43	44	44	41	43
C	43	44	45	44	42	41	40	38	44	44	44
D	41	43	44	40	47	46	45	43	42	40	42
E	41	41	43	43	47	45	42	43	46	42	42

Table B.19: Rebound hammer test results for Block 23

Rebound Hammer Testing

Performed by: XZ, EC
Date: 5/16/2003
Block #: 23

	1	**2**	**3**	**4**	**5**	**6**	**7**	**8**	**9**	**10**	**11**
A	40	32	39	36	36	39	39	38	35	42	36
B	41	42	42	42	36	41	43	43	40	40	43
C	40	43	43	41	40	38	38	36	39	41	43
D	45	42	44	44	45	42	42	40	41	40	42
E	40	46	39	40	39	49	43	42	36	48	40

	12	**13**	**14**	**15**	**16**	**17**	**18**	**19**	**20**	**21**	**22**
A	34	36	32	38	43	36	37	36	36	36	41
B	42	38	37	44	42	40	44	44	38	38	39
C	40	40	39	38	40	39	42	43	42	46	39
D	42	39	42	42	46	37	42	44	42	42	45
E	45	45	46	42	43	39	40	41	41	41	40

	23	**24**	**25**	**26**	**27**	**28**	**29**	**30**	**31**	**32**	**33**
A	40	38	36	37	39	37	36	35	36	38	39
B	37	42	36	42	41	41	36	41	42	40	42
C	44	42	37	42	38	40	40	43	44	42	42
D	42	44	42	36	40	41	46	41	42	43	42
E	40	36	43	36	41	38	43	46	38	42	40

Table B.20: Rebound hammer test results for Block 24

Rebound Hammer Testing

Performed by: XZ, EC
Date: 5/16/2003
Block #: 24

	1	**2**	**3**	**4**	**5**	**6**	**7**	**8**	**9**	**10**	**11**
A	44	41	38	46	42	38	41	43	46	40	46
B	46	43	43	43	42	43	41	44	41	42	48
C	53	43	45	43	40	40	41	43	39	40	48
D	44	45	40	42	44	42	42	44	40	41	40
E	44	47	42	48	48	45	42	47	41	44	46

	12	**13**	**14**	**15**	**16**	**17**	**18**	**19**	**20**	**21**	**22**
A	46	46	39	49	42	41	39	40	38	40	42
B	42	42	39	40	40	40	45	40	39	38	42
C	45	44	39	47	46	56	43	42	42	38	43
D	40	42	43	44	42	43	42	42	51	45	41
E	46	41	42	43	46	42	40	42	40	44	47

	23	**24**	**25**	**26**	**27**	**28**	**29**	**30**	**31**	**32**	**33**
A	41	40	39	46	39	40	40	38	39	40	42
B	41	40	40	43	40	42	42	42	43	42	41
C	44	44	44	44	46	46	46	53	44	46	47
D	42	42	38	43	44	46	43	39	44	42	39
E	44	52	44	48	47	43	40	46	40	40	40

Table B.21: Rebound hammer test results for Block 25

Rebound Hammer Testing

Performed by: SC, DL
Date: 7/11/2003
Block #: 25

	1	2	3	4	5	6	7	8	9	10	11
A	40	39	40	39	39	40	39	38	39	37	37
B	40	42	40	40	41	41	40	43	38	39	42
C	42	48	42	41	44	41	40	41	42	41	42
D	40	44	50	47	49	50	50	46	47	46	47
E	42	44	41	44	45	49	47	49	48	46	49

	12	13	14	15	16	17	18	19	20	21	22
A	40	36	36	39	41	40	40	41	40	41	39
B	37	37	40	37	37	36	39	38	39	36	42
C	42	42	40	40	40	41	42	42	45	44	42
D	49	47	47	46	47	48	48	49	47	47	46
E	48	50	48	47	46	47	48	49	47	50	49

	23	24	25	26	27	28	29	30	31	32	33
A	40	38	39	41	39	39	38	42	38	38	37
B	38	38	40	38	36	38	39	41	41	38	39
C	42	44	42	45	45	44	44	40	42	41	40
D	46	50	48	48	46	48	46	48	47	42	48
E	50	49	44	44	49	48	45	47	42	42	42

Table B.22: Rebound hammer test results for Block 26

Rebound Hammer Testing

Performed by: SC, DL
Date: 7/11/2003
Block #: 26

	1	**2**	**3**	**4**	**5**	**6**	**7**	**8**	**9**	**10**	**11**
A	36	36	32	34	33	34	32	33	31	33	32
B	44	41	40	35	35	34	36	36	35	36	36
C	40	42	35	35	40	38	38	38	42	41	42
D	42	39	39	39	41	41	46	43	42	45	44
E	41	41	41	40	38	42	42	41	41	41	44

	12	**13**	**14**	**15**	**16**	**17**	**18**	**19**	**20**	**21**	**22**
A	30	35	32	34	31	31	32	30	35	31	32
B	37	36	34	34	33	31	33	38	37	35	36
C	40	37	40	41	39	37	42	38	37	35	37
D	44	44	44	41	41	40	42	40	40	41	43
E	43	42	40	41	38	40	40	41	40	40	43

	23	**24**	**25**	**26**	**27**	**28**	**29**	**30**	**31**	**32**	**33**
A	33	34	36	38	33	32	34	34	32	33	28
B	36	39	37	38	41	39	35	38	37	37	36
C	42	39	42	39	42	39	42	39	41	41	38
D	42	42	42	42	42	43	44	42	42	39	41
E	44	44	40	40	45	46	46	43	42	44	42

Table B.23: Rebound hammer test results for Block 27

Rebound Hammer Testing

Performed by: SC, DL

Date: 7/11/2003

Block #: 27

	1	**2**	**3**	**4**	**5**	**6**	**7**	**8**	**9**	**10**	**11**
A	32	31	30	26	33	29	36	39	37	38	34
B	41	39	34	41	39	42	42	42	39	39	42
C	42	42	42	42	41	42	42	40	44	42	40
D	40	39	40	40	40	40	38	38	40	43	40
E	37	37	37	40	40	39	40	40	40	40	40

	12	**13**	**14**	**15**	**16**	**17**	**18**	**19**	**20**	**21**	**22**
A	32	38	42	39	35	37	38	35	32	36	38
B	44	44	42	40	42	42	40	44	39	38	42
C	42	42	42	40	44	42	44	42	41	42	42
D	42	41	41	44	42	41	41	44	44	48	44
E	39	39	40	40	40	40	42	42	40	41	41

	23	**24**	**25**	**26**	**27**	**28**	**29**	**30**	**31**	**32**	**33**
A	37	37	39	36	36	36	36	37	37	39	36
B	42	42	40	38	41	40	40	40	38	41	41
C	44	41	42	41	39	41	41	42	40	44	45
D	48	44	42	45	43	39	41	40	42	39	40
E	41	40	44	42	41	41	39	41	39	40	42

Table B.24: Rebound hammer test results for Block 28

Rebound Hammer Testing

Performed by: SC, DL

Date: 7/11/2003

Block #: 28

	1	2	3	4	5	6	7	8	9	10	11
A	39	36	38	38	36	38	39	38	37	38	36
B	36	41	38	41	40	40	39	41	36	37	37
C	41	41	39	40	39	41	42	39	40	39	41
D	38	38	38	38	40	40	42	42	44	40	38
E	39	41	40	39	39	39	41	45	40	44	41

	12	13	14	15	16	17	18	19	20	21	22
A	36	38	38	38	36	38	40	38	38	36	37
B	38	38	38	41	39	42	42	38	40	40	38
C	41	41	42	41	41	42	38	40	39	39	41
D	39	37	39	42	42	46	46	48	40	41	43
E	46	41	43	44	42	46	45	46	46	45	48

	23	24	25	26	27	28	29	30	31	32	33
A	37	38	38	35	36	37	36	35	35	38	36
B	36	38	36	36	36	36	36	36	36	36	37
C	39	39	39	40	38	38	38	38	41	42	43
D	42	41	40	40	39	40	38	39	38	40	39
E	44	43	43	44	44	42	40	44	44	43	40

APPENDIX C

CORE TEST RESULTS

Table C.1: Core data for Blocks 1 and 2

Block 1 & 2 Specimens

NDT	BQ, SC	f'c	SC		Age at removal
					365days
Date	2/3/2004	Date	2/10/2004		
f'st	SC	f'p	SC		Concrete Exposed to:
Date	2/11/2004	Date	2/28/2004		SO_4^{2-}

Core Name		Length cut (mm)	UPV Time dry(□s)	Pulse Velocity (m/s)	Resonant Frequency (Hz)	Ultimate Load (kN)	Ultimate Load (MPa)	Test Performed
1	1A	200.00	46.8	4273.5	2213	412.8	50.9	f'c
1	1B	201.50	46.2	4361.5	2598	458.9	56.6	f'c
1	1C	199.50	45.6	4375.0	2478	454.7	56.1	f'c
1	1D	209.00	46.7	4475.4	2548	150.5	4.5	f'st
1	1E	-	-	-	-	-	-	spare
1	1F	-	-	-	-	-	-	spare
1	2A	199.00	44.7	4451.9	2527	530.5	65.4	f'c
1	2B	200.00	45.0	4444.4	2546	613.2	75.6	f'c
1	2C	201.00	44.7	4496.6	2522	605.8	74.7	f'c
1	2D	-	-	-	-	-	-	spare
1	2E	-	-	-	-	-	-	spare
1	2F	208.00	45.6	4561.4	3061	504.5	62.2	f'c
1	3A	201.00	44.3	4537.2	2441	613.2	75.6	f'c
1	3B	200.00	44.1	4535.1	2399	643.7	79.4	f'c
1	3C	202.00	44.7	4519.0	2514	630.5	77.8	f'c
1	3D	-	-	-	-	-	-	spare
1	3E	-	-	-	-	-	-	spare
1	3F	207.00	45.3	4569.5	2997	159.1	4.8	f'st
2	1A	199.00	46.2	4307.4	2917	143.1	4.5	f'st
2	1B	204.50	46.5	4397.8	2995	154.6	4.7	f'st
2	1C	203.50	46.3	4395.2	2178	128.4	4.0	f'st
2	1D	203.50	46.0	4423.9	2691	-	7.6	f'p
2	1E	204.00	46.3	4406.0	2813	-	8.5	f'p
2	1F	204.50	46.8	4369.7	2477	-	7.6	f'p
2	2A	198.00	44.0	4500.0	2903	108.0	3.4	f'st
2	2B	200.00	44.5	4494.4	2957	175.9	5.5	f'st
2	2C	202.50	45.0	4500.0	2653	162.3	5.0	f'st
2	2D	201.50	44.7	4507.8	2997	-	9.5	f'p
2	2E	200.50	45.0	4455.6	2809	-	8.5	f'p
2	2F	200.00	44.2	4524.9	3384	-	8.7	f'p
2	3A	205.00	45.4	4515.4	2968	122.7	3.8	f'st
2	3B	208.00	45.9	4531.6	3045	179.1	5.4	f'st
2	3C	210.00	46.4	4525.9	2762	152.5	4.6	f'st
2	3D	207.50	45.8	4530.6	2984	-	8.8	f'p
2	3E	205.00	45.0	4555.6	2634	-	8.0	f'p
2	3F	203.00	44.5	4561.8	2651	-	8.7	f'p

Table C.1: Core data for Blocks 1 and 2 continued

Cylinder Name		Length cut (mm)	UPV Time dry(□s)	Pulse Velocity (m/s)	Resonant Frequency (Hz)	Ultimate Load (kN)	Ultimate Load (MPa)	Test Performed
1 & 2	1	199.00	44.2	4502.3	2791	616.5	76.0	f'c
1 & 2	2	197.00	43.9	4487.5	2703	610.1	75.3	f'c
1 & 2	3	197.00	43.8	4497.7	2702	595.8	73.5	f'c
1 & 2	4	195.50	43.9	4453.3	2644	-	10.2	f'p
1 & 2	5	196.50	44.0	4465.9	3037	-	8.5	f'p
1 & 2	6	193.00	42.8	4509.3	2849	-	9.9	f'p
1 & 2	7	195.50	43.2	4525.5	2550	190.7	6.1	f'st
1 & 2	8	199.50	44.0	4534.1	2904	187.9	5.9	f'st
1 & 2	9	194.00	43.5	4459.8	2657	180.5	5.8	f'st
1 & 2	10	199.50	44.4	4493.2	2982	-	10.0	f'p

Test	Location	Mean	Standard Deviation	Coefficient of Variance
f'c	Top	54.5	3.1	5.8
	Middle	71.9	5.6	7.8
	Bottom	77.6	1.9	2.4
	Cylinders	74.9	1.3	1.7
f'st	Top	4.6	0.1	2.9
	Middle	4.6	1.1	23.6
	Bottom	4.9	0.4	8.8
	Cylinders	5.9	0.1	2.4
f'p	Top	7.9	0.5	6.6
	Middle	8.9	0.5	5.9
	Bottom	8.5	0.4	5.2
	Cylinders	10.0	0.2	1.7

Table C.2: Core data for Blocks 3 and 4

Block 3 & 4 Specimens

NDT	BQ, SC	f'c	SC		Age at removal: 365days
Date	2/3/2004	Date	2/10/2004		
f'st	SC	f'p	SC		Concrete exposed to:
Date	2/11/2004	Date	3/1/2004		$Ca(OH)_2$

Core Name		Length cut (mm)	UPV Time dry(μs)	Pulse Velocity (m/s)	Resonant Frequency (Hz)	Ultimate Load (kN)	Ultimate Load (MPa)	Test Performed
3	1A	196.50	44.1	4455.8	2893	516.6	63.7	f'c
3	1B	196.00	44.9	4365.3	2455	503.9	62.2	f'c
3	1C	195.00	44.4	4391.9	2890	462.1	57.0	f'c
3	1D	-	-	-	-	-	-	spare
3	1E	-	-	-	-	-	-	spare
3	1F	-	-	-	-	-	-	spare
3	2A	195.00	43.0	4534.9	2191	621.4	76.6	f'c
3	2B	195.50	43.1	4536.0	2205	671.1	82.8	f'c
3	2C	196.00	43.3	4526.6	2276	594.9	73.4	f'c
3	2D	-	-	-	-	-	-	spare
3	2E	-	-	-	-	-	-	spare
3	2F	202.50	43.6	4644.5	2905	203.2	6.3	f'st
3	3A	120.00	26.8	4477.6	2254	701.6	86.5	f'c
3	3B	194.50	43.0	4523.3	2476	672.3	82.9	f'c
3	3C	195.50	42.8	4567.8	2477	640.9	79.1	f'c
3	3D	201.00	43.6	4610.1	2494	179.1	5.6	f'st
3	3E	-	-	-	-	-	-	spare
3	3F	193.00	42.2	4573.5	2593	659.5	81.4	f'c

4	1A	208.00	47.3	4397.5	2618	142.5	4.3	f'st
4	1B	209.50	47.5	4410.5	2894	149.2	4.5	f'st
4	1C	210.00	48.2	4356.8	2420	148.9	4.4	f'st
4	1D	210.50	48.0	4385.4	2166	-	7.9	f'p
4	1E	210.50	48.0	4385.4	2882	-	5.5	f'p
4	1F	208.00	47.5	4378.9	2999	-	6.3	f'p
4	2A	209.00	46.3	4514.0	3058	164.3	4.9	f'st
4	2B	212.50	47.0	4521.3	2731	172.1	5.1	f'st
4	2C	214.00	47.6	4495.8	2678	181.1	5.3	f'st
4	2D	214.00	48.0	4458.3	2755	-	8.5	f'p
4	2E	213.00	47.0	4531.9	2803	-	7.7	f'p
4	2F	209.00	46.1	4533.6	2868	-	7.9	f'p
4	3A	207.00	45.6	4539.5	2496	177.7	5.4	f'st
4	3B	211.00	46.5	4537.6	2632	188.7	5.6	f'st
4	3C	213.00	46.8	4551.3	2769	222.8	6.6	f'st
4	3D	214.00	47.5	4505.3	2597	-	8.5	f'p
4	3E	212.00	46.7	4539.6	2412	-	8.5	f'p
4	3F	209.00	46.3	4514.0	3513	-	8.6	f'p

Table C.2: Core data for Blocks 3 and 4 continued

Cylinder Name		Length cut (mm)	UPV Time dry(□s)	Pulse Velocity (m/s)	Resonant Frequency (Hz)	Ultimate Load (kN)	Ultimate Load (MPa)	Test Performed
3 & 4	1	200.50	44.4	4515.8	3085	610.9	75.3	f'c
3 & 4	2	199.50	44.4	4493.2	2556	611.2	75.4	f'c
3 & 4	3	199.50	44.0	4534.1	2647	599.4	73.9	f'c
3 & 4	4	198.50	44.2	4491.0	2956	-	7.6	f'p
3 & 4	5	196.00	43.5	4505.7	2755	-	8.4	f'p
3 & 4	6	199.00	44.5	4471.9	2741	-	8.0	f'p
3 & 4	7	199.00	44.1	4512.5	2889	184.2	5.8	f'st
3 & 4	8	199.00	44.2	4502.3	2524	197.6	6.2	f'st
3 & 4	9	199.00	44.4	4482.0	3004	184.1	5.8	f'st
3 & 4	10	199.50	44.1	4523.8	2912	-	8.5	f'p

Test	Location	Mean	Standard Deviation	Coefficient of Variance
f'c	Top	61.0	3.5	5.8
	Middle	77.6	4.8	6.2
	Bottom	81.1	1.9	2.4
	Cylinders	74.9	0.8	1.1
f'st	Top	4.4	0.1	2.1
	Middle	5.1	0.2	3.7
	Bottom	5.5	0.1	2.2
	Cylinders	5.9	0.2	4.1
f'p	Top	6.5	1.2	18.7
	Middle	8.0	0.4	5.5
	Bottom	8.5	0.0	0.4
	Cylinders	8.3	0.3	3.2

Table C.3: Core data for Blocks 5 and 6

Block 5 & 6 Specimens

NDT	EC	f'c	SC
Date	5/27/2003	Date	6/24/2003
f'st	SC	f'p	SC
Date	6/17/2003	Date	1/24/2004

Age at removal 91Days

Concrete Exposed to: SO_4^{2-}

Core Name		Length uncut (mm)	Length cut (mm)	UPV Time dry(□s)	Pulse Velocity (m/s)	Resonant Frequency (Hz)	Ultimate Load (kN)	Ultimate Load (MPa)	Test Performed
5	1A	-	205.0	47.1	4352.4	2998	469.3	57.9	f'c
5	1B	-	206.5	47.4	4356.5	2498	373.1	46.0	f'c
5	1C	-	205.0	46.8	4380.3	2584	371.1	45.8	f'c
5	1D	245.00	205.5	58.1	4216.9	2905	108.7	3.3	F'st
5	1E	246.00	-	57.7	4263.4	2289	-	5.2	f'p
5	1F	245.50	200.0	58.6	4189.4	2905	395.2	48.7	f'c
5	2A	245.00	198.0	57.1	4290.7	2580	387.0	47.7	f'c
5	2B	245.00	204.5	57.0	4298.2	2633	440.1	54.3	f'c
5	2C	245.00	205.0	56.5	4336.3	2480	405.3	49.9	f'c
5	2D	244.50	-	56.8	4304.6	-	-	-	spare
5	2E	244.50	-	56.4	4335.1	2879	-	7.1	f'p
5	2F	244.50	-	57.1	4282.0	-	-	-	spare
5	3A	241.50	208.0	55.4	4359.2	2603	503.0	62.0	f'c
5	3B	242.75	206.0	54.6	4446.0	2894	523.3	64.5	f'c
5	3C	242.00	205.0	53.9	4489.8	2453	519.3	64.1	f'c
5	3D	242.00	-	55.2	4384.1	-	-	-	spare
5	3E	242.00	-	55.3	4376.1	-	-	-	spare
5	3F	242.00	-	55.9	4329.2	-	-	-	spare
6	1A	-	208	47.7	4360.6	2806	122.1	3.7	f'st
6	1B	-	209	48.6	4300.4	2566	107.9	3.2	f'st
6	1C	-	206	47.6	4327.7	2704	94.2	2.9	f'st
6	1D	-	205.5	48.2	4263.5	2595	-	6.4	f'p
6	1E	-	207	48.7	4250.5	2299	-	8.1	f'p
6	1F	-	206.5	48.0	4302.1	2682	-	9.5	f'p
6	2A	-	205	47.0	4361.7	2876	120.6	3.7	f'st
6	2B	-	206	47.4	4346.0	2725	146.9	4.5	f'st
6	2C	-	209	47.5	4400.0	2880	137.9	4.1	f'st
6	2D	-	206.5	47.9	4311.1	2687	-	7.8	f'p
6	2E	-	207.3	47.2	4390.9	2685	-	8.8	f'p
6	2F	-	207	47.2	4385.6	2805	-	7.0	f'p
6	3A	-	209	47.0	4446.8	2101	149.0	4.5	f'st
6	3B	-	203.3	45.6	4457.2	2154	155.9	4.8	f'st
6	3C	-	207	46.3	4470.8	2732	161.6	4.9	f'st
6	3D	-	204.5	45.8	4465.1	2492	-	8.4	f'p
6	3E	-	208	46.6	4463.5	2702	-	8.6	f'p
6	3F	-	206.5	45.9	4498.9	2942	-	8.6	f'p

Table C.3: Core data for Blocks 5 and 6 continued

Cylinder Name			Length (mm)	UPV Time dry(□s)	Pulse Velocity (m/s)	Resonant Frequency (Hz)	Ultimate Load (kN)	Ultimate Load (MPa)	Test Performed
5 & 6	1S		206.00	46.0	4478.3	2160	133.3	4.1	f'st
5 & 6	2S		206.00	45.9	4488.0	2840	170.2	5.2	f'st
5 & 6	3S		206.00	46.3	4449.2	3000	182.7	5.6	f'st
5 & 6	4S		205.50	45.9	4477.1	2475	-	10.2	f'p
5 & 6	5S		205.25	46.1	4452.3	2670	-	11.3	f'p
5 & 6	6S		205.75	45.9	4482.6	2535	-	12.6	f'p
5 & 6	7S		201.00	45.8	4388.6	2203	473.7	58.4	f'c
5 & 6	8S		201.00	45.8	4388.6	2221	484.1	59.7	f'c
5 & 6	9S		198.50	45.4	4372.2	2696	510.3	62.9	f'c
5 & 6	10S		195.00	45.4	4295.2	2697	-	8.7	f'p

Test	Location	Mean	Standard Deviation	Coefficient of Variance
f'c	Top	46.8	1.6	3.5
	Middle	50.7	3.3	6.6
	Bottom	63.5	1.3	2.1
	Cylinders	60.4	2.3	3.9
f'st	Top	3.4	0.2	6.9
	Middle	4.1	0.4	9.6
	Bottom	4.6	0.2	5.2
	Cylinders	4.9	0.8	15.9
f'p	Top	8.0	1.5	19.0
	Middle	7.3	0.5	6.2
	Bottom	8.6	0.1	1.3
	Cylinders	11.4	1.2	10.6

Table C.4: Core data for Blocks 7 and 8

Block 7 & 8 Specimens

NDT	EC	F'c	SC
Date	5/27/2003	Date	6/24/2003
f'st	SC	f'p	SC
Date	6/17/2003	Date	1/24/2004

Age at removal 91days

Concrete Exposed to: $Ca(OH)_2$

Core Name		Length uncut (mm)	Length cut (mm)	UPV Time dry(□s)	Pulse Velocity (m/s)	Resonant Frequency (Hz)	Ultimate Load (kN)	Ultimate Load (MPa)	Test Performed
7	1A	246.50	200.00	57.1	4317.0	2678	445.8	55.0	f'c
7	1B	247.50	204.00	57.0	4342.1	2735	500.6	61.7	f'c
7	1C	247.00	204.50	57.0	4333.3	2415	398.0	49.1	f'c
7	1D	247.50	-	57.5	4304.3	-	-	5.5	f'p
7	1E	247.50	200.00	57.8	4282.0	2490	488.0	60.2	f'c
7	1F	246.25	-	57.4	4290.1	-	-	-	spare
7	2A	248.50	205.00	58.4	4255.1	2865	426.9	52.7	f'c
7	2B	250.00	204.00	58.1	4302.9	2630	506.9	62.5	f'c
7	2C	251.00	204.00	57.8	4342.6	1830	409.6	50.5	f'c
7	2D	250.50	-	57.9	4326.4	-	-	-	spare
7	2E	249.75	197.00	57.7	4328.4	2530	487.0	60.1	f'c
7	2F	247.00	-	57.8	4273.4	-	-	-	spare
7	3A	248.75	207.00	56.2	4426.2	2890	514.2	63.4	f'c
7	3B	252.00	205.00	57.4	4390.2	2591	398.5	49.2	f'c
7	3C	253.00	207.00	57.6	4392.4	2597	500.6	61.7	f'c
7	3D	253.50	-	57.4	4416.4	-	-	-	spare
7	3E	254.00	200.00	57.0	4456.1	2492	526.7	65.0	f'c
7	3F	250.75	207.00	56.2	4461.7	2924	152.7	4.6	f'st

8	1A	244.00	206.75	56.2	4341.6	2801	147.2	4.5	f'st
8	1B	243.00	206.75	56.3	4316.2	2944	168.1	5.1	f'st
8	1C	243.50	206.50	55.5	4387.4	2948	155.2	4.7	f'st
8	1D	244.00	207.25	56.1	4349.4	2752	-	8.4	f'p
8	1E	244.00	205.25	56.6	4311.0	2665	-	8.1	f'p
8	1F	243.00	205.00	56.4	4308.5	2873	-	6.0	f'p
8	2A	244.00	207.25	56.5	4318.6	2582	107.9	3.3	f'st
8	2B	244.00	205.00	55.7	4380.6	2991	111.4	3.4	f'st
8	2C	243.00	205.00	57.1	4255.7	2740	107.8	3.3	f'st
8	2D	244.00	207.75	56.3	4333.9	2606	-	7.6	f'p
8	2E	244.00	196.50	56.1	4349.4	2692	-	6.9	f'p
8	2F	243.50	205.50	56.4	4317.4	2898	-	7.6	f'p
8	3A	241.50	208.00	53.9	4480.5	2765	132.2	4.0	f'st
8	3B	241.50	206.00	53.9	4480.5	2844	161.1	4.9	f'st
8	3C	242.00	205.00	53.7	4506.5	2677	172.4	5.3	f'st
8	3D	241.50	207.50	54.0	4472.2	2889	-	10.4	f'p
8	3E	242.50	204.00	53.9	4499.1	2980	-	8.7	f'p
8	3F	242.00	208.50	54.4	4448.5	2996	-	9.4	f'p

Table C.4: Core data for Blocks 7 and 8 continued

Cylinder Name			Length (mm)	UPV Time dry(□s)	Pulse Velocity (m/s)	Resonant Frequency (Hz)	Ultimate Load (kN)	Ultimate Load (MPa)	Test Performed
7 & 8	1C		206.00	45.8	4497.8	2770	146.2	4.4	f'st
7 & 8	2C		206.00	45.7	4507.7	2350	94.4	2.9	f'st
7 & 8	3C		205.25	45.6	4501.1	2684	163.3	5.0	f'st
7 & 8	4C		205.50	45.7	4496.7	2520	174.0	5.3	f'st
7 & 8	5C		205.75	45.8	4492.4	2785	-	7.9	f'p
7 & 8	6C		205.00	45.9	4466.2	2484	-	9.2	f'p
7 & 8	7C		202.00	45.4	4449.3	2490	463.7	57.2	f'c
7 & 8	8C		201.00	45.2	4446.9	2590	441.8	54.5	f'c
7 & 8	9C		197.00	44.8	4397.3	2646	463.5	57.2	f'c
7 & 8	10C		200.00	45.2	4424.8	2619	-	7.8	f'p

Test	Location	Mean	Standard Deviation	Coefficient of Variance
f'c	Top	59.0	3.5	6.0
	Middle	58.4	5.1	8.8
	Bottom	63.4	1.6	2.5
	Cylinders	56.3	1.6	2.8
f'st	Top	4.8	0.3	6.7
	Middle	3.3	0.1	2.2
	Bottom	4.9	0.3	6.6
	Cylinders	4.9	0.4	8.8
f'p	Top	7.5	1.3	17.7
	Middle	7.4	0.4	5.6
	Bottom	9.5	0.8	8.6
	Cylinders	8.3	0.8	9.9

Table C.5: Core data for Blocks 9 and 10

Block 9 & 10 Specimens

NDT	XZ	f'c	SC	Age at removal	28days
Date	6/30/2003	Date	7/7/2003		
f'st	SC	f'p	SC	Concrete Exposed to:	
Date	7/17/2003	Date	2/3/2004	SO_4^{2-}	

Core Name		Length cut (mm)	UPV Time dry(□s)	Pulse Velocity (m/s)	Resonant Frequency (Hz)	Ultimate Load (kN)	Ultimate Load (MPa)	Test Performed
9	1A	204.00	48.3	4223.6	2768	285.8	35.2	f'c
9	1B	203.00	48.4	4194.2	2498	308.3	38.0	f'c
9	1C	203.00	48.0	4229.2	2656	331.0	40.8	f'c
9	1D	204.00	47.9	4258.9	2510	118.9	3.7	f'st
9	1E	203.50	47.8	4257.3	2685	-	4.6	f'p
9	1F	201.50	47.8	4215.5	2106	-	-	spare
9	2A	205.50	47.4	4335.4	2140	-	-	f'c
9	2B	204.00	48.2	4232.4	2247	342.6	42.3	f'c
9	2C	204.50	48.7	4199.2	2410	335.6	41.4	f'c
9	2D	205.00	47.9	4279.7	2628	-	-	spare
9	2E	202.00	46.8	4316.2	2809	444.8	54.9	f'c
9	2F	202.50	47.1	4299.4	2905	446.8	55.1	f'c
9	3A	206.50	46.4	4450.4	2903	482.7	59.5	f'c
9	3B	204.00	47.1	4331.2	2365	404.0	49.8	f'c
9	3C	202.50	46.5	4354.8	2502	400.4	49.4	f'c
9	3D	204.00	46.4	4396.6	2456	145.7	4.5	f'st
9	3E	204.00	46.5	4387.1	2771	154.0	4.7	f'st
9	3F	204.00	47.2	4322.0	2607	402.6	49.7	f'c
10	1A	202.50	48.2	4201.2	2360	114.2	3.5	f'st
10	1B	205.00	48.5	4226.8	2256	120.5	3.7	f'st
10	1C	203.00	47.6	4264.7	2080	98.4	3.0	f'st
10	1D	204.50	48.2	4242.7	2392	-	6.8	f'p
10	1E	205.50	48.1	4272.3	2701	-	5.4	f'p
10	1F	206.00	48.5	4247.4	2731	-	6.0	f'p
10	2A	205.50	48.2	4263.5	2335	129.5	3.9	f'st
10	2B	203.00	47.7	4255.8	2588	120.1	3.7	f'st
10	2C	205.00	47.6	4306.7	2607	128.9	3.9	f'st
10	2D	204.00	47.1	4331.2	2606	-	7.8	f'p
10	2E	201.00	46.7	4304.1	-	-	9.1	f'p
10	2F	205.00	48.0	4270.8	2485	-	6.7	f'p
10	3A	205.00	46.4	4418.1	2306	109.1	3.3	f'st
10	3B	202.00	48.3	4182.2	2060	155.8	4.8	f'st
10	3C	203.00	46.7	4346.9	2305	121.9	3.8	f'st
10	3D	202.00	45.8	4410.5	2258	-	8.2	f'p
10	3E	204.00	47.0	4340.4	2668	-	7.7	f'p
10	3F	204.50	47.0	4351.1	2560	-	7.7	f'p

Table C.5: Core data for Blocks 9 and 10

Cylinder Name		Length (mm)	UPV Time dry(□s)	Pulse Velocity (m/s)	Resonant Frequency (Hz)	Ultimate Load (kN)	Ultimate Load (MPa)	Test Performed
9 & 10	1	202.00	46.4	4353.4	2557	395.8	48.8	f'c
9 & 10	2	203.00	46.8	4337.6	2521	377.6	46.6	f'c
9 & 10	3	201.00	46.2	4350.6	2380	425.5	52.5	f'c
9 & 10	4	205.00	46.7	4389.7	2139	142.7	4.4	f'st
9 & 10	5	204.00	46.8	4359.0	2601	123.9	3.8	f'st
9 & 10	6	205.00	47.1	4352.4	2199	142.0	4.3	f'st
9 & 10	7	205.00	47.5	4315.8	2110	-	6.8	f'p
9 & 10	8	205.00	47.6	4306.7	1969	-	6.0	f'p
9 & 10	9	204.00	46.8	4359.0	2230	-	8.2	f'p
9 & 10	10	205.00	46.7	4389.7	2696	-	5.4	f'p

Test	Location	Mean	Standard Deviation	Coefficient of Variance
f'c	Top	38.0	2.8	7.3
	Middle	41.8	0.6	1.4
	Bottom	49.6	0.2	0.5
	Cylinder	49.3	3.0	6.0
f'st	Top	3.6	0.1	2.2
	Middle	3.9	0.1	3.5
	Bottom	4.7	0.2	4.0
	Cylinder	4.2	0.3	7.5
f'p	Top	6.1	0.7	11.4
	Middle	7.9	1.2	15.3
	Bottom	7.9	0.3	3.8
	Cylinder	6.1	0.7	11.2

Table C.6: Core data for Blocks 11 and 12

Block 11 & 12 Specimens

NDT	XZ	f'c	SC		Age at removal 28days
Date	6/30/2003	Date	7/7/2003		
f'st	SC	f'p	SC		Concrete Exposed to:
Date	7/17/2003	Date	2/2/2004		$Ca(OH)_2$

Core Name		Length cut (mm)	UPV Time dry(□s)	Pulse Velocity (m/s)	Resonant Frequency (Hz)	Ultimate Load (kN)	Ultimate Load (MPa)	Test Performed
11	1A	202.00	47.9	4217.1	2096	369.2	45.5	f'c
11	1B	202.50	47.9	4227.6	2646	340.8	42.0	f'c
11	1C	204.00	48.3	4223.6	2619	329.3	40.6	f'c
11	1D	203.00	47.4	4282.7	2640	106.9	3.3	f'st
11	1E	202.50	47.5	4263.2	2641	-	-	spare
11	1F	203.00	47.7	4255.8	2525	-	3.9	f'p
11	2A	203.00	47.1	4310.0	2630	406.4	50.1	f'c
11	2B	202.00	46.9	4307.0	2597	392.4	48.4	f'c
11	2C	203.00	47.3	4291.8	2706	394.8	48.7	f'c
11	2D	201.00	47.0	4276.6	2684	-	-	spare
11	2E	203.00	47.4	4282.7	2525	-	5.7	f'p
11	2F	204.00	47.7	4276.7	2475	-	-	spare
11	3A	203.00	46.8	4337.6	2590	412.9	50.9	f'c
11	3B	203.00	46.6	4356.2	2475	442.0	54.5	f'c
11	3C	203.00	46.3	4384.4	2532	430.1	53.1	f'c
11	3D	206.00	47.5	4336.8	2334	-	-	spare
11	3E	204.00	47.5	4294.7	2569	-	5.8	f'p
11	3F	204.00	46.1	4425.2	2401	-	-	spare
12	1A	204.00	48.0	4250.0	2535	105.5	3.2	f'st
12	1B	204.00	48.2	4232.4	2372	99.5	3.1	f'st
12	1C	203.00	48.2	4211.6	2274	129.2	4.0	f'st
12	1D	203.00	48.1	4220.4	2298	-	7.0	f'p
12	1E	203.00	48.3	4202.9	2509	-	6.5	f'p
12	1F	204.00	48.5	4206.2	2519	-	4.3	f'p
12	2A	203.00	47.7	4255.8	2341	107.8	3.3	f'st
12	2B	201.00	46.5	4322.6	2548	106.0	3.3	f'st
12	2C	205.00	47.0	4361.7	2511	105.2	3.2	f'st
12	2D	205.50	47.9	4290.2	2274	-	4.9	f'p
12	2E	204.00	47.4	4303.8	2342	-	6.7	f'p
12	2F	203.00	47.8	4246.9	2285	-	6.5	f'p
12	3A	203.00	46.5	4365.6	2182	136.5	4.2	f'st
12	3B	203.00	46.4	4375.0	2151	126.0	3.9	f'st
12	3C	203.00	46.8	4337.6	2569	137.1	4.2	f'st
12	3D	203.00	45.4	4471.4	2379	-	6.5	f'p
12	3E	202.00	46.6	4334.8	2493	-	8.7	f'p
12	3F	203.00	46.7	4346.9	2531	-	5.7	f'p

Table C.6: Core data for Blocks 11 and 12 continued

Cylinder Name		Length (mm)	UPV Time dry(μs)	Pulse Velocity (m/s)	Resonant Frequency (Hz)	Ultimate Load (kN)	Ultimate Load (MPa)	Test Performed
11 & 12	1	204.00	46.7	4368.3	2566	411.5	50.8	f'c
11 & 12	2	203.50	46.8	4348.3	2261	428.8	52.9	f'c
11 & 12	3	205.00	47.1	4352.4	2389	352.4	43.5	f'c
11 & 12	4	205.00	46.4	4418.1	2450	124.2	3.8	f'st
11 & 12	5	205.00	47.4	4324.9	2729	147.8	4.5	f'st
11 & 12	6	205.00	47.0	4361.7	2442	104.5	3.2	f'st
11 & 12	7	205.00	47.6	4306.7	2269	-	6.6	f'p
11 & 12	8	204.50	47.0	4351.1	2264	-	6.7	f'p
11 & 12	9	205.00	46.4	4418.1	2655	113.8	3.5	f'st
11 & 12	10	205.00	47.3	4334.0	2704	448.9	55.4	f'c

Test	Location	Mean	Standard Deviation	Coefficient of Variance
f'c	Top	42.7	2.5	5.9
	Middle	49.1	0.9	1.9
	Bottom	52.8	1.8	3.4
	Cylinders	53.0	2.3	4.4
f'st	Top	3.2	0.1	4.0
	Middle	3.3	0.1	1.8
	Bottom	4.1	0.2	4.7
	Cylinders	3.5	0.3	8.6
f'p	Top	5.9	1.4	24.4
	Middle	6.3	0.5	8.7
	Bottom	6.0	0.4	7.2
	Cylinders	6.7	0.1	1.8

Table C.7: Core data for Blocks 17 and 18

Block 17 & 18 Specimens

NDT	SC, BQ	f'c	SC	Age at removal 365days
Date	1/27/2004	Date	2/9/2004	
f'st	SC	f'p	SC	Concrete Exposed to:
Date	2/2/2004	Date	2/27/2004	$Ca(OH)_2$

Core Name		Length cut (mm)	UPV Time dry(□s)	Pulse Velocity (m/s)	Resonant Frequency (Hz)	Ultimate Load (kN)	Ultimate Load (MPa)	Test Performed
17	1A	184.50	47.4	3892.4	2019	226.0	27.9	f'c
17	1B	185.50	47.5	3905.3	1805	237.1	29.2	f'c
17	1C	182.00	47.3	3847.8	1846	235.3	29.0	f'c
17	1D	190.50	48.0	3968.8	2691	85.7	2.8	f'st
17	1E	-	-	-	-	-	-	spare
17	1F	-	-	-	-	-	-	spare
17	2A	186.50	44.7	4172.3	2296	327.8	40.4	f'c
17	2B	187.50	45.2	4148.2	2277	294.6	36.3	f'c
17	2C	186.00	45.2	4115.0	2378	300.8	37.1	f'c
17	2D	-	-	-	-	-	-	spare
17	2E	-	-	-	-	-	-	spare
17	2F	-	-	-	-	-	-	spare
17	3A	186.00	44.1	4217.7	2428	343.9	42.4	f'c
17	3B	184.50	44.1	4183.7	2385	322.1	39.7	f'c
17	3C	185.00	44.1	4195.0	1846	322.1	39.7	f'c
17	3D	-	-	-	-	-	-	spare
17	3E	-	-	-	-	-	-	spare
17	3F	-	-	-	-	-	-	spare
18	1A	197.00	50.9	3870.3	2673	91.0	2.9	f'st
18	1B	198.00	51.2	3867.2	2291	96.6	3.1	f'st
18	1C	199.00	50.7	3925.0	2255	73.7	2.3	f'st
18	1D	199.50	52.0	3836.5	2160	-	3.3	f'p
18	1E	198.50	51.6	3846.9	2079	-	4.0	f'p
18	1F	198.00	51.2	3867.2	2566	-	3.8	f'p
18	2A	198.50	48.3	4109.7	2350	111.8	3.5	f'st
18	2B	201.50	49.8	4046.2	2319	107.4	3.3	f'st
18	2C	202.00	49.9	4048.1	2249	99.7	3.1	f'st
18	2D	202.00	49.0	4122.4	2143	-	4.6	f'p
18	2E	201.00	48.5	4144.3	2614	-	5.4	f'p
18	2F	199.50	48.7	4096.5	2554	-	5.2	f'p
18	3A	201.75	48.3	4177.0	2366	124.2	3.9	f'st
18	3B	199.00	48.3	4120.1	2450	117.5	3.7	f'st
18	3C	205.00	48.6	4218.1	2286	112.9	3.5	f'st
18	3D	204.50	48.1	4251.6	2440	-	6.8	f'p
18	3E	205.00	48.2	4253.1	2298	-	7.1	f'p
18	3F	200.00	47.1	4246.3	2303	-	7.2	f'p

Table C.7: Core data for Blocks 17 and 18 continued

Cylinder Name		Length (mm)	UPV Time dry(μs)	Pulse Velocity (m/s)	Resonant Frequency (Hz)	Ultimate Load (kN)	Ultimate Load (MPa)	Test Performed
17 & 18	1	197.00	47.7	4130.0	2659	291.2	35.9	f'c
17 & 18	2	195.50	46.8	4177.4	2548	303.5	37.4	f'c
17 & 18	3	194.50	46.7	4164.9	2145	305.3	37.7	f'c
17 & 18	4	196.00	47.2	4152.5	2631	-	6.8	f'p
17 & 18	5	196.00	47.1	4161.4	2271	-	6.8	f'p
17 & 18	6	196.50	47.2	4163.1	2268	-	6.5	f'p
17 & 18	7	196.00	46.6	4206.0	2180	127.9	4.1	f'st
17 & 18	8	195.50	46.7	4186.3	1979	107.3	3.4	f'st
17 & 18	9	196.00	47.3	4143.8	2054	109.1	3.5	f'st
17 & 18	10	195.50	46.9	4168.4	2085	106.3	3.4	f'st

Test	Location	Mean	Standard Deviation	Coefficient of Variance
f'c	Top	28.7	0.7	2.6
	Middle	38.0	2.2	5.7
	Bottom	40.6	1.5	3.8
	Cylinders	37.0	0.9	2.6
f'st	Top	2.9	0.1	4.2
	Middle	3.3	0.2	6.6
	Bottom	3.7	0.2	5.6
	Cylinders	3.4	0.0	1.2
f'p	Top	3.7	0.3	9.0
	Middle	5.1	0.4	7.8
	Bottom	7.0	0.2	3.1
	Cylinders	6.7	0.2	2.9

Table C.8: Core data for Blocks 19 and 20

Block 19 & 20 Specimens

NDT	SC, BQ	f'c	SC		Age at removal 365days
Date	1/27/2004	Date	2/9/2004		
f'st	SC, XZ	f'p	SC		Concrete Exposed to:
Date	2/2/2004	Date	2/25/2004		SO_4^{2-}

Core Name		Length cut (mm)	UPV Time dry(μs)	Pulse Velocity (m/s)	Resonant Frequency (Hz)	Ultimate Load (kN)	Ultimate Load (MPa)	Test Performed
19	1A	191.00	50.7	3767.3	2181	213.7	26.4	f'c
19	1B	192.00	49.9	3847.7	2235	231.6	28.6	f'c
19	1C	194.00	51.0	3803.9	1940	220.8	27.2	f'c
19	1D	203.00	52.8	3844.7	2588	81.0	2.5	f'st
19	1E	-	-	-	-	-	-	spare
19	1F	-	-	-	-	-	-	spare
19	2A	194.00	48.4	4008.3	2036	265.7	32.8	f'c
19	2B	196.00	48.4	4049.6	2117	291.4	35.9	f'c
19	2C	197.50	48.5	4072.2	2362	283.6	35.0	f'c
19	2D	-	-	-	-	-	-	spare
19	2E	-	-	-	-	-	-	spare
19	2F	-	-	-	-	-	-	spare
19	3A	195.00	47.1	4140.1	2452	304.1	37.5	f'c
19	3B	201.00	48.8	4118.9	2359	287.3	35.4	f'c
19	3C	203.00	48.8	4159.8	2274	294.6	36.3	f'c
19	3D	-	-	-	-	-	-	spare
19	3E	-	-	-	-	-	-	spare
19	3F	-	-	-	-	-	-	spare
20	1A	202.00	52.9	3818.5	2273	92.9	2.9	f'st
20	1B	198.50	51.1	3884.5	2047	83.2	2.6	f'st
20	1C	199.50	51.5	3873.8	2348	73.5	2.3	f'st
20	1D	202.50	52.8	3835.2	2200	-	4.1	f'p
20	1E	201.00	52.3	3843.2	2155	-	3.6	f'p
20	1F	203.50	52.4	3883.6	2195	-	3.0	f'p
20	2A	202.00	49.8	4056.2	2051	107.8	3.3	f'st
20	2B	202.00	50.0	4040.0	2265	90.5	2.8	f'st
20	2C	203.00	50.2	4043.8	2726	102.5	3.2	f'st
20	2D	201.50	49.7	4054.3	2295	-	5.0	f'p
20	2E	201.00	49.8	4036.1	2292	-	5.1	f'p
20	2F	202.00	49.1	4114.1	2396	-	3.9	f'p
20	3A	202.00	48.4	4173.6	2310	108.3	3.4	f'st
20	3B	202.00	48.5	4164.9	2062	116.8	3.6	f'st
20	3C	203.00	49.1	4134.4	2112	98.6	3.0	f'st
20	3D	207.00	49.6	4173.4	2519	-	6.1	f'p
20	3E	192.50	46.5	4139.8	2322	-	5.8	f'p
20	3F	196.50	46.7	4207.7	2221	-	5.7	f'p

Table C.8: Core data for Blocks 19 and 20 continued

Cylinder Name		Length (mm)	UPV Time dry(□s)	Pulse Velocity (m/s)	Resonant Frequency (Hz)	Ultimate Load (kN)	Ultimate Load (MPa)	Test Performed
19 & 20	1	194.50	46.7	4164.9	2070	287.2	35.4	f'c
19 & 20	2	196.00	46.4	4224.1	2077	298.2	36.8	f'c
19 & 20	3	194.50	46.3	4200.9	2134	270.0	33.3	f'c
19 & 20	4	195.00	46.5	4193.5	2047	-	7.2	f'p
19 & 20	5	195.00	46.9	4157.8	2305	-	8.8	f'p
19 & 20	6	196.00	46.9	4179.1	2520	-	8.5	f'p
19 & 20	7	194.50	45.7	4256.0	2270	110.9	3.6	f'st
19 & 20	8	196.00	46.5	4215.1	2009	100.1	3.2	f'st
19 & 20	9	195.00	47.3	4122.6	2260	101.4	3.3	f'st
19 & 20	10	194.50	46.3	4200.9	2566	-	7.7	f'p

Test	Location	Mean	Standard Deviation	Coefficient of Variance
f'c	Top	27.4	1.1	4.1
	Middle	34.6	1.6	4.7
	Bottom	36.4	1.0	2.8
	Cylinders	35.2	1.8	5.0
f'st	Top	2.5	0.2	6.5
	Middle	3.1	0.3	8.8
	Bottom	3.3	0.3	8.7
	Cylinders	3.3	0.2	6.0
f'p	Top	3.6	0.6	15.5
	Middle	4.7	0.7	15.1
	Bottom	5.9	0.2	3.3
	Cylinders	8.3	0.6	6.9

Table C.9: Core data for Blocks 21 and 22

Block 21 & 22 Specimens

NDT	EC	f'c	SC	Age at removal	91days
Date	6/11/2003	Date	6/23/2003		
f'st	SC	f'p	SC	Concrete Exposed to:	
Date	6/16/2003	Date	1/20/2004	$Ca(OH)_2$	

Core Name		Length cut (mm)	UPV Time dry(□s)	Pulse Velocity (m/s)	Resonant Frequency (Hz)	Ultimate Load (kN)	Ultimate Load (MPa)	Test Performed
21	1A	208.50	52.5	3971.4	2214	244.7	30.2	f'c
21	1B	204.25	50.9	4012.8	2879	233.2	28.8	f'c
21	1C	208.75	52.8	3953.6	2401	230.2	28.4	f'c
21	1D	-	-	-	-	-	-	spare
21	1E	207.00	53.0	3905.7	2578	-	3.4	f'p
21	1F	-	-	-	-	-	-	spare
21	2A	206.00	49.5	4161.6	2940.0	292.7	36.1	f'c
21	2B	206.50	50.1	4121.8	2478.0	287.8	35.5	f'c
21	2C	207.00	50.2	4123.5	2702.0	275.9	34.0	f'c
21	2D	-	-	-	-	-	-	spare
21	2E	-	-	-	-	-	-	spare
21	2F	-	-	-	-	-	-	spare
21	3A	209.00	49.3	4239.4	2504	301.8	37.2	f'c
21	3B	205.25	48.6	4223.3	2670	285.1	35.2	f'c
21	3C	204.75	49.0	4178.6	2680	296.8	36.6	f'c
21	3D	-	-	-	-	-	-	spare
21	3E	-	-	-	-	-	-	spare
21	3F	-	-	-	-	-	-	spare
22	1A	206.00	51.3	4015.6	2690	105.0	3.2	f'st
22	1B	204.25	51.0	4004.9	2864	89.9	2.8	f'st
22	1C	206.50	52.6	3925.9	2486	99.5	3.0	f'st
22	1D	205.25	51.8	3962.4	2819	-	4.6	f'p
22	1E	206.00	52.1	3953.9	2990	-	5.8	f'p
22	1F	207.00	51.9	3988.4	2619	-	4.5	f'p
22	2A	203.25	49.4	4114.4	2636	117.3	3.6	f'st
22	2B	202.50	50.4	4017.9	2477	104.4	3.2	f'st
22	2C	207.00	49.8	4156.6	2318	116.4	3.5	f'st
22	2D	203.00	48.5	4185.6	2504	-	6.5	f'p
22	2E	204.50	49.4	4139.7	2581	-	6.2	f'p
22	2F	205.50	49.5	4151.5	2303	-	6.1	f'p
22	3A	204.50	49.0	4173.5	2977	90.8	2.8	f'st
22	3B	205.50	49.1	4185.3	3006	102.7	3.1	f'st
22	3C	205.00	49.7	4124.7	2563	104.2	3.2	f'st
22	3D	206.50	49.5	4171.7	2560	-	6.6	f'p
22	3E	206.00	48.1	4282.7	2957	-	7.4	f'p
22	3F	205.00	48.0	4270.8	2710	-	7.0	f'p

Table C.9: Core data for Blocks 21 and 22 continued

Cylinder Name		Length (mm)	UPV Time dry(□s)	Pulse Velocity (m/s)	Resonant Frequency (Hz)	Ultimate Load (kN)	Ultimate Load (MPa)	Test Performed
21 & 22	1	203.75	49.6	4107.9	2750	91.0	2.8	f'st
21 & 22	2	204.00	49.3	4137.9	2604	104.2	3.2	f'st
21 & 22	3	204.75	49.0	4178.6	2450	112.8	3.5	f'st
21 & 22	4	204.50	49.6	4123.0	2930	-	8.9	f'p
21 & 22	5	203.50	50.1	4061.9	2480	-	8.1	f'p
21 & 22	6	204.50	49.5	4131.3	2504			spare
21 & 22	7	199.00	48.0	4145.8	2702	274.5	33.9	f'c
21 & 22	8	198.00	47.8	4142.3	2600	278.3	34.3	f'c
21 & 22	9	198.00	48.2	4107.9	2645	274.6	33.9	f'c
21 & 22	10	199.00	48.6	4094.7	2536	-	8.9	f'p

Test	Location	Mean	Standard Deviation	Coefficient of Variance
f'c	Top	29.1	0.9	3.2
	Middle	35.2	1.1	3.0
	Bottom	36.3	1.1	2.9
	Cylinders	34.0	0.3	0.8
f'st	Top	3.0	0.2	7.4
	Middle	3.5	0.2	5.8
	Bottom	3.0	0.2	7.2
	Cylinders	3.2	0.3	10.5
f'p	Top	5.0	0.7	14.5
	Middle	6.3	0.2	3.4
	Bottom	7.0	0.4	5.9
	Cylinders	8.6	0.4	5.0

Table C.10: Core data for Blocks 23 and 24

Block 23 & 24 Specimens

NDT	EC	f'c	SC		Age at removal
Date	6/11/2003	Date	6/23/2003		91days
f'st	SC	f'p	SC		Concrete Exposed to:
Date	6/18/2003	Date	1/20/2004		SO_4^{2-}

Core Name		Length uncut (mm)	Length cut (mm)	UPV Time dry(□s)	Pulse Velocity (m/s)	Resonant Frequency (Hz)	Ultimate Load (kN)	Ultimate Load (MPa)	Test Performed
23	1A	-	206.50	52.5	3933.3	2473	239.8	29.6	f'c
23	1B	-	207.50	52.3	3967.5	2491	230.4	28.4	f'c
23	1C	-	207.50	51.6	4021.3	2405	239.1	29.5	f'c
23	1D	-	206.00	52.7	3908.9	2518	89.1	2.7	f'st
23	1E	-	-	-	-	-	-	-	spare
23	1F	-	207.00	51.8	3996.1	2049	-	2.3	f'p
23	2A	-	206.00	49.3	4178.5	2800	258.6	31.9	f'c
23	2B	-	208.00	49.9	4168.3	2670	281.9	34.8	f'c
23	2C	-	204.50	49.4	4139.7	2555	290.1	35.8	f'c
23	2D	-	207.00	50.1	4131.7	2613	-	3.8	f'p
23	2E	-	-	-	-	-	-	-	spare
23	2F	-	-	-	-	-	-	-	spare
23	3A	-	206.00	48.1	4282.7	2514	337.3	41.6	f'c
23	3B	-	205.00	47.7	4297.7	2620	345.3	42.6	f'c
23	3C	-	209.00	49.9	4188.4	2580	304.0	37.5	f'c
23	3D	-	206.00	50.1	4111.8	2384	-	3.6	f'p
23	3E	-	-	-	-	-	-	-	spare
23	3F	-	-	-	-	-	-	-	spare
24	1A	245.00	207.50	63.9	3834.1	2341	87.5	2.6	f'st
24	1B	244.00	203.00	62.7	3891.5	2359	93.5	2.9	f'st
24	1C	243.50	204.00	62.9	3871.2	2636	74.1	2.3	f'st
24	1D	243.50	205.00	62.7	3883.6	2228	-	3.8	f'p
24	1E	245.00	207.00	63.5	3858.3	2576	-	4.2	f'p
24	1F	245.25	207.00	63.8	3844.0	2260	-	3.4	f'p
24	2A	244.00	204.00	60.3	4046.4	2850	103.2	3.2	f'st
24	2B	244.00	205.50	60.7	4019.8	2622	96.1	2.9	f'st
24	2C	243.25	204.50	59.8	4067.7	2466	87.5	2.7	f'st
24	2D	243.50	207.00	60.7	4011.5	2437	-	4.9	f'p
24	2E	244.00	207.50	61.2	3986.9	2463	-	4.1	f'p
24	2F	244.25	205.00	61.2	3991.0	2622	-	4.2	f'p
24	3A	243.50	205.00	57.6	4227.4	2414	128.6	3.9	f'st
24	3B	243.00	209.00	57.4	4233.4	2915	128.3	3.8	f'st
24	3C	243.25	206.50	58.4	4165.2	2778	114.4	3.5	f'st
24	3D	243.00	205.00	59.2	4104.7	2777	-	6.5	f'p
24	3E	243.00	207.00	59.1	4111.7	2686	-	5.6	f'p
24	3F	244.00	205.00	58.6	4163.8	2595	-	5.4	f'p

Table C.10: Core data for Blocks 23 and 24 continued

Cylinder Name			Length (mm)	UPV Time dry(□s)	Pulse Velocity (m/s)	Resonant Frequency (Hz)	Ultimate Load (kN)	Ultimate Load (MPa)	Test Performed
23 & 24	1		205.50	49.7	4134.8	2560	85.5	2.6	f'st
23 & 24	2		204.50	49.0	4173.5	2290	103.5	3.2	f'st
23 & 24	3		204.75	49.3	4153.1	2580	87.3	2.7	f'st
23 & 24	4		204.25	49.0	4168.4	2460	-	6.5	f'p
23 & 24	5		205.00	50.3	4075.5	2600	-	6.2	f'p
23 & 24	6		205.00	49.6	4133.1	2436	-	6.8	f'p
23 & 24	7		199.00	48.6	4094.7	2761	273.9	33.8	f'c
23 & 24	8		198.50	48.3	4109.7	2500	249.7	30.8	f'c
23 & 24	9		199.00	48.3	4120.1	2580	285.0	35.2	f'c
23 & 24	10		198.00	48.3	4099.4	2415	79.2	2.5	f'st

Test	Location	Mean	Standard Deviation	Coefficient of Variance
f'c	Top	29.2	0.6	2.2
	Middle	34.2	2.0	5.9
	Bottom	40.6	2.7	6.7
	Cylinders	33.2	2.2	6.7
f'st	Top	2.7	0.1	4.6
	Middle	2.9	0.2	8.3
	Bottom	3.7	0.2	6.5
	Cylinders	2.6	0.1	3.2
f'p	Top	3.8	0.4	9.9
	Middle	4.0	0.2	4.7
	Bottom	5.8	0.6	9.8
	Cylinders	6.5	0.3	5.2

Table C.11: Core data for Blocks 25 and 26

Block 25 & 26 Specimens

NDT	XZ, EC	f'c	SC	Age at removal 28days
Date	7/18/2003	Date	7/27/2003	
f'st	SC	f'p	SC	Concrete Exposed to:
Date	7/28/2003	Date	1/14/2004	SO_4^{2-}

Core Name		Length cut (mm)	UPV Time dry(□s)	Pulse Velocity (m/s)	Resonant Frequency (Hz)	Ultimate Load (kN)	Ultimate Load (MPa)	Test Performed
25	1A	196.00	50.7	3865.9	2292	158.1	19.5	f'c
25	1B	198.00	50.7	3905.3	2357	206.5	25.5	f'c
25	1C	197.00	51.0	3862.7	2737	186.9	23.1	f'c
25	1D	204.00	53.2	3834.6	2490	-	-	spare
25	1E	200.00	53.0	3773.6	2528	-	-	spare
25	1F	202.00	52.4	3855.0	2293	200.4	24.7	f'c
25	2A	198.00	50.2	3944.2	2422	223.6	27.6	f'c
25	2B	191.00	47.5	4021.1	2477	248.8	30.7	f'c
25	2C	193.00	48.4	3987.6	2070	247.5	30.5	f'c
25	2D	202.00	51.4	3930.0	2863	92.8	2.9	f'st
25	2E	204.00	51.4	3968.9	2447	-	-	spare
25	2F	203.00	51.7	3926.5	2354	-	-	spare
25	3A	195.00	45.9	4248.4	2776	279.1	34.4	f'c
25	3B	197.00	46.3	4254.9	2175	310.9	38.3	f'c
25	3C	196.00	47.7	4109.0	2764	266.8	32.9	f'c
25	3D	205.00	48.5	4226.8	2279	91.7	2.8	f'st
25	3E	204.00	48.6	4197.5	2588	-	-	spare
25	3F	202.00	47.7	4234.8	2988	-	-	spare
26	1A	204.00	52.2	3908.0	2789	73.4	2.3	f'st
26	1B	203.00	53.0	3830.2	2836	67.0	2.1	f'st
26	1C	200.00	51.4	3891.1	2230	64.2	2.0	f'st
26	1D	203.00	51.9	3911.4	2730	-	3.8	f'p
26	1E	199.00	52.9	3761.8	2557	-	3.7	f'p
26	1F	204.00	51.6	3953.5	2722	-	3.8	f'p
26	2A	203.00	50.0	4060.0	2472	93.5	2.9	f'st
26	2B	203.00	51.4	3949.4	2707	87.6	2.7	f'st
26	2C	203.00	50.1	4051.9	2484	72.9	2.2	f'st
26	2D	204.00	50.1	4071.9	2646	-	5.6	f'p
26	2E	205.00	50.3	4075.5	2506	-	5.0	f'p
26	2F	203.00	50.1	4051.9	2679	-	5.8	f'p
26	3A	202.00	48.1	4199.6	2468	97.9	3.0	f'st
26	3B	203.00	48.2	4211.6	2317	82.2	2.5	f'st
26	3C	203.00	48.3	4202.9	2374	75.1	2.3	f'st
26	3D	203.00	47.8	4246.9	2521	-	6.4	f'p
26	3E	205.00	49.0	4183.7	2615	-	7.0	f'p
26	3F	203.00	48.8	4159.8	2516	-	6.8	f'p

Table C.11: Core data for Blocks 25 and 26 continued

Cylinder Name		Length (mm)	UPV Time dry(□s)	Pulse Velocity (m/s)	Resonant Frequency (Hz)	Ultimate Load (kN)	Ultimate Load (MPa)	Test Performed
25 & 26	1	203.00	49.4	4109.3	2451	208.3	25.7	f'c
25 & 26	2	204.50	49.4	4139.7	2459	230.8	28.5	f'c
25 & 26	3	203.00	49.5	4101.0	2570	245.5	30.3	f'c
25 & 26	4	204.00	49.6	4112.9	2255	111.4	3.4	f'st
25 & 26	5	203.00	49.4	4109.3	2286	81.5	2.5	f'st
25 & 26	6	203.50	49.3	4127.8	2216	93.6	2.9	f'st
25 & 26	7	196.00	47.6	4117.6	2236	-	-	spare
25 & 26	8	196.00	47.8	4100.4	2169	-	6.4	f'p
25 & 26	9	198.00	47.7	4150.9	2360	105.8	2.2	f'st
25 & 26	10	200.00	48.7	4106.8	2236	97.5	3.1	f'st

Test	Location	Mean	Standard Deviation	Coefficient of Variance
f'c	Top	24.4	1.2	5.1
	Middle	29.6	1.8	5.9
	Bottom	35.2	2.8	8.0
	Cylinders	28.1	2.3	8.2
f'st	Top	2.1	0.1	6.0
	Middle	2.8	0.1	3.7
	Bottom	2.8	0.2	9.0
	Cylinders	3.1	0.3	8.8
f'p	Top	3.8	0.1	1.9
	Middle	5.5	0.4	7.6
	Bottom	6.7	0.3	4.3
	Cylinders	6.4	0.0	0.0

Table C.12: Core data for Blocks 27 and 28

Block 27 & 28 Specimens

NDT	XZ, EC	f'c	SC		Age at removal 28days
Date	7/18/2003	Date	7/27/2003		
f'st	SC	f'p	SC		Concrete Exposed to:
Date	7/28/2003	Date	1/15/2004		$Ca(OH)_2$

Core Name		Length cut (mm)	UPV Time dry(□s)	Pulse Velocity (m/s)	Resonant Frequency (Hz)	Ultimate Load (kN)	Ultimate Load (MPa)	Test Performed
27	1A	203.00	52.7	3852.0	2604	176.2	21.7	f'c
27	1B	197.00	52.1	3781.2	2513	206.8	25.5	f'c
27	1C	193.00	51.3	3762.2	2292	187.7	23.2	f'c
27	1D	207.00	54.6	3791.2	2952	-	2.7	f'p
27	1E	202.00	53.6	3768.7	2976	56.6	1.8	f'st
27	1F	206.00	53.7	3836.1	2880	-	-	spare
27	2A	199.00	49.9	3988.0	2805	208.6	25.7	f'c
27	2B	196.00	49.6	3951.6	2855	251.5	31.0	f'c
27	2C	197.00	49.8	3955.8	2568	233.4	28.8	f'c
27	2D	204.00	51.5	3961.2	2489	-	-	spare
27	2E	203.00	51.4	3949.4	2926	76.4	2.4	f'st
27	2F	207.00	51.6	4011.6	2983	-	2.7	f'p
27	3A	191.00	45.2	4225.7	2406	313.8	38.7	f'c
27	3B	201.00	47.2	4258.5	2145	272.6	33.6	f'c
27	3C	200.00	47.1	4246.3	2551	298.6	36.8	f'c
27	3D	203.00	49.1	4134.4	2939	-	-	spare
27	3E	206.00	48.4	4256.2	2545	-	4.5	f'p
27	3F	201.00	46.5	4322.6	2414	87.5	2.7	f'st
28	1A	205.00	53.2	3853.4	2489	56.9	1.7	f'st
28	1B	205.00	52.5	3904.8	2836	75.0	2.3	f'st
28	1C	205.00	53.2	3853.4	2697	50.8	1.6	f'st
28	1D	204.00	52.4	3893.1	2550	-	2.2	f'p
28	1E	205.00	52.9	3875.2	2672	-	4.3	f'p
28	1F	204.00	52.8	3863.6	2430	-	3.8	f'p
28	2A	208.00	51.4	4046.7	2392	79.4	2.4	f'st
28	2B	207.00	51.9	3988.4	2615	67.7	2.0	f'st
28	2C	204.00	50.7	4023.7	2755	82.4	2.5	f'st
28	2D	204.00	51.1	3992.2	2805	-	4.8	f'p
28	2E	205.00	51.4	3988.3	2536	-	5.0	f'p
28	2F	208.00	50.1	4151.7	2912	-	3.5	f'p
28	3A	208.00	49.2	4227.6	2597	128.3	3.9	f'st
28	3B	205.00	49.7	4124.7	2766	88.4	2.7	f'st
28	3C	203.00	49.1	4134.4	2950	76.8	2.4	f'st
28	3D	207.00	49.8	4156.6	2738	-	5.2	f'p
28	3E	205.00	47.8	4288.7	2772	-	6.4	f'p
28	3F	202.00	48.3	4182.2	2779	-	5.6	f'p

Table C.12: Core data for Blocks 27 and 28 continued

Cylinder Name		Length (mm)	UPV Time dry(□s)	Pulse Velocity (m/s)	Resonant Frequency (Hz)	Ultimate Load (kN)	Ultimate Load (MPa)	Test Performed
27 & 28	1	202.00	49.1	4114.1	2364	251.3	31.0	f'c
27 & 28	2	201.50	48.3	4171.8	2238	255.6	31.5	f'c
27 & 28	3	204.00	49.4	4129.6	2310	242.0	29.8	f'c
27 & 28	4	205.00	49.5	4141.4	2165	83.2	2.5	f'st
27 & 28	5	204.00	49.0	4163.3	2347	97.4	3.0	f'st
27 & 28	6	204.00	49.5	4121.2	2020	70.2	2.2	f'st
27 & 28	7	205.00	49.6	4133.1	2830	105.9	3.2	f'st
27 & 28	8	205.00	48.7	4209.4	2620	-	5.5	f'p
27 & 28	9	204.00	49.5	4121.2	2274	-	4.7	f'p
27 & 28	10	205.50	49.6	4143.1	2430	90.9	2.8	f'st

Test	Location	Mean	Standard Deviation	Coefficient of Variance
f'c	Top	23.5	1.9	8.1
	Middle	28.5	2.7	9.3
	Bottom	36.4	2.6	7.1
	Cylinders	30.8	0.9	2.8
f'st	Top	1.7	0.1	6.7
	Middle	2.4	0.1	3.8
	Bottom	2.6	0.2	7.7
	Cylinders	3.0	0.2	7.7
f'p	Top	3.6	0.8	22.0
	Middle	4.4	0.8	17.9
	Bottom	5.7	0.6	10.3
	Cylinders	5.1	0.6	11.1

APPENDIX D

SCANNING ELECTRON MICROSCOPY IMAGES

Block 4
Exposed to Lime Solution 12 Months
Sample Location – Below Immersion Line

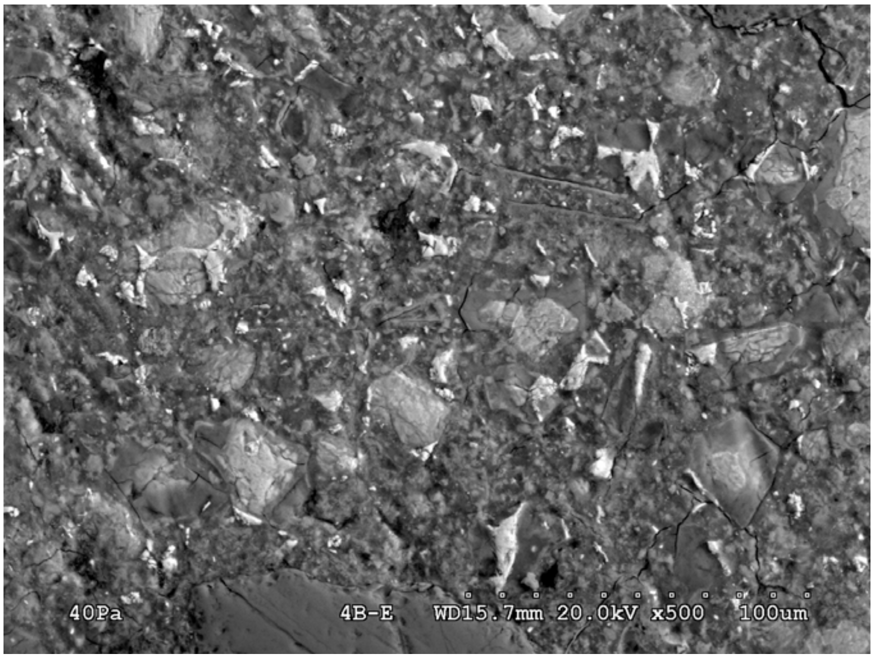

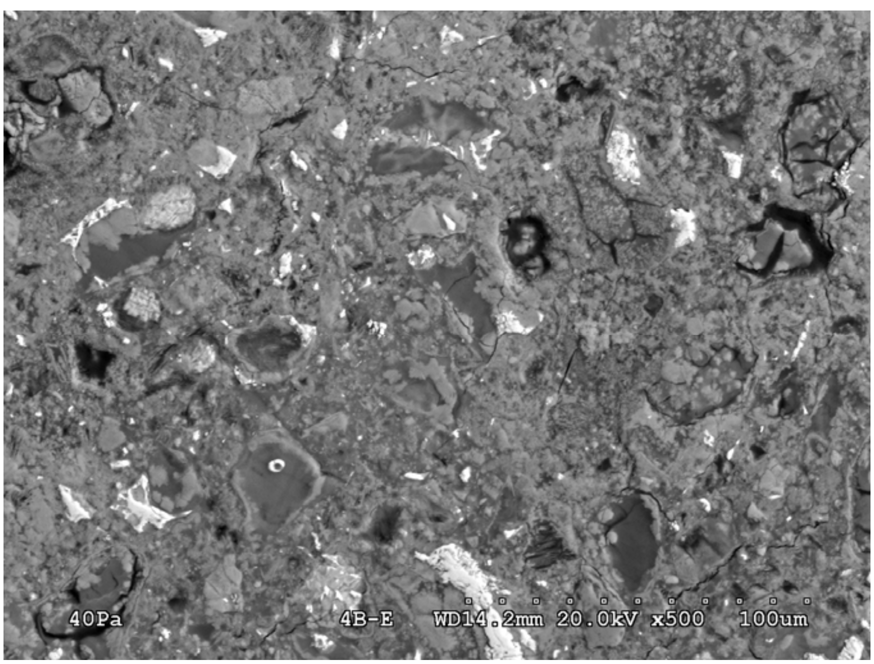

Block 4
Exposed to Lime Solution 12 Months
Sample Location – At Immersion Line

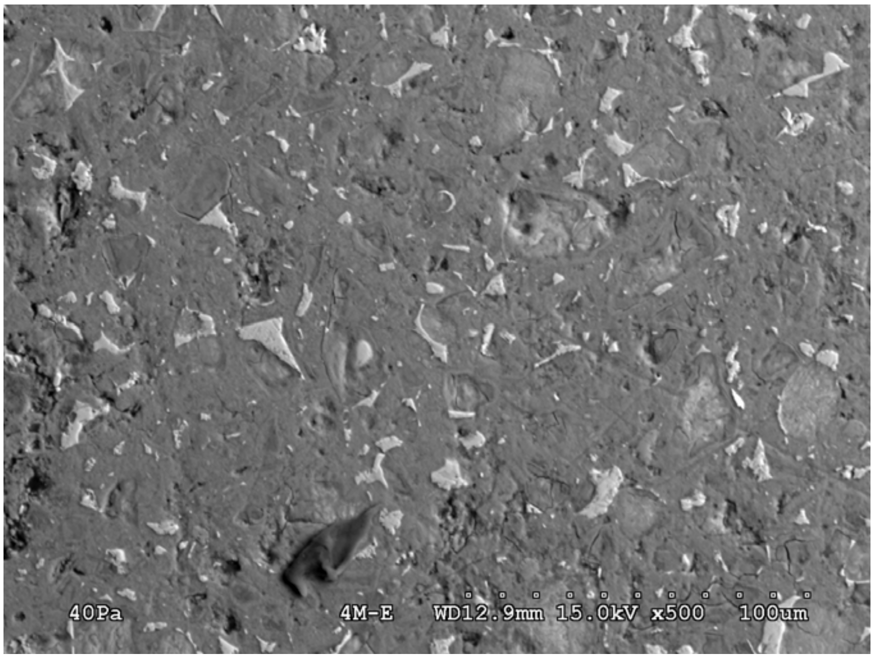

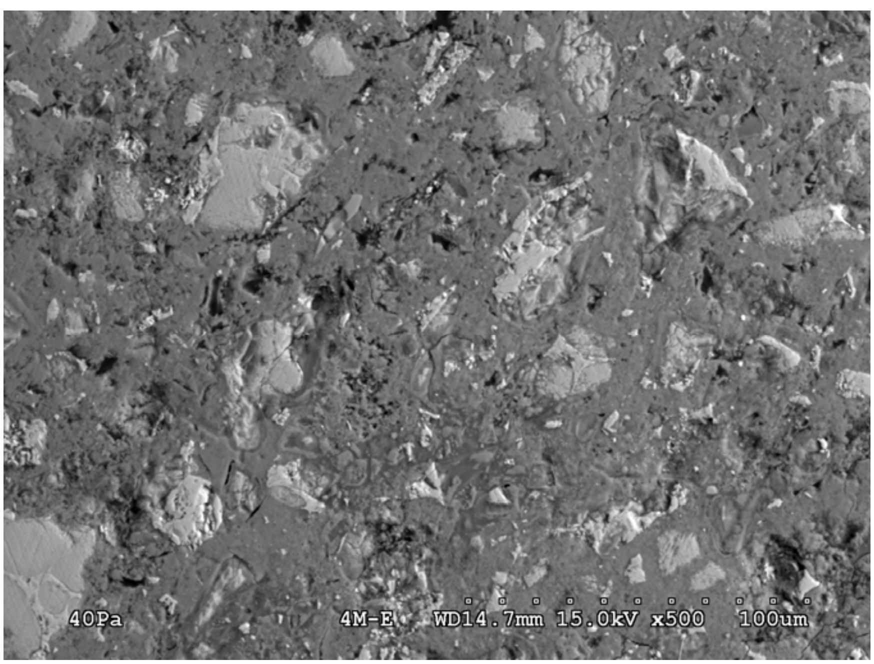

Block 4
Exposed to Lime Solution 12 Months
Sample Location – Above Immersion Line

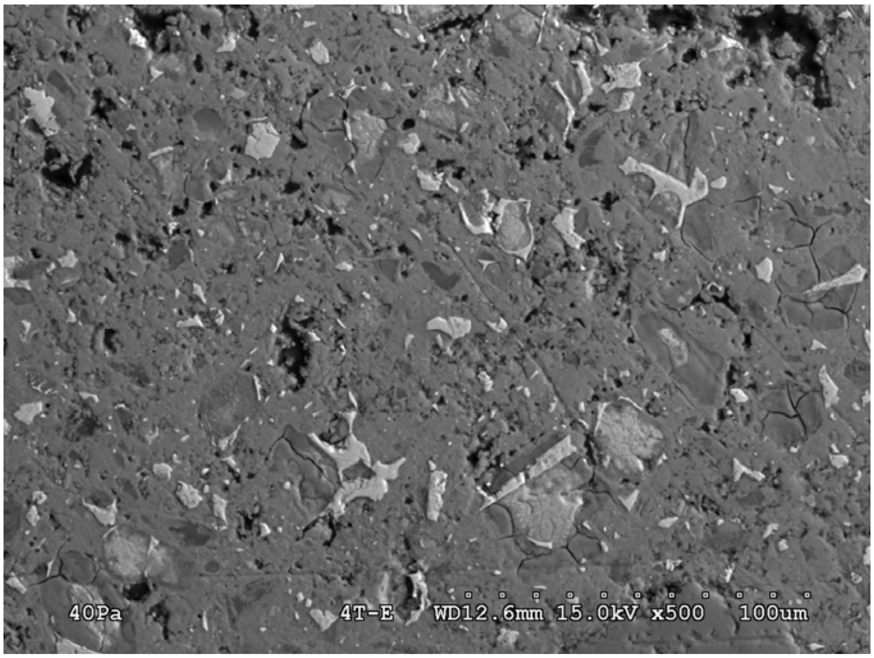

Block 17
Exposed to Lime Solution 12 Months
Sample Location – Below Immersion Line

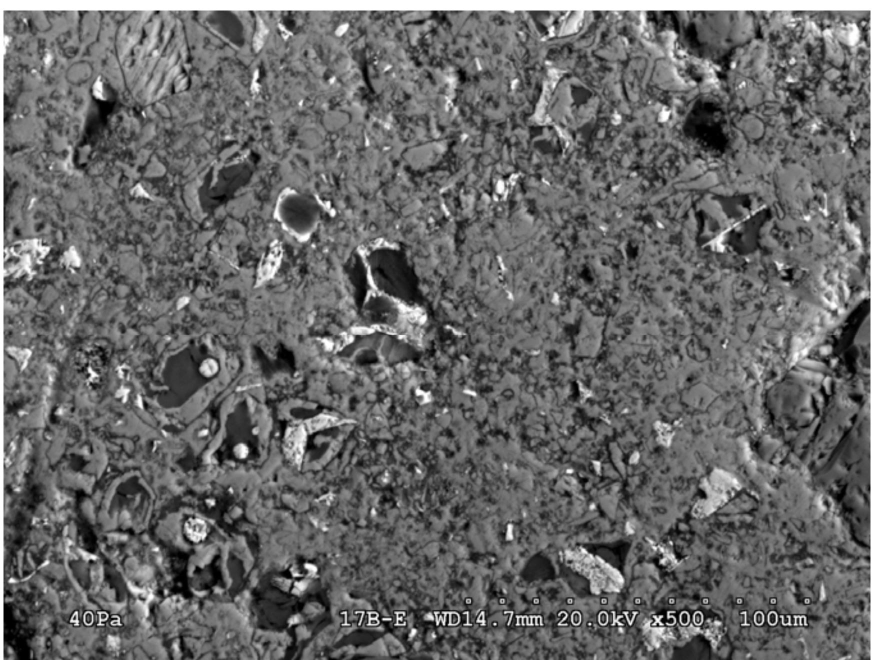

Block 17
Exposed to Lime Solution 12 Months
Sample Location – At Immersion Line

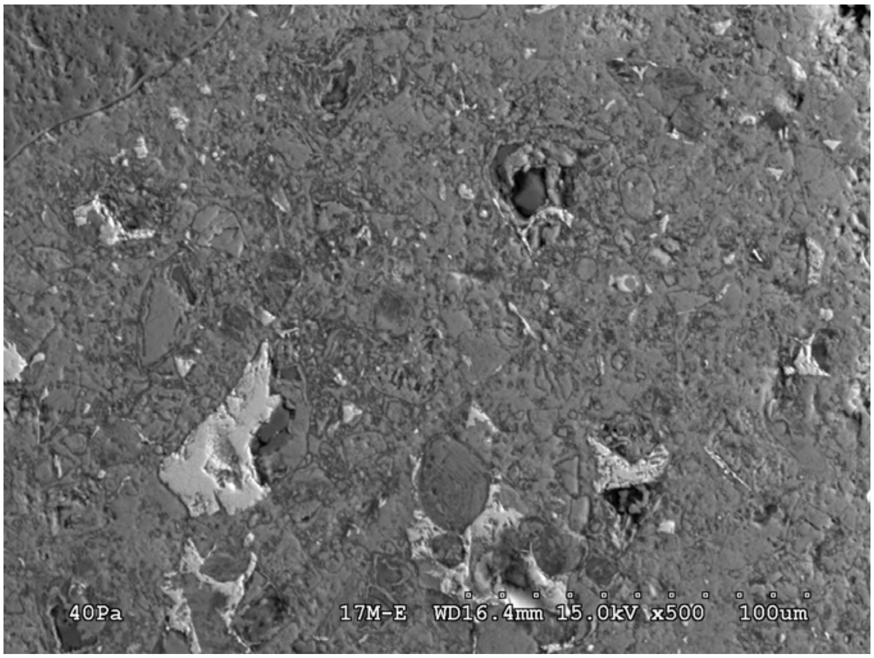

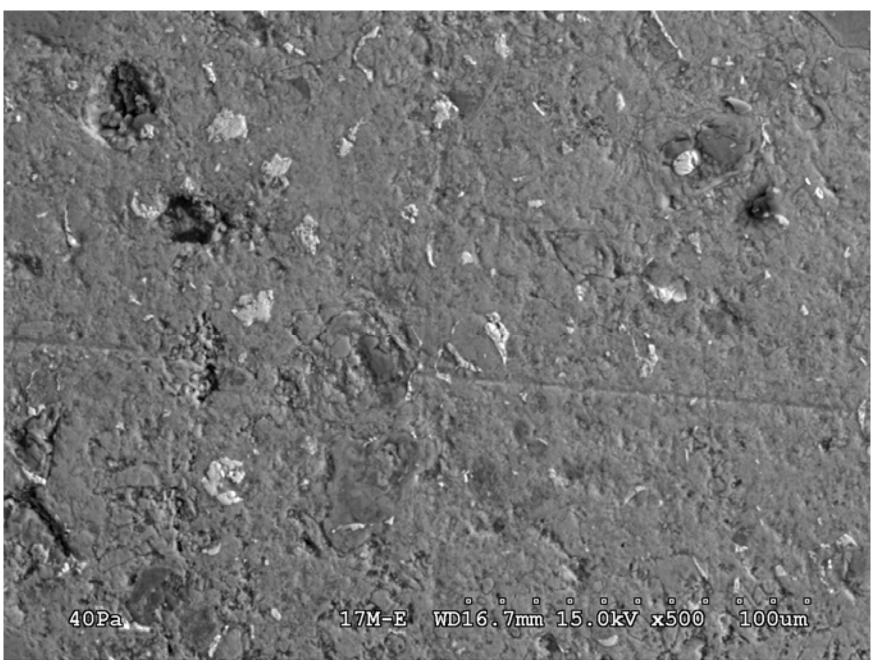

Block 17
Exposed to Lime Solution 12 Months
Sample Location – Above Immersion Line

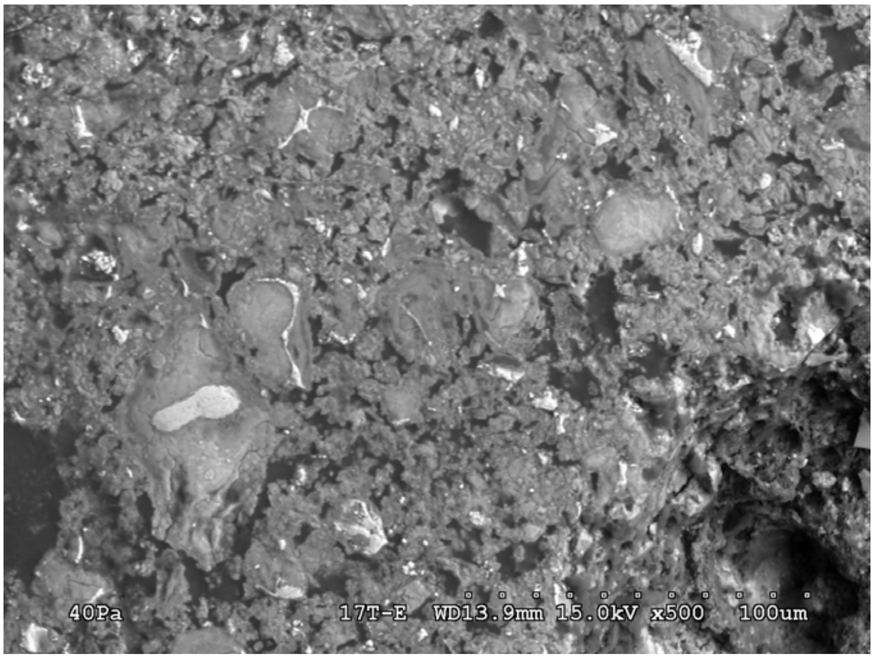

Block 1
Exposed to Sulfates 12 Months
Sample Location – Below Immersion Line

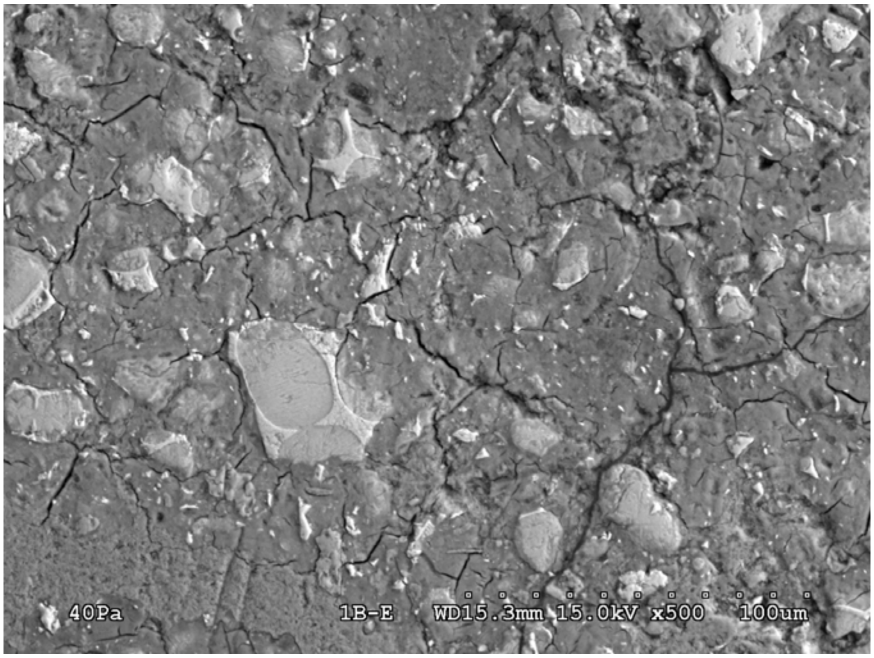

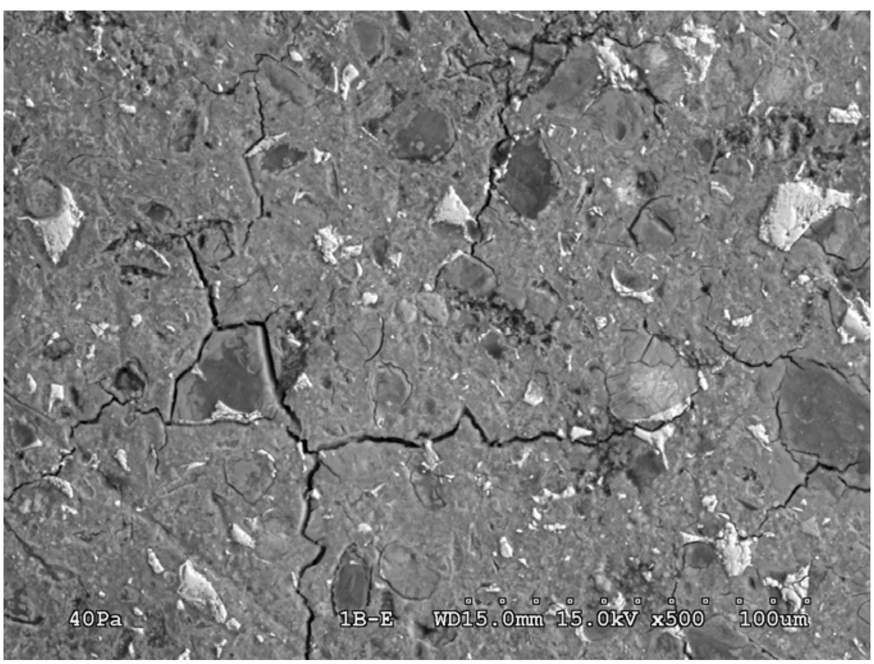

Block 1
Exposed to Sulfates 12 Months
Sample Location – At Immersion Line

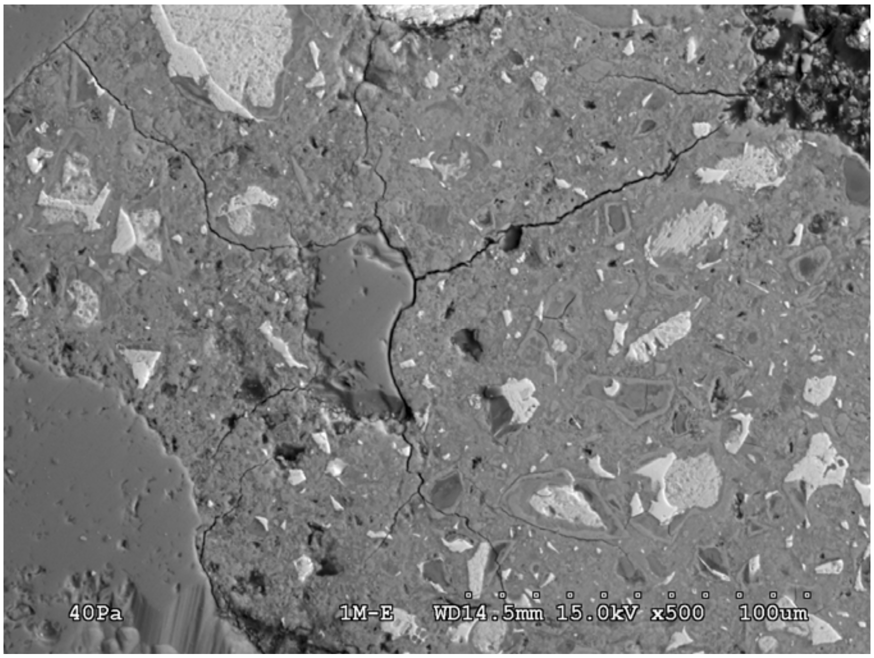

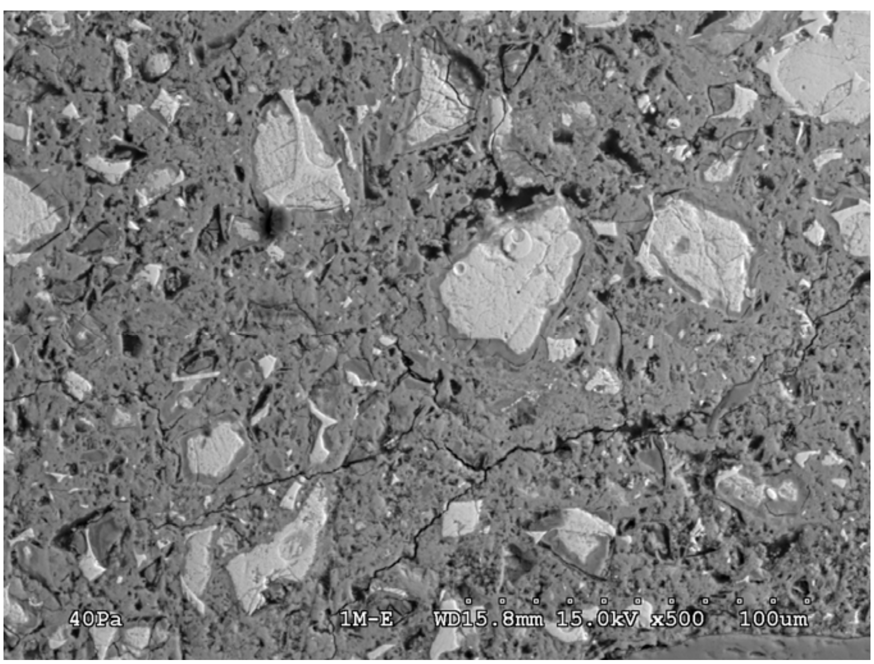

Block 1
Exposed to Sulfates 12 Months
Sample Location – Above Immersion Line

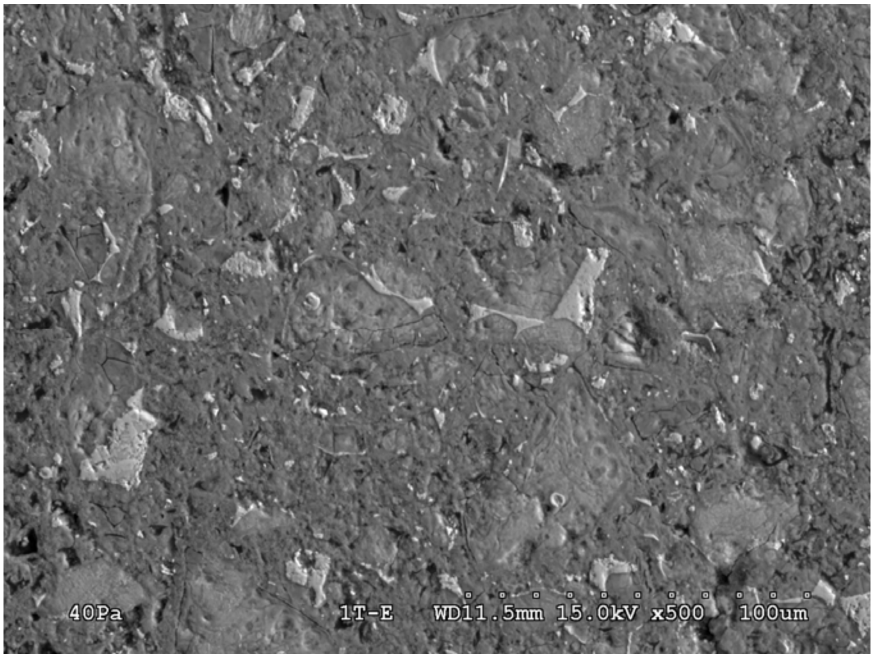

Block 20
Exposed to Sulfates 12 Months
Sample Location – Below Immersion Line

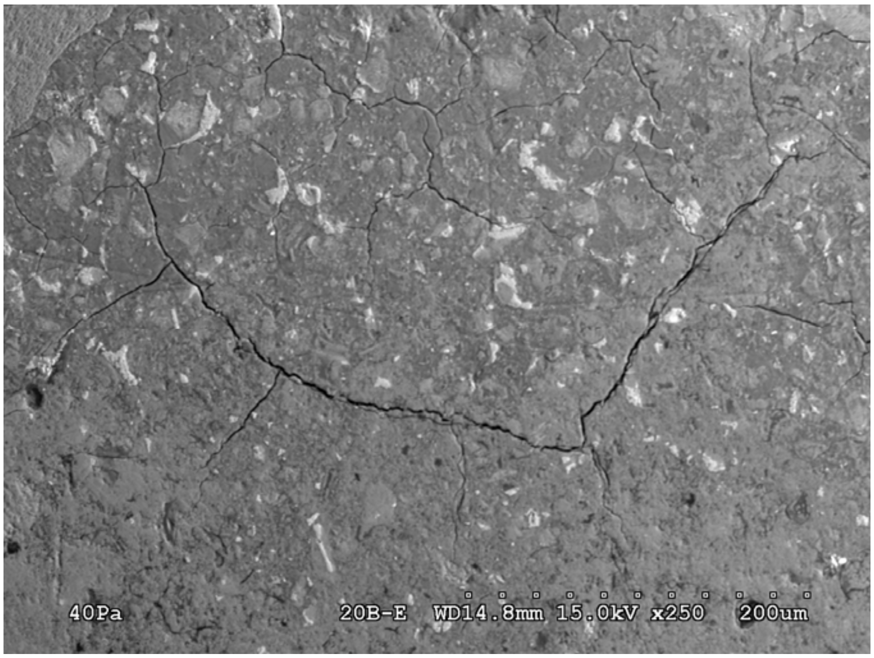

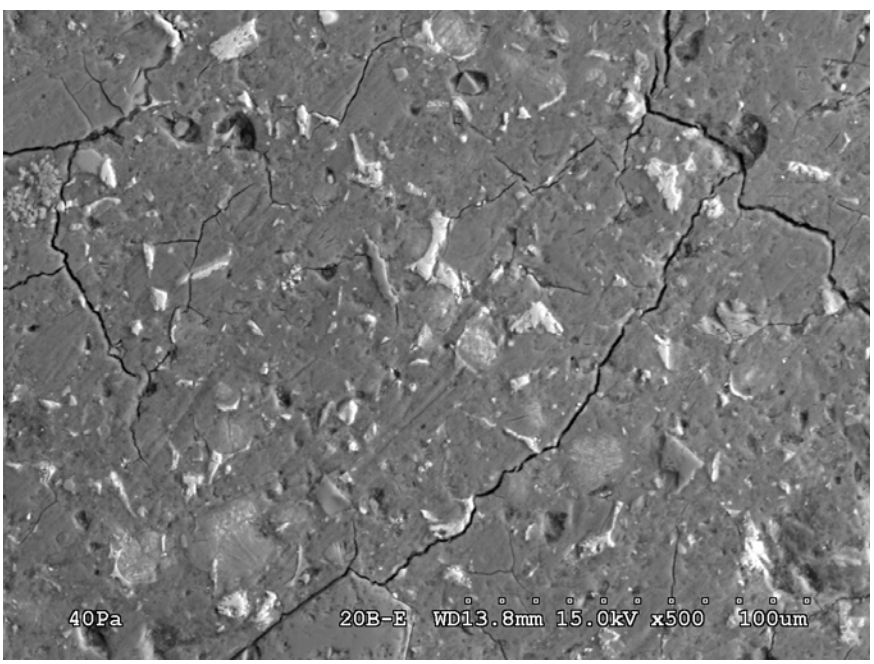

Block 20
Exposed to Sulfates 12 Months
Sample Location – At Immersion Line

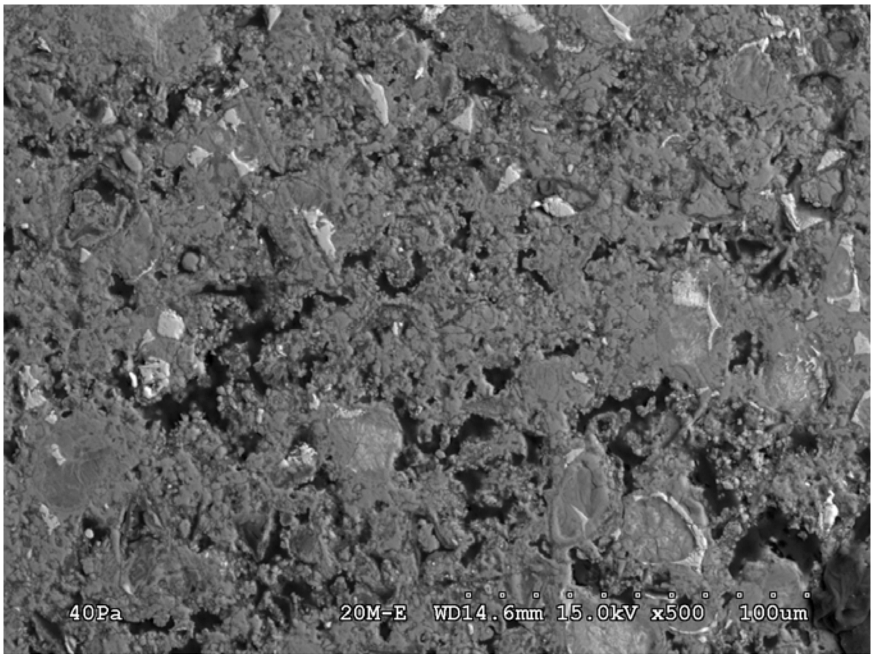

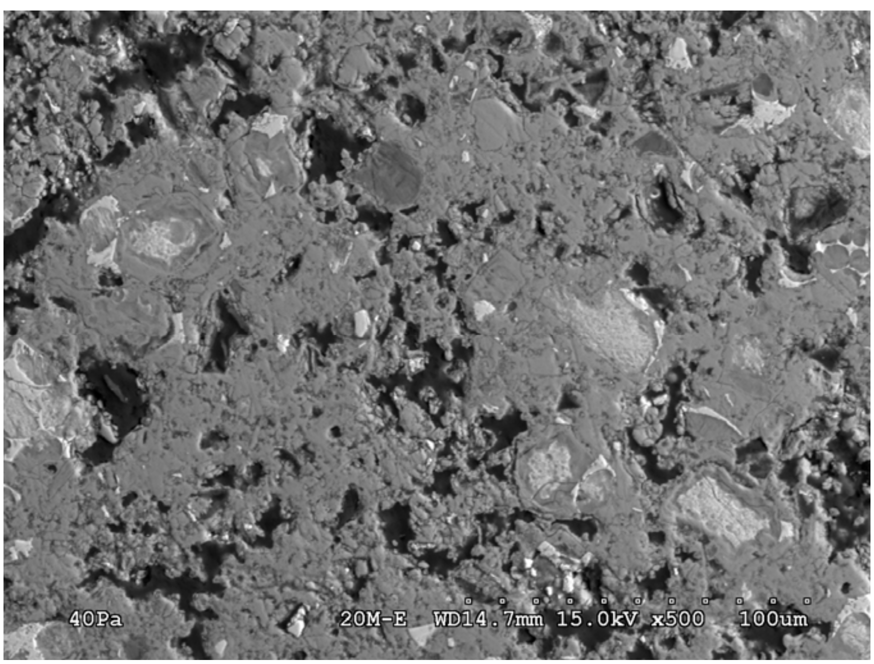

Block 20
Exposed to Sulfates 12 Months
Sample Location – Above Immersion Line